Eulerian droplet models: Mathematical analysis, improvement and applications

Sana Keita

Thesis submitted to the Faculty of Science in partial fulfillment of the requirements
for the degree of
Doctorate in Philosophy Mathematics and Statistics[1]

Department of Mathematics and Statistics
Faculty of Science
University of Ottawa

[1]The Ph.D. program is a joint program with Carleton University, administered by the Ottawa-Carleton Institute of Mathematics and Statistics

Abstract

The Eulerian description of dispersed two-phase flows results in a system of partial differential equations describing characteristics of the flow, namely volume fraction, density and velocity of the two phases, around any point in space over time. When pressure forces are neglected or a same pressure is considered for both phases, the resulting system is weakly hyperbolic and solutions may exhibit vacuum states (regions void of the dispersed phase) or localized unbounded singularities (delta shocks) that are not physically desirable. Therefore, it is crucial to find a physical way for preventing the formation of such undesirable solutions in weakly hyperbolic Eulerian two-phase flow models.

This thesis focuses on the mathematical analysis of an Eulerian model for air-droplet flows, here called the *Eulerian droplet model*. This model can be seen as the sticky particle system with a source term and is successfully used for the prediction of droplet impingement and more recently for the prediction of particle flows in airways. However, this model includes only one-way momentum exchange coupling, and develops delta shocks and vacuum states. The main goal of this thesis is to improve this model, especially for the prevention of delta shocks and vacuum states, and the adjunction of two-way momentum exchange coupling. Using a characteristic analysis, the condition for loss of regularity of smooth solutions of the inviscid Burgers equation with a source term is established. The same condition applies to the droplet model. The Riemann problems associated, respectively, to the Burgers equation with a source term and the droplet model are solved. The characteristics are curves that tend asymptotically to straight lines. The existence of an entropic solution to the generalized Rankine-Hugoniot conditions is proven. Next, a way for preventing the formation of delta shocks and vacuum states in the model is identified and a new Eulerian droplet model is proposed. A new hierarchy of two-way coupling Eulerian models is derived. Each model is analyzed and numerical comparisons of the models are carried out. Finally, 2D computations of air-particle flows comparing the new Eulerian droplet model with the standard Eulerian droplet model are presented.

Résumé

La description eulérienne des écoulements diphasiques dispersés donne lieu à un système d'équations aux dérivées partielles décrivant les caractéristiques de l'écoulement, à savoir la fraction volumique, la densité et la vitesse des deux phases, autour de tout point de l'espace en fonction du temps. Lorsque les forces de pression sont négligées ou qu'une même pression est considérée pour les deux phases, le système résultant est faiblement hyperbolique et les solutions peuvent présenter des zones de vacuum (régions dépourvues de la phase dispersée) ou des singularités non bornées localisées (delta chocs) physiquement indésirables. Par conséquent, il est crucial de trouver un moyen physique d'empêcher la formation de telles solutions indésirables dans les modèles eulériens faiblement hyperboliques pour les écoulements diphasiques.

Cette thèse porte sur l'analyse mathématique d'un modèle eulérien pour les écoulements d'air chargés de goutellettes, appelé ici le *modèle eulérien de gouttelettes*. Ce modèle peut être vu comme le système des particules collantes avec un terme source. Il a été utilisé avec succès pour la prédiction de l'impact de gouttelettes et plus récemment pour la prédiction du transport de particules dans les voies respiratoires. Cependant, ce modèle comprend un terme de couplage décrivant seulement le transfert de moment unidirectionnel. Sa solution développe aussi des delta chocs et des vacuums. L'objectif principal de cette thèse est d'améliorer ce modèle, en particulier pour prévenir les delta chocs et les vacuums, et pour inclure un transfert bidirectionnel du moment entre les phases. Via une analyse par caractéristiques, une condition de perte de régularité des solutions régulières de l'équation de Burgers avec terme source est établie. La même condition s'applique au modèle de gouttelettes. Les problèmes de Riemann associés respectivement à l'équation de Burgers avec terme source et au modèle de gouttelettes sont résolus. L'existence d'une solution entropique aux conditions généralisées de Rankine-Hugoniot est prouvée. Ensuite, un moyen d'empêcher la formation de delta chocs et de vacuums dans les solutions du modèle est identifié et un nouveau modèle eulérien de gouttelettes est proposé. Une nouvelle hiérarchie de modèles eulériens comprenant un transfert bidirectionnel du moment est dérivée. Chaque modèle est analysé et des comparaisons numériques des modèles sont présentées. Enfin, des calculs en 2D d'écoulements d'air chargés de particles sont présentés et permettent de comparer le nouveau modèle eulérien de gouttelettes au modèle eulérien de gouttelettes standard.

Acknowledgement

First, I would like to thank my thesis supervisor Dr. Yves Bourgault for his continuous guidance and his unconditional support both moral and financial. I would also like to thank him for his careful readings of this thesis.

I would like to express my sincere gratitude to the university of Ottawa for awarding me scholarships, and allowing me to achieve this work.

I owe fellow friend Cheikh Becaye Ndongo a special thank you for our (almost) daily conversations, and his unconditional moral support. Similarly, I would like to thank academic colleagues for their friendship and encouragement: Kak Choon Loy, Aminata Dite Tanti Keita, Saint Cyr Koyaguerebo Ime, Diane Fokoue, and Moussa Thiam. I appreciated the process of learning with/from each of you along the way.

Finally, I would like to take this opportunity to express my profound gratitude from the deepest part of my heart to my beloved parents for their entire support throughout my education. I cannot imagine my current position without their love and support. To them, I dedicate this thesis.

Contents

List of Figures

List of Tables

Chapter 1

Introduction

Flows of air carrying particles or droplets commonly occur in nature, for instance, convective flows within clouds [92, 48], atmospheric wind charged with particle aerosols [3, 58] and flows charged with ash during volcanic eruptions [94]. The prediction of such flows is also useful in industrial and medical applications. For instance, predicting the propagation and deposition of particles in the mouth-throat or the inner lung airways helps for designing inhalers [42, 88]. The prediction of in-flight icing droplet impingement can help to anticipate and prevent aircraft crashes [7, 2]. Applications in engineering also include diesel injection into engines [72] and coating spray processes [83].

There are two common approaches for describing a fluid in motion containing particles: Lagrangian and Eulerian. With the Lagrangian approach, the particles are individually tracked along their trajectories through the computational domain. The trajectory of each particle is established from the balance of forces exerted on the particle by using the fundamental dynamic relations. With the Eulerian approach, the particles are treated as a continuum interacting with the fluid phase. The motion of particles is described in function of their concentration and velocity on small control volumes around each point of the domain at any time. Of course, the particles are subject to the same dynamical relations with both approaches.

There are several mathematical models for air-particle flows proposed in the literature for both approaches. For a general presentation of models for two-phase flows, we refer to [57, 33, 44] and the references therein. Many numerical models for air flows charged with particles rely on the Lagrangian approach [98, 73, 4, 19]. Some comparisons of the Lagrangian and Eulerian approaches are available for specific applications [89, 47]. Recent works [89, 41, 99] suggest that the Eulerian approach may be a natural choice for the numerical prediction of air flows charged with particles.

In this thesis, we consider one of these Eulerian models for air-particle flow, which was used for the prediction of droplet impingement during in-flight icing [15]. The model corresponds to a dispersed phase subsystem, for instance a multi-phase

system for droplets or particles suspended in a carrier fluid. This model is known as the *Eulerian droplet model*, and will be introduced in the next section.

1.1 The Eulerian droplet model

Let $\mathcal{V}_x$ be a region of volume $vol(\mathcal{V}_x)$, containing the point $x \in \mathbb{R}^q$. This region is filled with spherical particles p. The volume fraction $\alpha = \alpha(x,t) \in \mathbb{R}$ and the velocity field $\mathbf{u} = \mathbf{u}(x,t) \in \mathbb{R}^q$ of particles at position x and time t are defined as follows:

$$\begin{aligned} \alpha &= \lim_{vol(\mathcal{V}_x)\to\varepsilon} \frac{\textit{total volume of the particles in } \mathcal{V}_x}{vol(\mathcal{V}_x)} = \lim_{vol(\mathcal{V}_x)\to\varepsilon} \frac{1}{vol(\mathcal{V}_x)} \sum_{p\subset\mathcal{V}_x} vol(p), \\ \mathbf{u} &= \lim_{vol(\mathcal{V}_x)\to\varepsilon} \frac{\sum_{p\subset\mathcal{V}_x} vol(p)\mathbf{u}_p}{\sum_{p\subset\mathcal{V}_x} vol(p)}, \end{aligned} \tag{1.1.1}$$

where *vol(p)* and $\mathbf{u}_p \in \mathbb{R}^q$ are the volume and velocity of particle p, respectively, and ε is a small positive number such that $\mathcal{V}_x$ contains a sufficiently large number $(10^3 - 10^4)$ of particles for α and $\mathbf{u}$ to be representative statistical averages.

1.1.1 Mass conservation

In fluid mechanics, the conservation of mass can be described by the continuity equation in different forms: conservative, non-conservative or integral form. The conservative form is the most used. The mass conservation equation for the particles can be written as

$$\frac{D\rho_l}{Dt} = \frac{\partial\rho_l}{\partial t} + \nabla\cdot(\rho_l\mathbf{u}) = 0, \tag{1.1.2}$$

where ρ_l represents the density of the particles, i.e. the mass of the material constituting the particles per unit volume.

1.1.2 Momentum conservation

A particle moving in a fluid experiences a *drag force* F_D. The drag force acts as a mechanism by which a particle tries to catch up with the changing velocities of the surrounding fluid. For a spherical particle moving in air flow, the drag force can be expressed (see [47]) as

$$F_D = \frac{\pi}{8} C_d Re_d \mu d(\mathbf{u}_a - \mathbf{u}), \tag{1.1.3}$$

where μ is the dynamic viscosity of air; d is the diameter of the particle; $\mathbf{u}_a$ is the air velocity field; $Re_d = \rho d|\mathbf{u}_a - \mathbf{u}|/\mu$ is the Reynolds number of the particle; ρ is the air density; and C_d is the drag coefficient. This coefficient depends on the particle Reynolds number, and will be defined later.

A particle in a gravitational field experiences a *gravitational force* in the direction of the gravitational acceleration $\mathbf{g}$. The particle also experiences another force in the opposite direction. This latter force is called *buoyancy force*. According to Archimedes' principle, the buoyancy force is equal to the weight of the displaced fluid volume. The net force F_G (the gravitational and buoyancy forces) for a spherical particle is given by (see [47])

$$F_G = (1 - \frac{\rho}{\rho_l})\mathbf{g}. \tag{1.1.4}$$

To simplify, we assume that the drag, gravitational and buoyancy forces are the only forces that act on the particles. For others types of forces that a particle in motion in a fluid can experience, we refer to [47]. Newton's second law states that

$$m\frac{d\mathbf{u}}{dt} = F_D + F_G \tag{1.1.5}$$

where m is the mass of the particle. An averaging procedure is performed on the equation (1.1.5) to get an Eulerian expression for momentum conservation. Details on the averaging procedure for these equations are given in [54]. After simplification, the mass and momentum conservation equations may be rewritten in their final non-dimensional form [15]:

$$\begin{aligned} &\frac{\partial \alpha}{\partial t} + \nabla \cdot (\alpha \mathbf{u}) = 0, \\ &\frac{\partial \mathbf{u}}{\partial t} + \mathbf{u} \cdot \nabla \mathbf{u} = \frac{C_D Re_d}{24K}(\mathbf{u}_a - \mathbf{u}) + (1 - \frac{\rho}{\rho_l})\frac{1}{Fr^2}\mathbf{g}, \end{aligned} \tag{1.1.6}$$

where $K = \rho_l d^2 U_\infty / 18 L\mu$ is an inertia parameter; $Fr = U_\infty / \sqrt{L g_0}$ is the Froude number; U_∞ is the speed of air at infinity; g_0 is a characteristic external field; and L is a characteristic length.

System (1.1.6) constitutes the *Eulerian droplet model* for air-particle flows [15]. It is important to notice that this model applies to particles with the same diameter. For particles of different sizes, one should consider the mean volume diameter (MVD) of the particles, or repeat system (1.1.6) for every particle diameter considered.

1.2 Some applications of the Eulerian droplet model

The Eulerian droplet model (1.1.6) yields volume fraction α and velocity field $\mathbf{u}$ of the particles in any specific location x in space at time t. The collection efficiency measures the fraction of particles approaching a surface, that actually deposit on this surface. The collection efficiency, denoted by β, can be then calculated as

$$\beta = \alpha \mathbf{u} \cdot \mathbf{n}, \tag{1.2.1}$$

where **n** is the outward normal of the domain. In [17], the collection efficiency profiles for a MVD of $16\mu m$ and a Langmuir-D distribution with a MVD of $16\mu m$ of droplets are computed with the Eulerian droplet model (1.1.6). Figure 1.1 (images are taken from [17]) shows the plot of the collection efficiency on the surface of a circular cylinder for both cases and the experimental data. One can see that the solution with a Langmuir-D distribution stays within the experimental repeatability range. Numeri-

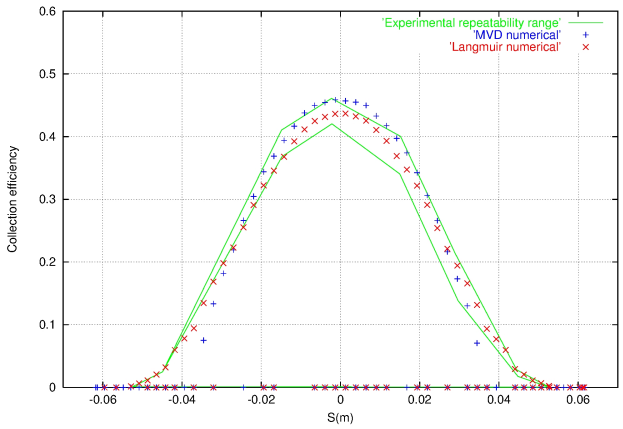

Figure 1.1: Comparison of the collection efficiency on the surface of a circular cylinder for the Langmuir-D distribution of droplet size and the MVD solution together with experimental data. The abscissa S is the distance along the circular arc from the stagnation point (reproduced from [17]).

cal computations using the Eulerian droplet model (1.1.6) were also conducted on the nose and cockpit of an aircraft [17]. Figure 1.2 shows the surface collection efficiency for a MVD of $400\mu m$. These numerical results show that the Eulerian droplet model can provide accurate droplet impingement predictions when an adequate droplet size distribution is provided.

The Eulerian droplet model (1.1.6) was also applied to particle flows in airways. Numerical computations of air-particle flows in a 2D prototype airway, computed with the Eulerian droplet model (1.1.6), were first presented in [14]. The model was also applied to aerosol propagation in a 3D patient-based geometry of the airway tract [16]. The air flow was obtained by solving the Navier-Stokes equations. Numerical results for aerosol propagation in this geometry were obtained by coupling the Eulerian droplet model (1.1.6) with the air flow solutions. Figure 1.3 shows the time-evolution of the aerosol volume fraction on a vertical cross-section of the airway tract. Figure 1.4 shows the collection efficiency computed on the walls of the airways. These numerical test cases show that the Eulerian droplet model could provide a viable approach to compute internal air-particle flows, even in the presence of recirculations.

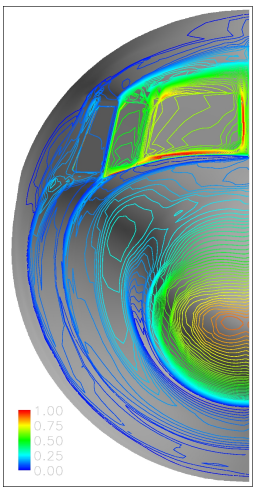

Figure 1.2: Collection efficiency on the nose and cockpit of a Convair-580 for droplets with MVD of $400\mu m$ (reproduced from [17]).

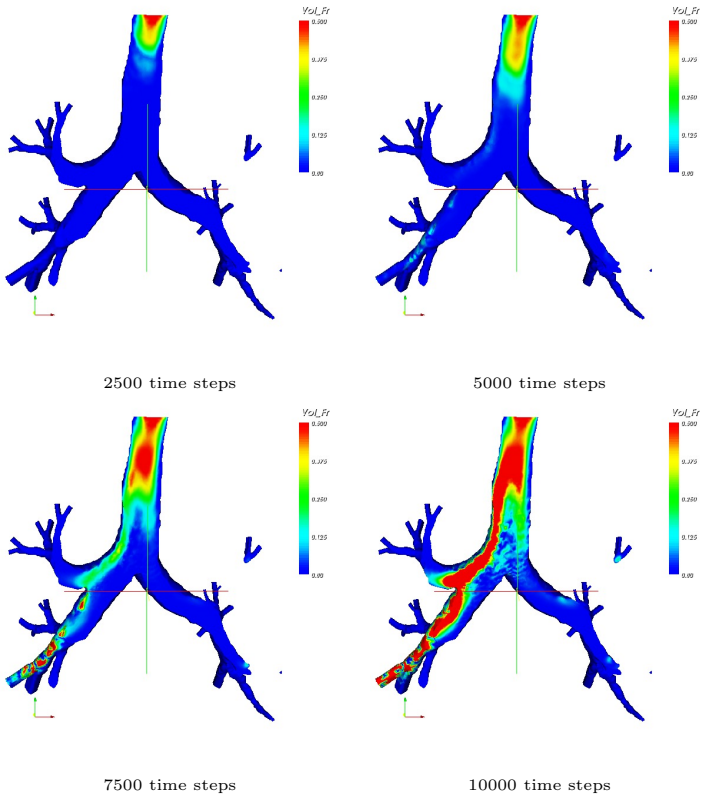

Figure 1.3: Volume fraction of aerosols at various times (reproduced from [16]).

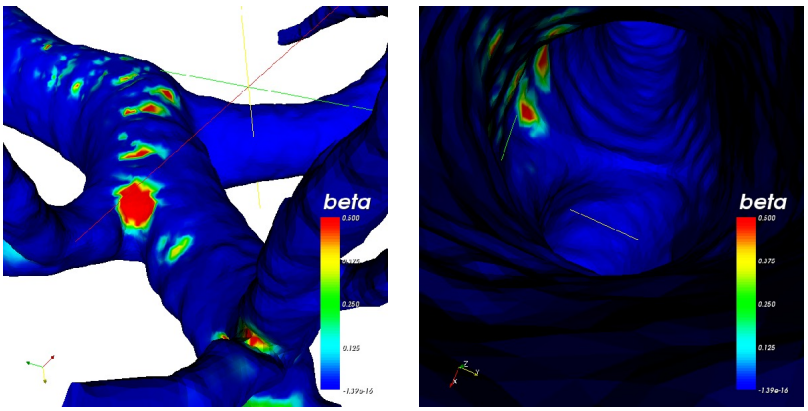

Right branch Endoscopic view

Figure 1.4: Collection efficiency on the walls of the airways (reproduced from [16]).

1.3 Problem statement and outline of the thesis

As most of the equations in fluid mechanics, the Eulerian droplet model (1.1.6) is a hyperbolic system that contains a nonlinear advection term (i.e. the advection velocity depends on the solution). The resolution of such problems encounters many difficulties among which we can mention:

- The loss of regularity for smooth initial data: For instance, considering the one-dimensional case, the second equation of (1.1.6) reduces to the inviscid Burgers equation (see [66, 46, 81, 64, 67]) with a zeroth order source term. It is well known that the solution of the inviscid Burgers equation develops discontinuities in finite time provided that the initial condition has negative slope somewhere in the domain. This is a difficulty for solving (1.1.6).

- The choice for the form of the equations, i.e. conservative versus non-conservative form: This choice is fundamental when dealing with solutions involving travelling waves with discontinuities. It also influences the choice of the numerical methods. For instance, equations in conservative form are usually solved with conservative schemes to avoid solutions that are not physically acceptable (e.g. solutions that violate the Rankine-Hugoniot conditions for shock waves). The presence of an advection term requires stabilized finite element methods for numerical stability. Such methods introduce numerical diffusion.

The numerical results shown in the previous section are obtained with smooth initial data. They show the usefulness of the Eulerian droplet model. Nevertheless, this model raises some concerns, particularly when discontinuities occur in the solutions. The main difficulties with the Eulerian droplet model are listed in the following.

i) The main drawback with the Eulerian droplet model lies in the fact that it may develop delta shocks, i.e. discontinuous unbounded solutions in the form of the Dirac delta function, within finite time, even with smooth initial conditions. For illustration, we solve system (1.1.6) in the one-dimensional case on the interval $[0, 3]$ using an upwind scheme. We take the initial conditions $\alpha(x, 0) = 0.5 \times \exp(-80(x - 0.5)^2)$ and $u(x, 0) = \exp(-80(x - 0.5)^2)$, and impose Dirichlet boundary conditions $\alpha = 0.5 \times \exp(-80(-0.5)^2)$ and $u = \exp(-80(-0.5)^2)$ on the inlet boundary ($x = 0$) of the domain. The outlet boundary ($x = 1$) is left free. To simplify, we take a constant drag coefficient ($\frac{C_D Re_d}{24K} = 1$), a constant air velocity $u_a = 1$, and we neglect the gravity force ($g = 0$). Numerical results are shown in Figure 1.5. We see

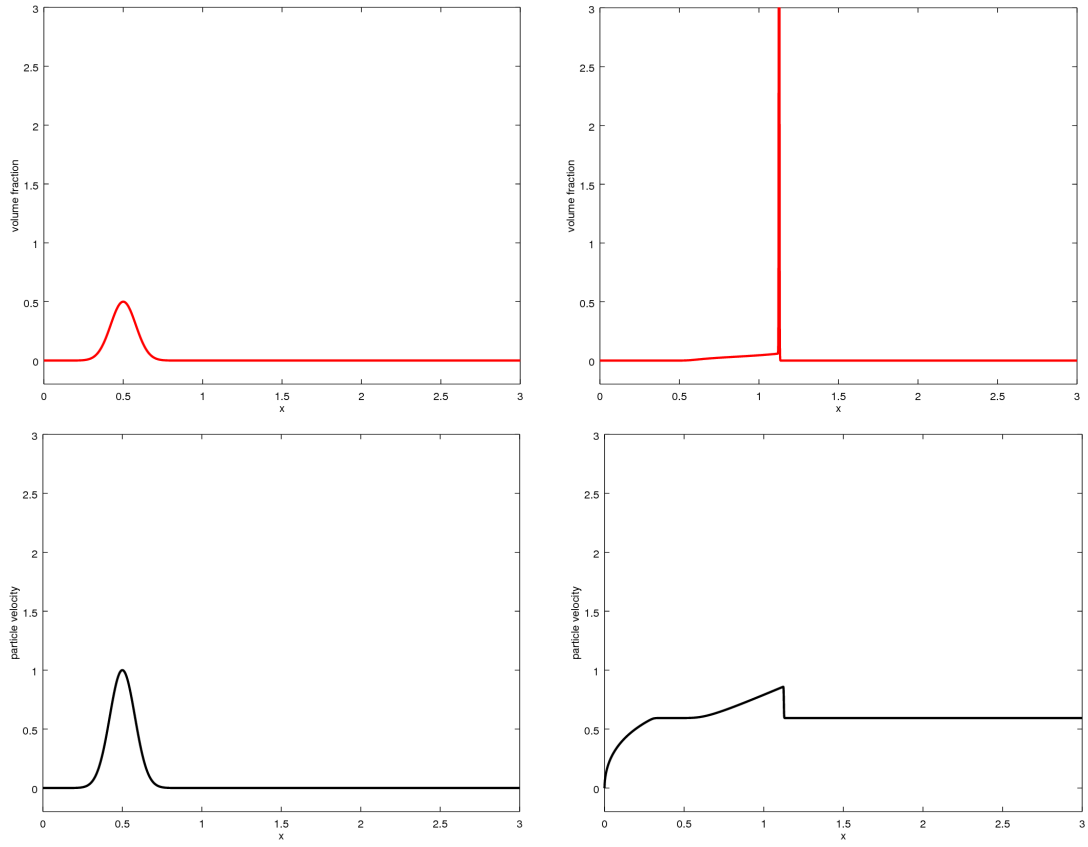

Figure 1.5: Formation of a delta shock in the solution of the Eulerian droplet model. $\frac{C_D Re_d}{24K} = 1$, $u_a = 1$, $g = 0$, $\Delta x = 5 \times 10^{-4}$ and $\Delta t = 3 \times 10^{-4}$.

the formation and propagation of a delta shock centered at the discontinuity in the velocity. Besides being problematic for numerical computations, this solution is not physically meaningful since the volume fraction should remain bounded.

ii) The momentum conservation equation (the second equation of (1.1.6)) is

written in non-conservative form. The conservative form of this equation, derived using the principles of continuum mechanics, reads as

$$\frac{\partial(\alpha\mathbf{u})}{\partial t} + \nabla\cdot(\alpha\mathbf{u}\otimes\mathbf{u}) = \frac{C_D Re_d}{24K}\alpha(\mathbf{u}_a - \mathbf{u}) + \alpha(1-\frac{\rho_a}{\rho_p})\frac{1}{Fr^2}\mathbf{g}, \tag{1.3.1}$$

where the tensor product $\alpha\mathbf{u}\otimes\mathbf{u}$ is defined as $(\alpha\mathbf{u}\otimes\mathbf{u})_{i,j} = \alpha u_i u_j$, $i,j = 1,...,d$. The passage from (1.3.1) to the second equation of (1.1.6) can be done first by subtracting α times the first equation of (1.1.6) from (1.3.1) and second, by dividing the so obtained equation by α. The Eulerian droplet model in conservative form is then written as

$$\begin{aligned} &\frac{\partial\alpha}{\partial t} + \nabla\cdot(\alpha\mathbf{u}) = 0, \\ &\frac{\partial(\alpha\mathbf{u})}{\partial t} + \nabla\cdot(\alpha\mathbf{u}\otimes\mathbf{u}) = \frac{C_D Re_d}{24K}\alpha(\mathbf{u}_a - \mathbf{u}) + \alpha(1-\frac{\rho_a}{\rho_p})\frac{1}{Fr^2}\mathbf{g}. \end{aligned} \tag{1.3.2}$$

In case $C_D = 0$ and $\mathbf{g} = 0$, the conservative form (1.3.2) of the Eulerian droplet model can be seen as the *pressureless gas equations* [9] or as the *sticky particle system* that arises in the modeling of particles hitting and sticking to each other to explain the formation of large scale-structures in the universe [36, 18]. The numerical results shown in section 1.2 are all computed with the non-conservative form (1.1.6). The use of the conservative form (1.3.2) has many advantages. For instance, it gives more possibilities for the choice of the numerical methods, including all conservative or kinetic schemes that were developed for hyperbolic conservation laws. However, the conservative form presents a main shortcoming: the velocity field is not defined in vacuum regions (for $\alpha = 0$). From the numerical point of view, the computation of the velocity field remains a challenge when the volume fraction tends to zero. The same problem is encountered with the pressureless gas equations when the particle density tends to zero. Some authors looked at this particular problem which is usually hard to handle. Boudin [13] suggested to take any value for the vector field when the particle density is null, for instance, by imposing a null velocity when the density of the particle tends to zero. This potentially leads to discontinuous solutions at the interface between the vacuum/non-vacuum regions. These discontinuities are artificial and create undesirable numerical difficulties. The conservative and non-conservative forms are equivalent for smooth solutions outside vacuum states. However, they may differ when discontinuities occur in the solution, as illustrated in Figure 1.6 for a delta shock wave computed with the two forms. A fundamental choice between the conservative and non-conservative forms must thus be made when using the Eulerian droplet model.

iii) Another weakness of the Eulerian droplet model is that it assumes one-way momentum transfer from the carrier fluid to the droplets but not vice-versa. The carrier fluid (air) is simply considered as a physical body acting on the droplets, and

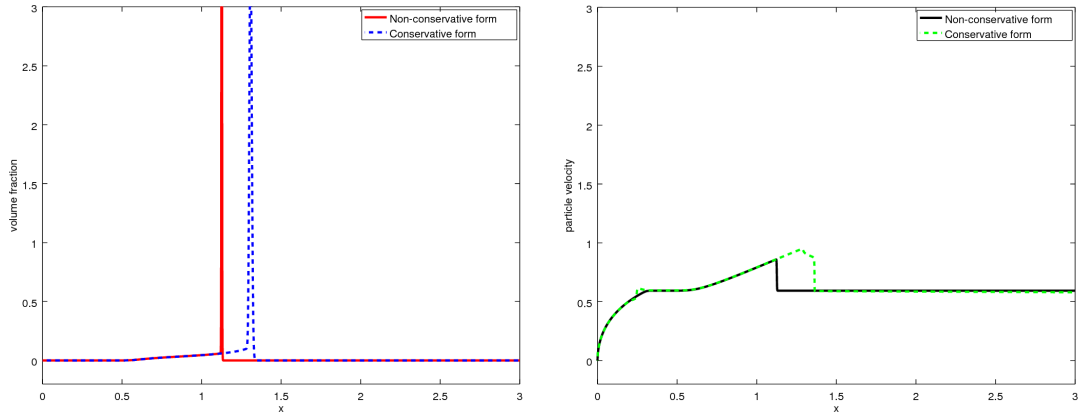

Figure 1.6: Delta shock wave with the conservative and non-conservative forms at $t = 0.9$. $\frac{C_D Re_d}{24K} = 1$, $u_a = 1$, $g = 0$, $\Delta x = 5\times10^{-4}$ and $\Delta t = 3\times10^{-4}$.

is modelled separately from the particle equations, by Euler or Navier-Stokes equations. To be more realistic, the effects of the droplets on the carrier fluid should also be taken into account, particularly when the particle mass loading is important.

The following questions are raised: **1)** Should one use the conservative or the non-conservative form? **2)** What is the cause of the formation of delta shocks? **3)** How can one improve the Eulerian droplet model to avoid delta shocks from occurring? **4)** How can one couple the Eulerian droplet model with the equations for the carrier fluid in order to take into account the effects of the droplets on the carrier fluid?

As far as we know, there is no theoretical study related to the pressureless gas equations including explicitly a zeroth-order source term as in the Eulerian droplet model. In this thesis, we are interested in the theoretical study of the Eulerian droplet model. The objective is to find an answer for each of the above questions. Our main goal is the improvement of the Eulerian droplet model, in particular preventing the formation of delta shocks without affecting its usefulness. We address these issues in the thesis as follows.

- **Chapter 2**: We first briefly recall the main mathematical tools for hyperbolic conservation laws, which are used throughout this thesis. We then introduce the hierarchy of Eulerian models for dispersed two-phase flows proposed by Bouchut in [10]. Finally, we discuss some numerical schemes proposed in the past for the simulation of hyperbolic conservation laws.

- **Chapter 3**: This chapter is devoted to the mathematical analysis of the Eulerian droplet model. The condition for loss of regularity of smooth solutions is

established. This partially answers the second question. The Riemann problem associated to the Eulerian droplet model is solved. The generalized Rankine-Hugoniot conditions for delta shocks are established and the existence of a solution to the generalized Rankine-Hugoniot conditions is proven. These results partially answer the first question when discontinuities occur in the solutions.

- **Chapter 4**: The responses to the second and third questions require a understanding of the process of delta shocks formation. We also want to find a way to prevent their occurrence. It is known that the formation of delta shocks and vacuum states in the pressureless gas system results from the vanishing pressure limit of the Euler equations for gas dynamics [23]. Due to the similarity between the Eulerian droplet model and the pressureless gas system, the isentropic Euler equations for gas dynamics and the process of formation of delta shocks in the vanishing limit pressure are reviewed in chapter 4. This gives a better understanding of the formation of delta shocks and vacuum states in pressureless gas system, and thus in the Eulerian droplet model. We also propose a proof of a result mentioned (but not proven) by Chen et Liu [23] in the vanishing pressure limit of the isentropic Euler equations.

- **Chapter 5**: Based on the results from the previous chapters, we propose an Eulerian droplet model with particle pressure. This new model is briefly analyzed. Numerical results illustrating the prevention of the formation of delta shocks and vacuum states in the solutions of the model are presented.

- **Chapter 6**: Starting from the hierarchy of two-phase models, which is presented in chapter 2, and using the same idea as in chapter 5, we propose a new hierarchy of Eulerian models for dispersed two-phase flows. Each model of this hierarchy is analyzed. A way of coupling the equations of the droplets with the equations modelling the carrier fluid is presented. This partially answers the fourth equation. Numerical comparisons of the different models are performed and the validity of each model is discussed.

- **Chapter 7**: This chapter is devoted to 2D numerical air-particle flow computations using the Eulerian droplet model proposed in chapter 5. The first goal of this chapter is to present theoretical arguments for the use of this model and the finite element methods for its simulation. The second goal is to compare the usefulness of this new model with the more standard Eulerian droplet model (1.1.6).

- **Appendix A**: All the models studied in this thesis are listed in the appendix.

Chapter 2

Literature review on hyperbolic systems and dispersed two-phase flow models

This chapter is devoted to a short review of the theory of conservation laws, hyperbolic systems, and dispersed two-phase flow models. We start by recalling the main mathematical tools used in the study of systems of conservation laws. Then, we present a hierarchy of Eulerian models for dispersed two-phase flows proposed by Bouchut [10]. Numerical schemes proposed for the simulation of conservation laws are discussed.

2.1 Conservation laws and hyperbolic systems

This section concerns the general form of systems of conservation laws and the main mathematical notions for such systems.

A system of **conservation laws** is a time-dependent system of partial differential equations (PDE) expressing conservation of mass, momentum, energy, charge, etc. In one space dimension, it takes the form (see [81])

$$\frac{\partial}{\partial t}u(x,t) + \frac{\partial}{\partial x}f\big(u(x,t)\big) = 0, \tag{2.1.1}$$

where $u : \mathbb{R} \times (0,\infty) \to \mathbb{R}^p$ is a p-dimensional vector of conserved quantities and $f : \mathbb{R}^p \to \mathbb{R}^p$ is a smooth vector-valued function called the **flux function**. Equation (2.1.1) must be augmented by some initial conditions

$$u(x,0) = u_0(x) \tag{2.1.2}$$

and eventually by boundary conditions if (2.1.1) is expressed on a bounded spatial domain.

System (2.1.1)-(2.1.2) may admit discontinuous solutions in some cases. Therefore, one needs to define what a solution with lower regularity is. To do that, one considers a test function $\psi \in \mathcal{C}_0^\infty(\overline{\mathbb{R} \times \mathbb{R}^+})$. Multiplying (2.1.1) by ψ and integrating by parts, one obtains the weak form of problem (2.1.1)-(2.1.2):

$$\int_0^\infty \int_{-\infty}^\infty \big(u\psi_t + f(u)\psi_x\big)\, dxdt = -\int_{-\infty}^\infty \psi(x,0)u(x,0)\, dx. \tag{2.1.3}$$

Note that a function u does not need to be differentiable or even continuous to satisfy (2.1.3). One has the following definition:

Definition 2.1.1. *A function u is a **weak solution** of the conservation law (2.1.1) if it satisfies (2.1.3) for all test functions $\psi \in \mathcal{C}_0^\infty(\overline{\mathbb{R} \times \mathbb{R}^+})$.*

Let $\Gamma = \{(x,t) : x = \xi(t), t \geq 0\}$ be a smooth curve with $\sigma(t) = \xi'(t)$ and u be a function defined as

$$u(x,t) = \begin{cases} u_l(x,t), & x < \xi(t), \\ u_r(x,t), & x > \xi(t), \end{cases} \tag{2.1.4}$$

where u_l and u_r are smooth functions. The following result characterizes a weak solution of the problem (2.1.1)-(2.1.2):

Theorem 2.1.2. *A function u defined as in (2.1.4) is a weak solution of the problem (2.1.1)-(2.1.2) if and only if the following properties are satisfied:*

- *i) u_l and u_r satisfies (2.1.1) in the classical sense;*
- *ii) $u(x,0) = u_0(x)$ for all $x \in \mathbb{R}$;*
- *iii) $\big(f(u_-(t)) - f(u_+(t))\big) = \sigma(t)\big(u_-(t) - u_+(t)\big)$,*
  where $u_-(t)$ and $u_+(t)$ are the limit of u as (x,t) approaches $(\xi(t),t)$ from the left and right, respectively.

Proof: See [81, 64, 63]. ∎

The relations *(iii)* are called **Rankine-Hugoniot conditions**. They reflect the exact relationship between the limit states on the two sides of the discontinuity curve Γ and the speed of propagation of this curve.

A weak solution to (2.1.1) is not necessarily unique. Hence, we need to find some criterion that enables us to choose the "physically relevant" solution among the weak solutions of (2.1.1). The criterion will be based on the concept of **entropy**.

Definition 2.1.3. *A pair of smooth functions (U,F) is called **entropy pair** if any continuously differentiable solution of (2.1.1) satisfies the additional conservation law*

$$U(u)_t + F(u)_x = 0. \tag{2.1.5}$$

*The functions U and F are called **entropy** and **entropy flux**, respectively.*

Definition 2.1.4. *A weak solution u is an **entropy solution** of (2.1.1) if, for all convex entropy functions and corresponding entropy fluxes, the inequality*

$$U(u)_t + F(u)_x \leqslant 0 \tag{2.1.6}$$

is satisfied in the weak sense.

The inequality (2.1.6) is called the **entropy inequality**. Let us introduce some other entropy conditions for scalar conservations laws:
Entropy condition I: A discontinuity propagating with speed σ given by the relations *(iii)* satisfies the entropy condition if

$$f'(u_+) < \sigma < f'(u_-). \tag{2.1.7}$$

The criterion (2.1.7) is known as **Lax's entropy condition** [64].

Entropy condition II: $u(x,t)$ is an entropy solution if all discontinuities satisfy

$$\frac{f(u) - f(u_+)}{u - u_+} \leqslant \sigma \leqslant \frac{f(u) - f(u_-)}{u - u_-} \tag{2.1.8}$$

for all u between u_- and u_+. The condition (2.1.8) is due to Oleinik [66]. For convex f, this requirement reduces to (2.1.7)

Entropy condition III: $u(x,t)$ is an entropy solution if there is a constant $E > 0$ such that for all $a > 0$, $t > 0$ and $x \in \mathbb{R}$,

$$\frac{u(x+a,t) - u(x,t)}{a} < \frac{E}{t}. \tag{2.1.9}$$

The condition (2.1.9) is also due to Oleinik [77].

For smooth solutions, system (2.1.1) can be written as

$$u_t + A(u)u_x = 0, \tag{2.1.10}$$

where $A(u)$ is the Jacobian matrix of the flux function f and is called **Jacobian matrix** associated to the conservation laws (2.1.1). System (2.1.1) written as in (2.1.10), is said to be in **quasilinear form**.

Definition 2.1.5. *A system of conservation laws is said **hyperbolic** if, for any $u \in \mathbb{R}^p$, the eigenvalues of the Jacobian matrix are real and the Jacobian matrix is diagonalizable, i.e. there is a complete set of p linearly independent eigenvectors. If, in addition, the eigenvalues are all distinct, the system is said **strictly hyperbolic**.*

Definition 2.1.6. *A system of conservation laws is said* ***weakly hyperbolic*** *if the Jacobian matrix has real eigenvalues but is not diagonalizable.*

Let λ_k, $k = 1, ..., p$, the set of eigenvalues of the Jacobian matrix of a system of conservation laws (2.1.1), and r_k, $k = 1, ..., q$, the corresponding eigenvectors. We have the following definitions:

Definition 2.1.7. *The curve $\chi_k(x, t; .)$ defined by*

$$\begin{cases} \dfrac{d\chi_k}{ds}(x, t; s) = \lambda_k(u(\chi(x, t; s), s)), \quad s \in [0, T], \\ \chi(x, t; t) = x, \end{cases} \tag{2.1.11}$$

*is called a k-****characteristic field****.*
A k-characteristic field is said to be ***genuinely nonlinear*** *if*

$$\nabla\lambda_k(u) \cdot r_k(u) \neq 0, \quad \forall u \in \mathbb{R}^p. \tag{2.1.12}$$

A k-characteristic field is said to be ***linearly degenerate*** *if*

$$\nabla\lambda_k(u) \cdot r_k(u) = 0, \quad \forall u \in \mathbb{R}^p. \tag{2.1.13}$$

Here, the differential ∇ is defined as $\nabla = (\partial_{u_1}, \partial_{u_2}, ..., \partial_{u_p})^T$.

Definition 2.1.8. *A smooth function $\mathcal{R}_k : \mathbb{R}^p \to \mathbb{R}$ is called a k-****Riemann invariant*** *if it satisfies*

$$\nabla\mathcal{R}_k(u) \cdot r_k(u) = 0, \quad \forall u \in \mathbb{R}^p. \tag{2.1.14}$$

These are the main mathematical tools for conservation laws that we will use throughout this thesis.

2.2 Dispersed two-phase flows

Under normal conditions, there are four states of matter: gas, liquid, solid and plasma. Two-phase flows occur when two of gas, liquid and solid are mixed together and flow subject to forces. There are several classifications of two-phase flows in the literature [57, 33, 44]. This is due to the variety of the problems involving these phenomena. Ishii [57] proposed a general classification by dividing the two-phase flows in four groups based on the components of the flow: gas-solid flows, gas-liquid flows, solid-liquid flows and the flows of two immiscible liquids.

Ishii [57] also proposed another classification depending on the flow topology, distinguishing three categories: separated two-phase flows, mixed two-phase flows and dispersed two-phase flows. We are interested here in this latter category. A dispersed two-phase flow corresponds to a simple configuration in which one of the

two phases is dispersed in the other continuous phase. In this situation, the continuous phase contains a large number of inclusions (discontinuous interfaces) of small size compared with the characteristic length of the flow domain. For example, the flow of dust in air, or the flow of droplets resulting from the disintegration of a jet of liquid in sprays.

There are two common approaches to model dispersed two-phases flows using differential equations based on the physical phenomenon of interest: Lagrangian and Eulerian. With the Lagrangian approach, the carrier fluid is modelled with Euler or Navier-Stokes equations while particles or groups of particles are tracked individually along their trajectory through the domain. For dispersed two-phase flows, the structure and the position of the interfaces of the two phases are in general very difficult to monitor and in many cases not so relevant for understanding the global behaviour of the system. In such cases, one can use an Eulerian approach based on averaging techniques, either in space, or in time, or both. Eulerian approach describes average characteristics of the flow around any point in space over time.

The general idea for deriving Eulerian models for dispersed two-phase flows is to formulate for each phase the conservation of mass, momentum and, if needed, energy, over a small control volume. The latter should contain a sufficiently large number of particles of the dispersed phase so that the conserved quantities are representative statistical averages. This conservation must be satisfied around any point of the control volume and at any time. This gives two types of local equations: an expression for the instantaneous local variation of each phase and another representing the interactions between the two phases at the interfaces. In general, this introduces more unknowns than equations in the system. So, closure laws are required for removing the indeterminacy of the system of equations.

2.2.1 Eulerian models for dispersed two-phase flows

In this subsection, we perform a brief literature review on Eulerian models for dispersed two-phase flow. This literature review is based on the hierarchy of Eulerian models proposed by Bouchut in [10]. We have chosen this particular hierarchy because it is composed of the most common Eulerian models for dispersed two-phase flow presented in the literature.

We consider a dispersed two-phase flow in a domain Ω, i.e. the flow of a mixture of gas and liquid particles (it could be solid particles). Around each point x of the domain Ω and at each time t, we define, using a control volume (as in (1.1.1)), the volume fractions α for the liquid phase and $1-\alpha$ for the gas phase, satisfying the condition

$$0 \leqslant \alpha \leqslant 1. \tag{2.2.1}$$

The velocity of the liquid and gas phases are denoted by u and v, respectively. Assume that there is no exchange of mass between the two phases. The mass conservation

for each phase (liquid and gas) gives rise to the pair of continuity equations [57]

$$\begin{cases} \partial_t((1-\alpha)\rho_g) + \partial_x((1-\alpha)\rho_g v) = 0, \\ \partial_t(\alpha\rho_l) + \partial_x(\alpha\rho_l u) = 0, \end{cases} \tag{2.2.2}$$

where ρ_g and ρ_l are the gas and liquid density, respectively. The conservation of momentum can be written as [57]

$$\begin{cases} \partial_t((1-\alpha)\rho_g v) + \partial_x((1-\alpha)\rho_g v^2) + (1-\alpha)\partial_x p + \tau_g = D_g, \\ \partial_t(\alpha\rho_l u) + \partial_x(\alpha\rho_l u^2) + \alpha\partial_x p + \tau_l = D_l, \end{cases} \tag{2.2.3}$$

where p is the common pressure; D_g and D_l represent the expressions of the drag force for the gas and liquid phases, respectively; and τ_g and τ_l are called *pressure correction* terms. The exact form of the equations for the conservation of momentum depends on the constitutive relations expressing the interaction between the two phases. The two most common constitutive relations are Stokes' and Newton's laws. In the first case, the drag force is taken linear with respect to the relative velocity $v-u$ of the two phases. For Newton's law, the friction force is quadratic with respect to the relative velocity, an assumption usually valid for larger relative velocities. Here, we will use Stokes' law in which the expression of the drag force is given by (see [57])

$$D_l = -D_g = \mu\alpha(1-\alpha)\rho_l(v-u), \tag{2.2.4}$$

where μ is called the drag coefficient.

System (2.2.2)-(2.2.3) contains more unknowns than equations. Therefore, we need closure relations. The common pressure evolution is assumed to be governed by an equation of state

$$p = p(\rho_g) = \kappa\rho_g^\gamma, \quad \kappa > 0, \quad \gamma > 1. \tag{2.2.5}$$

The pressure correction terms are differential terms which are mathematically relevant because they affect the well-posed nature of the system. Several pressure correction terms are developed in the literature. We consider here those proposed in [61], given by

$$\tau_g = 0, \quad \tau_l = C_p\rho_l(v-u)^2\partial_x\alpha, \tag{2.2.6}$$

where $C_p \geq 0$ is a constant. We could have considered any alternative pressure correction terms satisfying

$$\lim_{v\to u}\tau_g = \lim_{v\to u}\tau_l = 0. \tag{2.2.7}$$

This property is of physical relevance and many expressions for pressure correction used in industry satisfy (2.2.7) (for more details, see [10]).

The density perturbation method introduced in [28] provides a convenient way to analyze the well-posed nature of two-phase flow models. This method consists of

introducing two characteristic densities ρ_g^0 and ρ_l^0 for the gas and liquid phases. These characteristic densities allow to define the new variables

$$\tilde{\rho_g} = \frac{\rho_g}{\rho_g^0} \quad \text{and} \quad \tilde{\rho_l} = \frac{\rho_l}{\rho_l^0}. \tag{2.2.8}$$

To simplify, one assumes that the liquid density ρ_l is constant, and one takes $\rho_l^0 = \rho_l$. System (2.2.2)-(2.2.3) and (2.2.6) reads in term of the new variables (the subscript $\sim$ is omitted) as

$$\begin{cases} \partial_t((1-\alpha)\rho_g) + \partial_x((1-\alpha)\rho_g v) = 0, \\ \partial_t((1-\alpha)\rho_g v) + \partial_x((1-\alpha)\rho_g v^2) + (1-\alpha)\partial_x p = \dfrac{\mu}{\epsilon}\alpha(1-\alpha)(u-v), \\ \partial_t \alpha + \partial_x(\alpha u) = 0, \\ \partial_t(\alpha u) + \partial_x(\alpha u^2) + \epsilon\alpha\partial_x p + C_p(v-u)^2\partial_x\alpha = \mu\alpha(1-\alpha)(v-u), \end{cases} \tag{I}$$

where $\epsilon = \dfrac{\rho_g^0}{\rho_l}$ is a density ratio. System (I) with unknowns ρ_g, v, α and u is referred to as Model I by Bouchut [10].

The source term in Model I contains a relaxation term $\frac{\mu}{\epsilon}\alpha(1-\alpha)(u-v)$. Several authors [22, 71] showed that the long behaviour of hyperbolic systems with relaxation terms is governed by local equilibrium systems. Carrying out the Chapman-Enskog expansion for system (I), i.e. one seeks solution v in the form

$$v = u + \epsilon w, \tag{2.2.9}$$

one obtains (see details of the derivation in Appendix B)

$$\begin{cases} \partial_t((1-\alpha)\rho_g) + \partial_x((1-\alpha)\rho_g u) = \epsilon\partial_x(\dfrac{\rho_g}{\mu\alpha}(1-\alpha)\partial_x p), \\ \partial_t \alpha + \partial_x(\alpha u) = 0, \\ \partial_t(\alpha u) + \partial_x(\alpha u^2 + \epsilon p) = 0. \end{cases} \tag{II}$$

System (II) with unknowns ρ_g, α and u is referred to as Model II by Bouchut [10].

Considering only the two last equation of system (II) and ignoring the terms with the density ratio ϵ, one gets

$$\begin{cases} \partial_t \alpha + \partial_x(\alpha u) = 0, \\ \partial_t(\alpha u) + \partial_x(\alpha u^2) = 0. \end{cases} \tag{III}$$

System (III) with unknowns α and u is referred to as Model III by Bouchut [10]. System (III) is also known as the pressureless gas system [9] or the sticky particles system [36, 18]. It has been studied by several authors, for instance, see [10, 13, 18,

82, 23, 9, 11]. It is well known that Model III may develop delta shock solutions within finite time [10, 82].

Instead of ignoring the terms with the density ratio in Model II, Bouchut [10] proposed the following modification to resolve issues with unbounded α in Model III:

$$\lim_{\epsilon\to 0}\epsilon p=\Pi,\quad \text{with}\quad \Pi=0\quad \text{if}\quad 0\leqslant\alpha\leqslant 1. \tag{2.2.10}$$

Under the hypothesis (2.2.10), the last two equations of system (II) give rise to

$$\begin{cases}\partial_t\alpha+\partial_x(\alpha u)=0,\\ \partial_t(\alpha u)+\partial_x(\alpha u^2+\Pi)=0,\\ \lim\limits_{\epsilon\to 0}\epsilon p=\Pi,\ \text{with}\ \Pi=0\quad \text{if}\quad 0\leqslant\alpha\leqslant 1.\end{cases} \tag{IV}$$

System (IV) with unknowns α and u is referred to as Model IV by Bouchut [10].

2.2.2 Nature and well-posedness of the models

Model I is written in non-conservative form. Its hyperbolicity and well-posedness have been discussed in [28]. It can be shown [28] by using perturbation theory for linear operators that for ϵ small, $v\neq u$ and $C_p>0$, the Jacobian matrix of Model I has four distinct real eigenvalues, and thus it is diagonalizable. In this case, Model I is strictly hyperbolic and is expected to be well-posed. However, if $v=u$ or $C_p=0$, i.e. there is no pressure correction term, then Model I is ill-posed under some regimes for instance for subsonic flows because its Jacobian matrix has complex eigenvalues [28]. For more details on the eigenstructure of Model I, we refer to [28].

Model II is written in conservative form, perturbed with a second order differential term in ρ_g. For smooth solutions with $0<\alpha<1$, it can be written in quasilinear form as

$$\begin{pmatrix}\rho_g\\ \alpha\\ u\end{pmatrix}_t+\begin{pmatrix}u & 0 & \dfrac{\rho_g}{1-\alpha}\\ 0 & u & \alpha\\ \dfrac{\epsilon p'(\rho_g)}{\alpha} & 0 & u\end{pmatrix}\begin{pmatrix}\rho_g\\ \alpha\\ u\end{pmatrix}_x=\begin{pmatrix}\dfrac{\epsilon}{1-\alpha}\partial_x\big(\dfrac{\rho_g}{\mu\alpha}(1-\alpha)\partial_x p\big)\\ 0\\ 0\end{pmatrix}. \tag{2.2.11}$$

Its Jacobian matrix has three distinct real eigenvalues

$$u-\sqrt{\frac{\epsilon p'(\rho_g)\rho_g}{\alpha(1-\alpha)}},\quad u\quad\text{and}\quad u+\sqrt{\frac{\epsilon p'(\rho_g)\rho_g}{\alpha(1-\alpha)}}, \tag{2.2.12}$$

and is diagonalizable. Thus, Model II is a strictly hyperbolic system in conservative form perturbed with a second order term. With this perturbation, the first equation

of the system can be seen as an advection-diffusion equation in ρ_g, with the diffusion term leading to extra dissipation.

Model III is also written in conservative form. For smooth solutions, it can be written in quasilinear form as

$$\begin{pmatrix}\alpha\\ u\end{pmatrix}_t + \begin{pmatrix}u & \alpha\\ 0 & u\end{pmatrix}\begin{pmatrix}\alpha\\ u\end{pmatrix}_x = \begin{pmatrix}0\\ 0\end{pmatrix}. \tag{2.2.13}$$

Its Jacobian matrix has one double real eigenvalue u and is not diagonalizable. Thus, Model III is weakly hyperbolic.

For the properties of Model IV, we refer to [10].

2.3 Numerical methods for conservation laws

A numerical method for a conservation law may converge to a non-suitable solution. A simple and natural requirement one can impose on a numerical scheme to avoid this inconvenience is to be conservative (see [66, 46, 67]). In this section, we recall some important notions for numerical schemes, and present some numerical methods proposed in the literature for conservation laws, particularly for Model III.

We discretize the x-t plane by choosing a mesh width $h = \Delta x$ and a time step $k = \Delta t$, and define the discrete mesh points (x_i, t_n) in the x-t plane by

$$\begin{aligned} x_i &= ih, \quad i = ..., -2, -1, 0, 1, 2, ...\\ t_n &= nk, \quad n = 0, 1, 2, ... \end{aligned} \tag{2.3.1}$$

We denote $x_{i+\frac{1}{2}} = \frac{x_i + x_{i+1}}{2}$. Recall that the general form of a *conservative* finite difference scheme can be written as

$$U_i^{n+1} = U_i^n - \frac{k}{h}\Big(F(U_{i-p}^n, U_{i-p+1}^n, ..., U_{i+q}^n) - F(U_{i-p-1}^n, U_{i-p}^n, ..., U_{i+q-1}^n)\Big) \tag{2.3.2}$$

for some function F of $p + q + 1$ arguments, called the *numerical flux function*.
There are several ways to build a conservative numerical scheme for conservation laws (2.1.1). A common approach is based on the integration of (2.1.1) in space over the control cell $C_i = [x_{i-\frac{1}{2}}, x_{i+\frac{1}{2}}]$ and in time from t_n to t_{n+1}. This gives

$$\int_{C_i} u(x, t_{n+1})\, dx = \int_{C_i} u(x, t_n)\, dx + \int_{t_n}^{t_{n+1}} f(u(x_{i-\frac{1}{2}}, t))\, dt - \int_{t_n}^{t_{n+1}} f(u(x_{i+\frac{1}{2}}, t))\, dt. \tag{2.3.3}$$

Equation (2.3.3) is based on the integral form of the conservation laws (2.1.1). Dividing (2.3.3) by the mesh width h, one gets

$$\begin{aligned}\frac{1}{h}\int_{C_i} u(x,t_{n+1})\,dx =& \frac{1}{h}\int_{C_i} u(x,t_n)\,dx - \frac{1}{h}\int_{t_n}^{t_{n+1}} f(u(x_{i+\frac{1}{2}},t))\,dt \\ &+ \frac{1}{h}\int_{t_n}^{t_{n+1}} f(u(x_{i-\frac{1}{2}},t))\,dt.\end{aligned} \tag{2.3.4}$$

This latter equation can be written as

$$U_i^{n+1} = U_i^n - \frac{k}{h}\Big(F(U_i^n, U_{i+1}^n) - F(U_{i-1}^n, U_i^n)\Big), \tag{2.3.5}$$

where $F(U_i^n, U_{i+1}^n)$ and U_i^n are the average of $f(u(x_{i-\frac{1}{2}},t))$ on $[t_n, t_{n+1}]$ and u on C_i, respectively. The scheme (2.3.5) is in the form (2.3.2), with $p = 0$ and $q = 1$. Hence, it is conservative.

Another important notion for a numerical scheme is *consistency*. Given a partial differential equation $Pu = f$ and a finite difference scheme, $P_{k,h}v = f$, we say that the finite difference scheme is *consistent* with the partial differential equation if for any smooth function ϕ

$$P\phi - P_{k,h}\phi \to 0 \text{ as } \Delta t, \Delta x \to 0. \tag{2.3.6}$$

Consistency is a very important property for a numerical scheme. In fact, the Lax-Wendroff theorem [63] states that if a solution of a conservative and consistent numerical scheme converges when $h \to 0$ and $k \to 0$, then it converges to a weak solution of the conservation law. However, the theorem does not guarantee the convergence which requires some notion of stability. It also does not guarantee the uniqueness which requires some entropy condition.

There are several conservative and consistent numerical methods proposed in the literature for the numerical simulation of conservation laws. Among these methods, one has the Modified Lax-Friedrichs method proposed in [87]. This scheme reads for the conservation laws (2.1.1) as

$$u_i^{n+1} = \frac{1}{4}(u_{i-1}^n + 2u_i^n + u_{i+1}^n) - \frac{k}{h}\big(f(u_{i+1}^n) - f(u_{i-1}^n)\big). \tag{2.3.7}$$

It is shown in [87] that this scheme is consistent with the PDE (2.1.1) and it satisfies the entropy inequality.

Bouchut [12] introduced a numerical scheme for the simulation of the pressuleress gas system, i.e. Model III in Bouchut's hierarchy [10]. The same scheme was investigated by Boudin [13] in the form of an upwind scheme for the simulation of the same

problem. This scheme reads for (III) as

$$\begin{aligned}
\alpha_i^{n+1} =& \alpha_i^n - \frac{k}{h}\big(\alpha_i^n(u_i^n)_+ - \alpha_{i-1}^n(u_{i-1}^n)_+\big) - \frac{k}{h}\big(\alpha_{i+1}^n(u_{i+1}^n)_- - \alpha_i^n(u_i^n)_-\big),\\
q_i^{n+1} =& q_i^n - \frac{k}{h}\big(q_i^n(u_i^n)_+ - q_{i-1}^n(u_{i-1}^n)_+\big) - \frac{k}{h}\big(q_{i+1}^n(u_{i+1}^n)_- - q_i^n(u_i^n)_-\big),\\
u_i^{n+1} =& \frac{q_i^{n+1}}{\alpha_i^{n+1}}, \qquad \text{if} \quad \alpha_i^{n+1} \neq 0,
\end{aligned} \tag{2.3.8}$$

where $q_i^h = \alpha_i^h u_i^h$, a_+=max$(0,a)$ and a_-=min$(0,a)$ for a real a.

Another numerical scheme based on the Transport-Collapse technique is introduced in [9] for system (III). The Transport-Collapse method is introduced by Brenier [18] for the numerical resolution of conservation laws (2.1.1) with conservative and monotone schemes. It writes for system (III) as

$$\begin{aligned}
\alpha_i^{n+1} &= \alpha_i^n - \frac{k}{h}\Big(- \alpha_{i+1}^n(u_{i+1}^n)_- + \alpha_i^n(u_i^n)_+ + \alpha_i^n(u_i^n)_- - \alpha_{i-1}^n(u_{i-1}^n)_+\Big),\\
\alpha_i^{n+1}u_i^{n+1} &= \alpha_i^n u_i^n - \frac{k}{h}\Big(\alpha_{i+1}^n(u_{i+1}^n)_-^2 + \alpha_i^n(u_i^n)_+^2 - \alpha_i^n(u_i^n)_-^2 - \alpha_{i-1}^n(u_{i-1}^n)_+^2\Big),\\
u_i^{n+1} &= u_i^n + \frac{k}{h}\Big(\frac{\alpha_{i+1}^n(u_{i+1}^n)_-}{\alpha_i^{n+1}}(u_{i+1}^n - u_i^n) + \frac{\alpha_{i-1}^n(u_{i-1}^n)_+}{\alpha_i^{n+1}}(u_{i-1}^n - u_i^n)\Big).
\end{aligned} \tag{2.3.9}$$

Note that in (2.3.8) and (2.3.9) the discrete velocity u_i^n is defined for $\alpha_i^n \neq 0$. Boudin [13] proposed to take $u = 0$ if $\alpha = 0$. In practice, one can compute u by using the relation

$$u_i^n = \begin{cases} \dfrac{q_i^n}{\alpha_i^n} & \text{if} \quad |\alpha_i^n| > eps, \\ 0 \quad \text{otherwise}, \end{cases} \tag{2.3.10}$$

where eps is taken very small (10^{-10} to 10^{-15}). Under the discrete Courant-Friedrichs-Levy (CFL) condition $|u_i^n|k \leqslant h$, the schemes (2.3.8) and (2.3.9) preserve the positivity of the volume fraction α, satisfy the maximum principle, the total diminishing property and the entropy inequality [13, 9].

Chapter 3

Eulerian droplet model: Delta shocks and solution of the Riemann problem

In this chapter, we focus on the mathematical analysis of the Eulerian droplet model in its simplest form. We first discuss its hyperbolicity and the mechanisms of blowup in its solution. We then solve the Riemann problems associated to the non-conservative and conservative forms. Finally, numerical tests are performed for comparison with theoretical results.

3.1 Droplet model: mathematical analysis

We consider the Eulerian model for air-particle flow in the one-dimensional case:

$$\begin{cases} \partial_t \alpha + \partial_x(\alpha u) = 0, \\ \partial_t(\alpha u) + \partial_x(\alpha u^2) = K_D \alpha(u_a - u), \end{cases} \tag{E}$$

where $\alpha \geqslant 0$ and u are the volume fraction and velocity of the particles, respectively; K_D is the drag coefficient between the air and the particles; and u_a is the velocity of the air. For smooth solutions, the second equation of (E) is equivalent to

$$\alpha(\partial_t u + u\partial_x u) + u(\partial_t \alpha + \partial_x(\alpha u)) = K_D \alpha(u_a - u). \tag{3.1.1}$$

Using the first equation of (E) in (3.1.1) and simplifying by $\alpha \neq 0$, one obtains

$$\partial_t u + u\partial_x u = K_D(u_a - u). \tag{3.1.2}$$

This latter equation can be written as

$$\partial_t u + \partial_x \left(\frac{u^2}{2}\right) = K_D(u_a - u). \tag{B}$$

Hence, a smooth solution (α, u) with $\alpha \neq 0$ of (E) is also a solution to the problem

$$\begin{cases} \partial_t \alpha + \partial_x(\alpha u) = 0, \\ \partial_t u + \partial_x \left(\dfrac{u^2}{2}\right) = K_D(u_a - u). \end{cases} \tag{E'}$$

One easily shows that any smooth solution (α, u) of (E') is also a solution to (E).

In case $K_D \equiv 0$, equation (B) reduces to the classical inviscid Burgers equation. This latter is studied in most textbooks on conservation laws [66, 46, 81, 64, 67]. It is well known that the solution of the inviscid Burgers equation develops discontinuities in finite time provided that the initial condition has negative slope somewhere in the domain. The characteristic curves associated to the inviscid Burgers equation are straight lines and the solution u is constant along these characteristic curves. The solution of the Riemann problem is either a shock wave separating two constant states or a rarefaction wave.

Still regarding the case $K_D \equiv 0$, system (E) can be seen as the *pressureless gas equations* [9] or as the *sticky particle system* that arises in the modelling of particles hitting and sticking to each other to explain the formation of large scale structures in the universe [36, 18]. The pressureless gas equations have been studied by several authors [10, 9, 23, 11, 82, 70]. In particular, the existence of measure solutions for the Riemann problem, was first presented by Bouchut in [9]. The characteristic curves associated to the pressureless gas equations are straight lines. The solution of the Riemann problem is either a delta shock wave, a two-contact-discontinuity solution with vacuum state or a contact discontinuity [82]. The Rankine-Hugoniot conditions are linear ordinary differential equations (ODEs) [82] instead of algebraic equations as in classical bounded shocks.

In case $K_D > 0$, system (E) is known as the *Eulerian droplet model* [15]. Note that here the gravity and buoyancy forces are neglected since they are three orders of magnitude lower than the drag force for droplets or solid particles solid in air [15]. These forces could be important in some others cases. The Eulerian droplet model corresponds to a dispersed phase subsystem in its simplest form, for instance a multi-phase system for droplets or particles suspended in a carrier fluid. This model is successfully used for the prediction of droplets impingement on airfoils and ice accretion on airplane wings during in-flight icing events [15, 17, 75, 6, 50]. Extension to particle flows in airways was more recently attempted [14, 16].

In the present study, we are interested in the theoretical analysis of equation (B) and systems (E') and (E). In reality, the drag coefficient K_D is a function of the droplet (particle) Reynolds number (see [15]) but for performing the analysis, we assume that K_D and the air velocity u_a are constant. In the following, system (E) will also be referred to as Model E, and equation (B) as the *inviscid Burgers equation with source term*.

3.1.1 Hyperbolicity and shortcomings

The Eulerian droplet model (E) is a first-order system of conservation laws for the volume fraction α and the momentum αu. For smooth solutions, it is equivalent to system (E') which can be written in quasilinear form as

$$\begin{pmatrix}\alpha\\ u\end{pmatrix}_t + \begin{pmatrix}u & \alpha\\ 0 & u\end{pmatrix}\begin{pmatrix}\alpha\\ u\end{pmatrix}_x = \begin{pmatrix}0\\ K_D(u_a-u)\end{pmatrix}. \tag{3.1.3}$$

The Jacobian matrix (see section 2.1 for the definition) has one double eigenvalue $\lambda = u$ and is not diagonalizable. Hence, the Eulerian droplet model is *weakly hyperbolic*. Solutions of weakly hyperbolic systems can encounter many difficulties, particularly in terms of boundedness. To illustrate one recurrent difficulty with boundedness, consider the following linear first-order system of PDEs

$$\begin{cases}\begin{pmatrix}\alpha\\ u\end{pmatrix}_t + \begin{pmatrix}\mu & \beta\\ 0 & \mu\end{pmatrix}\begin{pmatrix}\alpha\\ u\end{pmatrix}_x = 0, \quad (x,t)\in\mathbb{R}\times\mathbb{R}^+,\\ (\alpha,u)(x,0) = (\alpha_0,u_0)(x), \quad \forall x\in\mathbb{R},\end{cases} \tag{3.1.4}$$

where $\mu,\beta\neq 0$, are constant. System (3.1.4) is weakly hyperbolic with one double eigenvalue $\lambda=\mu$. One can first solve the second equation of (3.1.4) by the method of characteristics to find

$$u(x,t) = u_0(x-\mu t) \tag{3.1.5}$$

and then, considering $-\beta\partial_x u$ as a source term, we calculate the solution of the first equation

$$\alpha(x,t) = \alpha_0(x-\mu t) - \beta t u_0'(x-\mu t). \tag{3.1.6}$$

We immediately note that α is not defined in the classical sense at points where the initial condition u_0 is not differentiable. For instance, if u_0 is a Heaviside function then α would contain a Dirac mass. These kind of shortcomings are often present in the solution of weakly hyperbolic problems, such as the pressureless gas system [82].

3.1.2 Loss of regularity for a smooth initial solution

Another difficulty with the solution of hyperbolic systems is the loss of regularity for smooth initial solution. Here, we analyze the loss of regularity for a smooth solution (α,u) of system (E), satisfying the initial condition

$$(\alpha,u)(x,0) = (\alpha_0,u_0)(x), \quad \alpha_0,u_0\in\mathcal{C}^1(\mathbb{R}). \tag{3.1.7}$$

Characteristic curves $\chi=\chi(x,t;s)$ associated to system (E) are the solutions of the ODE

$$\begin{cases}\dfrac{d\chi}{ds}(x,t;s) = u\big(\chi(x,t;s),s\big), \quad s\geqslant 0,\\ \chi(x,t;t) = x.\end{cases} \tag{3.1.8}$$

Recall that for a smooth solution (α, u) with $\alpha \neq 0$, the second equation of (E) is equivalent to (3.1.2), which can be written along the characteristics $\chi = \chi(x,t;s)$ as

$$\frac{Du}{dt} + K_D(u - u_a) = 0, \tag{3.1.9}$$

where $\frac{D}{dt} = \frac{\partial}{\partial t} + u\frac{\partial}{\partial x}$ is the material derivative. An integration with respect to t of (3.1.9) from 0 to s gives

$$u\big(\chi(x,t;s),s\big) = u_a + \big(u_0(\chi(x,t;0)) - u_a\big)e^{-K_D s}, \tag{3.1.10}$$

in particular for $s = t$, we get

$$u\big(\chi(x,t;t),t\big) = u(x,t) = u_a + \big(u_0(\chi(x,t;0)) - u_a\big)e^{-K_D s}. \tag{3.1.11}$$

By substituting (3.1.10) in (3.1.8) and then integrating from 0 to s, we get

$$\chi(x,t;s) = \chi(x,t;0) + u_a s + \frac{(u_0(\chi(x,t;0)) - u_a)(1 - e^{-K_D s})}{K_D}. \tag{3.1.12}$$

We denote $\chi(x,t;0)$ by x_0 (foot of the characteristic $\chi(x,t;s)$). Equations (3.1.11) and (3.1.12) can be written now as

$$u\big(\chi(x,t;t),t\big) = u(x,t) = u_a + \big(u_0(x_0)) - u_a\big)e^{-K_D t} \tag{3.1.13}$$

and

$$\chi(x,t;s) = x_0 + u_a s + \frac{u_0(x_0) - u_a}{K_D}(1 - e^{-K_D s}), \tag{3.1.14}$$

respectively. The first equation of (E) reads along the characteristics $\chi = \chi(x,t;s)$ as

$$\frac{D\alpha}{dt} = -\alpha\partial_x u. \tag{3.1.15}$$

Using (3.1.14) and the initial condition in (3.1.8), we get

$$x = \chi(x,t;t) = x_0 + u_a t + \frac{u_0(x_0) - u_a}{K_D}(1 - e^{-K_D t}). \tag{3.1.16}$$

Hence, x can be viewed as a function of the foot x_0 of the characteristic and time t. Thus, $\partial_x u$ can be written as

$$\partial_x u = \frac{\partial u}{\partial x_0}\frac{\partial x_0}{\partial x} + \frac{\partial u}{\partial t}\frac{\partial t}{\partial x}. \tag{3.1.17}$$

Now, consider the map h from $\mathbb{R} \times \mathbb{R}_0^+$ to $\mathbb{R} \times \mathbb{R}_0^+$, defined by

$$h : (\chi(x,t;0),t) = (x_0,t) \mapsto (\chi(x,t;t),t) = (x,t).$$

This function is bijective as long as the characteristics do not intersect. Its Jacobian is given by

$$J_h(x_0,t)=\begin{pmatrix}\frac{\partial x}{\partial x_0} & \frac{\partial x}{\partial t}\\ \frac{\partial t}{\partial x_0} & \frac{\partial t}{\partial t}\end{pmatrix}=\begin{pmatrix}\frac{\partial x}{\partial x_0} & \frac{\partial x}{\partial t}\\ 0 & 1\end{pmatrix}. \tag{3.1.18}$$

The inverse of the Jacobian J_h is given by

$$\big(J_h(x_0,t)\big)^{-1}=\frac{1}{\frac{\partial x}{\partial x_0}}\begin{pmatrix}1 & -\frac{\partial x}{\partial t}\\ 0 & \frac{\partial x}{\partial x_0}\end{pmatrix}. \tag{3.1.19}$$

The Jacobian of the inverse of h is given by

$$J_{h^{-1}}(x,t)=\begin{pmatrix}\frac{\partial x_0}{\partial x} & \frac{\partial x_0}{\partial t}\\ \frac{\partial t}{\partial x} & \frac{\partial t}{\partial t}\end{pmatrix}=\begin{pmatrix}\frac{\partial x_0}{\partial x} & \frac{\partial x_0}{\partial t}\\ \frac{\partial t}{\partial x} & 1\end{pmatrix} \tag{3.1.20}$$

As $\big(J_h(x_0,t)\big)^{-1}= J_{h^{-1}}(x,t)$, we obtain by identification that

$$\frac{\partial t}{\partial x}=0 \quad \text{and} \quad \frac{\partial x_0}{\partial x}=\frac{1}{\frac{\partial x}{\partial x_0}}.$$

Hence, (3.1.17) reduces to

$$\partial_x u=\frac{\partial u}{\partial x_0}\frac{1}{\frac{\partial x}{\partial x_0}}. \tag{3.1.21}$$

From (3.1.13) and (3.1.16), we get

$$\frac{\partial u}{\partial x_0}=u_0'(x_0)e^{-K_D t} \quad \text{and} \quad \frac{\partial x}{\partial x_0}=\frac{K_D+u_0'(x_0)(1-e^{-K_D t})}{K_D}, \tag{3.1.22}$$

respectively. Hence, (3.1.21) gives

$$\partial_x u=\frac{K_D e^{-K_D t}u_0'(x_0)}{K_D+(1-e^{-K_D t})u_0'(x_0)}. \tag{3.1.23}$$

Substituting (3.1.23) in (3.1.15), we obtain

$$\frac{D\alpha}{dt}=-\frac{K_D\alpha e^{-K_D t}u_0'(x_0)}{K_D+(1-e^{-K_D t})u_0'(x_0)}. \tag{3.1.24}$$

For $\alpha\neq 0$, one can divide by α and integrate (3.1.24) on both sides in time from 0 to t to obtain

$$\log\big(\alpha(x,t)\big)=-\log\big(K_D+(1-e^{-K_D t})u_0'(x_0)\big)+\log(K_D)+\log\big(\alpha_0(x_0)\big).$$

This last equality leads to

$$\alpha(x,t)=\frac{K_D\alpha_0(x_0)}{K_D+(1-e^{-K_D t})u_0'(x_0)}. \tag{3.1.25}$$

We have the following result:

Proposition 3.1.1. ***(Loss of regularity)***
Let (α, u) be a smooth solution of (E)*, satisfying the initial conditions* (3.1.7)*. Then α and $\partial_x u$ blow up if and only if there exists x_0 in the domain such that*

$$u_0'(x_0) < -K_D. \tag{3.1.26}$$

Moreover, the blowup occurs at

$$t = \inf_{u_0'(x_0)<-K_D} \Big\{ -\frac{\log(1+\frac{K_D}{u_0'(x_0)})}{K_D} \Big\}. \tag{3.1.27}$$

Proof: As $\alpha_0 \in \mathcal{C}^1(\mathbb{R})$ then α and $\partial_x u$ blow up if and only if

$$K_D + (1 - e^{-K_D t})u_0'(x_0) = 0, \quad \text{for some } x_0 \in \mathbb{R}. \tag{3.1.28}$$

As $K_D > 0$ and $1 - e^{-K_D t} \geq 0$ for any $t \geq 0$, then (3.1.28) holds if and only if

$$u_0'(x_0) < 0 \quad \text{and} \quad 1 - e^{-K_D t} = \frac{-K_D}{u_0'(x_0)} \Longleftrightarrow t = -\frac{\log(1+\frac{K_D}{u_0'(x_0)})}{K_D}. \tag{3.1.29}$$

Since $1 - e^{-K_D t} < 1$ for any $t \geq 0$, we obtain $u_0'(x_0) < -K_D$. The smallest time satisfying (3.1.29) is given by (3.1.27). ∎

Remark 3.1.2. ***i)*** *Proposition 3.1.1 stipulates that the volume fraction α and the gradient of the velocity $\partial_x u$ blow up simultaneously if and only if* (3.1.26) *holds. Inequality* (3.1.26) *is also a necessary and sufficient condition for the characteristics to intersect. In fact, two characteristics $\chi_1(x,t;s)$ and $\chi_2(x,t;s)$ with distinct foots x_1 and x_2, respectively, intersect if and only if there is $s^* > 0$ such that $\chi_1(x,t;s^*) = \chi_2(x,t;s^*)$. Using* (3.1.14)*, the equality $\chi_1(x,t;s^*) = \chi_2(x,t;s^*)$ gives*

$$x_2 - x_1 + \frac{(1 - e^{-K_D s})(u_0(x_2) - u_0(x_1))}{K_D} = 0$$

which implies (since $x_1 \neq x_2$ and $1 - e^{-K_D s} \neq 0$ for all $s > 0$) that

$$\frac{u_0(x_2) - u_0(x_1)}{x_2 - x_1} = \frac{-K_D}{1 - e^{-K_D s}}.$$

Using the fact that $0 < 1 - e^{-K_D s} < 1$ for all $s > 0$ and $K_D > 0$, this last equation reduces to

$$\frac{u_0(x_2) - u_0(x_1)}{x_2 - x_1} < -K_D. \tag{3.1.30}$$

As $u_0 \in \mathcal{C}^1(\mathbb{R})$, the mean value theorem ensures the existence of a point x_0 between x_1 and x_2 such that

$$u_0'(x_0) = \frac{u_0(x_2) - u_0(x_1)}{x_2 - x_1} < -K_D. \tag{3.1.31}$$

ii) *The condition* (3.1.26) *for loss of regularity also applies to system* (E') *and equation* (B).

The blowup of $\partial_x u$ leads to a discontinuity in the velocity. The blowup of α leads to an unbounded volume fraction. Hence, the solution of (E) is not bounded in regions where the characteristic curves meet.

3.2 Riemann problem for the inviscid Burgers equation with source term

Recall that the inviscid Burgers equation with source term reads as

$$\partial_t u + \partial_x \left(\frac{1}{2}u^2\right) = K_D(u_a - u), \tag{B}$$

with an initial condition

$$u(x,0) = u_0(x), \tag{3.2.1}$$

where u_0 is a piecewise smooth function. Equation (B) can be written along characteristics curves (3.1.8) as in (3.1.9). The latter has solution given by (3.1.13). We showed in subsection 3.1.2 that a solution of (B) loses its regularity if and only if (3.1.26) is satisfied. To better understand the propagation of discontinuities in the solution, we look for the solution of the Riemann problem, i.e. the solution of problem (B) and (3.2.1), where u_0 satisfies

$$u_0(x) = \begin{cases} u_-, & x < 0, \\ u_+, & x > 0, \end{cases} \tag{3.2.2}$$

with constants $u_-, u_+ \in \mathbb{R}$. Substituting (3.2.2) in (3.1.14), one obtains

$$\chi(x,t;s) = \begin{cases} x_0 + u_a s + \dfrac{(u_a - u_-)(e^{-K_D s} - 1)}{K_D}, & x_0 < 0, \\ x_0 + u_a s + \dfrac{(u_a - u_+)(e^{-K_D s} - 1)}{K_D}, & x_0 > 0. \end{cases} \tag{3.2.3}$$

Hence, the characteristic curves for (B) are no longer straight lines, but only asymptotic to straight lines, and the solution u given by (3.1.13) is no longer constant along these characteristic curves, as opposed to the classical Burgers equation.

3.2.1 Shock waves

We first assume that $u_- > u_+$. In this case, the characteristics intersect since (3.1.26) is satisfied. Some characteristic curves are represented in Figure 3.1 for three different values of the air velocity u_a. The solution is discontinuous. By the method

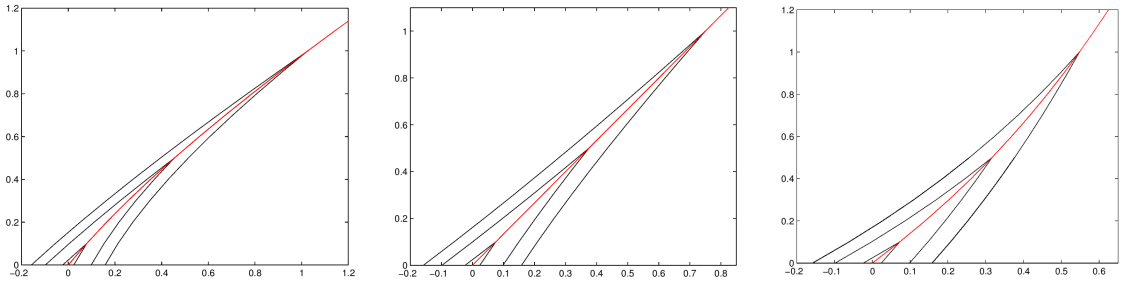

Figure 3.1: Characteristic curves on the x-t plane for $u_- = 1.0$, $u_+ = 0.5$ and $K_D = 1.0$. Left: $u_a = 1.5$, middle: $u_a = 0.75$ and right: $u_a = 0.2$.

of characteristics, the solution is a shock wave, i.e. a smooth curve $\Gamma = \{(x,t) : x = \xi(t), t \geq 0\}$ in the x-t plane moving at some speed $\sigma(t) = \xi'(t)$, separating left and right states denoted by $u_l(x,t)$ and $u_r(x,t)$, respectively. As we are considering solutions that may be discontinuous, these should be taken in the weak sense. We have the following definition.

Definition 3.2.1. *We say that u is a **weak solution** of* (B) *and* (3.2.1) *if*

$$\int_0^\infty \int_{-\infty}^\infty \Big(u\psi_t + \frac{u^2}{2}\psi_x + K_D(u_a - u)\psi\Big)dxdt = -\int_{-\infty}^\infty u_0(x)\psi(x,0)\,dx, \qquad (3.2.4)$$

for all test functions $\psi \in \mathcal{C}_0^\infty(\overline{\mathbb{R}\times\mathbb{R}^+})$.

Notice that a weak solution u need not be differentiable or even continuous to satisfy (3.2.4). Let u be a function regular on both sides of the curve Γ, while being discontinuous across Γ. We have the following result.

Theorem 3.2.2. *The function u is a weak solution of* (B) *and* (3.2.1) *if and only if the following properties hold:*

i) u satisfies (B) *in the classical sense on both sides of the curve $x = \xi(t)$;*

ii) $u(x,0) = u_0(x)$ for all $x \in \mathbb{R}$;

iii) the following Rankine-Hugoniot condition is satisfied:

$$\big(u_r(t) - u_l(t)\big)\sigma(t) = \frac{1}{2}\big(u_r(t)^2 - u_l(t)^2\big), \qquad (3.2.5)$$

where $u_l(t)$ and $u_r(t)$ are the limit of the solution u when (x,t) approaches $(\xi(t),t)$ from the left and the right, respectively.

Proof: Let $\psi \in \mathcal{C}_0^\infty(\overline{\mathbb{R}\times\mathbb{R}^+})$. We have

$$\begin{aligned}
&\int_0^\infty\int_{-\infty}^\infty \Big(u\psi_t+\frac{1}{2}u^2\psi_x+K_D(u-u_a)\psi\Big)\,dxdt=\\
&\quad\int_0^\infty\int_{-\infty}^{\xi(t)} \Big((u\psi)_t+\frac{1}{2}(u^2\psi)_x\Big)\,dxdt+\int_0^\infty\int_{\xi(t)}^\infty \Big((u\psi)_t+\frac{1}{2}(u^2\psi)_x\Big)\,dxdt\\
&\qquad-\int_0^\infty\int_{-\infty}^{\xi(t)} \Big(u_t+\frac{1}{2}(u^2)_x)-K_D(u-u_a)\Big)\psi\,dxdt\\
&\qquad-\int_0^\infty\int_{\xi(t)}^{\infty} (u_t+\frac{1}{2}(u^2)_x)-K_D(u-u_a)\Big)\psi\,dxdt.
\end{aligned}$$

Applying Green's formula in the first two integrals on the r.h.s, we obtain

$$\begin{aligned}
&\int_0^\infty\int_{-\infty}^\infty \Big(u\psi_t+\frac{1}{2}u^2\psi_x+K_D(u-u_a)\psi\Big)\,dxdt=\\
&\qquad\int_{x=\xi(t)}\psi(\xi(t),t)\Big(-u_l(t)\,dx+\frac{1}{2}u_l(t)^2\,dt\Big)-\int_{-\infty}^\infty u(0,x)\psi(x,0)\,dx\\
&\qquad-\int_{x=\xi(t)}\psi(\xi(t),t)\Big(-u_r(t)\,dx+\frac{1}{2}u_r(t)^2\,dt\Big)\\
&\qquad-\int_0^\infty\int_{-\infty}^{\xi(t)} \Big(u_t+\frac{1}{2}(u^2)_x)-K_D(u-u_a)\Big)\psi\,dxdt\\
&\qquad-\int_0^\infty\int_{\xi(t)}^{\infty} (u_t+\frac{1}{2}(u^2)_x)-K_D(u-u_a)\Big)\psi\,dxdt.
\end{aligned}$$

Using the fact that $dx=\xi'(t)dt=\sigma(t)dt$ on the curve $x=\xi(t)$ and reorganizing this last equation, we end up with

$$\begin{aligned}
&\int_0^\infty\int_{-\infty}^\infty \Big(u\psi_t+\frac{1}{2}u^2\psi_x+K_D(u-u_a)\psi\Big)\,dxdt=\\
&\qquad\int_0^\infty \Big(\frac{1}{2}\big(u_l(t)^2-u_r(t)^2\big)+\big(u_r(t)-u_l(t)\big)\sigma(t)\Big)\psi(\xi(t),t)\,dt\\
&\qquad-\int_0^\infty\int_{-\infty}^{\xi(t)} \Big(u_t+\frac{1}{2}(u^2)_x)-K_D(u-u_a)\Big)\psi\,dxdt\\
&\qquad-\int_0^\infty\int_{\xi(t)}^{\infty} (u_t+\frac{1}{2}(u^2)_x)-K_D(u-u_a)\Big)\psi\,dxdt\\
&\qquad-\int_{-\infty}^\infty u(0,x)\psi(x,0)\,dx. \qquad (3.2.6)
\end{aligned}$$

1) If u is a weak solution of (B) and (3.2.1) then for all $\psi \in \mathcal{C}_0^\infty(\overline{\mathbb{R}\times\mathbb{R}^+})$ we get,

by substituting (3.2.6) in (3.2.4), that

$$
\begin{aligned}
-\int_{-\infty}^{\infty} u_0(x)\psi(x,0)\,dx = \int_{x=\xi(t)} \Big(\frac{1}{2}\big(u_l(t)^2 - u_r(t)^2\big) + u_r(t) - u_l(t))\sigma(t)\Big)\psi(\xi(t),t)\,dt \\
- \int_0^{\infty}\int_{-\infty}^{\xi(t)} \Big(u_t + \frac{1}{2}(u^2)_x) - K_D(u-u_a)\Big)\psi\,dxdt \\
- \int_0^{\infty}\int_{\xi(t)}^{\infty} (u_t + \frac{1}{2}(u^2)_x) - K_D(u-u_a)\Big)\psi\,dxdt \\
- \int_{-\infty}^{\infty} u(0,x)\psi(x,0)\,dx. \qquad (3.2.7)
\end{aligned}
$$

<u>*Case 1*</u>: if $\psi(x,0) = \psi(\xi(t),t) = 0$, then (3.2.7) reduces to

$$
\begin{aligned}
0 = &\int_0^{\infty}\int_{-\infty}^{\xi(t)} \big(u_t + \frac{1}{2}(u^2)_x - K_D(u-u_a)\big)\psi\,dxdt \\
&+ \int_0^{\infty}\int_{-\infty}^{\xi(t)} \big(u_t + \frac{1}{2}(u^2)_x - K_D(u-u_a)\big)\psi\,dxdt,
\end{aligned}
$$

which implies property (i) because ψ is arbitrary.
<u>*Case 2*</u>: if $\psi(\xi(t),t) = 0$ for all $t \geq 0$ then by using (i), (3.2.7) reduces to

$$
-\int_{-\infty}^{\infty} u_0(x)\psi(x,0)\,dx = -\int_{-\infty}^{\infty} u(x,0)\psi(x,0)\,dx
$$

which implies that $u_0(x) = u(x,0)$ for all $x \in \mathbb{R}$. Hence, (ii) holds.
<u>*Case 3*</u>: if $\psi(x,0) = 0$ for all $x \in \mathbb{R}$ then by using (i), (3.2.7) reduces to

$$
0 = \int_0^{\infty} \Big(\big(u_r(t) - u_l(t)\big)\sigma(t) - \frac{1}{2}\big(u_r^2(t) - u_l^2(t)\big)\Big)\psi(\xi(t),t)\,dt
$$

which implies that (iii) is satisfied.

2) Conversely, if (i), (ii) and (iii) are satisfied then (3.2.6) gives rise to

$$
\int_0^{\infty}\int_{-\infty}^{\infty} \Big(u\psi_t + \frac{1}{2}u^2\psi_x + K_D(u-u_a)\psi\Big)\,dxdt = -\int_{-\infty}^{\infty} u_0(x)\psi(x,0)\,dx,
$$

for any $\psi \in \mathcal{C}_0^{\infty}(\overline{\mathbb{R}\times\mathbb{R}^+})$, i.e. the function u is a week solution of (B) and (3.2.1). This completes the proof of the theorem. ∎

We now return to the Riemann problem. A solution of the Riemann problem satisfies (B) in the classical sense on both sides of Γ. Hence, the left and right states are determined from (3.1.13), that is

$$
u_l(x,t) = u_a + (u_- - u_a)e^{-K_D t}, \qquad (3.2.8)
$$

$$u_r(x,t) = u_a + (u_+ - u_a)e^{-K_D t}, \tag{3.2.9}$$

respectively. These left and right states depend only on time. Therefore, the limit states are given by $u_l(t) = u_l(x,t)$ and $u_r(t) = u_r(x,t)$. The propagation speed σ calculated from the Rankine-Hugoniot conditions (3.2.5) is given by

$$\sigma(t) = \frac{1}{2}\Big(u_l(t) + u_r(t)\Big) = u_a + \frac{1}{2}\Big(u_- + u_+ - 2u_a\Big)e^{-K_D t}, \tag{3.2.10}$$

and satisfies

$$u_l(t) - \sigma(t) = \sigma(t) - u_r(t) = \frac{u_- - u_+}{2}e^{-K_D t} > 0, \quad \forall t \geq 0, \tag{3.2.11}$$

which leads to the inequality

$$u_l(t) > \sigma(t) > u_r(t). \tag{3.2.12}$$

Remark 3.2.3. ***i)*** *Inequality* (3.2.12) *is nothing else but the* ***Lax entropy condition*** *for the inviscid Burgers equation.*
ii) *We have that*

$$\lim_{t\to\infty}\big(u_l(t) - \sigma(t)\big) = \lim_{t\to\infty}\big(\sigma(t) - u_r(t)\big) = 0. \tag{3.2.13}$$

This means that the Lax entropy condition (3.2.12) *for the inviscid Burgers equation with source term degenerates as time goes to infinity. This degeneracy is not observed with the classical inviscid Burgers equation.*

The shock curve for the inviscid Burgers equation with source term (B) is then given by

$$\xi(t) = \int_0^t \sigma(s)ds = u_a t + \frac{\big(2u_a - (u_- + u_+)\big)\big(e^{-K_D t} - 1\big)}{2K_D}. \tag{3.2.14}$$

We reach the following result.

Corollary 3.2.4. *If $u_- > u_+$ the entropy solution of the Riemann problem for the inviscid Burgers equation with source term* (B) *and* (3.2.2) *is given by*

$$u(x,t) = \begin{cases} u_l(x,t), & x < \xi(t), \\ \sigma(t), & x = \xi(t), \\ u_r(x,t), & x > \xi(t), \end{cases} \tag{3.2.15}$$

where u_l, u_r are given by (3.2.8) *and* (3.2.9)*, respectively, σ is given by* (3.2.10) *and ξ is given by* (3.2.14)*.*

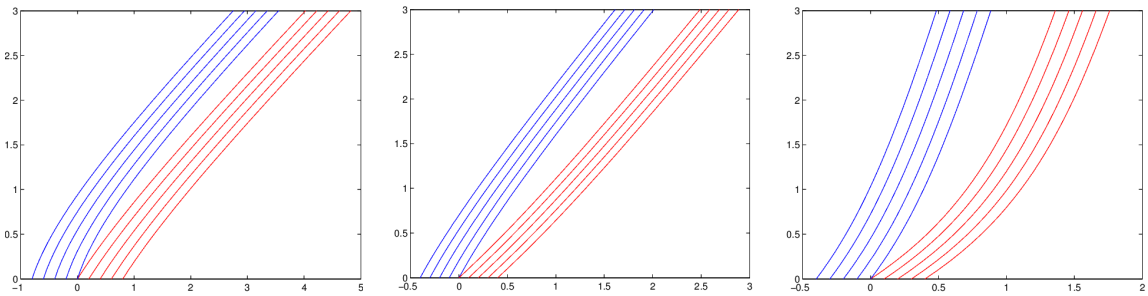

Figure 3.2: Characteristic curves on the x-t plane for $u_- = 0.5$, $u_+ = 1.0$ and $K_D = 1.0$. Left: $u_a = 1.5$, middle: $u_a = 0.75$ and right: $u_a = 0.2$.

3.2.2 Rarefaction waves

We now assume that $u_- < u_+$. We draw some characteristic curves. They are represented in Figure 3.2. In this case, the characteristics do not intersect but do not cover the whole x-t plane. The uncovered region $\mathcal{S}$ is delimited by the curves

$$X_1(t) = \int_0^t u_l(s)ds = u_a t + \frac{(u_a - u_-)(e^{-K_D t} - 1)}{K_D} \tag{3.2.16}$$

and

$$X_2(t) = \int_0^t u_r(s)ds = u_a t + \frac{(u_a - u_+)(e^{-K_D t} - 1)}{K_D}. \tag{3.2.17}$$

The characteristics fill the whole domain except the region $\mathcal{S}$. By the method of characteristics, the solution of the Riemann problem outside $\mathcal{S}$ is given by (3.2.8) if $x < X_1(t)$ and by (3.2.9) if $x > X_2(t)$. To find the solution inside $\mathcal{S}$, we have to cover this region by a family of characteristics starting at the origin, i.e. to solve (3.1.8) with the initial condition $\chi(x,t;0) = 0$. Figure 3.3 shows the region $\mathcal{S}$ (delimited by $x = X_1(t)$ (in blue) and $x = X_2(t)$ (in red)) filled with characteristics (in black) starting all at the origin. From (3.1.10), we obtain the following value of u at the foot x_0 of the characteristics

$$u_0(x_0) = u_0(\chi(x,t;0)) = u_a + \big(u(\chi(x,t;s),s) - u_a\big)e^{K_D s}. \tag{3.2.18}$$

Substituting (3.2.18) in (3.1.14) (recall that all the characteristics belonging to $\mathcal{S}$ start from the origin $x_0 = 0$), one obtains

$$\begin{aligned} \chi(x,t;s) &= u_a s + \frac{u_a + \big(u(\chi(x,t;s),s) - u_a\big)e^{K_D s} - u_a}{K_D}\big(1 - e^{-K_D s}\big) \\ &= u_a s + \frac{\big(u(\chi(x,t;s),s) - u_a\big)}{K_D}\big(e^{K_D s} - 1\big). \end{aligned} \tag{3.2.19}$$

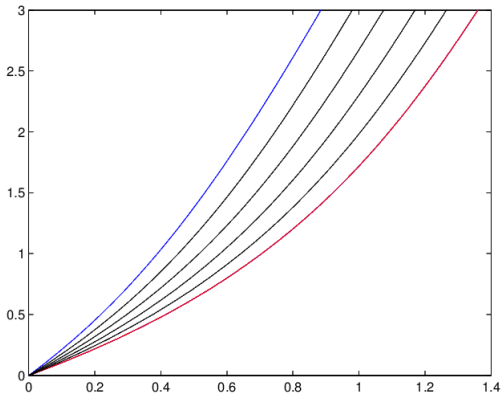

Figure 3.3: Region $\mathcal{S}$ filled with characteristic curves stating at the origin. $u_- = 0.5$, $u_+ = 1.0$, $K_D = 1.0$ and $u_a = 0.2$.

Hence,

$$u(\chi(x,t;s),s) = u_a + \frac{K_D\big(\chi(x,t;s) - u_a s\big)}{e^{K_D s} - 1}. \tag{3.2.20}$$

At $s = t$, we obtain

$$u(x,t) = u_a + \frac{K_D\big(x - u_a t\big)}{e^{K_D t} - 1}. \tag{3.2.21}$$

We define the smooth function $\overline{u}$ on $\mathbb{R} \times \mathbb{R}^+$ by

$$\overline{u}(x,t) = u_a + \frac{K_D(x - u_a t)}{e^{K_D t} - 1}. \tag{3.2.22}$$

The following result holds.

Theorem 3.2.5. *If $u_- < u_+$ then the solution of Riemann problem for the inviscid Burgers equation with source term* (B) *is given by*

$$u(x,t) = \begin{cases} u_l(x,t), & x < X_1(t), \\ \overline{u}(x,t), & X_1(t) \le x \le X_2(t), \\ u_r(x,t), & x > X_2(t), \end{cases} \tag{3.2.23}$$

where u_l, u_r are given by (3.2.8) *and* (3.2.9)*, respectively, X_1, X_2 are given by* (3.2.16) *and* (3.2.17)*, respectively, and $\overline{u}$ is given by* (3.2.22)*.*

Proof: The functions u_l, u_r are smooth and satisfy (B). The function $\overline{u}(x,t)$ is continuous at points $X_1(t)$ and $X_2(t)$ for $t > 0$. In fact, by replacing $X_1(t)$ (resp. $X_2(t)$) in (3.2.22), one gets u_l (resp. $u_r(t)$). Furthermore $\overline{u}(x,t)$ is differentiable for

$t > 0$ and we have

$$\begin{aligned}
\partial_t \overline{u} + \partial_x(\frac{1}{2}\overline{u}^2) = & \\
& \frac{-K_D u_a\big(e^{K_D t}-1\big) - {K_D}^2\big(x-u_a t\big)e^{K_D t}}{\big(e^{K_D t}-1\big)^2} + \frac{K_D}{e^{K_D t}-1}\Big(u_a + \frac{K_D\big(x-u_a t\big)}{e^{K_D t}-1}\Big) \\
= & \frac{-K_D u_a\big(e^{K_D t}-1\big) - {K_D}^2\big(x-u_a t\big)e^{K_D t}}{\big(e^{K_D t}-1\big)^2} + \frac{K_D u_a\big(e^{K_D t}-1\big) + {K_D}^2\big(x-u_a t\big)}{\big(e^{K_D t}-1\big)^2} \\
= & \frac{-{K_D}^2\big(x-u_a t\big)\big(e^{K_D t}-1\big)}{\big(e^{K_D t}-1\big)^2} \\
= & K_D\big(u_a - \big(u_a + \frac{K_D(x-u_a t)}{e^{K_D t}-1}\big)\big) \\
= & K_D\big(u_a - \overline{u}\big).
\end{aligned}$$

Hence, the function u defined in (3.2.23) satisfies (B) and (3.2.2). ∎

In summary, the inviscid Burgers equation with source term (B) develops discontinuities if and only if the slope of the initial condition u_0 is sufficiently negative with respect to the drag coefficient K_D somewhere in the domain. This is a generalization of the condition of loss of regularity for the classical inviscid Burgers equation. The characteristic curves associated to the inviscid Burgers equation with source term are no longer straight lines but are curves that tend asymptotically to straight lines, as time goes to infinity. The solution of the Riemann problem is still a shock or rarefaction wave, depending on the sign of $u_+ - u_-$. The Lax entropy condition degenerates as time goes to infinity. The left and right states are no longer constant. Instead, the states u_l and u_r depend on time (only) while asymptotically approaching u_a as time goes to infinity on both sides of the shock. These are the main differences with the inviscid Burgers equation where the strength of the shock does not weaken and the Lax entropy condition remains satisfied as time goes to infinity. Thus, the zeroth order source term acts as a relaxation force preventing shocks from occurring if the slope of u is not sufficiently negative, and weakening shocks as time grows.

3.3 Riemann problem for system E'

In this section, we are interested in system (E') which can be written as

$$\begin{cases} \partial_t \alpha + \partial_x(\alpha u) = 0, \\ \partial_t u + \partial_x\left(\dfrac{u^2}{2}\right) = K_D(u_a - u), \end{cases} \tag{E'}$$

satisfying the following initial condition

$$\big(\alpha, u\big)(x,0) = \big(\alpha_0, u_0\big)(x), \tag{3.3.1}$$

where α_0 and u_0 are piecewise smooth functions. We are interested in system (E') because any smooth solution of it is also a solution to the Eulerian droplet model (E). This implication is an equivalence when one is far away vacuum states, i.e. for $\alpha \neq 0$. Note that the second equation of (E') is exactly the inviscid Burgers equation with source term (B). This is one of the reasons why we studied the latter equation in the previous section. Recall that a solution of (E') develops discontinuities if and only if (3.1.26) is satisfied. To understand the propagation of discontinuities in (E'), we look for the solution of the Riemann problem, i.e. the solution of problem (E') and (3.3.1), where (α_0, u_0) satisfies

$$\big(\alpha_0, u_0\big)(x) = \begin{cases} (\alpha_-, u_-), & x < 0, \\ (\alpha_+, u_+), & x > 0, \end{cases} \tag{3.3.2}$$

with constants $\alpha_-, \alpha_+ \in \mathbb{R}^+$ and $u_-, u_+ \in \mathbb{R}$.

Recall that the solution u of the second equation of (E') is given along the characteristics (3.1.8) by

$$u(x,t) = u_a + \big(u_0(x_0) - u_a\big)e^{-K_D t}, \tag{3.3.3}$$

where x_0 (foot of the characteristic $\chi(x,t;s)$) can be determined from (3.1.16) and is given by the implicit equation

$$x_0 = x - u_a t + \frac{\big(u_0(x_0) - u_a\big)\big(e^{-K_D t} - 1\big)}{K_D}. \tag{3.3.4}$$

3.3.1 Contact discontinuity

Assume that $u_- = u_+ = u_*$. Then $u_0(x) = u_*$ for all $x \in \mathbb{R}$, and (3.3.4) reduces to

$$x_0 = x - u_a t + \frac{(u_* - u_a)(e^{-K_D t} - 1)}{K_D}. \tag{3.3.5}$$

Using this last equality in (3.3.3), we get the solution u given by

$$u(x,t) = u_a + \big(u_* - u_a\big)e^{-K_D t}. \tag{3.3.6}$$

The first equation of (E') then becomes

$$\partial_t \alpha + \partial_x(\alpha u) = \partial_t \alpha + u\partial_x \alpha = 0, \tag{3.3.7}$$

which can be written along the characteristics as $\frac{D\alpha}{dt} = 0$, has the solution

$$\alpha(x,t) = \alpha_0(x_0). \tag{3.3.8}$$

Again, using (3.3.2) and (3.3.5), we find

$$\alpha(x,t) = \begin{cases} \alpha_-, & \text{if} \quad x < u_a t + \dfrac{\big(u_a - u_*\big)\big(e^{-K_D t} - 1\big)}{K_D}, \\ \alpha_+, & \text{if} \quad x > u_a t + \dfrac{\big(u_a - u_*\big)\big(e^{-K_D t} - 1\big)}{K_D}. \end{cases} \tag{3.3.9}$$

Hence, if $u_- = u_+$ the solution of the Riemann problem (E') and (3.3.2) is given by

$$(\alpha,u)(x,t) = \begin{cases} \big(\alpha_-, u_a + \big(u_- - u_a\big)e^{-K_D t}\big), & \text{if} \quad x < u_a t + \dfrac{\big(u_a - u_-\big)\big(e^{-K_D t} - 1\big)}{K_D}, \\ \big(\alpha_+, u_a + \big(u_- - u_a\big)e^{-K_D t}\big), & \text{if} \quad x > u_a t + \dfrac{\big(u_a - u_-\big)\big(e^{-K_D t} - 1\big)}{K_D}. \end{cases} \tag{3.3.10}$$

Note that u is continuous across the curve

$$x = \xi(t) = u_a t + \frac{(u_a - u_*)(e^{-K_D t} - 1)}{K_D}, \tag{3.3.11}$$

while α might be discontinuous across this curve. This type of solution is called a *contact discontinuity*.

3.3.2 Delta shock waves

Now assume that $u_- > u_+$. In this case, the characteristics intersect. As pointed out at the end of the section 3.1.2, the solution u is discontinuous and α is not bounded. As in [82], we look for a solution (α, u) of the form

$$\alpha(x,t) = \alpha^0(x,t) + \omega(t)\delta(x - \xi(t)), \quad u(x,t) = u^0(x,t), \tag{3.3.12}$$

where α^0, u^0 are smooth functions on both sides of a curve

$$\Gamma = \{(x,t) : x = \xi(t), t \geq 0\},$$

while being discontinuous across Γ, and ω is a smooth function defined on $\mathbb{R}_0^+$ and satisfying the initial condition

$$\omega(0) = \omega_0 \in \mathbb{R}_0^+. \tag{3.3.13}$$

We call **δ-shock**, a pair of distributions (α, u) as given in (3.3.12). As in [82], we define a weighted δ-function $\omega(t)\delta_\xi$ supported on the curve Γ as follows

$$\langle \omega(t)\delta_\xi, \psi\rangle = \int_0^\infty \omega(t)\psi(\xi(t), t)dt, \tag{3.3.14}$$

for all test function $\psi \in \mathcal{C}_0^\infty(\mathbb{R}\times\mathbb{R}^+)$. We also define the following duality products between the δ-shock (α, u) and test functions in $\mathcal{C}_0^\infty(\mathbb{R}\times\mathbb{R}^+)$:

$$\begin{cases} \langle \alpha, \psi\rangle = \displaystyle\int_0^\infty\int_{-\infty}^\infty \alpha^0\psi\, dxdt + \langle \omega(t)\delta_\xi, \psi\rangle, \\ \langle \alpha u, \psi\rangle = \displaystyle\int_0^\infty\int_{-\infty}^\infty \alpha^0 u^0\psi\, dxdt + \langle \omega(t)\xi'(t)\delta_\xi, \psi\rangle. \end{cases} \tag{3.3.15}$$

We introduce the following definition.

Definition 3.3.1. *We say that a δ-shock (α,u) is a **weak solution** of* (E') *and* (3.3.1) *if*

$$\begin{cases} \langle \alpha, \psi_t\rangle + \langle \alpha u, \psi_x\rangle = -\displaystyle\int_{-\infty}^\infty \alpha_0(x)\psi(x,0)\, dx - \omega_0\psi(\xi(0),0), \\ \displaystyle\int_0^\infty\int_{-\infty}^\infty (u\psi_t + \frac{1}{2}u^2\psi_x)\, dxdt = -\int_0^\infty\int_{-\infty}^\infty K_D(u_a - u)\psi\, dxdt - \int_{-\infty}^\infty u_0(x)\psi(x,0)\, dx, \end{cases} \tag{3.3.16}$$

hold for all test functions $\psi \in \mathcal{C}_0^\infty(\overline{\mathbb{R}\times\mathbb{R}^+})$.

The above definition of δ-shock was first used by Sheng [82] to construct δ-shock solutions of the Riemann problem for the pressureless gas system. The classical Rankine-Hugoniot conditions of shocks have been generalized to those of δ-shocks to describe the relationship among the propagation speed, the location and the weight of δ-shocks. The Lax entropy condition is used to ensure the uniqueness of the solution [82]. Since the volume fraction may develop a Dirac measure in finite time, it is natural to seek for solution of (E') and (3.3.1) in the sense of measures, i.e. in the sense of distributions which are signed measures. The Cauchy problem for the pressureless gas system was solved in [26] using measure solutions in the space of signed Borel measures on $\mathbb{R}$, denoted $\mathcal{M}(\mathbb{R})$. The entropy inequality is not sufficient to obtain the uniqueness of measure solutions. For initial conditions taken in the space of bounded measurable functions, the uniqueness of measure solutions to the pressureless gas system was proven in [93] with the Oleinik entropy condition. For initial data in the space of measures, it was proven in [68] that the Oleinik condition is not sufficient to ensure uniqueness for measure solutions but it has to be complemented with a cohesion condition. The δ-shock solutions are particular measure solutions defined in [26], and belong to $\mathcal{M}(\mathbb{R})$. We use the approach of Sheng [82] to construct a δ-shock solution of the Riemann problem for (E'). We have the following result.

Theorem 3.3.2. *A δ-shock (α, u) is a weak solution of* (E') *and* (3.3.1) *if and only if the following properties are satisfied:*

i) (α^0, u^0) *satisfies* (E') *in the classical sense on both sides of the curve* Γ*;*

ii) $\big(\alpha, u\big)(x,0) = \big(\alpha_0, u_0\big)(x)$ *for all* $x \in \mathbb{R}$*;*

iii) the following system of differential-algebraic equation (DAE) in (ω, σ) *is satisfied on* Γ*:*

$$\begin{cases} \dfrac{d\omega}{dt}(t) = \big(\alpha_r(t) - \alpha_l(t)\big)\sigma(t) - \big(\alpha_r(t)u_r(t) - \alpha_l(t)u_l(t)\big), \\ \big(u_r(t) - u_l(t)\big)\sigma(t) = \dfrac{1}{2}\big(u_r(t)^2 - u_l(t)^2\big), \end{cases} \tag{3.3.17}$$

where $\alpha_l(t)$ *and* $\alpha_r(t)$ *are the limit of the solution* α *when* (x,t) *approaches* $(\xi(t),t)$ *from the left and the right, respectively;*

iv)

$$\omega(0) = \omega_0. \tag{3.3.18}$$

Proof: By Theorem 3.2.2, the function $u = u^0$ is a weak solution of the second equation of (E') and the second equation of (3.3.1) if and only if u^0 satisfies the second equation of (E') in the classical sense on both sides of the curve Γ, the initial condition $u(x,0) = u^0(x,0) = u_0(x)$ and the second equation of (3.3.17) is satisfied at the discontinuity. It remains to prove the properties (i)-(iv) for the first equation of (3.3.16). Let $\psi \in \mathcal{C}_0^\infty(\overline{\mathbb{R}\times\mathbb{R}^+})$. We have

$$\begin{aligned} \langle \alpha, \psi_t\rangle + \langle \alpha u, \psi_x\rangle &= \int_0^\infty \int_{-\infty}^\infty \alpha^0\psi_t\, dxdt + \langle \omega(t)\delta_\xi, \psi_t\rangle + \int_0^\infty \int_{-\infty}^\infty \alpha^0 u^0\psi_x\, dxdt \\ &\qquad + \langle \omega(t)\xi'(t)\delta_\xi, \psi_x\rangle \\ &= \int_0^\infty \int_{-\infty}^\infty \alpha^0\psi_t\, dxdt + \int_0^\infty \omega(t)\psi_t(\xi(t),t)\, dt + \int_0^\infty \int_{-\infty}^\infty \alpha^0 u^0\psi_x\, dxdt \\ &\qquad + \int_0^\infty \omega(t)\xi'(t)\psi_x(\xi(t),t)\, dt \\ &= \int_0^\infty \int_{-\infty}^\infty (\alpha^0\psi_t + \alpha^0 u^0\psi_x)\, dxdt + \int_0^\infty \omega(t)\frac{d\psi}{dt}(\xi(t),t)\, dt. \end{aligned}$$

Integrating by parts the right-hand side integrals, we obtain

$$\begin{aligned} \langle \alpha, \psi_t\rangle + \langle \alpha u, \psi_x\rangle &= -\int_0^\infty \int_{-\infty}^{\xi(t)} \big(\alpha_t^0 + (\alpha^0 u^0)_x\big)\psi\, dxdt - \int_0^\infty \int_{\xi(t)}^\infty \big(\alpha_t^0 + (\alpha^0 u^0)_x\big)\psi\, dxdt \\ &+ \int_0^\infty \Big(\big(\alpha_r(t) - \alpha_l(t)\big)\sigma(t) - \big(\alpha_r(t)u_r(t) - \alpha_l(t)u_l(t)\big) - \frac{d\omega}{dt}(t)\Big)\psi(\xi(t),t)\, dt \end{aligned}$$

$$-\int_{-\infty}^{\infty}\alpha^0(x,0)\psi(x,0)\,dx-\omega(0)\psi(\xi(0),0). \tag{3.3.19}$$

1) If a δ-shock (α,u) is a weak solution of (E') and (3.3.1), then (3.3.19) implies that

$$\begin{aligned}-\int_{-\infty}^{\infty}\alpha_0(x)\psi(x,0)dx-\omega_0\psi(\xi(0),0)&=-\int_0^{\infty}\int_{-\infty}^{\xi(t)}\big(\alpha_t^0+(\alpha^0u^0)_x\big)\psi\,dxdt\\&-\int_0^{\infty}\int_{\xi(t)}^{\infty}\big(\alpha_t^0+(\alpha^0u^0)_x\big)\psi\,dxdt-\int_{-\infty}^{\infty}\alpha^0(x,0)\psi(x,0)\,dx-\omega(0)\psi(\xi(0),0)\\&+\int_{x=\xi(t)}\Big(\big(\alpha_r(t)-\alpha_l(t)\big)\sigma(t)-\big(\alpha_r(t)u_r(t)-\alpha_l(t)u_l(t)\big)-\frac{d\omega}{dt}(t)\Big)\psi(\xi(t),t)\,dt.\end{aligned} \tag{3.3.20}$$

Firstly, we need to prove that (α^0,u^0) satisfies the first equation of (E) in the classical sense in both sides of the shock curve $x=\xi(t)$. To do this, we consider $\psi\in\mathcal{C}_0^{\infty}(\mathbb{R}\times\mathbb{R}^+)$ satisfying $\psi(\xi(t),t)=0$ for all $t\geq 0$. Equation (3.3.20) becomes

$$0=-\int_0^{\infty}\int_{-\infty}^{\xi(t)}\big(\alpha_t^0+(\alpha^0u^0)_x\big)\psi\,dxdt-\int_0^{\infty}\int_{\xi(t)}^{\infty}\big(\alpha_t^0+(\alpha^0u^0)_x\big)\psi\,dxdt.$$

Since ψ is arbitrary, this last equation implies that (α^0,u^0) satisfies the first equation of (E) in the classical sense on both sides of the curve Γ.
Secondly, we have to show that α^0 satisfies the initial condition (3.4.2), i.e. $\alpha^0(x,0)=\alpha_0(x)$. To achieve this, we consider $\psi\in\mathcal{C}_0^{\infty}(\overline{\mathbb{R}\times\mathbb{R}^+})$ satisfying $\psi(\xi(t),t)=0$ for all $t\geq 0$. Using (i) then (3.3.20) becomes

$$-\int_{-\infty}^{\infty}\alpha_0(x)\psi(x,0)dx=-\int_{-\infty}^{\infty}\alpha^0(x,0)\psi(x,0)dx. \tag{3.3.21}$$

which is equivalent to $\alpha^0(x,0)=\alpha_0(x)$ since ψ is arbitrary.
Next, we have to prove that the first equation of (3.3.17) is satisfied. For that, we take an arbitrary $\psi\in\mathcal{C}_0^{\infty}(\mathbb{R}\times\mathbb{R}^+)$. Using (i), (3.3.20) becomes

$$0=\int_0^{\infty}\Big(\big(\alpha_r(t)-\alpha_l(t)\big)\sigma(t)-\big(\alpha_r(t)u_r(t)-\alpha_l(t)u_l(t)\big)-\frac{d\omega}{dt}(t)\Big)\psi(\xi(t),t)\,dt.$$

Since ψ is arbitrary, the first equation of (3.3.17) is satisfied.
It remains to show that the initial condition $\omega(0)=\omega_0$ holds. To prove this, we consider $\psi\in\mathcal{C}_0^{\infty}(\overline{\mathbb{R}\times\mathbb{R}^+})$. Using (i), (ii) and (iii) then (3.3.20) becomes

$$-\omega_0\psi(\xi(0),0)=-\omega(0)\psi(\xi(0),0),$$

which implies, by taking $\psi(\xi(0),0)\neq 0$, that (iv) holds.

2) Conversely, if (i), (ii), (iii) and (iv) are satisfied then it is easy to deduce form (3.3.19) that

$$\langle \alpha, \psi_t \rangle + \langle \alpha u, \psi_x \rangle = -\int_{-\infty}^{\infty} \alpha_0(x)\psi(x,0)\,dx - \omega_0\psi(\xi(0),0).$$

for all $\psi \in \mathcal{C}_0^\infty(\overline{\mathbb{R}\times\mathbb{R}^+})$. This completes the proof of the theorem. ∎

We now return to the Riemann problem. Theorem 3.2.4 states that the solution u of the second equation of (E') is given by (3.2.15). This solution depends only on time, which implies, as

$$\frac{D\alpha}{dt} = \alpha\partial_x u = 0, \tag{3.3.22}$$

that the solution $\alpha = \alpha_0(x_0)$ is constant on both sides of the curve (3.2.14). Hence, the left and right states for α are determined by the Riemann data, that is

$$\alpha_l(x,t) \equiv \alpha_-, \tag{3.3.23}$$

$$\alpha_r(x,t) \equiv \alpha_+. \tag{3.3.24}$$

The limit states for the solution α are then given by $\alpha_l(t) = \alpha_-$ and $\alpha_r(t) = \alpha_+$. Substituting (3.2.8), (3.2.9), (3.2.10), (3.3.23) and (3.3.24) in the first equation of (3.3.17) and integrating the latter, we obtain

$$\begin{aligned}\omega(t) = \omega_0 &+ \big(\alpha_+ - \alpha_-\big)\big(u_a t + \frac{(u_a - u_- + u_a - u_+)(e^{-K_D t} - 1)}{2K_D}\big) \\ &+ \alpha_-\big(u_a t + \frac{(u_a - u_-)(e^{-K_D t} - 1)}{K_D}\big) - \alpha_+\big(u_a t + \frac{(u_a - u_+)(e^{-K_D t} - 1)}{K_D}\big).\end{aligned} \tag{3.3.25}$$

Reorganizing this last equation, we end up with

$$\omega(t) = \omega_0 + \frac{(\alpha_+ + \alpha_-)(u_- - u_+)(1 - e^{-K_D t})}{2K_D}. \tag{3.3.26}$$

For the solution of the Riemann problem (E') and (3.3.2), we take $\omega_0 = 0$ since the initial condition (3.3.2) stipulates that α does not initially contain a Dirac mass. In general, one can start with a δ-shock as an initial condition. In such case, ω_0 is not necessarily zero. We can now state the following result.

Corollary 3.3.3. *If $u_- > u_+$ then the entropy solution of the Riemann problem* (E') *and* (3.3.2) *is given by*

$$(\alpha,u)(x,t) = \begin{cases} \big(\alpha_-, u_l(t)\big), & x < \xi(t), \\ \big(\omega(t)\delta(x-\xi(t)), \sigma(t)\big), & x = \xi(t), \\ \big(\alpha_+, u_r(t)\big), & x > \xi(t), \end{cases} \tag{3.3.27}$$

where ω is given by (3.3.26) *with $\omega_0 = 0$, u_l, u_r are given by* (3.2.8) *and* (3.2.9), *respectively, σ is given by* (3.2.10) *and ξ is given by* (3.2.14).

In the following of this thesis, a solution to a PDE problem that takes the form given in (3.3.27) will also be called a *delta shock wave*.

3.3.3 Two contact discontinuities with a vacuum state

Assume that $u_- < u_+$. Then the solution u of the second equation of (E') is given by (3.2.23). This solution only depends on time t outside the region $\mathcal{S}$ delimited by the curves $X_1(t)$ and $X_2(t)$ defined in subsection 3.2.2. Hence, $\partial_x u \equiv 0$ for $(x,t) \notin \overline{\mathcal{S}}$. As the first equation of (E') can be written along characteristics as

$$\frac{D\alpha}{dt} = -\alpha \partial_x u, \tag{3.3.28}$$

we see that α is constant outside the region $\mathcal{S}$, and thus it is equal to its initial value on the foot of characteristic curves, that is

$$\alpha(x,t) = \alpha_0(x_0) \quad = \begin{cases} \alpha_-, & x_0 < 0, \\ \alpha_+, & x_0 > 0, \end{cases} \quad (x,t) \notin \overline{\mathcal{S}}. \tag{3.3.29}$$

As u is given by (3.2.23) outside region $\mathcal{S}$, we get from (3.1.8) that

$$\begin{aligned} x = \chi(x,t;t) &= \chi(x,t;0) + \int_0^t u(\chi(x,t;s),s)\, ds \\ &= x_0 + \begin{cases} \displaystyle\int_0^t u_l(x,s)ds, & \text{if} \quad x < X_1(t), \\ \displaystyle\int_0^t u_r(x,s)ds, & \text{if} \quad x > X_1(t) \end{cases} \\ &= \begin{cases} x_0 + X_1(t), & \text{if} \quad x < X_1(t), \\ x_0 + X_2(t), & \text{if} \quad x > X_2(t). \end{cases} \end{aligned} \tag{3.3.30}$$

Hence,

$$x_0 = \begin{cases} x - X_1(t), & \text{if} \quad x < X_1(t), \\ x - X_2(t), & \text{if} \quad x > X_2(t). \end{cases} \tag{3.3.31}$$

Therefore, by substituting (3.3.31) in (3.3.29), one obtains the solution α outside the region $\mathcal{S}$:

$$\alpha(x,t) = \begin{cases} \alpha_-, & x < X_1(t), \\ \alpha_+, & x > X_2(t). \end{cases} \quad (x,t) \notin \overline{\mathcal{S}}. \tag{3.3.32}$$

Inside the region $\mathcal{S}$, the solution u of the second equation of (E') is given by (3.2.22). So, equation (3.3.28) can be written on $\mathcal{S}$ as

$$\frac{D\alpha}{dt} = -\alpha \partial_x \overline{u}, \quad \forall (x,t) \in \mathcal{S}. \tag{3.3.33}$$

The function $\alpha = 0$ satisfies (3.3.33). Let $\epsilon > 0$ and assume $\alpha \neq 0$. Ones divides (3.3.33) by α and integrates on both sides from $s = \epsilon$ to $s = t$ to obtain

$$\begin{aligned}
\log(\alpha(x,t)) &= -\int_\epsilon^t \partial_x \overline{u}(x,s)ds + \log(\alpha(x,\epsilon)) \\
&= -\int_\epsilon^t \frac{K_D ds}{e^{K_D s}-1} + \log\big(\alpha(x,\epsilon)\big) \\
&= -\int_\epsilon^t \Big(\frac{K_D e^{K_D s}}{e^{K_D s}-1} - K_D\Big)ds + \log\big(\alpha(x,\epsilon)\big) \\
&= -\log\big(e^{K_D t}-1\big) + K_D t + \log\big(e^{K_D\epsilon}-1\big) - K_D\epsilon + \log\big(\alpha(x,\epsilon)\big) \\
&= \log\Big(\frac{\big(e^{K_D\epsilon}-1\big)\alpha(x,\epsilon)}{e^{K_D t}-1}\Big) + K_D\big(t-\epsilon\big).
\end{aligned}$$

This last equation gives

$$\alpha(x,t) = \frac{(1-e^{-K_D\epsilon})e^{K_D t}\alpha(x,\epsilon)}{e^{K_D t}-1}, \quad \forall (x,t) \in \mathcal{S}. \tag{3.3.34}$$

Taking $\epsilon \to 0$ in (3.3.34), one obtains

$$\alpha(x,t) \equiv 0, \quad \forall (x,t) \in \mathcal{S}, \tag{3.3.35}$$

leading to a contradiction. Hence, $\alpha = 0$ inside the region $\mathcal{S}$. We reach the following result.

Corollary 3.3.4. *If $u_- < u_+$ then the solution of the Riemann problem* (E') *and* (3.3.2) *is given by*

$$(\alpha,u)(x,t) = \begin{cases} \big(\alpha_-, u_l(x,t)\big), & x < X_1(t), \\ \big(0, \overline{u}(x,t)\big), & X_1(t) \le x \le X_2(t), \\ \big(\alpha_+, u_r(x,t)\big), & x > X_2(t), \end{cases} \tag{3.3.36}$$

where u_l and u_r are given by (3.2.8) *and* (3.2.9)*, respectively, $\overline{u}$ is given by* (3.2.22)*, and X_1 and X_2 are given by* (3.2.16) *and* (3.2.17)*, respectively.*

Note that u is continuous while α might be discontinuous across each of the two curves $x = X_1(t)$ and $x = X_2(t)$. This type of solution is called a *two-contact-discontinuity*.

In summary, the solution of the Riemann problem for system (E') is either a δ-shock solution or a two-contact-discontinuity with a vacuum state or a contact discontinuity, depending on the sign of $u_- - u_+$. The Rankine-Hugoniot conditions are given by a differential-algebraic equation. The solution α is constant outside of the shock trajectory Γ and is uniquely determined by the initial Riemann data, and u is given by the solution of the inviscid Burgers equation with source term (B).

3.4 Riemann problem for the Eulerian droplet model

Recall that the Eulerian droplet model in conservative form in the one-dimensional case reads as

$$\begin{cases} \partial_t \alpha + \partial_x(\alpha u) = 0, \\ \partial_t(\alpha u) + \partial_x(\alpha u^2) = K_D \alpha(u_a - u), \end{cases} \tag{E}$$

with the initial conditions

$$\big(\alpha, u\big)(x,0) = \big(\alpha_0, u_0\big)(x), \tag{3.4.1}$$

where α_0 and u_0 are piecewise smooth functions. Recall that any smooth solution to system (E') is also a solution to system (E). As in system (E'), the solution of (E) develops discontinuities if and only if (3.1.26) is satisfied (see subsection 3.1.2). To investigate the propagation of discontinuities in (E), we consider the Riemann problem, i.e. we look for the solution of problem (E) and (3.4.1), where (α_0, u_0) satisfies

$$\big(\alpha_0, u_0\big)(x) = \begin{cases} (\alpha_-, u_-), & x < 0, \\ (\alpha_+, u_+), & x > 0, \end{cases} \tag{3.4.2}$$

with constants $\alpha_-, \alpha_+ \in \mathbb{R}^+$ and $u_-, u_+ \in \mathbb{R}$.

3.4.1 Contact discontinuity

Assume that $u_- = u_+$. In this case, the characteristics do not intersect and fill the whole domain. From Remark 3.1.2, the velocity u is continuous and the volume fraction α does not blow up, i.e. the solution (α, u) is bounded. A bounded and eventual discontinuous (in α) solution across a curve satisfies the classical Rankine-Hugoniot conditions given by

$$\sigma(t) = \frac{\alpha_l(t)u_l(t) - \alpha_r(t)u_r(t)}{\alpha_l(t) - \alpha_r(t)} = \frac{\alpha_l(t)u_l(t)^2 - \alpha_r(t)u_r(t)^2}{\alpha_l(t)u_l(t) - \alpha_r(t)u_r(t)} = u^*(t), \tag{3.4.3}$$

where $u^*(t)$ is the common limit state of the solution u when (x,t) approaches the discontinuity curve. Equation (3.4.3) means the discontinuity curve moves at speed equal to the common limit state $u^*(t)$. We proved in subsection 3.3.1 that if $u_- = u_+$ then the Riemann solution of system (E') is a contact discontinuity, i.e. u is continuous and an eventual discontinuity in α moves at speed $\sigma(t) = \xi'(t)$, where ξ is given by (3.3.11). As the systems (E) and (E') are equivalent on both sides of the discontinuity curve and u is continuous across this curve, then $u^*(t) = \sigma(t) = \xi'(t)$. Thus, if $u_- = u_+$ then the solution of the Riemann problem (E) and (3.4.2) is given by (3.3.10).

3.4.2 Delta shock waves

Assume that $u_- > u_+$. The characteristics overlap and as pointed out in subsection 3.1.2, a bounded solution of (E) does not exist. We seek for δ-shock solutions for system (E). Recall that a δ-shock (α, u) is as follows:

$$\alpha(x,t) = \alpha^0(x,t) + \omega(t)\delta_\xi, \qquad u(x,t) = u^0(x,t), \quad (x,t) \in \mathbb{R} \times \mathbb{R}^+, \tag{3.4.4}$$

where α^0, u^0 are piecewise smooth functions on both sides of a smooth curve

$$\Gamma = \{(x,t) : x = \xi(t), t \geq 0\}, \tag{3.4.5}$$

while being discontinuous across Γ and ω is a smooth function defined on $[0,\infty)$ and satisfying the initial condition

$$\omega(0) = \omega_0 \in \mathbb{R}_0^+. \tag{3.4.6}$$

As in the previous section, we define the following duality products between δ-shock (seen as distributions) and test functions in $\mathcal{C}_0^\infty(\mathbb{R} \times \mathbb{R}^+)$:

$$\begin{cases} \langle \alpha, \psi \rangle = \displaystyle\int_0^\infty \int_{-\infty}^\infty \alpha^0 \psi dx dt + \langle \omega(t)\delta_\xi, \psi \rangle, \\ \langle \alpha u, \psi \rangle = \displaystyle\int_0^\infty \int_{-\infty}^\infty \alpha^0 u^0 \psi dx dt + \langle \omega(t)\xi'(t)\delta_\xi, \psi \rangle, \\ \langle \alpha u^2, \psi \rangle = \displaystyle\int_0^\infty \int_{-\infty}^\infty \alpha^0 (u^0)^2 \psi dx dt + \langle \sigma(t)\omega(t)\xi'(t)\delta_\xi, \psi \rangle, \\ \langle \alpha(u_a - u), \psi \rangle = \displaystyle\int_0^\infty \int_{-\infty}^\infty \alpha^0 (u_a - u^0) \psi dx dt + \langle (u_a - \sigma(t))\omega(t)\delta_\xi, \psi \rangle, \end{cases} \tag{3.4.7}$$

where $\sigma(t) = \xi'(t)$ satisfies $\sigma(0) = \sigma_0 \in \mathbb{R}$.

Definition 3.4.1. *We say that a δ-shock (α, u) is a **weak solution** of* (E) *and* (3.4.1) *if*

$$\begin{cases} \langle \alpha, \psi_t \rangle + \langle \alpha u, \psi_x \rangle = -\displaystyle\int_{-\infty}^\infty \alpha_0(x)\psi(x,0)dx - \omega_0 \psi(\xi(0),0), \\ \langle \alpha u, \psi_t \rangle + \langle \alpha u^2, \psi_x \rangle + K_D \langle \alpha(u_a - u), \psi \rangle = -\displaystyle\int_{-\infty}^\infty \alpha_0(x)u_0(x)\psi(x,0)dx \\ \qquad\qquad\qquad\qquad\qquad\qquad\qquad\qquad - \sigma_0\omega_0\psi(\xi(0),0), \end{cases} \tag{3.4.8}$$

hold for all test functions $\psi \in \mathcal{C}_0^\infty(\overline{\mathbb{R} \times \mathbb{R}^+})$.

We have the following result.

Theorem 3.4.2. *A δ-shock (α, u) is a weak solution of* (E) *and* (3.4.1) *if and only if the following properties are satisfied:*

i) (α^0, u^0) *satisfies* (E) *in the classical sense on both sides of the curve* Γ*;*

ii) $\alpha(x,0) = \alpha_0(x)$ *and* $\alpha^0(x,0)u^0(x,0) = \alpha_0(x)u_0(x)$ *for all* $x \in \mathbb{R}$*;*

iii) the following ODEs are satisfied on the curve Γ*:*

$$\begin{cases} \dfrac{d\omega}{dt}(t) = \big(\alpha_r(t) - \alpha_l(t)\big)\sigma(t) - \big(\alpha_r(t)u_r(t) - \alpha_l(t)u_l(t)\big), \\ \dfrac{d\big(\omega(t)\sigma(t)\big)}{dt} = \big(\alpha_r(t)u_r(t) - \alpha_l(t)u_l(t)\big)\sigma(t) - \big(\alpha_r(t)u_r(t)^2 - \alpha_l(t)u_l(t)^2\big) \\ \qquad\qquad + K_D\big(u_a - \sigma(t)\big)\omega(t); \end{cases} \tag{3.4.9}$$

iv) the following initial conditions are satisfied:

$$\omega(0) = \omega_0, \quad \omega(0)\sigma(0) = \omega_0\sigma_0. \tag{3.4.10}$$

Proof: Let $\psi \in \mathcal{C}_0^\infty(\overline{\mathbb{R}\times\mathbb{R}^+})$. Proceeding as in the proof of theorem 3.3.2, we get

$$\begin{aligned} \langle \alpha, \psi_t\rangle + \langle \alpha u, \psi_x\rangle &= -\int_0^\infty \int_{-\infty}^{\xi(t)} \big(\alpha_t^0 + (\alpha^0 u^0)_x\big)\psi \, dxdt - \int_0^\infty \int_{\xi(t)}^{\infty} \big(\alpha_t^0 + (\alpha^0 u^0)_x\big)\psi \, dxdt \\ &+ \int_{x=\xi(t)} \Big(\big(\alpha_r(t) - \alpha_l(t)\big)\sigma(t) - \big(\alpha_r(t)u_r(t) - \alpha_l(t)u_l(t)\big) - \frac{d\omega}{dt}(t)\Big)\psi(\xi(t),t)\, dt \\ &- \int_{-\infty}^{\infty} \alpha^0(x,0)\psi(x,0)\, dx - \omega(0)\psi(\xi(0),0). \end{aligned} \tag{3.4.11}$$

We also have

$$\begin{aligned} &\langle \alpha u, \psi_t\rangle + \langle \alpha u^2, \psi_x\rangle + \langle K_D\alpha(u_a - u), \psi\rangle = \int_0^\infty \int_{-\infty}^{\infty} \alpha^0 u^0 \psi_t dxdt + \langle \omega(t)\xi'(t)\delta_\xi, \psi_t\rangle \\ &+ \int_0^\infty \int_{-\infty}^{\infty} \alpha^0 (u^0)^2 \psi_x dxdt + \langle \sigma(t)\omega(t)\xi'(t)\delta_\xi, \psi_x\rangle + \int_0^\infty \int_{-\infty}^{\infty} K_D\alpha^0(u_a - u^0)\psi dxdt \\ &\qquad + \langle K_D(u_a - \sigma(t))\omega(t)\delta_\xi, \psi\rangle \\ &= \int_0^\infty \int_{-\infty}^{\infty} \big(\alpha^0 u^0\psi_t + \alpha^0(u^0)^2\psi_x\big)dxdt + \int_0^\infty \int_{-\infty}^{\infty} K_D\alpha^0(u_a - u^0)\psi dxdt \\ &\qquad + \int_0^\infty \sigma(t)\omega(t)\frac{d\psi}{dt}(\xi(t),t)dt + \int_0^\infty K_D(u_a - \sigma(t))\omega(t)\psi(\xi(t),t)dt. \end{aligned} \tag{3.4.12}$$

Integrating by part the first and the third terms in this last expression, we obtain

$$\langle \alpha u, \psi_t\rangle + \langle \alpha u^2, \psi_x\rangle + \langle K_D\alpha(u_a - u), \psi\rangle = -\int_{-\infty}^{\infty} \alpha^0(x,0)u^0(x,0)\psi(x,0)\, dx$$

$$
\begin{aligned}
&- \int_0^\infty \int_{-\infty}^{\xi(t)} \Big((\alpha^0 u^0)_t + (\alpha^0 (u^0)^2)_x - K_D \alpha^0 (u_a - u^0) \Big) \psi \, dxdt \\
&- \int_0^\infty \int_{\xi(t)}^{\infty} \Big((\alpha^0 u^0)_t + (\alpha^0 (u^0)^2)_x - K_D \alpha^0 (u_a - u^0) \Big) \psi \, dxdt \\
&+ \int_{x=\xi(t)} \Big[\Big(\alpha_r(t) u_r(t) - \alpha_l(t) u_l(t) \Big) \sigma(t) - \Big(\alpha_r(t) u_r(t)^2 - \alpha_l(t) u_l(t)^2 \Big) \\
&\qquad\qquad + K_D \big(u_a - \sigma(t) \big) \omega(t) - \frac{d(\omega(t)\sigma(t))}{dt} \Big] \psi(\xi(t), t) \, dt \\
&- \omega(0)\sigma(0)\psi(\xi(0), 0). \qquad (3.4.13)
\end{aligned}
$$

1) If the δ-shock (α, u) is a weak solution of (E) and (3.4.1) then (3.4.11) and (3.4.13) can be written as

$$
\begin{aligned}
&- \int_{-\infty}^\infty \alpha_0(x)\psi(x,0)dx - \omega_0 \psi(\xi(0),0) = - \int_0^\infty \int_{-\infty}^{\xi(t)} \big(\alpha_t^0 + (\alpha^0 u^0)_x \big) \psi \, dxdt \\
&- \int_0^\infty \int_{\xi(t)}^{\infty} \big(\alpha_t^0 + (\alpha^0 u^0)_x \big) \psi \, dxdt - \int_{-\infty}^\infty \alpha^0(x,0)\psi(x,0) \, dx - \omega(0)\psi(\xi(0),0) \\
&+ \int_{x=\xi(t)} \Big(\big(\alpha_r(t) - \alpha_l(t) \big) \sigma(t) - \big(\alpha_r(t) u_r(t) - \alpha_l(t) u_l(t) \big) - \frac{d\omega}{dt}(t) \Big) \psi(\xi(t), t) \, dt,
\end{aligned}
\qquad (3.4.14)
$$

$$
\begin{aligned}
&- \int_{-\infty}^\infty \alpha_0(x) u_0(x) \psi(x,0) \, dx - \sigma_0 \omega_0 \psi(\xi(0),0) = - \int_{-\infty}^\infty \alpha^0(x,0) u^0(x,0) \psi(x,0) \, dx \\
&\qquad - \int_0^\infty \int_{-\infty}^{\xi(t)} \Big((\alpha^0 u^0)_t + (\alpha^0 (u^0)^2)_x - K_D \alpha^0 (u_a - u^0) \Big) \psi \, dxdt \\
&\qquad - \int_0^\infty \int_{\xi(t)}^{\infty} \Big((\alpha^0 u^0)_t + (\alpha^0 (u^0)^2)_x - K_D \alpha^0 (u_a - u^0) \Big) \psi \, dxdt \\
&\qquad + \int_{x=\xi(t)} \Big(\big(\alpha_r(t) u_r(t) - \alpha_l(t) u_l(t) \big) \sigma(t) - \big(\alpha_r(t) u_r(t)^2 - \alpha_l(t) u_l(t)^2 \big) \\
&\qquad\qquad + K_D \big(u_a - \sigma(t) \big) \omega(t) - \frac{d(\omega(t)\sigma(t))}{dt} \Big) \psi(\xi(t), t) \, dt \\
&\qquad - \omega(0)\sigma(0)\psi(\xi(0),0), \qquad (3.4.15)
\end{aligned}
$$

respectively.
Case 1: If $\psi(x,0) = 0$, $\forall x \in \mathbb{R}$ and $\psi(\xi(t), t) = 0$, $\forall t \in \mathbb{R}^+$ then (3.4.14) and (3.4.15) reduce to

$$
0 = - \int_0^\infty \int_{-\infty}^{\xi(t)} \big(\alpha_t^0 + (\alpha^0 u^0)_x \big) \psi \, dxdt - \int_0^\infty \int_{\xi(t)}^{\infty} \big(\alpha_t^0 + (\alpha^0 u^0)_x \big) \psi \, dxdt,
$$

$$0=-\int_0^{\infty}\int_{-\infty}^{\xi(t)}\Big((\alpha^0u^0)_t+(\alpha^0(u^0)^2)_x-K_D\alpha^0(u_a-u^0)\Big)\psi\,dxdt$$
$$-\int_0^{\infty}\int_{\xi(t)}^{\infty}\Big((\alpha^0u^0)_t+(\alpha^0(u^0)^2)_x-K_D\alpha^0(u_a-u^0)\Big)\psi\,dxdt,$$

respectively. These two equalities imply that (i) is satisfied because ψ is arbitrary.
Case 2: If $\psi(\xi(t),t)=0$ for all $t\geq 0$ then by using (i) , the equations (3.4.14) and (3.4.15) reduce to

$$-\int_{-\infty}^{\infty}\alpha_0(x)\psi(x,0)\,dx=-\int_{-\infty}^{\infty}\alpha^0(x,0)\psi(x,0)\,dx,$$
$$-\int_{-\infty}^{\infty}\alpha_0(x)u_0(x)\psi(x,0)\,dx=-\int_{-\infty}^{\infty}\alpha^0(x,0)u^0(x,0)\psi(x,0)\,dx,$$

respectively. So, (ii) is satisfied.
Case 3: If $\psi(x,0)=0$ for all $x\in\mathbb{R}$ then by using (i), the equations (3.4.14) and (3.4.15) reduce to

$$0=\int_0^{\infty}\Big(\big(\alpha_r(t)-\alpha_l(t)\big)\sigma(t)-\big(\alpha_r(t)u_r(t)-\alpha_l(t)u_l(t)\big)-\frac{d\omega}{dt}(t)\Big)\psi(\xi(t),t)\,dt,$$

$$0=\int_{x=\xi(t)}\Big(\big(\alpha_r(t)u_r(t)-\alpha_l(t)u_l(t)\big)\sigma(t)-\big(\alpha_r(t)u_r(t)^2-\alpha_l(t)u_l(t)^2\big)$$
$$+K_D\big(u_a-\sigma(t)\big)\omega(t)-\frac{d(\omega(t)\sigma(t))}{dt}\Big)\psi(\xi(t),t)\,dt,$$

respectively. These two last equations imply (iii) .
Case 4: Combining (i), (ii) and (iii), the equations (3.4.14) and (3.4.15) give rise to

$$-\sigma_0\psi(\xi(0),0)=-\sigma(0)\psi(\xi(0),0),\tag{3.4.16}$$
$$-\sigma_0\omega_0\psi(\xi(0),0)=-\omega(0)\sigma(0)\psi(\xi(0),0),\tag{3.4.17}$$

respectively. By taking $\psi(\xi(0),0)\neq 0$, we obtain (iv).
2) Conversely, if (i), (ii), (iii) and (iv) are satisfied then (3.4.11) and (3.4.13) imply that (3.4.8) holds. This completes the proof of the theorem. ∎

Remark 3.4.3. *The initial value problem* (3.4.9)-(3.4.10) *reflects the exact relationship between the limit states* $(\alpha_l(t),u_l(t))$, $(\alpha_r(t),u_t(t))$ *on the two sides of the delta shock curve* Γ, *the weight* ω *and propagation speed* σ *of the delta shock, as the classical*

Rankine-Hugoniot conditions do for a bounded shock wave. It is called ***generalized Rankine-Hugoniot (GRH) conditions*** *for delta shock waves. It is a nonlinear system of ordinary differential equations of first order. We will prove in the next subsection, at least for the solution of the Riemann problem* (E) *and* (3.4.2)*, the existence of a solution* (ω, σ) *to the GRH conditions* (3.4.9)-(3.4.10) *satisfying the Lax entropy condition* (3.2.12)*.*

The solution of the Riemann problem (E') and (3.3.2) is smooth on both sides of the curve given by the differential-algebraic equation (3.3.17)-(3.3.18) (see corollary 3.3.3). In theorem 3.4.2, the solution of (E) is smooth on both sides of the curve (3.4.5). The systems (E) and (E') are equivalent for smooth solutions. According to the above discussion, we have the following result.

Corollary 3.4.4. *If* $u_- > u_+$ *then a solution of the Riemann problem* (E) *and* (3.4.2) *is given by*

$$(\alpha, u)(x,t) = \begin{cases} \big(\alpha_-, u_l(x,t)\big), & x < \xi(t), \\ \big(\omega(t)\delta(x-\xi(t)), \sigma(t)\big), & x = \xi(t), \\ \big(\alpha_+, u_r(x,t)\big), & x > \xi(t), \end{cases} \tag{3.4.18}$$

where u_l*,* u_r *are given by* (3.2.8) *and* (3.2.9)*, respectively,* (ω, σ) *is the solution of the GRH conditions* (3.4.9) *with the initial conditions* (3.4.48)*, and*

$$\xi(t) = \int_0^t \sigma(s)ds. \tag{3.4.19}$$

3.4.3 Two contact discontinuities with a vacuum state

Assume that $u_- < u_+$. The characteristics do not intersect nor fill the region $\mathcal{S}$ (see subsection 3.3.3). The Riemann solution is constructed as in subsection 3.3.3. Therefore, it is given by the two-contact-discontinuity solution with a vacuum state in (3.3.36).

In summary, the characteristic curves for the Eulerian droplet model (E) (seen as the pressureless gas system with zeroth-order source term) are curves (due to the presence of the source term) tending asymptotically to straight lines. The GRH conditions are given by a nonlinear system of ODEs which might be hard to solve analytically. As system (E'), the solution of the Riemann problem for system (E) is either a δ-shock solution, a two-contact-discontinuity with a vacuum state or a contact discontinuity.

3.4.4 Existence of an entropy solution to the GRH conditions for the Eulerian droplet model

Recall that the generalized Rankine-Hugoniot conditions for system (E) can be written as

$$\begin{cases} \dfrac{d\omega}{dt}(t) = \big(\alpha_r(t) - \alpha_l(t)\big)\sigma(t) - \big(\alpha_r(t)u_r(t) - \alpha_l(t)u_l(t)\big), \\ \dfrac{d(\omega\sigma)}{dt}(t) = \big(\alpha_r(t)u_r(t) - \alpha_l(t)u_l(t)\big)\sigma(t) + K_D\big(u_a - \sigma(t)\big)\omega(t) \\ \qquad\qquad - \big(\alpha_r(t)u_r(t)^2 - \alpha_l(t)u_l(t)^2\big), \end{cases} \tag{3.4.20}$$

satisfying the initial conditions

$$\omega(0) = \omega_0, \quad \omega(0)\sigma(0) = \omega_0\sigma_0, \tag{3.4.21}$$

where (α_l, u_l) and (α_r, u_r) are the left and right limits of the solution (α, u) of system (E) when (x, t) approaches the shock curve (3.4.5). We look for the existence of a solution to (3.4.20)-(3.4.21). The following results hold.

Lemma 3.4.5. *(**Growth of the weight ω of the δ-shock**)*
Assume that $\alpha_l(t), \alpha_r(t) > 0$ and $u_l(t) > u_r(t)$ for all $t \geq 0$. Suppose that there exists a solution $(\omega, \sigma) \in \mathcal{C}^1(\mathbb{R}^+) \times \mathcal{C}^1(\mathbb{R}^+)$ to the initial value problem (3.4.20)-(3.4.21). *If σ satisfies*

$$u_r(t) < \sigma(t) < u_l(t), \quad \forall t \geq 0, \tag{3.4.22}$$

then

$$\omega(t_2) > \omega(t_1) \quad \forall t_2 > t_1. \tag{3.4.23}$$

In particular, for the solution of the Riemann problem (E) *and* (3.4.2), *we have*

$$\omega(t) \geq \omega_0 + \frac{C(1 - e^{-K_D t})}{K_D}, \quad \forall t \geq 0, \tag{3.4.24}$$

where C is a positive constant.

Proof: We proceed by cases. Let $t \geq 0$.
Case 1: Assume that $\alpha_l(t) = \alpha_r(t)$. The first equation of (3.4.20) reduces to

$$\frac{d\omega}{dt}(t) = \alpha_l(t)\big(u_l(t) - u_r(t)\big) > 0.$$

Case 2: Assume that $\alpha_l(t) < \alpha_r(t)$. Using the first inequality from (3.4.22) in the first equation of (3.4.20), we obtain

$$\frac{d\omega}{dt}(t) = \big(\alpha_r(t) - \alpha_l(t)\big)\sigma(t) - \big(\alpha_r(t)u_r(t) - \alpha_l(t)u_l(t)\big)$$

$$> \big(\alpha_r(t) - \alpha_l(t)\big)u_r(t) - \big(\alpha_r(t)u_r(t) - \alpha_l(t)u_l(t)\big)$$
$$> \alpha_l(t)\big(u_l(t) - u_r(t)\big) > 0.$$

Case 3: Assume that $\alpha_l(t) > \alpha_r(t)$. Using the second inequality from (3.4.22) in the first equation of (3.4.20), we obtain

$$\frac{d\omega}{dt}(t) = \big(\alpha_r(t) - \alpha_l(t)\big)\sigma(t) - \big(\alpha_r(t)u_r(t) - \alpha_l(t)u_l(t)\big)$$
$$> \big(\alpha_r(t) - \alpha_l(t)\big)u_l(t) - \big(\alpha_r(t)u_r(t) - \alpha_l(t)u_l(t)\big)$$
$$> \alpha_r(t)\big(u_l(t) - u_r(t)\big) > 0.$$

Combining these three cases, we obtain

$$\frac{d\omega}{dt}(t) > 0, \quad \forall t \geq 0. \tag{3.4.25}$$

Hence, ω is an increasing function, and thus (3.4.23) holds. In particular, for the solution of the Riemann problem (E) and (3.4.2), the limit states are given by $\alpha_l(t) = \alpha_-$, $\alpha_r(t) = \alpha_+$, $u_l(t) = u_a + (u_- - u_a)e^{-K_D t}$ and $u_l(t) = u_a + (u_+ - u_a)e^{-K_D t}$. By setting $C = \min\{\alpha_-, \alpha_+\}(u_- - u_+) > 0$, one obtains

$$\frac{d\omega}{dt}(t) \geq Ce^{-K_D t}, \quad \forall t \geq 0. \tag{3.4.26}$$

Integrating this last inequality on both sides from 0 to t, we get

$$\omega(t) \geq \omega(0) + C\int_0^t e^{-K_D s}\,ds = \omega_0 + \frac{C(1 - e^{-K_D t})}{K_D}, \quad \forall t \geq 0. \tag{3.4.27}$$

∎

Inequality (3.4.22) is nothing else but the Lax entropy condition (3.2.12).

Proposition 3.4.6. *(**Entropic δ-shock speed**)*
Assume that $\alpha_l(t), \alpha_r(t) > 0$, $u_l(t) > u_r(t)$ for all $t \geq 0$ and $\sigma_0 \in (u_r(0), u_l(0))$. If $(\omega, \sigma) \in \mathcal{C}^1(\mathbb{R}^+) \times \mathcal{C}^1(\mathbb{R}^+)$ is a solution to the initial value problem (3.4.20)-(3.4.21) *then σ satisfies the Lax entropy condition* (3.4.22) *for all $t \geq 0$.*

Proof: We proceed by contradiction. Suppose that there exists $t \geq 0$ such that (3.4.22) is not satisfied. From $\sigma(0) = \sigma_0 \in (u_r(0), u_l(0))$ and the continuity of σ, there exists a smallest $t > 0$, denoted by t^*, such that

$$\sigma(t^*) = u_l(t^*) \text{ or } \sigma(t^*) = u_r(t^*) \text{ and } \sigma \text{ satisfies (3.4.22)}, \ \forall t \in [0, t^*). \tag{3.4.28}$$

By lemma 3.4.5, ω satisfies (3.4.23) on $[0, t^*)$. Combining this with the continuity of ω, we get

$$\omega(t^*) > \omega(0) = \omega_0 \geqslant 0. \tag{3.4.29}$$

Assume that $\sigma(t^*) = u_l(t^*)$. Substituting $\sigma(t^*)$ by $u_l(t^*)$ in the first equation of (3.4.20), we get

$$\begin{aligned}\frac{d\omega}{dt}(t^*) &= \big(\alpha_r(t^*) - \alpha_l(t^*)\big)u_l(t^*) - \big(\alpha_r(t^*)u_r(t^*) - \alpha_l(t^*)u_l(t^*)\big)\\ &= \alpha_r(t^*)\big(u_l(t^*) - u_r(t^*)\big).\end{aligned} \tag{3.4.30}$$

Substituting $\sigma(t^*)$ by $u_l(t^*)$ in the second equation of (3.4.20), we obtain

$$\begin{aligned}\frac{d(\omega\sigma)}{dt}(t^*) &= \big(\alpha_r(t^*)u_r(t^*) - \alpha_l(t^*)u_l(t^*)\big)u_l(t^*) + \alpha_l(t^*)u_l^2(t^*)\\ &\qquad - \alpha_r(t^*)u_r(t^*)^2 + K_D\big(u_a - u_l(t^*)\big)\omega(t^*)\\ &= \alpha_r(t^*)u_r(t^*)\big(u_l(t^*) - u_r(t^*)\big) + K_D\big(u_a - u_l(t^*)\big)\omega(t^*).\end{aligned} \tag{3.4.31}$$

From (3.4.30) and (3.4.31), one calculates

$$\begin{aligned}\omega(t^*)\frac{d\sigma}{dt}(t^*) &= \frac{d(\omega\sigma)}{dt}(t^*) - \sigma(t^*)\frac{d\omega}{dt}(t^*)\\ &= \frac{d(\omega\sigma)}{dt}(t^*) - u_l(t^*)\frac{d\omega}{dt}(t^*)\\ &= -\alpha_r(t^*)\big(u_l(t^*) - u_r(t^*)\big)^2 + K_D\big(u_a - u_l(t^*)\big)\omega(t^*).\end{aligned} \tag{3.4.32}$$

Using this last equation, one calculates

$$\begin{aligned}\omega(t^*)\frac{d(\sigma - u_l)}{dt}(t^*) &= \omega(t^*)\frac{d\sigma}{dt}(t^*) - \omega(t^*)\frac{du_l}{dt}(t^*)\\ &= -\alpha_r(t^*)\big(u_l(t^*) - u_r(t^*)\big)^2 - \Big(\frac{du_l}{dt}(t^*) - K_D(u_a - u_l(t^*))\Big)\omega(t^*)\\ &= -\alpha_r(t^*)\big(u_l(t^*) - u_r(t^*)\big)^2 < 0,\end{aligned} \tag{3.4.33}$$

since u_l satisfies (E) in the classical sense. Using (3.4.29), we deduce from (3.4.33) that

$$\frac{d(\sigma - u_l)}{dt}(t^*) < 0.$$

By the continuity of the function $t \mapsto \dfrac{d(\sigma - u_l)}{dt}(t)$, there exists $\epsilon > 0$ such that

$$\frac{d(\sigma - u_l)}{dt}(t) < 0, \quad \forall t \in]t^* - \epsilon, t^*[.$$

Integrating, this last inequality from $t^* - \epsilon$ to t^* on both sides, we obtain

$$0 \geq \int_{t^*-\epsilon}^{t^*} \frac{d(\sigma - u_l)}{ds}(s)ds = (\sigma - u_l)(t^*) - (\sigma - u_l)(t^* - \epsilon) = -\sigma(t^* - \epsilon) + u_l(t^* - \epsilon).$$

This last inequality implies that $\sigma(t^*-\epsilon) \geq u_l(t^*-\epsilon)$ which contradicts (3.4.28). Assume that $\sigma(t^*) = u_r(t^*)$. A similar reasoning as above also leads to a contradiction of (3.4.28). Hence, such $t^* > 0$ does not exist. Thus, the shock speed σ satisfies (3.4.22) for all $t \geq 0$. ∎

To simplify notations, we set

$$\begin{aligned} &a(t) = \alpha_r(t) - \alpha_l(t), \quad b(t) = \alpha_r(t)u_r(t) - \alpha_l(t)u_l(t), \\ &c(t) = \alpha_r(t)u_r(t)^2 - \alpha_l(t)u_l(t)^2, \quad \theta(t) = \omega(t)\sigma(t). \end{aligned} \tag{3.4.34}$$

The functions a, b and c are continuous and bounded for all $t \geqslant 0$ since the limit states (α_l, u_l) and (α_r, u_r) are continuous and bounded. Substituting a, b, c and θ in (3.4.20), this system can be written as

$$\begin{cases} \dfrac{d\omega}{dt}(t) = a(t)\dfrac{\theta(t)}{\omega(t)} - b(t), \\ \dfrac{d\theta}{dt}(t) = b(t)\dfrac{\theta(t)}{\omega(t)} + K_D\big(u_a\omega(t) - \theta(t)\big) - c(t). \end{cases} \tag{3.4.35}$$

The initial value problem (3.4.20)-(3.4.21) can then be written in the following condensed form

$$\begin{cases} \dfrac{d\mathbf{z}}{dt} = \mathbf{f}(\mathbf{z}, t), \\ \mathbf{z}(0) = (\omega_0, \theta_0)^T, \text{ with } \theta_0 = \omega_0\sigma_0, \end{cases} \tag{3.4.36}$$

where

$$\mathbf{z}(t) = \begin{pmatrix} \omega(t) \\ \theta(t) \end{pmatrix} \quad \text{and} \quad \mathbf{f}(\mathbf{z}, t) = \begin{pmatrix} f_1(\mathbf{z}, t) \\ f_2(\mathbf{z}, t) \end{pmatrix} = \begin{pmatrix} a(t)\dfrac{\theta(t)}{\omega(t)} - b(t) \\ b(t)\dfrac{\theta(t)}{\omega(t)} + K_D\big(u_a\omega(t) - \theta(t)\big) - c(t) \end{pmatrix}. \tag{3.4.37}$$

We have the following result for the existence of a solution to the GRH conditions (3.4.20)-(3.4.21) in case of a δ-shock solution for the Riemann problem (E) and(3.4.2):

Theorem 3.4.7. *(**Existence of a solution to the GRH**)*
If $\alpha_-, \alpha_+ > 0$, $u_- > u_+$ and $\sigma_0 \in (u_+, u_-)$ then the generalized Rankine-Hugoniot conditions (3.4.20)-(3.4.21) *for the solution of the Riemann problem* (E) *and* (3.4.2) *have a $\mathcal{C}^1$-solution (ω, σ) which satisfies the Lax entropy condition* (3.4.22).

Proof: If $\alpha_-, \alpha_+ > 0$ and $u_- > u_+$ then the limit states α_l, α_r, u_l and u_r of the solution to the Riemann problem (E) and (3.4.2) satisfy $\alpha_l(t), \alpha_r(t) > 0$ and $u_l(t) > u_r(t)$ for all $t \geq 0$.

i) Let us first suppose that $\omega_0 > 0$. As the functions a, b and c are continuous for all $t \geqslant 0$, the functions f_i, $i = 1, 2$, are continuous at $t = 0$. The Cauchy-Péano

theorem (see [29], p.59) ensures the existence of a $\mathcal{C}^1$-solution (ω, θ) to (3.4.36) on some interval $[0, t_1]$. From Proposition 3.4.6 and Lemma 3.4.5, ω satisfies (3.4.24) on $[0, t_1]$. This implies that

$$\omega(t) = \omega_0 + \frac{C(1 - e^{-K_D t})}{K_D} > 0 \quad \forall t \in [0, t_1].$$

The partial derivatives $\frac{\partial f_i}{\partial z_i}$ exist and are continuous on $\mathbb{R}^+ \times \mathbb{R} \times [0, t_1]$. The Cauchy-Lipschitz existence theorem (see [29], p.65) ensures the uniqueness of the solution (ω, θ) on the interval $[0, t_1]$. We define

$$\sigma(t) = \frac{\theta(t)}{\omega(t)} \quad \forall t \in [0, t_1].$$

Clearly, the pair (ω, σ) is a $\mathcal{C}^1$-solution of (3.4.20)-(3.4.21) on $[0, t_1]$. Uniqueness of (ω, σ) follows from the uniqueness of (ω, θ). From Lemma 3.2 in [29], there exists a maximal solution extending the local solution (ω, σ). We claim that this maximal solution is global, i.e. it is defined for all $t \geq 0$. In fact, if this maximal solution is not global then lemma 3.3 in [29] stipulates that it is defined on an interval of the form $[0, T_0)$, for some $0 < T_0 < \infty$. Then, using Proposition 3.4.6 and lemma 3.4.5, this maximal solution could be extended beyond T_0 since $\lim_{t \to T_0} \omega(t) > 0$, contradicting the maximality of the solution.

ii) Now suppose that $\omega_0 = 0$. Take any finite $T > 0$. Let $F_1 = \{(\omega_n, \theta_n)\}_{n \geq 1}$ be a family of functions such that (ω_n, θ_n) is a $\mathcal{C}^1$-solution to (3.4.36) on the interval $[0, T]$ satisfying the initial conditions $\omega_n(0) = \frac{1}{n}$ and $\theta_n(0) = \frac{\sigma_0}{n}$. Moreover, the functions ω_n satisfy (3.4.23) and (3.4.24). The existence of the family F_1 follows from part (i). Let us prove that F_1 is a family of bounded and equicontinuous functions on the interval $[0, T]$. For all $n \geq 1$, we have

$$\begin{cases} \dfrac{d\omega_n}{dt}(t) = a(t)\sigma_n(t) - b(t), \\ \dfrac{d\theta_n}{dt}(t) = b(t)\sigma_n(t) + K_D\big(u_a - \sigma_n(t)\big)\omega_n(t) - c(t). \end{cases} \tag{3.4.38}$$

Taking the absolute value in the first equation of (3.4.38), we get

$$\begin{aligned} \left|\frac{d\omega_n}{dt}(t)\right| &= \big|a(t)\sigma_n(t) - b(t)\big)\big| \\ &\leqslant |a(t)|\,|u_l(t)| + |b(t)| \\ &\leqslant M, \text{ where } M = \max_{s \in [0,T]}\{|a(s)||u_l(s)| + |b(s)|\}. \end{aligned} \tag{3.4.39}$$

Integrating ω_n' from 0 to t, taking the absolute value and using (3.4.39), we get

$$|\omega_n(t)| = \left|\omega_n(0) + \int_0^t \omega_n'(s)\,ds\right|$$

$$\begin{aligned}
&\leqslant \frac{1}{n} + \int_0^t |\omega_n'(s)|\, ds \\
&\leqslant 1 + MT, \quad \forall t \in [0,T].
\end{aligned}$$

Hence, the functions ω_n and their first derivative are uniformly bounded on $[0,T]$. For all $n \geq 1$, $\theta_n = \omega_n \sigma_n$ is bounded as a product of two bounded functions since σ_n satisfies (3.4.22) and $u_r(t)$, $u_l(t)$ are bounded. Furthermore, $\theta_n'(t)$ is also bounded since

$$\begin{aligned}
\left|\frac{d\theta_n}{dt}(t)\right| &= \big|b(t)\sigma_n(t) + K_D\big(u_a - \sigma_n(t)\big)\omega_n(t) - c(t)\big| \\
&\leqslant |b(t)|\,|u_l(t)| + K_D|\omega_n(t)|\big(\,|u_a| + |u_l(t)|\,\big) + |c(t)| \\
&\leqslant |b(t)|\,|u_l(t)| + K_D\big(1+MT\big)\big(\,|u_a| + |u_l(t)|\,\big) + |c(t)| \\
&\leqslant Q = \max_{t\in[0,T]}\big\{|b(t)|\,|u_l(t)| + K_D\big(1+MT\big)\big(\,|u_a| + |u_l(t)|\,\big) + |c(t)|\big\} < \infty.
\end{aligned}$$

Hence, F_1 is a family of bounded and equicontinuous functions at every point of the interval $[0,T]$. The Arzelà-Ascoli theorem ensures the existence of a subsequence $\{(\omega_{n_k}, \theta_{n_k})\} \subset F_1$ that converges uniformly to a continuous functions (ω, θ) on the interval $[0,T]$. Since ω_{n_k} satisfies (3.4.24), we have

$$\begin{aligned}
\omega(t) = \lim_{n_k\to\infty} \omega_{n_k}(t) &\geq \lim_{n_k\to\infty}\Big(\omega_{n_k}(0) + \frac{C(1-e^{-K_D t})}{K_D}\Big) \\
&\geq \lim_{n_k\to\infty}\Big(\frac{1}{n_k} + \frac{C(1-e^{-K_D t})}{K_D}\Big) \qquad (3.4.40) \\
&\geq \frac{C(1-e^{-K_D t})}{K_D} > 0, \quad \forall t \in (0,T].
\end{aligned}$$

Inequality (3.4.40) means that the limit function ω is positive on any interval of the form $[\eta, T]$, with $0 < \eta \leqslant T$. Now, we define the sequence of functions

$$\sigma_{n_k}(t) = \frac{\theta_{n_k(t)}}{\omega_{n_k}(t)}, \quad \forall t \in [0,T], \qquad (3.4.41)$$

and the function

$$\sigma(t) = \frac{\theta(t)}{\omega(t)}, \quad \forall t \in [\eta, T]. \qquad (3.4.42)$$

Clearly, σ is a continuous function on the interval $[\eta, T]$ as a quotient of two continuous functions. Let us prove that σ_{n_k} converges uniformly to σ on the interval $[\eta, T]$. Let

$t \in [\eta, T]$. We have

$$\begin{aligned}
|\sigma_{n_k}(t) - \sigma(t)| &= \left|\frac{\theta_{n_k}(t)}{\omega_{n_k}(t)} - \frac{\theta(t)}{\omega(t)}\right| = \left|\frac{\theta_{n_k}(t)\omega(t) - \omega_{n_k}(t)\theta(t)}{\omega_{n_k}(t)\omega(t)}\right| \\
&\leqslant \left|\frac{\theta_{n_k}(t)\omega(t) + \theta(t)\omega(t) - \theta(t)\omega(t) - \omega_{n_k}(t)\theta(t)}{\omega_{n_k}(\eta)\omega(\eta)}\right| \quad \text{(from (3.4.23))} \\
&\leqslant \frac{{K_D}^2|\theta(t)|}{C^2(1-e^{-K_D\eta})^2}\,|\omega_{n_k}(t) - \omega(t)| \\
&\qquad + \frac{{K_D}^2\,|\omega(t)|}{C^2(1-e^{-K_D\eta})^2}\,|\theta_{n_k}(t) - \theta(t)| \quad \text{(from (3.4.24))} \\
&\leqslant \frac{{K_D}^2}{C^2(1-e^{-K_D\eta})^2}\Big(|\theta(t)|\,|\omega_{n_k}(t) - \omega(t)| + |\omega(t)|\,|\theta_{n_k}(t) - \theta(t)|\Big).
\end{aligned} \tag{3.4.43}$$

Set

$$P = \frac{\max_{t\in[\eta,T]}\{|\theta(t)|, |\omega(t)|\}{K_D}^2}{C^2(1-e^{-K_D\eta})^2} < \infty.$$

Taking the supremum in (3.4.43), we get

$$\sup_{t\in[\eta,T]} |\sigma_{n_k}(t) - \sigma(t)| \leqslant P\Big(\sup_{t\in[\eta,T]} |\omega_{n_k}(t) - \omega(t)| + \sup_{t\in[\eta,T]} |\theta_{n_k}(t) - \theta(t)|\Big). \tag{3.4.44}$$

Hence, the sequence σ_{n_k} converges uniformly to σ on the interval $[\eta, T]$ since ω_{n_k} and θ_{n_k} uniformly converge to ω and θ, respectively, on the interval $[0, T]$.
Let us prove that (ω, σ) is a $\mathcal{C}^1$-solution to (3.4.20) on the interval $[\eta, T]$. For all $n_k \geq 1$, we have

$$\begin{cases}
\dfrac{d\omega_{n_k}}{dt}(t) = a(t)\sigma_{n_k}(t) - b(t), \\
\dfrac{d(\omega_{n_k}\sigma_{n_k})}{dt} = b(t)\sigma_{n_k}(t) + K_D\big(u_a - \sigma_{n_k}(t)\big)\omega_{n_k}(t) - c(t).
\end{cases} \tag{3.4.45}$$

As ω_{n_k} and σ_{n_k} converge uniformly to ω and σ, respectively, on the interval $[\eta, T]$ then the terms on the r.h.s of each equation of (3.4.45) also converge uniformly on the interval $[\eta, T]$, i.e. the sequence $\{(\frac{d\omega_{n_k}}{dt}, \frac{d(\omega_{n_k}\sigma_{n_k})}{dt})\}_{k\geq 1}$ converges uniformly on the interval $[\eta, T]$. Take $n_k \to \infty$ in (3.4.45). Then, using Theorem 7.17 in [80], we obtain

$$\begin{cases}
\dfrac{d\omega}{dt}(t) = \lim\limits_{n_k\to\infty} \dfrac{d\omega_{n_k}}{dt}(t) = \lim\limits_{n_k\to\infty} \Big(a(t)\sigma_{n_k}(t) - b(t)\Big) = a(t)\sigma(t) - b(t), \\
\dfrac{d(\omega\sigma)}{dt}(t) = \lim\limits_{n_k\to\infty} \dfrac{d(\omega_{n_k}\sigma_{n_k})}{dt}(t) = \lim\limits_{n_k\to\infty} \Big(b(t)\sigma_{n_k}(t) + K_D\big(u_a - \sigma_{n_k}(t)\big)\omega_{n_k}(t) - c(t)\Big) \\
\qquad\qquad\qquad\qquad = b(t)\sigma(t) + K_D\big(u_a - \sigma(t)\big)\omega(t) - c(t).
\end{cases} \tag{3.4.46}$$

As the terms on the r.h.s of each equation of (3.4.46) are continuous then $\frac{d\omega}{dt}$ and $\frac{d\theta}{dt}$ are continuous on the interval $[\eta, T]$. Hence, the pair (ω, σ) is a $\mathcal{C}^1$-solution to (3.4.20) on the interval $[\eta, T]$. Since $\eta > 0$ is arbitrary then the $\mathcal{C}^1$-solution (ω, σ) can be extended to all t in $(0, T]$. From the uniform convergence of ω_{n_k} to ω on the interval $[0, T]$, we get

$$\omega(0) = \lim_{n_k \to \infty} \omega_{n_k}(0) = \lim_{n_k \to \infty} \frac{1}{n_k} = 0 = \omega_0. \tag{3.4.47}$$

We set

$$\sigma(0) = \sigma_0 \in (u_+, u_-) = (u_r(0), u_l(0)).$$

Thus, the $\mathcal{C}^1$ functions (ω, σ) satisfy the initial value problem (3.4.20)-(3.4.21) for all $t \in (0, T]$. Since $T > 0$ is arbitrary then this solution can be extended to all $t > 0$. By proposition 3.4.6, σ satisfies the Lax entropy condition (3.4.22) for all $t \geqslant 0$. ∎

We also have the following result for existence of a solution to the GRH conditions (3.4.20)-(3.4.21) in case of a contact discontinuity or a two-contact-discontinuity solution for the Riemann problem (E) and (3.4.2):

Corollary 3.4.8. *If $u_- = u_+$ then $(\omega, \sigma) = (0, u_l)$ is a solution to the problem* (3.4.20).

Proof: If $u_- = u_+$ then the solution u is continuous, and thus $u_l(t) = u_r(t)$ for all $t \geqslant 0$. Substituting u_r, ω and σ by u_l, 0 and u_l, respectively, we obtain 0 on both sides of equation (3.4.20). Hence, $(0, u_l)$ satisfies (3.4.20). ∎

Remark 3.4.9. *The generalized Rankine-Hugoniot conditions* (3.4.20) *reduce to the classical Rankine-Hugoniot conditions for a contact discontinuity or a two-contact-discontinuity-solution. In fact, if $u_- = u_+$ then the solution of the Riemann problem* (E) *and* (3.4.2) *is bounded and thus, $\omega \equiv 0$. Applying the classical Rankine-Hugoniot conditions for* (E)*, we get $\sigma = \frac{\alpha_r u_r - \alpha_l u_l}{\alpha_r - \alpha_l} = \frac{\alpha_r u_r^2 - \alpha_l u_l^2}{\alpha_r u_r - \alpha_l u_l} = u_l$. Hence, we recover the solution of the classical Rankine-Hugoniot conditions* (3.4.20) *from the generalized Rankine-Hugoniot conditions.*

Proposition 3.4.6 stipulates that the initial delta shock speed σ_0 should belong to the interval (u_+, u_-). A choice for an entropic σ_0 is given by the following result.

Proposition 3.4.10. *Assume that $\alpha_l(0), \alpha_r(0) > 0$. Let $(\omega, \sigma) \in \mathcal{C}^1(\mathbb{R}_0^+) \times \mathcal{C}^1(\mathbb{R}_0^+)$ be a solution to the GRH conditions* (3.4.20)-(3.4.21)*. If $\omega_0 = 0$ then an entropic initial shock speed σ_0 satisfying the GRH conditions and the Lax entropy condition* (3.4.22) *at the origin is given by*

$$\sigma_0 = \frac{\sqrt{\alpha_r(0)}u_r(0) + \sqrt{\alpha_l(0)}u_l(0)}{\sqrt{\alpha_r(0)} + \sqrt{\alpha_l(0)}}. \tag{3.4.48}$$

Proof: By using the first equation of (3.4.20), the second equation can be written as

$$\omega(t)\frac{d\sigma}{dt}(t) = -a(t)\sigma(t)^2 + 2b(t)\sigma(t) - c(t) + K_D\big(u_a - \sigma(t)\big)\omega(t). \tag{3.4.49}$$

At $t = 0$, $\omega(0) = \omega_0 = 0$ and (3.4.49) reduces to

$$-a(0)\sigma(0)^2 + 2b(0)\sigma(0) - c(0) = 0. \tag{3.4.50}$$

If $a(0) = 0$, i.e. $\alpha_l(0) = \alpha_r(0)$ then (3.4.50) has one solution given by

$$\sigma(0) = \frac{c(0)}{2b(0)} = \frac{\alpha_r(0)u_r(0)^2 - \alpha_l(0)u_l(0)^2}{2(\alpha_r(0)u_r(0) - \alpha_l(0)u_l(0))} = \frac{u_r(0) + u_l(0)}{2} \in (u_r(0), u_l(0)), \tag{3.4.51}$$

If $a(0) \neq 0$, i.e. $\alpha_l(0) \neq \alpha_r(0)$ then (3.4.50) has two roots given by

$$\sigma(0)_1 = \frac{b(0) - \sqrt{b(0)^2 - a(0)c(0)}}{a(0)} = \frac{\sqrt{\alpha_r(0)}u_r(0) - \sqrt{\alpha_l(0)}u_l(0)}{\sqrt{\alpha_r(0)} - \sqrt{\alpha_l(0)}}, \tag{3.4.52}$$

$$\sigma(0)_2 = \frac{b(0) + \sqrt{b(0)^2 - a(0)c(0)}}{a(0)} = \frac{\sqrt{\alpha_r(0)}u_r(0) + \sqrt{\alpha_l(0)}u_l(0)}{\sqrt{\alpha_r(0)} + \sqrt{\alpha_l(0)}}. \tag{3.4.53}$$

The first root $\sigma(0)_1$ does not always satisfy the Lax entropy condition at the origin. In fact,

$$\begin{aligned}
\sigma_{01} - u_l(0) =& \frac{\sqrt{\alpha_r(0)}u_r(0) - \sqrt{\alpha_l(0)}u_l(0)}{\sqrt{\alpha_r(0)} - \sqrt{\alpha_l(0)}} - u_l(0) \\
=& \frac{\sqrt{\alpha_r(0)}u_r(0) - \sqrt{\alpha_l(0)}u_l(0) - \sqrt{\alpha_r(0)}u_l(0) + \sqrt{\alpha_l(0)}u_l(0)}{\sqrt{\alpha_r(0)} - \sqrt{\alpha_l(0)}} \\
=& \frac{\sqrt{\alpha_r(0)}(u_r(0) - u_l(0))}{\sqrt{\alpha_r(0)} - \sqrt{\alpha_l(0)}} > 0, \quad \text{if } \alpha_l(0) > \alpha_r(0).
\end{aligned} \tag{3.4.54}$$

The second root $\sigma(0)_2 \in (u_r(0), u_l(0))$ for all $\alpha_l(0), \alpha_r(0) > 0$. Moreover, if $\alpha_l(0) = \alpha_r(0)$ then $\sigma(0)_2$ reduces to (3.4.51). Thus, an initial shock speed σ_0 satisfying the Lax entropy condition (3.4.22) at the origin is given by (3.4.48). ∎

We proved the existence of a solution to the generalized Rankine-Hugoniot conditions (3.4.9)-(3.4.10) for the Riemann problem (E) and (3.4.2), satisfying the Lax entropy condition. In general, it might be hard to find the analytical solution of the initial value problem associated to the GRH conditions. At least for the Riemann problem, one can solve numerically this initial value problem since the limit states

$(\alpha_l(t), u_l(t))$ and $(\alpha_r(t), u_r(t))$ are known. The systems (E') and (E) are equivalent for smooth, two-contact-discontinuity or contact discontinuity solutions but they differ for δ-shock solutions. In fact, one can, by a tedious substitution, check that the solution (given in (3.3.26) and (3.2.10)) of the GRH conditions (3.3.17) for system (E') does not satisfy the GRH conditions (3.4.9)-(3.4.10) for the Eulerian droplet model (E). Hence, the conservative form of the Eulerian droplet model is to be used when discontinuous traveling waves (shocks, contact discontinuities) are present in the solutions.

3.5 Droplet model with non constant air velocity

Consider again the Eulerian droplet model

$$\begin{cases} \partial_t \alpha + \partial_x(\alpha u) = 0, \\ \partial_t(\alpha u) + \partial_x(\alpha u^2) = K_D \alpha (u_a - u), \end{cases} \tag{E}$$

with the initial condition

$$(\alpha, u)(x, 0) = (\alpha_0, u_0)(x), \quad \alpha_0, u_0 \in \mathcal{C}^1(\mathbb{R}), \tag{3.5.1}$$

where now the air velocity $u_a = u_a(x, t)$ is no longer constant. The hyperbolicity of the system is not affected by the air velocity function since this latter is in the zeroth-order right-hand side term. All the properties from subsection 3.1.1 are still valid. Recall that for smooth solutions, the second equation of (E) is equivalent to

$$\partial_t u + u\partial_x u = K_D(u_a - u) \tag{3.5.2}$$

which can be written along characteristics $\chi(x, t; s)$ (solution of (3.1.8)) as

$$\frac{Du}{dt} = K_D(u_a - u). \tag{3.5.3}$$

We have

$$\frac{D(e^{K_D s}u)}{ds} = e^{K_D s}\frac{Du}{ds} + K_D e^{K_D s}u. \tag{3.5.4}$$

Using (3.5.3) in this last equation, we get

$$\begin{aligned} \frac{D(e^{K_D s}u)}{ds} &= e^{K_D s}K_D(u_a - u) + K_D e^{K_D s}u, \\ &= K_D e^{K_D s}u_a. \end{aligned} \tag{3.5.5}$$

Integrating (3.5.5) from 0 to s on both sides, we obtain

$$u(\chi(x,t;s),s) = u_0(x_0)e^{-K_D s} + \int_0^s K_D e^{K_D(r-s)} u_a(\chi(x,t;r),r)\,dr, \tag{3.5.6}$$

where $x_0 = \chi(x,t;0)$. By substituting (3.5.6) in the characteristic equation (3.1.8) and integrating the latter equation on both sides from 0 to t, we obtain an equation for the characteristic curves

$$\begin{aligned} x = \chi(x,t;t) &= x_0 + \int_0^t u(\chi(x,t;s),s)ds \\ &= x_0 + \frac{u_0(x_0)}{K_D}(1-e^{-K_D t}) + \int_0^t g(\chi(x,t;s),s)\,ds, \end{aligned} \tag{3.5.7}$$

where

$$g(\chi(x,t;s),s) = \int_0^s K_D e^{K_D(r-s)} u_a(\chi(x,t;r),r)\,dr. \tag{3.5.8}$$

As in section 3.1.2, g can be seen as a function of x_0. In section 3.1.2, we proved that $\partial_x u$ can be written along the characteristics as

$$\partial_x u = \frac{\partial u}{\partial x_0}\frac{1}{\frac{\partial x}{\partial x_0}} \tag{3.5.9}$$

as long as the characteristics do not intersect. From (3.5.6), we get

$$\begin{aligned} \frac{\partial u}{\partial x_0}(\chi(x,t;s),s) &= u_0'(x_0)e^{-K_D t} + \partial_{x_0}\Big(\int_0^s K_D e^{K_D(r-s)} u_a(\chi(x,t;r),r)dr\Big) \\ &= u_0'(x_0)e^{-K_D t} + \frac{\partial g}{\partial x_0}(\chi(x,t;s),s). \end{aligned} \tag{3.5.10}$$

From (3.5.7), we calculate

$$\begin{aligned} \frac{\partial x}{\partial x_0} &= 1 + \frac{u_0'(x_0)}{K_D}(1-e^{-K_D t}) + \partial_{x_0}\Big(\int_0^t g(\chi(x,t;s),s)ds\Big) \\ &= 1 + \frac{u_0'(x_0)}{K_D}(1-e^{-K_D t}) + \int_0^t \frac{\partial g}{\partial x_0}(\chi(x,t;s),s)ds. \end{aligned} \tag{3.5.11}$$

Thus, (3.5.9) gives

$$\begin{aligned} \partial_x u &= \frac{\partial u}{\partial x_0}\frac{1}{\frac{\partial x}{\partial x_0}} \\ &= \frac{u_0'(x_0)e^{-K_D t} + \frac{\partial g}{\partial x_0}(\chi(x,t;s),s)}{1 + \frac{u_0'(x_0)}{K_D}(1-e^{-K_D t}) + h(x_0,t)}, \end{aligned} \tag{3.5.12}$$

where

$$h(x_0,t)=\int_0^t \frac{\partial g}{\partial x_0}(\chi(x,t;s),s)\,ds. \tag{3.5.13}$$

Recall also that the first equation of (E) can be written along the characteristics as

$$\frac{D\alpha}{dt}=-\alpha\partial_x u. \tag{3.5.14}$$

Substituting (3.5.12) in (3.5.14), this latter equation leads to

$$\frac{D\alpha}{dt}\big(\chi(x,t;s),s\big)=-\alpha\frac{u_0'(x_0)e^{-K_Dt}+\dfrac{\partial g}{\partial x_0}\big(\chi(x,t;s),s\big)}{1+\frac{u_0'(x_0)}{K_D}(1-e^{-K_Dt})+h(x_0,t)}. \tag{3.5.15}$$

Assuming $\alpha\neq 0$ and for $s=t$, we divide by α and integrate (3.5.15) on both sides from 0 to t to obtain

$$\log\big(\alpha(x,t)\big)=\log\big(\alpha_0(x_0)\big)-\log\big(1+\frac{u_0'(x_0)}{K_D}(1-e^{-K_Dt})+h(x_0,t)\big)+\log\big(1+h(x_0,0)\big).$$

This last equation gives rise to

$$\alpha\big(x,t\big)=\frac{\big(1+h(x_0,0)\big)\alpha_0(x_0)}{1+\frac{u_0'(x_0)}{K_D}(1-e^{-K_Dt})+h(x_0,t)}. \tag{3.5.16}$$

We show in the same way as in the proof of proposition 3.1.1 that α and $\partial_x u$ blow up simultaneously if and only if

$$u_0'(x_0)=-\frac{K_D\big(1+h(t,x_0)\big)}{1-e^{-K_Dt}} \tag{3.5.17}$$

for some x_0 in the domain. In particular, if the air velocity u_a is constant then $h\equiv 0$ and we recover all the results that we have established in proposition 3.1.1 for u_a constant.

In general, equation (3.5.17) states that the loss of regularity for a smooth initial solution of the Eulerian droplet model (E) and (3.5.1) depends on the slope of the initial velocity with respect to the air velocity and the drag coefficient. For a non constant air velocity, it is hard to integrate along the characteristics and we are not able to derive an explicit expression for this condition. The solution of the Riemann problem can also not be established for the same reason. These are some difficulties encountered when studying the Eulerian droplet model with a non-constant air velocity. This explains why we have assumed the air velocity to be constant in the previous sections.

3.6 Numerical results

In this section, we present some numerical results to illustrate the theoretical analysis of delta shock waves and vacuum states for the Eulerian droplet model (E). All the numerical solutions are computed using the Transport-Collapse method (see section 2.3).

3.6.1 Riemann problem for (E): Exact vs numerical solutions

This test case is devoted to the comparison of the numerical and exact solutions of the Riemann problem for (E). We look at the solution on the whole real line. However, we solve (E) on the bounded domain $[-0.5, 2.5]$. We impose a zero slope for each variable on the inlet boundary $x = -0.5$ and the outlet boundary $x = 2.5$ of the computational domain. The drag coefficient is $K_D = 0.2$ and the air velocity $u_a = 1$.

Firstly, we take the following Riemann initial conditions:

$$\big(\alpha, u\big)(x,0) = \begin{cases} (0.8, 1.5), & x \leqslant 0, \\ (0.3, 0.5), & x > 0, \end{cases} \tag{3.6.1}$$

which correspond to the physical case where initially the droplets at the left of the origin move faster. We numerically solve the GRH conditions (3.4.9) satisfying the initial conditions $\omega_0 = 0$ and σ_0 given by (3.4.48) with the forward Euler time-stepping scheme with a small time step to ensure accuracy and stability. This allows us to get a numerical approximation for the weighted ω, the speed σ and the location $x = \xi$ of the delta shock wave, and thus to calculate the "exact solution" for the Riemann problem. Exact and numerical solutions are shown in Figure 3.4. The droplets behind catch those in front resulting in a huge concentration of particles on the shock trajectory. This corresponds theoretically to the formation of a delta shock wave.

Secondly, we consider the Riemann initial data:

$$\big(\alpha, u\big)(x,0) = \begin{cases} (0.3, 1.0), & x \leqslant 0, \\ (0.8, 2.0), & x > 0, \end{cases} \tag{3.6.2}$$

which corresponds to the physical case where initially the droplets downstream of the origin move faster. The exact and numerical solutions are presented in Figure 3.5. We observe a left and right non-vacuum states of droplets delimiting a vacuum state and moving at a continuous velocity. This corresponds theoretically to two-contact-discontinuity solution with a vacuum state.

In both cases, the exact and numerical solutions match very well. This shows the efficiency of the numerical scheme for computing solutions involving delta shock waves.

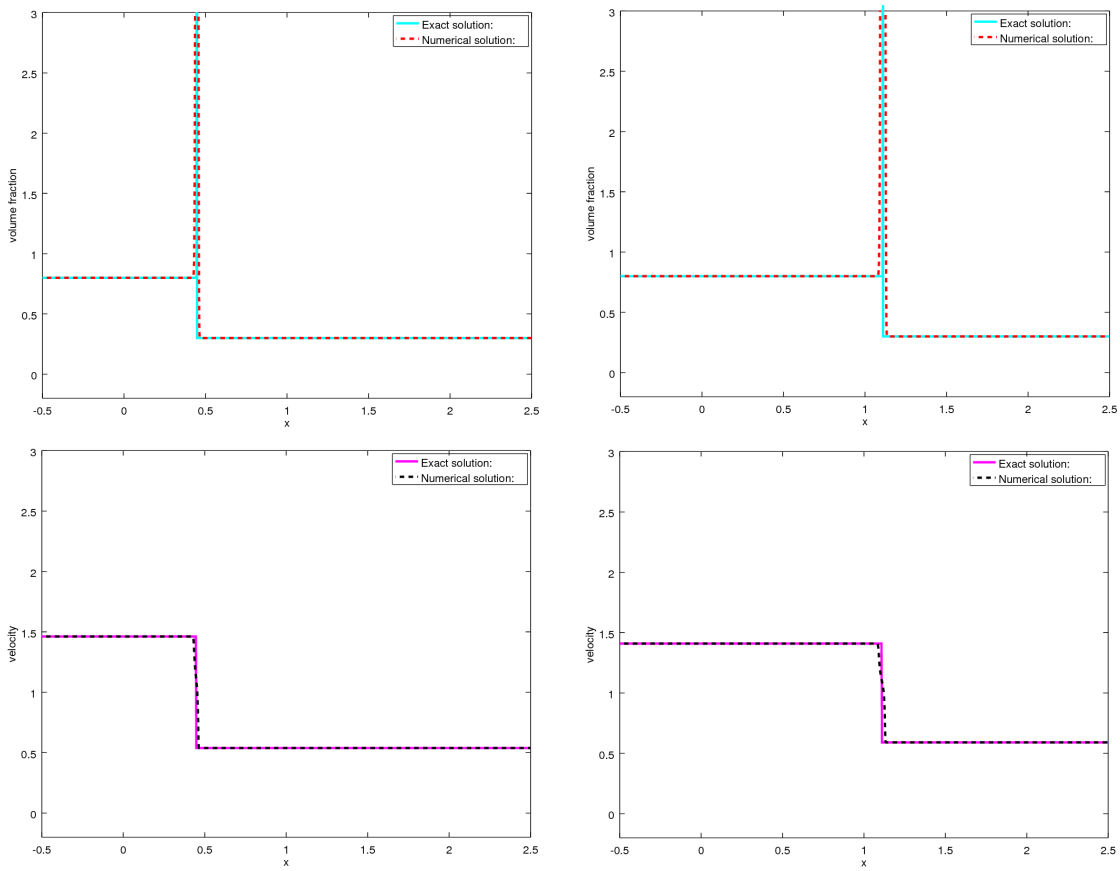

$t = 0.4$ $t = 1$

Figure 3.4: A delta shock wave of Model E: exact and numerical solutions in time. $K_D = 0.2$, $u_a = 1$, $\Delta x = 10^{-3}$ and $\Delta t = 10^{-4}$.

3.6.2 Impact of the source term on the solution

If there is no source term, i.e. $K_D \equiv 0$, system (E) reduces to the pressureless gas system for which the Riemann problem was solved in [82]. In this second test case, we compare the numerical solution of model (E) with/without the zeroth-order source term in order to highlight the impact of the zeroth-order source term on the solution. The computational domain and the boundary conditions are the same as in first test case. We take the air velocity $u_a = 5$, the drag coefficient $K_D = 1.5$ and the following Riemann initial data:

$$\big(\alpha, u\big)(x,0) = \begin{cases} (0.3, 2), & x \leqslant 0 \\ (0.8, 1), & x > 0. \end{cases} \tag{3.6.3}$$

Numerical results for $K_D = 0$ and $K_D = 1.5$ are displayed in Figure 3.6. The solutions

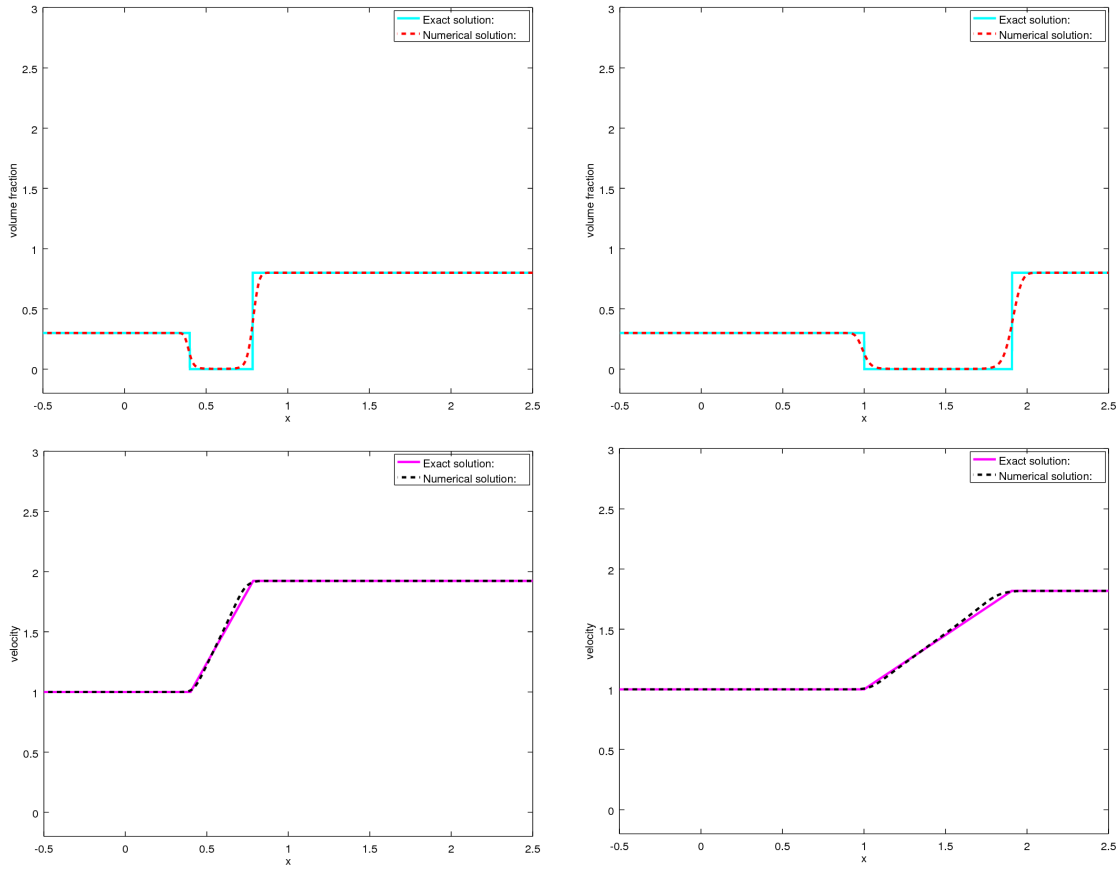

$t = 0.4$ $t = 1$

Figure 3.5: A two-contact-discontinuity solution with a vacuum state of Model E: exact and numerical solutions in time. $K_D = 0.2$, $u_a = 1$, $\Delta x = 10^{-3}$ and $\Delta t = 10^{-4}$.

shown are obtained numerically, hence delta shocks can only have limited amplitude. The amplitude of the delta shocks goes to infinity as the mesh is refined. We notice that the zeroth-order source term has significant impact on the solution. It acts as a relaxation term by weakening the weighted of the delta shock (seen as the difference in amplitude in the numerical solutions), affecting the propagation speed, and thus the location of the delta shock. It also affects the velocity solution. As one can see in Figure 3.7, the left and right states of the velocity are no longer constant over time and tend to the air velocity, which behaves as an equilibrium point.

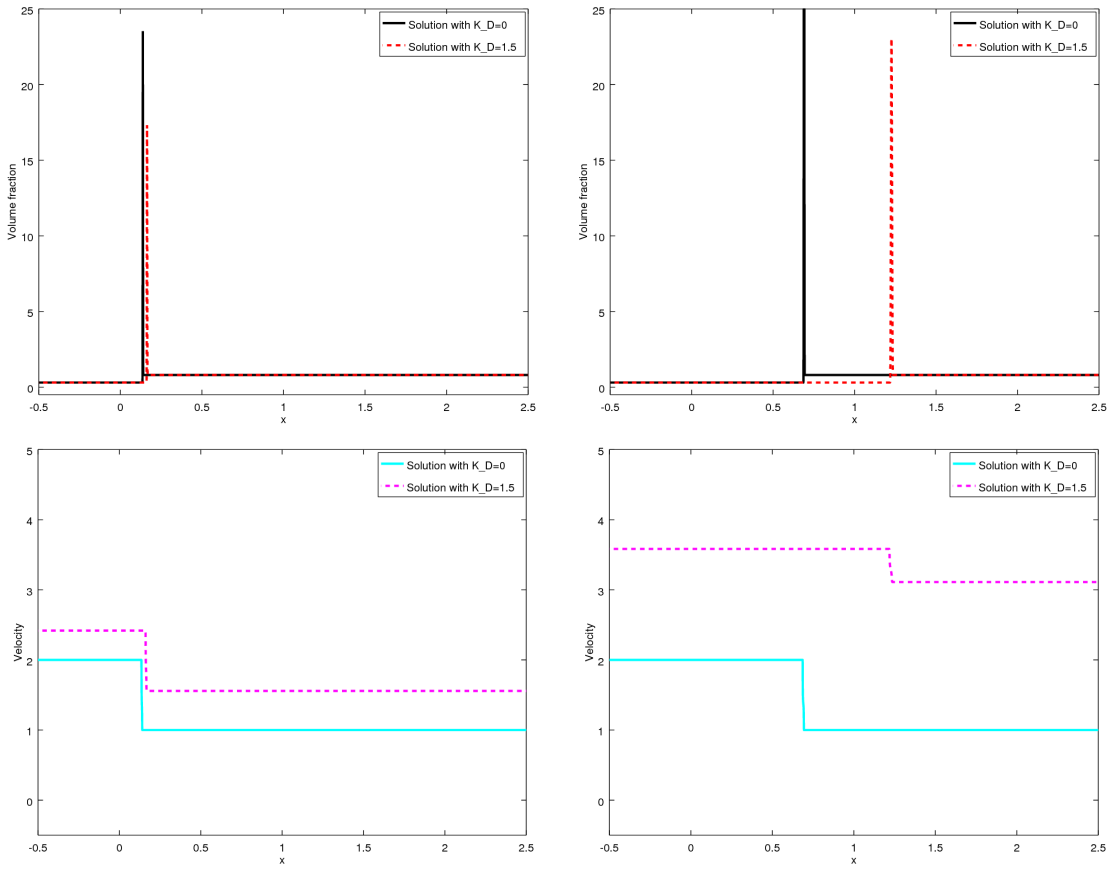

$t = 0.1$ $t = 0.5$

Figure 3.6: Evolution of a delta shock wave in Model E. Solution with/without the zeroth order source term. $u_a = 5$, $\Delta x = 10^{-4}$ and $\Delta t = 10^{-5}$.

3.7 Conclusion

In this chapter, we generalized the condition for loss of regularity for the inviscid Burgers equation and solved the Riemann problem associated to the Burgers equation with a zeroth-order source term. As for the classical inviscid Burgers equation, the solution of the Riemann problem is either a shock wave or a rarefaction wave but the characteristic curves are no longer straight lines. The left and right states are no longer constant and the Lax entropy condition degenerates as time goes to infinity.

It is already known that delta shock waves and vacuum states appear in the solution of the Riemann problem for the pressureless gas system [82]. The Rankine-Hugoniot conditions are no longer algebraic equations as for bounded shock waves but they form a system of linear ODEs of first order, which one can solve to obtain

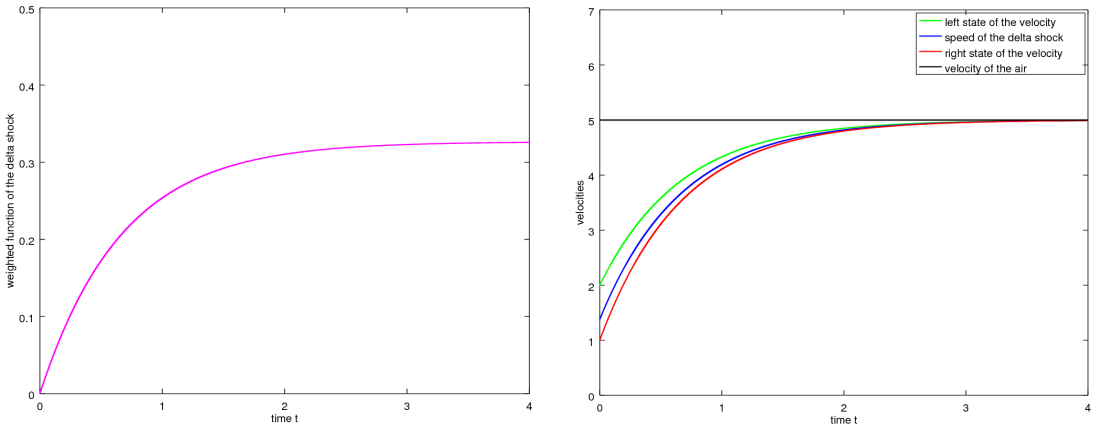

Figure 3.7: Numerical solution of the GRH conditions (3.4.9) with the initial conditions $\omega_0 = 0$ and σ_0 given (3.4.48) and the Riemann data (3.6.3). At left: weight of the delta shock. At right: velocities as a functions of time. $K_D = 1.5$ and $\Delta t = 10^{-4}$.

the shock speed and the weight of the delta shock [82]. In this chapter, we showed that delta shock waves and vacuum states also appear in the solution of the Riemann problem for system (E), which can be seen as the pressureless gas system with a zeroth-order linear source term. The Rankine-Hugoniot conditions for (E) are given by a nonlinear system of ODEs of first order that is hard or impossible to solve analytically. The difficulty in the analysis comes from the contribution of the source term which leads to characteristic curves that are no longer straight lines. The zeroth-order source term acts as a relaxation term by weakening the delta shocks.

In practice, α represents the volume fraction of droplets (or solid particles) and, therefore, it should be nonnegative and bounded. We showed that the volume fraction blows up for some choices of the initial velocity with respect to the air velocity and the drag coefficient. This blowup leads to unbounded volume fraction solution, and thus nonphysical solutions. Improvements are required in Model E to prevent nonphysical solutions to occur.

Chapter 4

Note on the isentropic Euler equations

The one-dimensional isentropic Euler equations of gas dynamics read as

$$\begin{cases} \partial_t \rho + \partial_x(\rho v) = 0, \\ \partial_t(\rho v) + \partial_x(\rho v^2 + p) = 0, \end{cases} \tag{IE}$$

where $\rho > 0$, v and p are the density, velocity and pressure of the gas, respectively. The pressure p is a function of the density and is determined from the constitutive thermodynamic relation of the gas under consideration. We restrict ourselves to polytropic perfect gases for which the state equation for the pressure is given by

$$p = p(\rho) = \kappa \rho^\gamma, \quad \kappa > 0, \ \gamma > 1. \tag{4.0.1}$$

System (IE) describes the isentropic flow of compressible fluids. There has been a great interest in the analysis of the isentropic Euler equation of gas dynamics [84, 25, 81, 31, 46, 23, 65]. In 2003, Chen and Liu [23] analyzed the behaviour of the solutions of the Riemann problem for the Euler equations (IE) and (4.0.1) when the pressure vanishes. The first goal of this chapter is to review the mechanisms of formation of delta shocks and vacuum states in the vanishing pressure limit of the isentropic Euler equations which can be seen as the Eulerian droplet model (E) without a source term. This helps to better understand the formation of delta shocks and vacuum states in the Eulerian droplet model, and thus to find a way of preventing the formation of delta shocks and vacuum states in the solutions of (E). Two cases were only partially covered by the analysis of Chen and Liu [23] in the vanishing pressure limit of the isentropic Euler equations, namely the 1-shock combined with the 2-rarefaction and the 1-rarefaction combined with the 2-shock wave. As far as we know, the proof and complete analysis of these two cases have not been discussed in the literature. The second goal of this chapter is to analyze the behaviour of these two cases in the vanishing pressure limit.

This chapter is organized as follows. In section 4.1, we establish the characteristic variables of system (IE) and (4.0.1). In section 4.2, we recall the relations for shock and rarefaction waves for the Riemann problem of (IE) and(4.0.1). In section 4.3, we analyze the behaviour of a solution composed of a 1-shock wave combined with a 2-rarefaction wave and a solution composed of a 1-rarefaction wave combined with a 2-shock wave, when the pressure coefficient vanishes. Numerical illustrations are carried out in section 4.4.

4.1 Hyperbolicity and characteristic variables

The isentropic Euler equations of gas dynamics (IE) and (4.0.1) can be written in quasilinear form as

$$\partial_t \mathbf{v} + J_{IE}(\mathbf{v})\partial_x \mathbf{v} = 0, \tag{4.1.1}$$

where $\mathbf{v} = (\rho, \rho v)^T$ and the Jacobian matrix J_{IE} is given by

$$J_{IE} = \begin{pmatrix} 0 & 1 \\ -v^2 + p'(\rho) & 2v \end{pmatrix}. \tag{4.1.2}$$

The eigenvalues of the Jacobian matrix are given by

$$\lambda_1(\rho, \rho v) = v - c \quad \text{and} \quad \lambda_2(\rho, \rho v) = v + c, \tag{4.1.3}$$

where

$$c = c(\rho) = \sqrt{p'(\rho)} = \sqrt{\kappa\gamma\rho^{\gamma-1}} \tag{4.1.4}$$

is called the *speed of sound*. A general set of eigenvectors associated to the eigenvalues (4.1.3) is given by

$$r_1(\rho, \rho v) = \beta_1 \begin{pmatrix} 1 \\ \lambda_1 \end{pmatrix} \quad \text{and} \quad r_2(\rho, \rho v) = \beta_2 \begin{pmatrix} 1 \\ \lambda_2 \end{pmatrix}, \tag{4.1.5}$$

where $\beta_1 = \beta_1(\rho, \rho v)$ and $\beta_2 = \beta_2(\rho, \rho v)$ are nonzero scalar functions. The Jacobian matrix (4.1.2) can be diagonalized by using the transformation matrix whose columns are given by the eigenvectors in (4.1.5), i.e. the Jacobian matrix can be written as $J_{IE} = P_{IE}\mathbf{\Lambda}_{IE}{P_{IE}}^{-1}$, where

$$P_{IE} = \begin{pmatrix} \beta_1 & \beta_2 \\ \beta_1\lambda_1 & \beta_2\lambda_2 \end{pmatrix} \quad \text{and} \quad \mathbf{\Lambda}_{IE} = \begin{pmatrix} \lambda_1 & 0 \\ 0 & \lambda_2 \end{pmatrix}. \tag{4.1.6}$$

Thus, the isentropic Euler equations (IE) and (4.0.1) form a *strictly hyperbolic* system (see Definition 2.1.5).

Assume that there exists $\boldsymbol{\phi} = (\phi_1, \phi_2)$ such that

$$d\boldsymbol{\phi} = {P_{IE}}^{-1} d\mathbf{v}, \tag{4.1.7}$$

where d is a differential operator that can be used as $d\phi_j = \partial_x \phi_j$ or $d\phi_j = \partial_t \phi_j$. On one hand, if we substitute the Jacobian matrix J_{IE} in (4.1.1) by $P_{IE}\boldsymbol{\Lambda}_{IE}{P_{IE}}^{-1}$ and take the differential operator $d\phi_j = \partial_x \phi_j$ in (4.1.7) we obtain

$$\partial_t \mathbf{v} + P_{IE}\boldsymbol{\Lambda}_{IE}\partial_x \boldsymbol{\phi} = 0. \tag{4.1.8}$$

We multiple equation (4.1.8) by ${P_{IE}}^{-1}$ from the left and take the differential operator $d\phi_j = \partial_t \phi_j$ in (4.1.7). This leads to the diagonalized system

$$\partial_t \boldsymbol{\phi} + \boldsymbol{\Lambda}_{IE}(\mathbf{v})\partial_x \boldsymbol{\phi} = 0. \tag{4.1.9}$$

On the other hand, expanding (4.1.7) directly gives rise to

$$\begin{aligned} d\phi_1 &= \frac{1}{2c\beta_1\beta_2}\big((v+c)\beta_2 d\rho - \beta_2 d(\rho v)\big) = \frac{1}{2c\beta_1}\big(cd\rho - \rho dv\big), \\ d\phi_2 &= \frac{1}{2c\beta_1\beta_2}\big((c-v)\beta_1 d\rho + \beta_1 d(\rho v)\big) = \frac{1}{2c\beta_2}\big(cd\rho + \rho dv\big). \end{aligned} \tag{4.1.10}$$

In particular, for $\beta_1(\rho, \rho v) = -\beta_2(\rho, \rho v) = -\dfrac{\rho}{2c}$, these two last equations reduce to

$$d\phi_1 = dv - \frac{c}{\rho}d\rho \quad \text{and} \quad d\phi_2 = dv + \frac{c}{\rho}d\rho, \tag{4.1.11}$$

respectively. Rewrite the term $\frac{c}{\rho}d\rho$ as dg with

$$g : \rho \mapsto \int \frac{c(\rho)}{\rho}\, d\rho. \tag{4.1.12}$$

Equation (4.1.11) gives rise to

$$d\phi_1 = dv - dg = d(v-g) \quad \text{and} \quad d\phi_2 = dv + dg = d(v+g). \tag{4.1.13}$$

These equations are easy to integrate. By using (4.1.4), we find

$$\phi_1 = v - g = v - \frac{2}{\gamma - 1}c \quad \text{and} \quad \phi_2 = v + g = v + \frac{2}{\gamma - 1}c. \tag{4.1.14}$$

We check by a straightforward calculation that $\boldsymbol{\phi} = (\phi_1, \phi_2)$ given by (4.1.14) satisfies (4.1.7). The variables ϕ_j are called *characteristic variables* [64]. Finally, the isentropic Euler equations for gas dynamics (IE) and (4.0.1) can be rewritten as

$$\begin{cases} \partial_t \phi_1 + (v-c)\partial_x \phi_1 = 0, \\ \partial_t \phi_2 + (v+c)\partial_x \phi_2 = 0. \end{cases} \tag{4.1.15}$$

System (4.1.15) means that each characteristic variable $\phi_j = (-1)^j \frac{2}{\gamma-1}c + v$ is simply advected at speed λ_j as time evolves, i.e. the quantity ϕ_j is constant along the j-characteristic field $\chi_j(x, t; .)$ (see definition 2.1.7).

4.2 Solution of the Riemann problem

The Riemann problem for the isentropic Euler equation for gas dynamics consists of system (IE) and (4.0.1) with the Riemann initial data

$$(\rho, v)(x,0) = \begin{cases} (\rho_-, v_-), & x < 0, \\ (\rho_+, v_+), & x > 0, \end{cases} \tag{4.2.1}$$

where ρ_-, $\rho_+ \in \mathbb{R}^+$ and v_-, $v_+ \in \mathbb{R}$, are given constants. The solution of this problem was established in [84, 25]. We recall this solution since it is needed below.

4.2.1 Rarefaction wave curves

We seek a solution of the form $\big(\rho, \rho v\big)(x,t) = \big(\rho, \rho v\big)(\xi)$, where $\xi = \dfrac{x}{t}$. A solution of this form is called *self-similar solution*. The system (IE) can be written in term of the new variables $\rho(\xi)$ and $\rho(\xi)v(\xi)$ as

$$\begin{cases} -\xi\rho_\xi + (\rho v)_\xi = 0, \\ -\xi(\rho v)_\xi + (\rho v^2 + p)_\xi = 0, \end{cases} \tag{4.2.2}$$

which can be written in the condensed form

$$(J_{IE} - \xi I)\mathbf{v}_\xi = 0. \tag{4.2.3}$$

This last equation leads either to the general solution

$$\mathbf{v}_\xi = 0 \Longrightarrow \mathbf{v}(\xi) = \big(\rho, \rho v\big)(\xi) = const, \tag{4.2.4}$$

or to the relation

$$J_{IE}\mathbf{v}_\xi = \xi\mathbf{v}_\xi, \tag{4.2.5}$$

which means that ξ is an eigenvalue of the Jacobian matrix J_{IE} with a corresponding eigenvector $\mathbf{v}_\xi$. From (4.1.3), we have

$$\xi = \lambda_j = (-1)^j c + v, \quad j = 1, 2. \tag{4.2.6}$$

A continuous self-similar solution $\big(\rho(\xi), v(\xi)\big)$, where ξ satisfies (4.2.6), is called a *j-rarefaction wave* [81].

Given a state (ρ_-, v_-), we look for the set of states (ρ_*, v_*) that can be connected from the left to the state (ρ_-, v_-) by a 1-rarefaction wave. The states (ρ_*, v_*) depend on the pressure p which is parametrized by the parameter κ. Therefore, in the following, these states are denoted by $(\rho_*^\kappa, v_*^\kappa)$. A straightforward calculation shows that

$$\nabla\phi_2 \cdot r_1 = \nabla\phi_1 \cdot r_2 = 0, \tag{4.2.7}$$

where ϕ_j is given in (4.1.14), r_j is given in (4.1.5) with $\beta_1 = -\beta_2 = -\dfrac{\rho}{2c}$. Note that in this section, the gradient operator is with respect to the conservative variables ρ and ρv. Hence, from Definition 2.1.8, a j-Riemann invariant φ_j for the isentropic Euler equations (IE) and (4.0.1) is given by

$$\varphi_j = \phi_{j+(-1)^{j+1}}, \quad j = 1, 2. \tag{4.2.8}$$

Recall that in a j-rarefaction wave, a j-Riemann invariant is constant (see [81], theorem 3.2). Hence, we have $\varphi_1(\rho_-, \rho_- v_-) = \varphi_1(\rho_*^\kappa, \rho_*^\kappa v_*^\kappa)$ which implies that

$$v_*^\kappa = v_- + \frac{2}{\gamma - 1}(c_- - c_*^\kappa), \tag{4.2.9}$$

where $c_- = c(\rho_-)$ and $c_*^\kappa = c(\rho_*^\kappa)$. For a 1-rarefaction, we get from (4.2.6) that $\xi = \frac{x}{t} = \lambda_1$. As ξ increases from the left to the right, λ_1 also increases in this way. Therefore,

$$\lambda_1(\rho_-, \rho_- v_-) < \lambda_1(\rho_*^\kappa, \rho_*^\kappa v_*^\kappa) \Longleftrightarrow v_- - c_- < v_*^\kappa - c_*^\kappa. \tag{4.2.10}$$

Combining (4.2.9) and (4.2.10), we get

$$\frac{\gamma + 1}{\gamma - 1} c_- > \frac{\gamma + 1}{\gamma - 1} c_*^\kappa, \tag{4.2.11}$$

which implies that $\rho_*^\kappa < \rho_-$ since the function $\rho \mapsto c(\rho)$ is increasing due to condition (4.0.1). Hence, the state $(\rho_*^\kappa, v_*^\kappa)$ satisfies

$$v_*^\kappa = v_- + \frac{2}{\gamma - 1}(c_- - c_*^\kappa) = v_- + \frac{2\sqrt{\kappa\gamma}}{\gamma - 1}\big(\rho_-^{\frac{\gamma-1}{2}} - (\rho_*^\kappa)^{\frac{\gamma-1}{2}}\big), \quad \rho_*^\kappa < \rho_-. \tag{4.2.12}$$

In the same way, we find the set of states $(\rho_*^\kappa, v_*^\kappa)$ that can be connected from the right to a given state (ρ_+, v_+) by a 2-rarefaction wave. We obtain

$$v_*^\kappa = v_+ - \frac{2\sqrt{\kappa\gamma}}{\gamma - 1}\big(\rho_+^{\frac{\gamma-1}{2}} - (\rho_*^\kappa)^{\frac{\gamma-1}{2}}\big), \quad \rho_*^\kappa < \rho_+. \tag{4.2.13}$$

4.2.2 Shock wave curves

Now we look for discontinuous solutions, particularly for shock waves. A j-shock wave is characterized by a curve $x = \xi_j(t)$ in the x-t plane across which the variables are discontinuous with finite jump. The eigenvalues (4.1.3) of system (IE) and (4.0.1) satisfy

$$\begin{aligned} \nabla\lambda_1 \cdot r_1 &= -\big(c' + \frac{c}{\rho}\big)\beta_1 = -\frac{(\gamma + 1)\beta_1}{2}\sqrt{\kappa\gamma\rho^{\gamma-3}} \neq 0, \\ \nabla\lambda_2 \cdot r_2 &= \big(c' + \frac{c}{\rho}\big)\beta_2 = \frac{(\gamma + 1)\beta_2}{2}\sqrt{\kappa\gamma\rho^{\gamma-3}} \neq 0. \end{aligned} \tag{4.2.14}$$

Hence, the two characteristics fields of the isentropic Euler equations are *genuinely nonlinear* (see Definition 2.1.7). Recall that for conservation laws with genuinely nonlinear characteristic fields, discontinuous solutions are shock waves [64]. An admissible j-shock wave solution will satisfy the *Rankine-Hugoniot conditions* [64] which are given for (IE) and (4.0.1) by

$$\sigma_j = \frac{\rho_r v_r - \rho_l v_l}{\rho_r - \rho_l}, \quad \sigma_j = \frac{\rho_r v_r^2 + \kappa {\rho_r}^\gamma - \rho_l v_l^2 - \kappa {\rho_l}^\gamma}{\rho_r v_r - \rho_l v_l}, \tag{4.2.15}$$

where (ρ_l, v_l) and (ρ_r, v_r) are the limit of the solution (ρ, v) when x approaches the shock curve $\xi_j(t)$ from the left and right, respectively, and $\sigma_j = \xi_j'(t)$ is the propagation speed of the j-shock wave. In addition, this shock speed σ_j satisfies the *Lax entropy conditions* [64]

$$\lambda_j(\rho_r, \rho_r v_r) < \sigma_j < \lambda_j(\rho_l, \rho_l v_l). \tag{4.2.16}$$

Given a state (ρ_-, v_-), we look for the set of states $(\rho_*^\kappa, v_*^\kappa)$ that can be connected from the left to the state (ρ_-, v_-) by a 1-shock wave. On one hand, the Rankine-Hugoniot conditions (4.2.15) lead to

$$v_*^\kappa = v_- \pm \sqrt{\frac{\kappa\big((\rho_*^\kappa)^\gamma - {\rho_-}^\gamma\big)}{\rho_*^\kappa \rho_-(\rho_*^\kappa - \rho_-)}}(\rho_*^\kappa - \rho_-). \tag{4.2.17}$$

On the other hand, the Lax entropy condition (4.2.16) leads to

$$\begin{aligned} v_*^\kappa - c_*^\kappa < \frac{\rho_*^\kappa v_*^\kappa - \rho_- v_-}{\rho_*^\kappa - \rho_-} < v_- - c_- &\Longrightarrow -\frac{c_*^\kappa}{\rho_-} < \frac{v_*^\kappa - v_-}{\rho_*^\kappa - \rho_-} < -\frac{c_-}{\rho_*^\kappa} \\ &\Longrightarrow \rho_*^\kappa c_*^\kappa > \frac{\rho_*^\kappa \rho_-(v_- - v_*^\kappa)}{\rho_*^\kappa - \rho_-} > \rho_- c_-, \end{aligned} \tag{4.2.18}$$

which implies that $\rho_*^\kappa > \rho_-$ since the function $\rho \mapsto \rho c(\rho)$ is positive and strictly increasing. Hence, (4.2.17) reduces to

$$v_*^\kappa = v_- - \sqrt{\frac{\kappa\big((\rho_*^\kappa)^\gamma - {\rho_-}^\gamma\big)}{\rho_*^\kappa \rho_-(\rho_*^\kappa - \rho_-)}}(\rho_*^\kappa - \rho_-), \quad \rho_*^\kappa > \rho_-. \tag{4.2.19}$$

In an analogous way, we find that the state $(\rho_*^\kappa, v_*^\kappa)$ that can be connected from the right to a given state (ρ_+, v_+) by a 2-shock, is given by

$$v_*^\kappa = v_+ + \sqrt{\frac{\kappa\big({\rho_+}^\gamma - (\rho_*^\kappa)^\gamma\big)}{\rho_+ \rho_*^\kappa(\rho_+ - \rho_*^\kappa)}}(\rho_*^\kappa - \rho_+), \quad \rho_*^\kappa > \rho_+. \tag{4.2.20}$$

4.2.3 Intermediate states of the Riemann solution

A solution of the Riemann problem for the isentropic Euler equation (IE) is composed of three constant states connected by either rarefaction or shock waves. The left and right states are uniquely determined by the initial data. There are four possible configurations for a solution of the Riemann problem, depending on the initial data. For more details, we refer to [84, 25]. We shall be content here to determine the intermediate state $(\rho_*^\kappa, v_*^\kappa)$ between the left and right states for each of the four possible configurations of the solution which are listed below:

1) 1-*rarefaction and* 2-*rarefaction waves:*
For a 1-rarefaction and 2-rarefaction waves Riemann solution, the intermediate state for the velocity v_*^κ satisfies both (4.2.12) and (4.2.13). Combining these two equations, we get the intermediate state for the density

$$\rho_*^\kappa = \Big(\frac{\frac{\gamma-1}{2}(v_- - v_+) + \sqrt{\kappa\gamma}(\rho_-^{\frac{\gamma-1}{2}} + \rho_+^{\frac{\gamma-1}{2}})}{2\sqrt{\kappa\gamma}}\Big)^{\frac{2}{\gamma-1}}. \tag{4.2.21}$$

From this, one can determine v_*^κ from (4.2.12) or (4.2.13).

2) 1-*rarefaction and* 2-*shock waves:*
For a 1-rarefaction and 2-shock wave Riemann solution, the intermediate state for the velocity v_*^κ satisfies both (4.2.12) and (4.2.20). Combining these two equations, we obtain the following nonlinear equation for the intermediate state for the density

$$v_- - v_+ + \frac{2}{\gamma-1}\sqrt{\kappa\gamma}\big(\rho_-^{\frac{\gamma-1}{2}} - (\rho_*^\kappa)^{\frac{\gamma-1}{2}}\big) - \sqrt{\frac{\kappa\big({\rho_+}^\gamma - (\rho_*^\kappa)^\gamma\big)}{\rho_*^\kappa\rho_+(\rho_+ - \rho_*^\kappa)}}(\rho_*^\kappa - \rho_+) = 0. \tag{4.2.22}$$

Once ρ_*^κ is found then v_*^κ can be calculated using either (4.2.12) or (4.2.20).

3) 1-*shock and* 2-*shock waves:*
For a 1-shock and 2-shock wave Riemann solution, the intermediate state for the velocity v_*^κ satisfies both (4.2.19) and (4.2.20) leading to the nonlinear equation for the intermediate state for the density

$$v_- - v_+ - \sqrt{\frac{\kappa\big((\rho_*^\kappa)^\gamma - \rho_-^\gamma\big)}{\rho_*^\kappa\rho_-(\rho_*^\kappa - \rho_-)}}(\rho_*^\kappa - \rho_-) - \sqrt{\frac{\kappa\big({\rho_+}^\gamma - (\rho_*^\kappa)^\gamma\big)}{\rho_*^\kappa\rho_+(\rho_+ - \rho_*^\kappa)}}(\rho_*^\kappa - \rho_+) = 0. \tag{4.2.23}$$

Once ρ_*^κ is obtained, one can calculate v_*^κ using (4.2.19) or (4.2.20).

4) 1-*shock and* 2-*rarefaction waves:*

For a 1-shock and a 2-rarefaction wave solution, the intermediate state for the velocity v_*^κ satisfies both (4.2.13) and (4.2.19) leading to the nonlinear equation for the intermediate state for the density

$$v_- - v_+ - \sqrt{\frac{\kappa\big((\rho_*^\kappa)^\gamma - \rho_-^\gamma\big)}{\rho_*^\kappa \rho_-(\rho_*^\kappa - \rho_-)}}(\rho_*^\kappa - \rho_-) - \frac{2}{\gamma-1}\sqrt{\kappa\gamma}\big((\rho_*^\kappa)^{\frac{\gamma-1}{2}} - \rho_+^{\frac{\gamma-1}{2}}\big) = 0. \quad (4.2.24)$$

Once ρ_*^κ is determined, v_*^κ can be calculated from (4.2.19) or (4.2.13).

Thus, the intermediate state (except for a 1-rarefaction and 2-rarefaction situation) is given by a nonlinear equation which is usually solved numerically, for instance using Newton's method.

4.3 Behaviour of solutions of the Riemann problem in the vanishing pressure limit

Formally, the limit system of the isentropic Euler equations as the pressure vanishes forms the pressureless gas system

$$\begin{cases} \partial_t \rho + \partial_x(\rho v) = 0, \\ \partial_t(\rho v) + \partial_x(\rho v^2) = 0. \end{cases} \quad (4.3.1)$$

This system models the motion of free particles that stick under collision [10, 9, 82, 23, 11, 70]. It has been extensively analyzed, see for instance [9, 18, 82, 69, 11, 70, 36]. Bouchut [9] first established the existence of measure solutions of the Riemann problem. The problem with the Riemann data (4.2.1) was solved by Sheng and Zhang [82]. In the case $v_- < v_+$, the Riemann solution consists of two contact discontinuities and a vacuum state, that is

$$(\rho, v)(x,t) = (\rho, v)(\frac{x}{t}) = \begin{cases} (\rho_-, v_-), & -\infty < \dfrac{x}{t} \leqslant v_-, \\ (0, v(\dfrac{x}{t})), & v_- \leqslant \dfrac{x}{t} \leqslant v_+, \\ (\rho_+, v_+), & v_+ \leqslant \dfrac{x}{t} < \infty, \end{cases} \quad (4.3.2)$$

where $v(\frac{x}{t})$ is any smooth function satisfying $v(v_\pm) = v_\pm$. In the case $v_- > v_+$, the Riemann solution is given by a δ-shock wave, that is

$$(\rho, v)(x,t) = \begin{cases} (\rho_-, v_-), & -\infty < x < \sigma t, \\ (\omega(t)\delta(x - \sigma t), \sigma), & x = \sigma t, \\ (\rho_+, v_+), & \sigma t < x < \infty, \end{cases} \quad (4.3.3)$$

where

$$\sigma = \frac{\sqrt{\rho_-}v_+ + \sqrt{\rho_+}v_+}{\sqrt{\rho_-} + \sqrt{\rho_+}}, \qquad \omega(t) = \frac{t}{\sqrt{1+\sigma^2}}\big((\rho_+v_+ - \rho_-v_-) - \sigma(\rho_+ - \rho_-)\big)$$

and δ is the Dirac delta distribution centered at the origin. For more details, we refer to the previous chapter and [82].

In 2003, Chen and Liu [23] identified and analyzed the formation of δ-shock waves and vacuum states in Riemann solutions to the system (IE) and (4.0.1) as the pressure vanishes. They considered vanishing viscosity solutions and established the two following results.

Theorem 4.3.1. *Let $v_- > v_+$. For sufficiently small and positive $\kappa > 0$, assume that $(\rho^\kappa, \rho^\kappa v^\kappa)$ is a 1-shock wave and 2-shock wave solution of* (IE) *and* (4.0.1) *with Riemann data* (4.2.1). *Then, when $\kappa \to 0$, ρ^κ and $\rho^\kappa v^\kappa$ converge in the sense of distributions, and the limit solutions ρ and ρv are sums of a step function and a δ-measure with weights*

$$\frac{t}{1+\sigma^2}\big(\sigma(\rho_+ - \rho_-) - (\rho_+v_+ - \rho_-v_-)\big) \quad \textit{and} \quad \frac{t}{1+\sigma^2}\big(\sigma(\rho_+v_+ - \rho_-v_-) - (\rho_+v_+^2 - \rho_-v_-^2)\big),$$

respectively, which form the δ-shock solution (4.3.3) *of the pressureless gas system* (4.3.1) *with the same Riemann data.*

Proof: See the proof of theorem 3.1 in [23]. ∎

Theorem 4.3.2. *Let $v_- < v_+$ and $\rho_\pm > 0$. Assume that $(\rho^\kappa, \rho^\kappa v^\kappa)$ is a 1-rarefaction wave and 2-rarefaction wave solution of* (IE) *and* (4.0.1) *with Riemann data* (4.2.1). *Then, when $\kappa \to 0$, the solution $(\rho^\kappa, \rho^\kappa v^\kappa)$ tends to a two-contact discontinuity solution* (4.3.2) *of the pressureless gas system* (4.3.1) *with the same initial data.*

Proof: See section 4, in [23]. ∎

These two results show rigorously that any two-shock Riemann solution of the Euler equations for isentropic fluids (IE) and (4.0.1) tends to a δ-shock solution of the Euler equations for pressureless fluids (4.3.1), and the intermediate density between the two shocks tends to a weighted δ-measure that forms a δ-shock. By contrast, any two-rarefaction Riemann solution of the Euler equations for isentropic fluids (IE) and (4.0.1) tends to a two-contact-discontinuity solution of the Euler equations for pressureless fluids (4.3.1), whose intermediate state between the two contact discontinuities is a vacuum state even when the initial data stays away from the vacuum.

These results were also extended to nonisentropic flows [24], to the relativistic Euler equations for polytropic gases [96], and recently to the modified Chaplygin gas

pressure law [95]. These papers only cover solutions that contain two shocks or two rarefactions waves.

Without giving details, Chen and Liu [23] also mentioned that the behaviour of the Riemann solution for the two others possible configurations of the Riemann problem, namely a 1-shock wave combined with a 2-rarefaction wave and a 1-rarefaction wave combined with a 2-shock wave, can be deduced from the two above cases. Since the proofs in these situations are non trivial, we provide a complete proof.

4.3.1 Behaviour of a 1-shock and 2-rarefaction solution in the vanishing pressure limit

Let $v_- > v_+$ and $\rho_\pm > 0$. For $\kappa > 0$, let $(\rho_*^\kappa, \rho_*^\kappa v_*^\kappa)$ be the intermediate state of a solution $(\rho^\kappa, \rho^\kappa v^\kappa)$ of the system (IE) and (4.0.1) with Riemann data (4.2.1), in the sense that v_- and v_*^κ are connected by a 1-shock wave, and v_*^κ and u_+ are connected by a 2-rarefaction wave. Then, this intermediate state is determined by (4.2.13) and (4.2.19), from which we immediately deduce that $\rho_+ > \rho_-$. The following results also hold.

Lemma 4.3.3.

$$v_- > v_*^\kappa > v_+, \forall \kappa \in (0, \kappa_{sr}), \ \textit{with } v_*^\kappa = v_+ \Leftrightarrow \kappa = \kappa_{sr} := \frac{\rho_-\rho_+(v_- - v_+)^2}{(\rho_+^\gamma - \rho_-^\gamma)(\rho_+ - \rho_-)}. \tag{4.3.4}$$

Proof: Let $\kappa > 0$. We first prove the equivalence in (4.3.4). Assume that $v_*^\kappa = v_+$. From (4.2.13), we get $\rho_*^\kappa = \rho_+$. Using the equalities $v_*^\kappa = v_+$ and $\rho_*^\kappa = \rho_+$ in (4.2.19), we obtain

$$v_+ - v_- = -\sqrt{\frac{\kappa\big(\rho_+^\gamma - {\rho_-}^\gamma\big)}{\rho_+\rho_-(\rho_+ - \rho_-)}}(\rho_+ - \rho_-) = -\sqrt{\frac{\kappa\big(\rho_+^\gamma - {\rho_-}^\gamma\big)(\rho_+ - \rho_-)}{\rho_+\rho_-}}$$

which implies, by taking the square on both sides, that

$$(v_+ - v_-)^2 = \frac{\kappa\big(\rho_+^\gamma - {\rho_-}^\gamma\big)(\rho_+ - \rho_-)}{\rho_+\rho_-}.$$

This last relation gives rise to $\kappa = \kappa_{sr}$. Conversely, suppose that $\kappa = \kappa_{sr}$. Then

$$v_- - v_+ = \sqrt{\frac{\kappa_{sr}\big(\rho_+^\gamma - {\rho_-}^\gamma\big)}{\rho_+\rho_-(\rho_+ - \rho_-)}}(\rho_+ - \rho_-). \tag{4.3.5}$$

We claim that $\rho_*^{\kappa_{sr}} = \rho_+$. In fact, assume that $\rho_*^{\kappa_{sr}} < \rho_+$. By combining (4.2.13) and (4.2.19), we obtain

$$v_- - v_+ = \sqrt{\frac{\kappa_{sr}\big((\rho_*^{\kappa_{sr}})^\gamma - \rho_-^\gamma\big)}{\rho_*^{\kappa_{sr}}\rho_-(\rho_*^{\kappa_{sr}} - \rho_-)}}(\rho_*^{\kappa_{sr}} - \rho_-) - \frac{2\sqrt{\kappa_{sr}\gamma}}{\gamma - 1}\big({\rho_+}^{\frac{\gamma-1}{2}} - (\rho_*^{\kappa_{sr}})^{\frac{\gamma-1}{2}}\big), \tag{4.3.6}$$

with $\rho_- < \rho_*^{\kappa_{sr}} < \rho_+$. Consider the function $h_1 : \rho \to (\rho^\gamma - \rho_-^\gamma)(1 - \frac{\rho_-}{\rho})$ which is strictly increasing since its derivative $h_1'(\rho) = \gamma\rho^{\gamma-1}(1 - \frac{\rho_-}{\rho}) + (\rho^\gamma - \rho_-^\gamma)\frac{\rho_-}{\rho^2} > 0$ for all $\rho > \rho_-$. We have:

$$
\begin{aligned}
h_1(\rho_+) > h_1(\rho_*^{\kappa_{sr}}) &\Longrightarrow \\
\frac{\big(\rho_+^\gamma - {\rho_-}^\gamma\big)(\rho_+ - \rho_-)}{\rho_+} &> \frac{\big((\rho_*^{\kappa_{sr}})^\gamma - {\rho_-}^\gamma\big)(\rho_*^{\kappa_{sr}} - \rho_-)}{\rho_*^{\kappa_{sr}}} \Longrightarrow \\
\frac{\kappa_{sr}\big(\rho_+^\gamma - {\rho_-}^\gamma\big)(\rho_+ - \rho_-)}{\rho_+\rho_-} &> \frac{\kappa_{sr}\big((\rho_*^{\kappa_{sr}})^\gamma - {\rho_-}^\gamma\big)(\rho_*^{\kappa_{sr}} - \rho_-)}{\rho_*^{\kappa_{sr}}\rho_-} \Longrightarrow \\
\sqrt{\frac{\kappa_{sr}\big(\rho_+^\gamma - {\rho_-}^\gamma\big)}{\rho_+\rho_-(\rho_+ - \rho_-)}}(\rho_+ - \rho_-) &> \sqrt{\frac{\kappa_{sr}\big((\rho_*^{\kappa_{sr}})^\gamma - {\rho_-}^\gamma\big)}{\rho_*^{\kappa_{sr}}\rho_-(\rho_*^{\kappa_{sr}} - \rho_-)}}(\rho_*^{\kappa_{sr}} - \rho_-) \\
&> \sqrt{\frac{\kappa_{sr}\big((\rho_*^{\kappa_{sr}})^\gamma - {\rho_-}^\gamma\big)}{\rho_*^{\kappa_{sr}}\rho_-(\rho_*^{\kappa_{sr}} - \rho_-)}}(\rho_*^{\kappa_{sr}} - \rho_-) - \frac{2\sqrt{\kappa_{sr}\gamma}}{\gamma - 1}\big({\rho_+}^{\frac{\gamma-1}{2}} - (\rho_*^{\kappa_{sr}})^{\frac{\gamma-1}{2}}\big).
\end{aligned}
$$

This last inequality implies that (4.3.5) and (4.3.6) cannot both be true. Hence, $\rho_*^{\kappa_{sr}} = \rho_+$. Using this equality in (4.2.19), we obtain

$$
v_- - v_*^{\kappa_{sr}} = \sqrt{\frac{\kappa_{sr}\big(\rho_+^\gamma - {\rho_-}^\gamma\big)}{\rho_+\rho_-(\rho_+ - \rho_-)}}(\rho_+ - \rho_-), \tag{4.3.7}
$$

which combined with (4.3.5) implies that $v_*^{\kappa_{sr}} = v_*^{\kappa} = v_+$. So, the equivalence in (4.3.4) holds.

From (4.2.19), we get

$$
v_*^{\kappa} - v_- = -\sqrt{\frac{\kappa\big((\rho_*^{\kappa})^\gamma - {\rho_-}^\gamma\big)}{\rho_*^{\kappa}\rho_-(\rho_*^{\kappa} - \rho_-)}}(\rho_*^{\kappa} - \rho_-) < 0.
$$

It remains to prove that $v_*^{\kappa} > v_+$ for all $\kappa \in (0, \kappa_{sr})$. We proceed by contradiction. Suppose there exists $\kappa_1 \in (0, \kappa_{sr})$ such that $v_*^{\kappa_1}$ and v_+ are connected by a 2-rarefaction wave. On the one hand, as $\kappa_1 < \kappa_{sr}$ then from the definition of κ_{sr} in (4.3.4), we get

$$
v_- - v_+ > \sqrt{\frac{\kappa_1\big(\rho_+^\gamma - {\rho_-}^\gamma\big)}{\rho_+\rho_-(\rho_+ - \rho_-)}}(\rho_+ - \rho_-). \tag{4.3.8}
$$

On the other hand, as the intermediate state $(\rho_*^{\kappa_1}, v_*^{\kappa_1})$ satisfies both (4.2.13) and (4.2.19), then

$$
v_- - v_+ = \sqrt{\frac{\kappa_1\big((\rho_*^{\kappa_1})^\gamma - {\rho_-}^\gamma\big)}{\rho_*^{\kappa_1}\rho_-(\rho_*^{\kappa_1} - \rho_-)}}(\rho_*^{\kappa_1} - \rho_-) - \frac{2\sqrt{\kappa_1\gamma}}{\gamma - 1}\big({\rho_+}^{\frac{\gamma-1}{2}} - (\rho_*^{\kappa_1})^{\frac{\gamma-1}{2}}\big), \tag{4.3.9}
$$

with $\rho_- < \rho_*^{\kappa_1} < \rho_+$. We have:

$$h_1(\rho_+) > h_1(\rho_*^{\kappa_1}) \Longrightarrow$$
$$\sqrt{\frac{\kappa_1\big(\rho_+^{\gamma} - \rho_-{}^{\gamma}\big)}{\rho_+\rho_-(\rho_+ - \rho_-)}}(\rho_+ - \rho_-) > \sqrt{\frac{\kappa_1\big((\rho_*^{\kappa_1})^{\gamma} - \rho_-{}^{\gamma}\big)}{\rho_*^{\kappa_1}\rho_-(\rho_*^{\kappa_1} - \rho_-)}}(\rho_*^{\kappa_1} - \rho_-)$$
$$> \sqrt{\frac{\kappa_1\big((\rho_*^{\kappa_1})^{\gamma} - \rho_-{}^{\gamma}\big)}{\rho_*^{\kappa_1}\rho_-(\rho_*^{\kappa_1} - \rho_-)}}(\rho_*^{\kappa_1} - \rho_-) - \frac{2\sqrt{\kappa_1\gamma}}{\gamma - 1}\big(\rho_+{}^{\frac{\gamma-1}{2}} - (\rho_*^{\kappa_1})^{\frac{\gamma-1}{2}}\big).$$

This last inequality implies that (4.3.8) and (4.3.9) cannot both be true. Hence, for all $\kappa \in (0, \kappa_{sr})$ then v_*^{κ} and v_+ are connected by a 2-shock wave. This implies that $v_*^{\kappa} > v_+$ for all $\kappa \in (0, \kappa_{sr})$. ∎

Theorem 4.3.4. *Let $v_- > v_+$ and $\rho_\pm > 0$. For some $\kappa > 0$, assume that $(\rho^\kappa, \rho^\kappa v^\kappa)$ is a 1-shock wave and 2-rarefaction wave solution of* (IE) *and* (4.0.1) *with the Riemann data* (4.2.1)*. Then, when $\kappa \to 0$, the solution $(\rho^\kappa, \rho^\kappa v^\kappa)$ tends to the δ-shock solution* (4.3.3) *of the pressureless gas system* (4.3.1) *with the same Riemann data.*

Proof: Lemma 4.3.3 says that the solution $(\rho^\kappa, \rho^\kappa v^\kappa)$ gives rise to a 1-shock wave and 2-shock wave solution of (IE) and (4.0.1) when κ gets smaller than κ_{sr}. From theorem 4.3.1, we conclude that, when $\kappa \to 0$, the solution $(\rho^\kappa, \rho^\kappa v^\kappa)$ tends to the δ-shock solution of (4.3.1) with the same initial data. ∎

Remark 4.3.5. *The coefficient κ_{sr} defined in* (4.3.4) *represents the critical value for which a 1-shock wave and 2-rarefaction wave solution of the isentropic Euler equation* (IE) *and* (4.0.1) *converts to a two-shock solution when the pressure coefficient κ decreases. We use the index sr for referring to the shock wave at the left and the rarefaction wave at the right.*

4.3.2 Behaviour of a 1-rarefaction and 2-shock solution in the vanishing pressure limit

Let $v_- < v_+$ and $\rho_\pm > 0$. For $\kappa > 0$, let $(\rho_*^\kappa, \rho_*^\kappa v_*^\kappa)$ be the intermediate state of a solution $(\rho^\kappa, \rho^\kappa v^\kappa)$ of (IE) and (4.0.1) with Riemann data (4.2.1) in the sense that v_- and v_*^κ are connected by a 1-rarefaction wave, and v_*^κ and u_+ are connected by a 2-shock wave. Then this intermediate state is determined by (4.2.12) and (4.2.20), which imply that $\rho_- > \rho_+$. The following results also hold.

Lemma 4.3.6.

$$v_- < v_*^\kappa < v_+, \forall \kappa \in (0, \kappa_{rs}), \text{ with } v_*^\kappa = v_+ \Leftrightarrow \kappa = \kappa_{rs} := \left(\frac{(v_+ - v_-)(\gamma - 1)}{2\sqrt{\gamma}(\rho_-^{\frac{\gamma-1}{2}} - \rho_+^{\frac{\gamma-1}{2}})} \right)^2. \tag{4.3.10}$$

Proof: Let $\kappa > 0$. We first prove the equivalence in (4.3.10). Assume that $v_*^\kappa = v_+$. Using this equality in (4.2.20), we get $\rho_*^\kappa = \rho_+$. Now take $v_*^\kappa = v_+$ and $\rho_*^\kappa = \rho_+$ in (4.2.12), we obtain

$$v_+ = v_- + \frac{2\sqrt{\kappa\gamma}}{\gamma - 1}(\rho_-^{\frac{\gamma-1}{2}} - \rho_+^{\frac{\gamma-1}{2}}), \tag{4.3.11}$$

which implies that $\kappa = \kappa_{rs}$. Conversely, suppose that $\kappa = \kappa_{rs}$. Then

$$v_+ - v_- = \frac{2\sqrt{\kappa_{rs}\gamma}}{\gamma - 1}(\rho_-^{\frac{\gamma-1}{2}} - \rho_+^{\frac{\gamma-1}{2}}). \tag{4.3.12}$$

We claim that $\rho_*^{\kappa_{rs}} = \rho_+$. In fact, assume that $\rho_+ < \rho_*^{\kappa_{rs}}$. Combining (4.2.12) and (4.2.20), we obtain

$$v_+ - v_- = \frac{2\sqrt{\kappa_{rs}\gamma}}{\gamma - 1}\big(\rho_-{}^{\frac{\gamma-1}{2}} - (\rho_*^{\kappa_{rs}})^{\frac{\gamma-1}{2}}\big) - \sqrt{\frac{\kappa_{rs}\big((\rho_*^{\kappa_{rs}})^\gamma - \rho_+^\gamma\big)}{\rho_*^{\kappa_{rs}}\rho_+(\rho_*^{\kappa_{rs}} - \rho_+)}}(\rho_*^{\kappa_{rs}} - \rho_+) \tag{4.3.13}$$

with $\rho_+ < \rho_*^{\kappa_{rs}} < \rho_-$. Consider the function $h_2 : \rho \to \rho^{\frac{\gamma-1}{2}} - \rho_-^{\frac{\gamma-1}{2}}$ which is strictly increasing since its derivative $h_2'(\rho) = \frac{\gamma-1}{2}\rho^{\frac{\gamma-3}{2}} > 0$ for all $\rho > 0$. We have:

$$\begin{aligned}
h_2(\rho_+) < h_2(\rho_*^{\kappa_{rs}}) &\Longrightarrow \\
\big(\rho_+^{\frac{\gamma-1}{2}} - \rho_-^{\frac{\gamma-1}{2}}\big) < \big((\rho_*^{\kappa_{rs}})^{\frac{\gamma-1}{2}} - \rho_-^{\frac{\gamma-1}{2}}\big) &\Longrightarrow \\
\big(\rho_-^{\frac{\gamma-1}{2}} - \rho_+^{\frac{\gamma-1}{2}}\big) > \big(\rho_-^{\frac{\gamma-1}{2}} - (\rho_*^{\kappa_{rs}})^{\frac{\gamma-1}{2}}\big) &\Longrightarrow \\
\frac{2\sqrt{\kappa_{rs}\gamma}}{\gamma - 1}\big(\rho_-^{\frac{\gamma-1}{2}} - \rho_+^{\frac{\gamma-1}{2}}\big) > \frac{2\sqrt{\kappa_{rs}\gamma}}{\gamma - 1}\big(\rho_-^{\frac{\gamma-1}{2}} - (\rho_*^{\kappa_{rs}})^{\frac{\gamma-1}{2}}\big) & \\
> \frac{2\sqrt{\kappa_{rs}\gamma}}{\gamma - 1}\big(\rho_-^{\frac{\gamma-1}{2}} - (\rho_*^{\kappa_{rs}})^{\frac{\gamma-1}{2}}\big) - \sqrt{\frac{\kappa_{rs}\big((\rho_*^{\kappa_{rs}})^\gamma - \rho_+{}^\gamma\big)}{\rho_*^{\kappa_{rs}}\rho_+(\rho_*^{\kappa_{rs}} - \rho_+)}}(\rho_*^{\kappa_{rs}} - \rho_+). &
\end{aligned}$$

This last inequality implies that (4.3.12) and (4.3.13) cannot both be true. Hence, $\rho_*^{\kappa_{rs}} = \rho_+$. Taking this equality in (4.2.12), we obtain

$$v_*^{\kappa_{rs}} - v_- = \frac{2\sqrt{\kappa_{rs}\gamma}}{\gamma - 1}(\rho_-^{\frac{\gamma-1}{2}} - \rho_+^{\frac{\gamma-1}{2}}), \tag{4.3.14}$$

which, combined with (4.3.12), implies that $v_*^\kappa = v_*^{\kappa_{sr}} = v_+$. So, the equivalence in (4.3.10) holds.

From (4.2.12), we get

$$v_*^\kappa - v_- = \frac{2\sqrt{\kappa\gamma}}{\gamma-1}\big(\rho_-{}^{\frac{\gamma-1}{2}} - (\rho_*^\kappa)^{\frac{\gamma-1}{2}}\big) > 0.$$

It remains to prove that $v_*^\kappa < v_+$ for all $\kappa \in (0, \kappa_{rs})$. We proceed by contradiction. Suppose that there exists $\kappa_2 \in (0, \kappa_{rs})$ such that $v_*^{\kappa_2}$ and v_+ are connected by a 2-shock wave. As $\kappa_2 < \kappa_{rs}$ then from the definition of κ_{rs} in (4.3.10), we get

$$v_+ - v_- > \frac{2\sqrt{\kappa_2\gamma}}{\gamma-1}(\rho_-^{\frac{\gamma-1}{2}} - \rho_+^{\frac{\gamma-1}{2}}). \tag{4.3.15}$$

As the intermediate state $(\rho_*^{\kappa_2}, v_*^{\kappa_2})$ satisfies both (4.2.12) and (4.2.20) then

$$v_+ - v_- = \frac{2\sqrt{\kappa_2\gamma}}{\gamma-1}\big(\rho_-{}^{\frac{\gamma-1}{2}} - (\rho_*^{\kappa_2})^{\frac{\gamma-1}{2}}\big) - \sqrt{\frac{\kappa_2\big((\rho_*^{\kappa_2})^\gamma - \rho_+{}^\gamma\big)}{\rho_*^{\kappa_2}\rho_+(\rho_*^{\kappa_2}-\rho_+)}}(\rho_*^{\kappa_2} - \rho_+) \tag{4.3.16}$$

with $\rho_+ < \rho_*^{\kappa_2} < \rho_-$. We have:

$$\begin{aligned} &h_2(\rho_+) < h_2(\rho_*^{\kappa_2}) \Longrightarrow \\ \frac{2\sqrt{\kappa_2\gamma}}{\gamma-1}\big(\rho_-^{\frac{\gamma-1}{2}} - \rho_+^{\frac{\gamma-1}{2}}\big) &> \frac{2\sqrt{\kappa_2\gamma}}{\gamma-1}\big(\rho_-^{\frac{\gamma-1}{2}} - (\rho_*^{\kappa_2})^{\frac{\gamma-1}{2}}\big) \\ &> \frac{2\sqrt{\kappa_2\gamma}}{\gamma-1}\big(\rho_-^{\frac{\gamma-1}{2}} - (\rho_*^{\kappa_2})^{\frac{\gamma-1}{2}}\big) - \sqrt{\frac{\kappa_2\big((\rho_*^{\kappa_2})^\gamma - \rho_+{}^\gamma\big)}{\rho_*^{\kappa_2}\rho_+(\rho_*^{\kappa_2}-\rho_+)}}(\rho_*^{\kappa_2} - \rho_+). \end{aligned}$$

This last inequality implies that (4.3.15) and (4.3.16) cannot both be true. Hence, for all $\kappa_2 \in (0, \kappa_{rs})$, the states $v_*^{\kappa_2}$ and v_+ are connected by a 2-rarefaction wave. This implies that $v_*^\kappa < v_+$ for all $\kappa \in (0, \kappa_{rs})$. ∎

Theorem 4.3.7. *Let $v_- < v_+$ and $\rho_\pm > 0$. For some $\kappa > 0$, assume that $(\rho^\kappa, \rho^\kappa v^\kappa)$ is a 1-rarefaction wave and 2-shock wave solution of* (IE) *and* (4.0.1) *with the Riemann initial data* (4.2.1)*. Then, when $\kappa \to 0$, the solution $(\rho^\kappa, \rho^\kappa v^\kappa)$ tends to the two-contact-discontinuity solution* (4.3.2) *of the pressureless gas system* (4.3.1) *with the same Riemann data.*

Proof: Lemma 4.3.6 says that the solution $(\rho^\kappa, \rho^\kappa v^\kappa)$ gives rise to a 1-rarefaction wave and 2-rarefaction wave solution of (IE) and (4.0.1) when κ gets smaller than κ_{rs}. From theorem 4.3.2, we conclude that, when $\kappa \to 0$, the solution $(\rho^\kappa, \rho^\kappa v^\kappa)$ tends to the two-contact-discontinuity solution of (4.3.1) with the same initial data. ∎

Remark 4.3.8. *The coefficient κ_{rs} defined in* (4.3.10) *represents the critical value for which a* 1*-rarefaction wave and* 2*-shock wave solution of the isentropic Euler equation* (IE) *and* (4.0.1) *converts to a two-rarefaction solution when the pressure coefficient κ decreases. We use the index rs for referring to the rarefaction wave at the left and the shock wave at the right.*

The two news results (Theorems 4.3.4 and 4.3.7) show how one can deduce in the vanishing pressure limit, the behaviour of a 1-shock wave and 2-rarefaction wave solution and a 1-rarefaction wave and 2-shock wave solution from the behaviour of a two-shock solution and a two-rarefaction solution, respectively, as mentioned by Chen and Liu [23] without proof. Now, one can state that any Riemann solution of the isentropic Euler equations of gas dynamics (IE) and (4.0.1) tends to the Riemann solution of the pressureless Euler equations (4.3.1) with the same Riemann data as the pressure tends to zero.

4.4 Numerical illustrations

This section is devoted to some numerical illustrations of the theoretical results mentioned in the previous sections of this chapter. We use the modified Lax-Friedrich scheme (see section 2.3) to discretize equations (IE) and (4.0.1). We look at the solution on the whole real line. However, we solve (IE) and (4.0.1) in the bounded domain $[-1, 3]$. So, we impose a zero slope for each variable on the inlet boundary $x = -1$ of the computational domain.

We first illustrate the four possible configurations of the Riemann solution to (IE) and (4.0.1), depending on the initial data. The initial conditions for each configuration are listed below:

(a) 1-rarefaction and 2-rarefaction:

$$(\rho, v)(x,0) = \begin{cases} (1.2, 0.5) & \text{for} \quad x < 0, \\ (1.0, 1.5) & \text{for} \quad x > 0, \end{cases}$$

(b) 1-rarefaction and 2-shock:

$$(\rho, v)(x,0) = \begin{cases} (1.0, 0.8) & \text{for} \quad x < 0, \\ (0.5, 1.0) & \text{for} \quad x > 0, \end{cases}$$

(c) 1-shock and 2-shock:

$$(\rho, v)(x,0) = \begin{cases} (1.0, 1.5) & \text{for} \quad x < 0, \\ (1.2, 0.5) & \text{for} \quad x > 0, \end{cases}$$

(d) 1-shock and 2-rarefaction:

$$(\rho, v)(x,0) = \begin{cases} (0.2, 1.5) & \text{for} \quad x < 0, \\ (0.7, 1.0) & \text{for} \quad x > 0. \end{cases}$$

The intermediate state for the 1-rarefaction and 2-rarefaction solution is calculated from (4.2.12) and (4.2.21) and is given by $(\rho_*^\kappa, v_*^\kappa) = (0.62, 1.08)$. Note that the intermediate states for the others configurations are computed numerically from their corresponding nonlinear equations using the function *fsolve* in Matlab [74]. They

are given by $(\rho_*^\kappa, v_*^\kappa) = (0.63, 1.19)$, $(\rho_*^\kappa, v_*^\kappa) = (1.80, 0.91)$ and $(\rho_*^\kappa, v_*^\kappa) = (0.52, 0.75)$ for the 1-rarefaction and 2-shock solution, the 1-shock and 2-shock solution and the 1-shock and 2-rarefaction solution, respectively. These numerical approximations are used to calculate solutions called "exact solutions". Numerical and exact solutions are represented in Figure 4.1.

Next, we illustrate the formation of vacuum state starting with the 1-rarefaction wave and 2-shock wave solution from Figure 4.1(b), when the pressure vanishes. Numerical results are represented in Figure 4.2. We notice that for $\kappa = \kappa_{rs} \approx 0.68$ (calculated from (4.3.10) by using the initial data for the 1-rarefaction and 2-shock wave solution) the 2-shock wave disappears. For $\kappa < \kappa_{rs}$, the solution gives rise to a 1-rarefaction and 2-rarefaction that tends to a two-contact-discontinuity solution, whose intermediate state between the two contact discontinuities tends to a vacuum state.

The process of delta shock formation when the pressure vanishes is illustrated starting with the 1-shock and 2-rarefaction wave solution from Figure 4.1(d). Numerical solutions are shown in Figure 4.3. We see that that for $\kappa = \kappa_{sr} \approx 0.14$ (calculated form (4.3.4) by using the initial data for the 1-shock wave and 2-rarefaction wave solution) the 2-rarefaction wave disappears. For $\kappa < \kappa_{rs}$, the solution gives rise to a 1-shock and 2-shock solution that tends to a delta shock wave.

4.5 Conclusion

In this chapter, we reviewed the work of Chen and Liu [23] on the behaviour of the solution to the Riemann problem for the isentropic Euler equations in the vanishing pressure limit. It is also shown that any Riemann solution composed of a 1-shock wave combined with a 2-rarefaction wave tends to two-shock waves when the pressure coefficient gets smaller than a fixed value determined by the Riemann data. In contrast, any Riemann solution composed of a 1-rarefaction wave combined with a 2-shock wave converts to a two-rarefaction waves when the pressure coefficient gets smaller than a fixed value determined by the Riemann data. These new results show how one can deduce, in the vanishing pressure limit, the behaviour of a 1-shock wave and 2-rarefaction wave solution, or a 1-rarefaction wave and 2-shock wave solution from the work of Chen and Liu [23]. Our analysis completes the picture on the degeneracy of the isentropic Euler equations to the pressureless Euler equations.

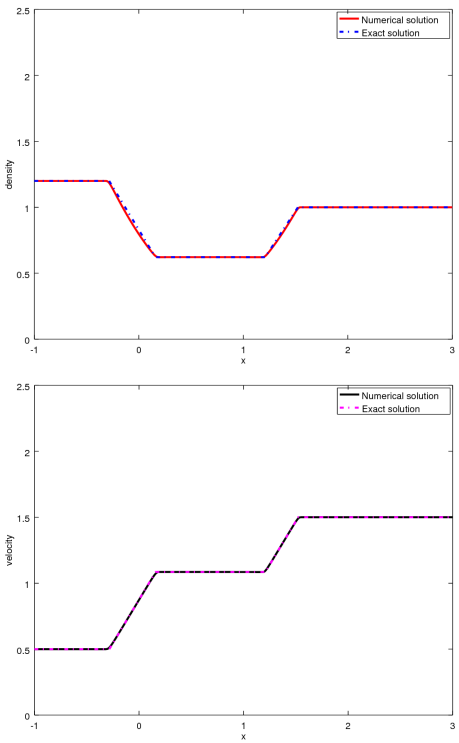

(a): 1-rarefaction and 2-rarefaction

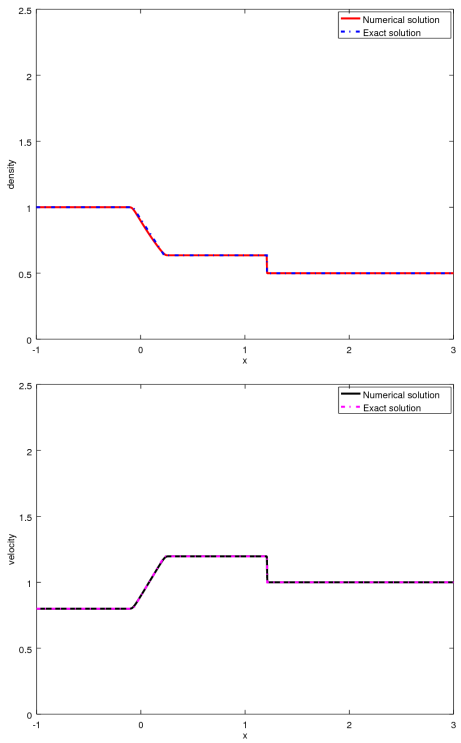

(b): 1-rarefaction and 2-shock

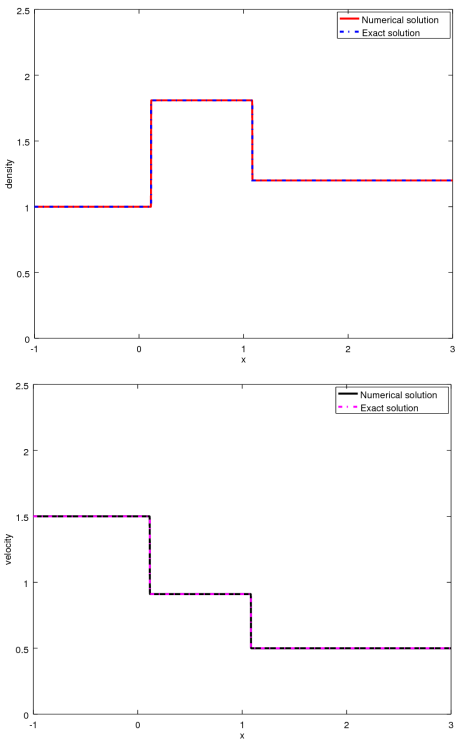

(c): 1-shock and 2-shock

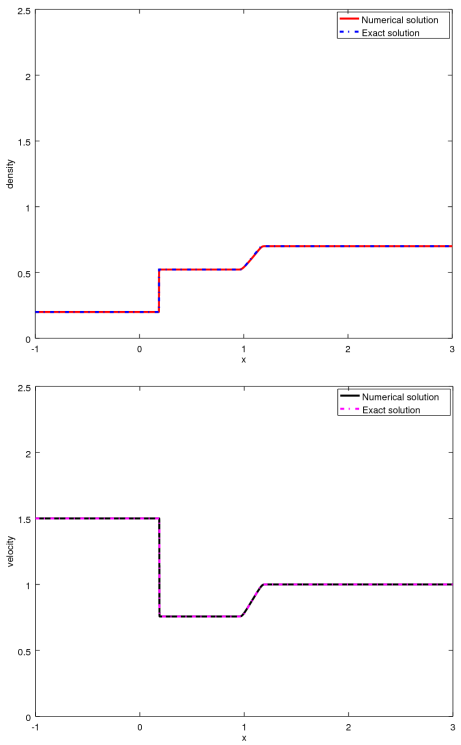

(d): 1-shock and 2-rarefaction

Figure 4.1: Exact and numerical Riemann solutions of the isentropic Euler equations at $t = 0.63$, $\kappa = 0.6$, $\gamma = 1.4$, $\Delta x = 10^{-4}$ and $\Delta t = 2 \times 10^{-5}$.

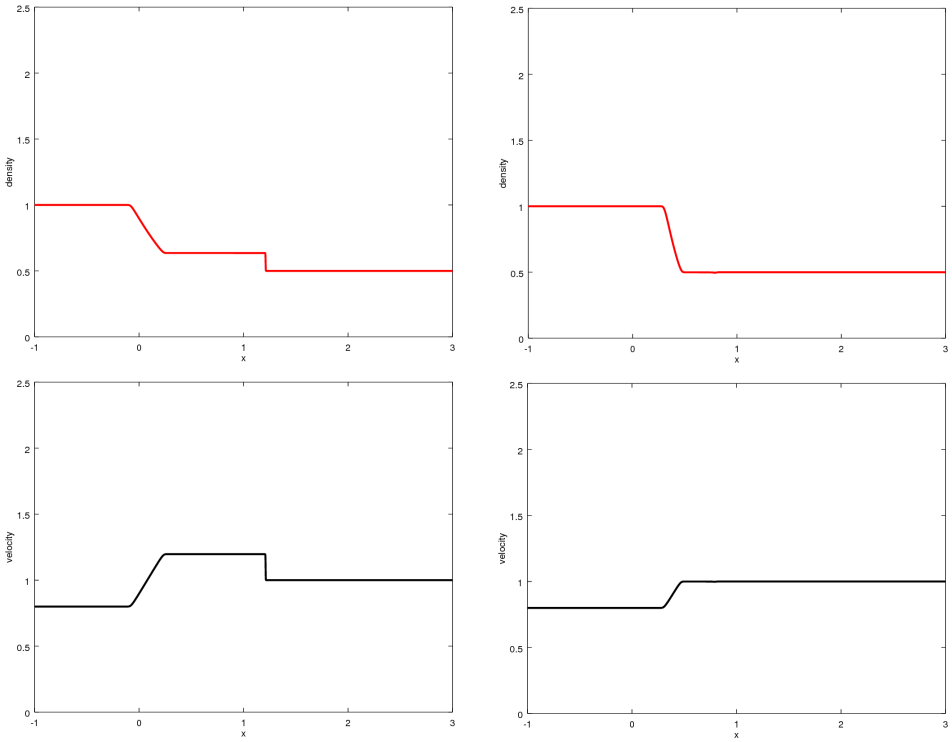

$\kappa = 0.6$ $\kappa = \kappa_{rs} \approx 0.068$

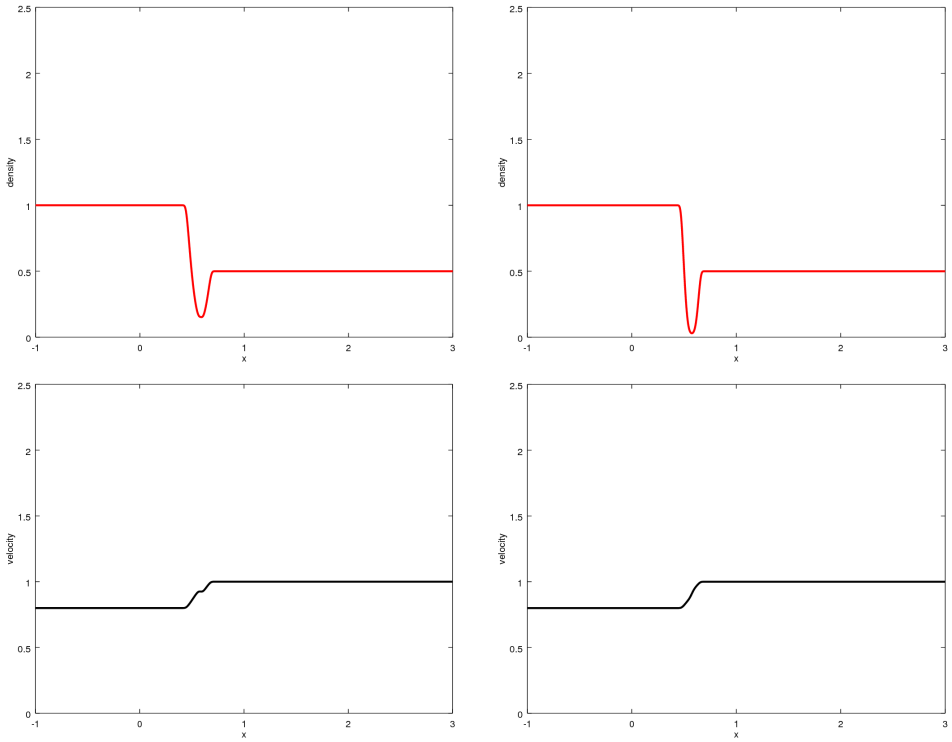

$\kappa = 0.005$ $\kappa = 0.001$

Figure 4.2: Formation of a vacuum state in the isentropic Euler equations as the pressure vanishes. $t = 0.63$, $\gamma = 1.4$, $\Delta x = 10^{-4}$ and $\Delta t = 2 \times 10^{-5}$.

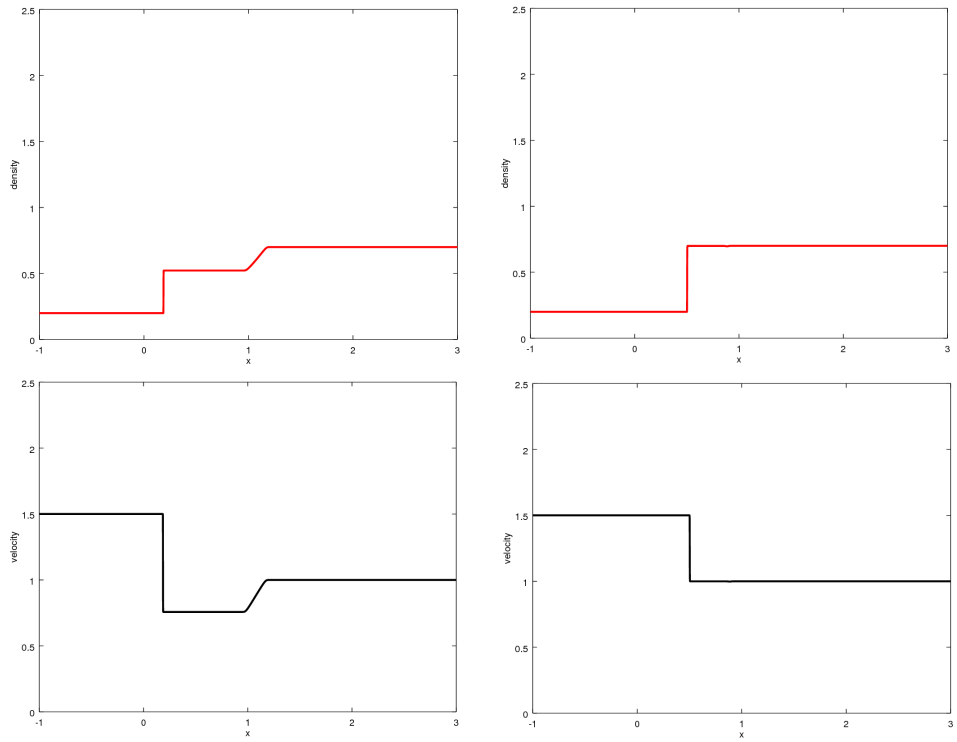

$\kappa = 0.6$ $\kappa = \kappa_{sr} \approx 0.14$

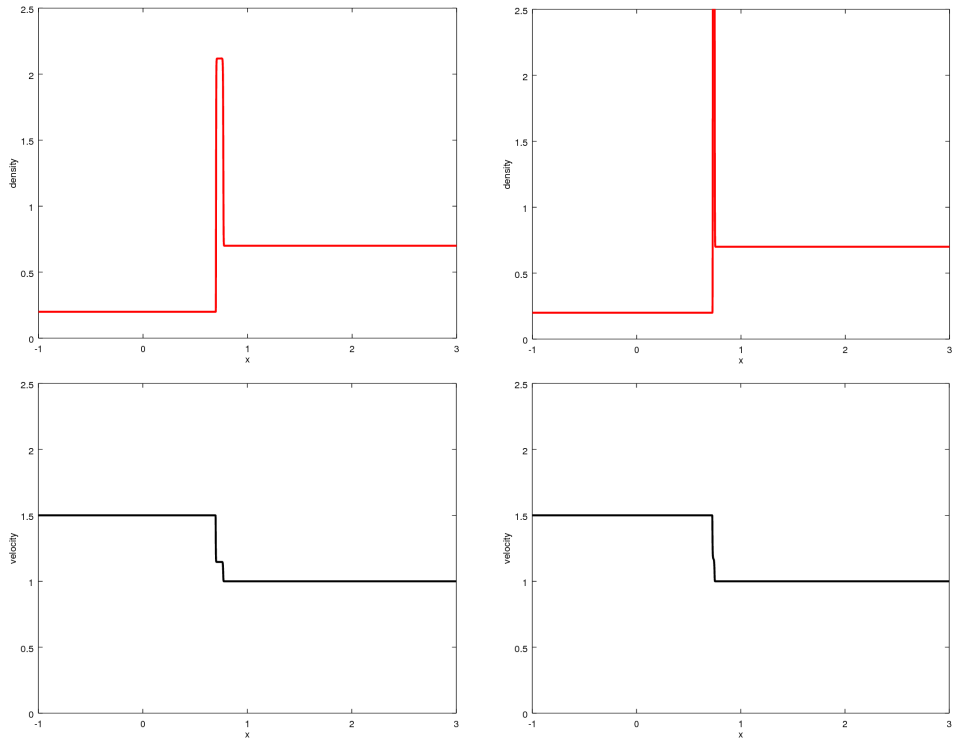

$\kappa = 0.01$ $\kappa = 0.001$

Figure 4.3: Formation of a delta shock wave in the isentropic Euler equations as the pressure vanishes. $t = 0.63$, $\gamma = 1.4$, $\Delta x = 10^{-4}$ and $\Delta t = 2 \times 10^{-5}$.

Chapter 5

A new Eulerian droplet model

The non-conservative form of Model E was successfully used for the prediction of droplets impingement on airfoils and ice accretion on airplane wings during in-flight icing events [15, 17, 75, 6, 50]. Extension to particle flows in airways was more recently attempted [14, 16]. However, we saw in chapter 3 that this model may develop vacuum states and delta shocks. Moreover, the conservative form should be used when discontinuous solutions appear. In vacuum states, the velocity field is not defined. From the numerical point of view, the computation of the velocity field with the conservative form remains a challenge when the volume fraction approaches zero. In the presence of delta shocks, the solution is physically undesirable since the volume fraction violates the primordial saturation constraint $0 \leqslant \alpha \leqslant 1$. A natural question arises: *How can one improve Model E to avoid vacuum states and delta shocks without affecting its usefulness*? We saw in chapter 4 that the formation of delta shocks and vacuum states in the pressureless gas system (which can be seen as Model E without the zeroth-order source term) results from the vanishing pressure in the Euler equations for gas dynamics (Model IE). This motivates the introduction of a new Eulerian droplet model with particle pressure:

$$\begin{cases} \partial_t \alpha + \partial_x(\alpha u) = 0, \\ \partial_t(\alpha u) + \partial_x(\alpha(u^2 + \pi)) = K_D \alpha(u_a - u), \end{cases} \tag{EP}$$

where $\alpha > 0$, u and π are the volume fraction, velocity and pressure of the droplets, respectively; u_a is the air velocity; K_D is the drag coefficient between the droplets and the air. Here, the droplet density ρ_l (density of the material constituting the droplets) is assumed to be constant, and thus is factorized from the second equation of (EP). There is a ratio $\frac{1}{\rho_l}$ (coming from this factorization) that multiplies the particle pressure π and the drag coefficient K_D. To simplify the notation, this ratio is included in the particle pressure and the drag coefficient. In the following, system (EP) will also be referred to as Model EP.

This chapter is divided as follows. In section 5.1, we give some theoretical justifications for adding a particle pressure in Model E. In section 5.2, the hyperbolicity and the characteristic variables of Model EP are discussed. In section 5.3, the difficulties encountered in the analysis of model EP are highlighted. Numerical illustrations are carried out in section 5.4.

5.1 Theoretical arguments for the use of a particle pressure

Consider again the linear first-order system of PDEs given in (3.1.4). We saw in subsection 3.1.1 that this system is weakly hyperbolic and develops delta shock solutions when the initial condition u_0 is not differentiable at some point x_0. We modify this system by adding the differential term $\epsilon\partial_x\alpha$ in the second equation. We obtain the new system

$$\begin{cases} \begin{pmatrix}\alpha\\ u\end{pmatrix}_t + \begin{pmatrix}\mu & \beta\\ \epsilon & \mu\end{pmatrix}\begin{pmatrix}\alpha\\ u\end{pmatrix}_x = 0, \quad (x,t)\in\mathbb{R}\times\mathbb{R}^+, \\ (\alpha,u)(x,0) = (\alpha_0,u_0)(x), \quad \forall x\in\mathbb{R}, \end{cases} \tag{5.1.1}$$

where $\epsilon > 0$ is constant. The Jacobian matrix of system (5.1.1) has two distinct real eigenvalues

$$\lambda_1 = \mu - c_\epsilon \quad \text{and} \quad \lambda_2 = \mu + c_\epsilon, \tag{5.1.2}$$

where $c_\epsilon = \sqrt{\epsilon\beta} > 0$. Corresponding eigenvectors are given by $r_1 = (c_\epsilon, -\epsilon)^T$ and $r_2 = (c_\epsilon, \epsilon)^T$, respectively. System (5.1.2) is diagonalizable, and thus is *strictly hyperbolic*. By the change of variable

$$\begin{pmatrix}w_1\\ w_2\end{pmatrix} = \begin{pmatrix}c_\epsilon & c_\epsilon\\ -\epsilon & \epsilon\end{pmatrix}^{-1}\begin{pmatrix}\alpha\\ u\end{pmatrix}, \tag{5.1.3}$$

system (5.1.1) transforms into two independent linear transport equations

$$\begin{pmatrix}w_1\\ w_2\end{pmatrix}_t + \begin{pmatrix}\mu - c_\epsilon & 0\\ 0 & \mu + c_\epsilon\end{pmatrix}\begin{pmatrix}w_1\\ w_2\end{pmatrix}_x = 0, \tag{5.1.4}$$

that can be solved by the method of characteristics to obtain

$$w_1(x,t) = w_1^0(x - (\mu - c_\epsilon)t), \quad w_2(x,t) = w_2^0(x - (\mu + c_\epsilon)t). \tag{5.1.5}$$

Using again (5.1.3), one retrieves the solution

$$\begin{aligned}\alpha(x,t) =& \frac{\alpha_0\big(x-(\mu-c_\epsilon)t\big)+\alpha_0\big(x-(\mu+c_\epsilon)t\big)}{2}\\ &-\beta t\frac{u_0\big(x-(\mu-c_\epsilon)t\big)-u_0\big(x-(\mu+c_\epsilon)t\big)}{2c_\epsilon t},\\ u(x,t) =& \frac{u_0\big(x-(\mu-c_\epsilon)t\big)+u_0\big(x-(\mu+c_\epsilon)t\big)}{2}\\ &-\epsilon t\frac{\alpha_0\big(x-(\mu-c_\epsilon)t\big)-\alpha_0\big(x-(\mu+c_\epsilon)t\big)}{2c_\epsilon t},\end{aligned} \tag{5.1.6}$$

of system (5.1.1). We see that this solution remains bounded as long as the initial condition (α_0, u_0) is bounded. Formally, system (3.1.4) is the limit system of (5.1.1) as the term $\epsilon\partial_x\alpha$ vanishes. Now take $\epsilon \to 0$. This implies that $c_\epsilon = \sqrt{\epsilon\beta} \to 0$. On the one hand, the two eigenvalues (5.1.2) of system (5.1.1) degenerate to the double eigenvalue $\lambda = u$ of system (3.1.4). On the other hand, solution (5.1.6) of system (5.1.1) gives rise to

$$\alpha(x,t) = \alpha_0(x-\mu t) - \beta t u_0'(x-\mu t), \quad u(x,t) = u_0(x-\mu t) - \lim_{\epsilon\to 0}\epsilon t\alpha_0'(x-\mu t) \tag{5.1.7}$$

which, if α_0' is bounded, reduces to

$$\alpha(x,t) = \alpha_0(x-\mu t) - \beta t u_0'(x-\mu t), \quad u(x,t) = u_0(x-\mu t). \tag{5.1.8}$$

This equation is nothing else but the solution of system (3.1.4). The introduction of $\epsilon\partial_x\alpha$ in (3.1.4) eliminates delta shocks.

The same phenomenon also occurs with nonlinear systems. In fact, we saw in chapter 4 that the occurrence of delta shocks and vacuum states in the pressureless gas system (4.3.1) results from the vanishing pressure limit of the isentropic Euler equations (IE).

Based on the above considerations, we speculate that adding a suitable term in the basic equation of the Eulerian droplet model (E) may prevent delta shocks and vacuum states formation. A simple and physically acceptable way to add such differential term in Model E is to consider a pressure that depends on the droplet volume fraction. Hence, we introduce a new Eulerian droplet model with a pressure gradient. Such a pressure is called *particle pressure* and could be seen as generated by particles, for instance during particle-particle collisions or through particle-particle interaction by the carrier fluid when particles get close to each other without necessarily colliding. There are several formulations for adding a pressure gradient in the momentum equation for a phase. The formulation that we have adopted here and the reason behind our choice will be discussed later.

5.2 Hyperbolicity and characteristic variables

In this section, we assume that the particle pressure π satisfies

$$\pi = \pi(\alpha) \geqslant 0, \quad \pi'(\alpha) > 0, \quad \pi''(\alpha) \geqslant 0. \tag{5.2.1}$$

We will give the reason behind these assumptions later. To simplify notation, we set

$$\tilde{\pi}(\alpha) = \alpha\pi(\alpha). \tag{5.2.2}$$

For smooth solutions, the Jacobian matrix of system (EP) and (5.2.1) is given by

$$J_{EP}(\alpha, \alpha u) = \begin{pmatrix} 0 & 1 \\ -u^2 + \tilde{\pi}'(\alpha) & 2u \end{pmatrix}, \tag{5.2.3}$$

and has two eigenvalues

$$\lambda_1(\alpha, \alpha u) = u - c_\pi, \quad \text{and} \quad \lambda_2(\alpha, \alpha u) = u + c_\pi, \tag{5.2.4}$$

where

$$c_\pi = c_\pi(\alpha) = \sqrt{\tilde{\pi}'(\alpha)} = \sqrt{\pi(\alpha) + \alpha\pi'(\alpha)} > 0, \tag{5.2.5}$$

since we assume that $\alpha > 0$ and π satisfies (5.2.1). A general set of eigenvectors associated to the eigenvalues (5.2.4) is given by

$$r_1(\alpha, \alpha u) = b_1 \begin{pmatrix} 1 \\ \lambda_1 \end{pmatrix} \quad \text{and} \quad r_2(\alpha, \alpha u) = b_2 \begin{pmatrix} 1 \\ \lambda_2 \end{pmatrix}, \tag{5.2.6}$$

respectively, where $b_1 = b_1(\alpha, \alpha u)$ and $b_2 = b_2(\alpha, \alpha u)$ are nonzero scalar functions. The Jacobian matrix (5.2.3) is diagonalizable. Hence, Model EP is *strictly hyperbolic*.

To find the characteristic variables of Model EP, we proceed as we did with the isentropic Euler equations (IE) in section 4.1. We assume there exists $\boldsymbol{\psi} = (\psi_1, \psi_2)$ such that

$$d\boldsymbol{\psi} = (P_{EP})^{-1} d\mathbf{u}, \tag{5.2.7}$$

where $\mathbf{u} = (\alpha, \alpha u)^T$, d is a differential operator that satisfies $d\psi_j = \partial_x \psi_j$ or $d\psi_j = \partial_t \psi_j$, and P_{EP} is the transformation matrix

$$P_{EP} = \begin{pmatrix} b_1 & b_2 \\ b_1\lambda_1 & b_2\lambda_2 \end{pmatrix}. \tag{5.2.8}$$

We rewrite system (EP) and (5.2.1) in the diagonalized form

$$\partial_t \boldsymbol{\psi} + \boldsymbol{\Lambda}_{EP}(\mathbf{u}) \partial_x \boldsymbol{\psi} = (P_{EP})^{-1} F(\mathbf{u}), \tag{5.2.9}$$

where

$$\mathbf{\Lambda}_{EP}(\mathbf{u}) = \begin{pmatrix} \lambda_1(\mathbf{u}) & 0 \\ 0 & \lambda_2(\mathbf{u}) \end{pmatrix}, \quad F(\mathbf{u}) = \begin{pmatrix} 0 \\ K_D\alpha(u_a - u) \end{pmatrix}. \tag{5.2.10}$$

Then, by the particular choice $b_1 = -b_2 = -\frac{\alpha}{2c_\pi}$, we find the characteristic variables

$$\psi_1 = u - g_\pi, \qquad \psi_2 = u + g_\pi, \tag{5.2.11}$$

where g_π is defined as

$$g_\pi = \int \frac{c_\pi(\alpha)}{\alpha}\, d\alpha. \tag{5.2.12}$$

Finally, system (EP) and (5.2.1) can be written as

$$\begin{aligned} \frac{\partial \psi_1}{\partial t} + (u - c_\pi)\frac{\partial \psi_1}{\partial x} &= K_D(u_a - u), \\ \frac{\partial \psi_2}{\partial t} + (u + c_\pi)\frac{\partial \psi_2}{\partial x} &= K_D(u_a - u). \end{aligned} \tag{5.2.13}$$

Equation (5.2.13) means that the characteristic variable ψ_j is not constant along the characteristic field $\chi_j(x, t; .)$. We are not able to find an analytical solution of the corresponding nonlinear system ODEs. This is a difficulty in the analysis of Model EP. Others difficulties will be discussed in the next section.

If $\lambda_j(\mathbf{u}) > 0$ then the characteristics emanate from a point on either the initial line $t = 0$ or the left boundary of the domain. This means that we have to prescribe the characteristic variable ψ_j at time $t = 0$ and at the left boundary. Similarly, if $\lambda_j(\mathbf{u}) < 0$ then the characteristics emanate from a point on either the initial line $t = 0$ or the right boundary, and thus we have to prescribe the characteristic variable ψ_j at $t = 0$ and at the right boundary. In most applications c_π is small since the volume fraction is small, and thus we fall in a supersonic regime, i.e. $u > c_\pi$. In this case, we only need boundary conditions on the inflow boundaries. Table 5.1 summarizes the location and the characteristic variables for which a boundary condition should be prescribed. The characteristic variables can be written as $(\psi_1, \psi_2) = H(\alpha, u)$. Formally, inverting this function H, we find the boundary conditions for the physical variables α and u.

	$u \geq c_\pi$	$\lvert u\rvert < c_\pi$	$u \leqslant -c_\pi$
left boundary	ψ_1, ψ_2	ψ_2	not required
right boundary	not required	ψ_1	ψ_1, ψ_2

Table 5.1: Boundary conditions for Model EP.

Remark 5.2.1. *The above results are valid provided that $c_\pi > 0$. This explains the assumption* (5.2.1) *on the particle pressure π to ensure the positivity of c_π.*

5.3 Difficulties with the analysis of Model EP

In this section, we highlight the difficulties encountered in the analysis of Model EP, particularly with the solution of the Riemann problem, i.e. problem (EP) and (5.2.1) augmented with the initial conditions

$$(\alpha, u)(x, 0) = \begin{cases} (\alpha_-, u_-), & x < 0, \\ (\alpha_+, u_+), & x > 0, \end{cases} \tag{5.3.1}$$

where α_-, $\alpha_+ \in \mathbb{R}^+$ and u_-, $u_+ \in \mathbb{R}$ are given constants.

5.3.1 Rarefaction waves

The characteristic variables of Model EP are not constant along their corresponding characteristic fields. This is due to the zeroth-order source term. We do not have Riemann invariants for system (EP), and thus we cannot establish its rarefaction curves as we did for the isentropic Euler equations. This is another difficulty in the analysis of the Riemann problem for Model EP.

5.3.2 Shock waves

We are looking for a shock wave, i.e. a solution that is discontinuous across a continuous curves $x = \xi_j(t)$. The eigenvalues (5.2.4) and eigenvectors (5.2.6) of system (EP) and (5.2.1) satisfy

$$\begin{aligned} \nabla\lambda_1 \cdot r_1 &= -b_1 \left(c'_\pi(\alpha) + \frac{c_\pi(\alpha)}{\alpha} \right) = -b_1 \left(\frac{2\pi'(\alpha) + \alpha\pi''(\alpha)}{2\sqrt{\pi(\alpha) + \alpha\pi'(\alpha)}} + \frac{c_\pi(\alpha)}{\alpha} \right) \neq 0, \\ \nabla\lambda_2 \cdot r_2 &= b_2 \left(c'_\pi(\alpha) + \frac{c_\pi(\alpha)}{\alpha} \right) = b_2 \left(\frac{2\pi'(\alpha) + \alpha\pi''(\alpha)}{2\sqrt{\pi(\alpha) + \alpha\pi'(\alpha)}} + \frac{c_\pi(\alpha)}{\alpha} \right) \neq 0, \end{aligned} \tag{5.3.2}$$

since π satisfies (5.2.1). Note that here the gradient operator is taken with respect to the conservative variables α and αu. Hence, the two characteristic fields of (EP) and (5.2.1) are *genuinely nonlinear*. Thus, discontinuous solutions of problem (EP) and (5.2.1) are shock waves [64]. Such solutions satisfy the *Rankine-Hugoniot conditions* [64] given by

$$\begin{aligned} \sigma_j(t) &= \frac{\alpha(\xi_j^+, t)u(\xi_j^+, t) - \alpha(\xi_j^-, t)u(\xi_j^-, t)}{\alpha(\xi_j^+, t) - \alpha(\xi_j^-, t)}, \\ \sigma_j(t) &= \frac{\alpha(\xi_j^+, t)u(\xi_j^+, t)^2 + \tilde{\pi}(\alpha(\xi_j^+, t)) - \alpha(\xi_j^-, t)u(\xi_j^-, t)^2 - \tilde{\pi}(\alpha(\xi_j^-, t))}{\alpha(\xi_j^+, t)u(\xi_j^+, t) - \alpha(\xi_j^-, t)u(\xi_j^-, t)}, \end{aligned} \tag{5.3.3}$$

where $\big(\alpha(\xi_j^-,t),u(\xi_j^-,t)\big)$ and $\big(\alpha(\xi_j^+,t),u(\xi_j^+,t)\big)$ denote the limits of the solution (α,u) when x approaches the j-shock curve ξ_j from the left and right, respectively, and $\sigma_j = \xi_j'(t)$ is the speed of propagation of the j-shock curve. Note that for classical shock wave solutions, the zeroth-order source term disappears in the Rankine-Hugoniot conditions as we have shown in the proof of theorem 3.2.2 for the Burgers equation with source term (B). In addition, the j-shock speed σ_j also satisfies the *Lax entropy conditions* [64]

$$\begin{aligned}\lambda_{j-1}\big(\alpha(\xi_j^-,t),\alpha(\xi_j^-,t)u(\xi_j^-,t)\big) < \sigma_j(t) < \lambda_j\big(\alpha(\xi_j^-,t),\alpha(\xi_j^-,t)u(\xi_j^-,t)\big),\\ \lambda_j\big(\alpha(\xi_j^+,t),\alpha(\xi_j^+,t)u(\xi_j^+,t)\big) < \sigma_j(t) < \lambda_{j+1}\big(\alpha(\xi_j^+,t),\alpha(\xi_j^+,t)u(\xi_j^+,t)\big),\end{aligned} \tag{5.3.4}$$

where $\lambda_0 = -\infty$ and $\lambda_3 = \infty$.

Suppose that (α,u) is a solution of (EP) and (5.2.1) that contains a 1-shock wave. We want to establish a relation between a given left state (α_l,u_l) and a right state (α,u), separated by the 1-shock curve. On the one hand, the Rankine-Hugoniot conditions (5.3.3) lead to

$$u(\xi_1^+,t) = u_l(\xi_1^-,t) \pm \sqrt{\frac{\tilde\pi(\alpha(\xi_1^+,t)) - \tilde\pi(\alpha_l(\xi_1^-,t))}{\alpha(\xi_1^+,t)\alpha_l(\xi_1^-,t)(\alpha(\xi_1^+,t)-\alpha_l(\xi_1^-,t))}}\big(\alpha(\xi_1^+,t)-\alpha_l(\xi_1^-,t)\big). \tag{5.3.5}$$

On the other hand, the Lax entropy conditions (5.3.4) lead to

$$c_\pi(\alpha(\xi_1^+,t))\alpha(\xi_1^+,t) > \frac{\alpha(\xi_1^+,t)\alpha_l(\xi_1^-,t)\big(u_l(\xi_1^-,t)-u(\xi_1^+,t)\big)}{\alpha(\xi_1^+,t)-\alpha_l(\xi_1^-,t)} > c_\pi(\alpha_l(\xi_1^-,t))\alpha_l(\xi_1^-,t). \tag{5.3.6}$$

Since the function $\alpha \mapsto \alpha c_\pi(\alpha)$ is positive and strictly increasing (from assumption (5.2.1)), then condition (5.3.6) implies that $\alpha(\xi_1^+,t) > \alpha_l(\xi_1^-,t)$ and $u(\xi_1^+,t) < u_l(\xi_1^-,t)$. Hence, (5.3.5) reduces to

$$u(\xi_1^+,t) = u_l(\xi_1^-,t) - \sqrt{\frac{\big(\tilde\pi(\alpha(\xi_1^+,t)) - \tilde\pi(\alpha_l(\xi_1^-,t))\big)\big(\alpha(\xi_1^+,t)-\alpha_l(\xi_1^-,t)\big)}{\alpha(\xi_1^+,t)\alpha_l(\xi_1^-,t)}}, \tag{5.3.7}$$

with $\alpha(\xi_1^+,t) > \alpha_l(\xi_1^-,t)$.

In an analogous way, we establish a relation between a left state (α,u) and a given right state (α_r,u_r), separated by a 2-shock wave, that is

$$u(\xi_2^-,t) = u_r(\xi_2^+,t) + \sqrt{\frac{\big(\tilde\pi(\alpha_r(\xi_2^+,t)) - \tilde\pi(\alpha(\xi_2^-,t))\big)\big(\alpha_r(\xi_2^+,t)-\alpha(\xi_2^-,t)\big)}{\alpha_r(\xi_2^+,t)\alpha(\xi_2^-,t)}}, \tag{5.3.8}$$

with $\alpha(\xi_2^-,t) > \alpha_r(\xi_2^+,t)$.

The presence of the zeroth-order source term combined with the particle pressure makes the analysis of Model EP very challenging since they leads to non-constant states for the Riemann solution on both sides of the shock trajectory. In particular, we could not find an analytical expression for the intermediate state between the two shocks. From the numerical results in the next section there is no reason to think that the intermediate state is constant for a given time t (as with the left and right states) or has trivial limits while approaching the shock curves at fixed t.

5.4 Numerical illustrations

This section is devoted to the numerical illustration that a particle pressure prevents the formation of delta shocks and vacuum states in Model EP. The test cases performed in subsection 3.6.1 showed the formation of delta shocks and vacuum states in Model E. We repeat these test cases with Model EP to highlight the prevention of delta shocks and vacuum states formation. We use the modified Lax-Friedrich scheme (see section 2.3) to discretize the balance laws (EP). We take $\pi = \kappa_0 \alpha$, where κ_0 is a constant coefficient. We will see in the next chapter the reason behind this particular choice of the particle pressure.

We first solve (EP) for the initial data (3.6.1). Numerical results for different values of the particle pressure coefficient κ_0 are represented in Figure 5.1. We obtain a delta shock wave centered on the velocity discontinuity with the solution without particle pressure (Model E). In the presence of a particle pressure, i.e. for $\kappa_0 > 0$, the discontinuity in the velocity breaks down in two discontinuities. This gives rise to a left, intermediate and right states. The amplitude of the volume fraction for the intermediate state between these two discontinuities becomes bounded and decreases as the particle pressure coefficient κ_0 increases. Note that here the variables are scaled. This explains why the displayed volume fraction is bigger than one in some cases. Moreover, for a particle pressure coefficient κ_0 big enough, the volume fraction remains smaller than one. The particle pressure prevents the formation of a delta shock by giving rise to a two-shock solution.

Secondly, we solve (EP) for the initial conditions (3.6.2). Numerical results for different values of the particle pressure coefficient κ_0 are represented in Figure 5.2. We obtain a two-contact discontinuity solution with a vacuum state with the solution without particle pressure (Model E). In presence of a particle pressure, the solution turns into a two-rarefaction solution without vacuum state.

We clearly see from these two test cases that particle pressure can prevent delta shocks and vacuum states formation. These results show the mathematical and physical relevance of including a particle pressure gradient in Model E.

5.5 Conclusion

In this chapter we proposed a new Eulerian model for air-droplets flows. This model is written in conservative form and is strictly hyperbolic as opposed to the standard Eulerian droplet model, which is weakly hyperbolic with one double eigenvalue. We tried to perform for the new Eulerian droplet model, an analysis similar to the one we did for the isentropic Euler equations of gas dynamics in chapter 4, but the zeroth-order source term leads to a more complicated analysis. The classical theory for hyperbolic conservation laws do not apply to the conservation laws with zeroth-order source (EP). We have illustrated numerically how delta shocks and vacuum states formation is prevented in this new Eulerian droplet model. These results show the mathematical and physical relevance of a particle pressure gradient in the momentum equation of the particulate phase. Model EP could extend the validity range of model (E) to those situations where delta shocks could appear in model (E). However, mathematical proofs are needed to confirm these numerical observations.

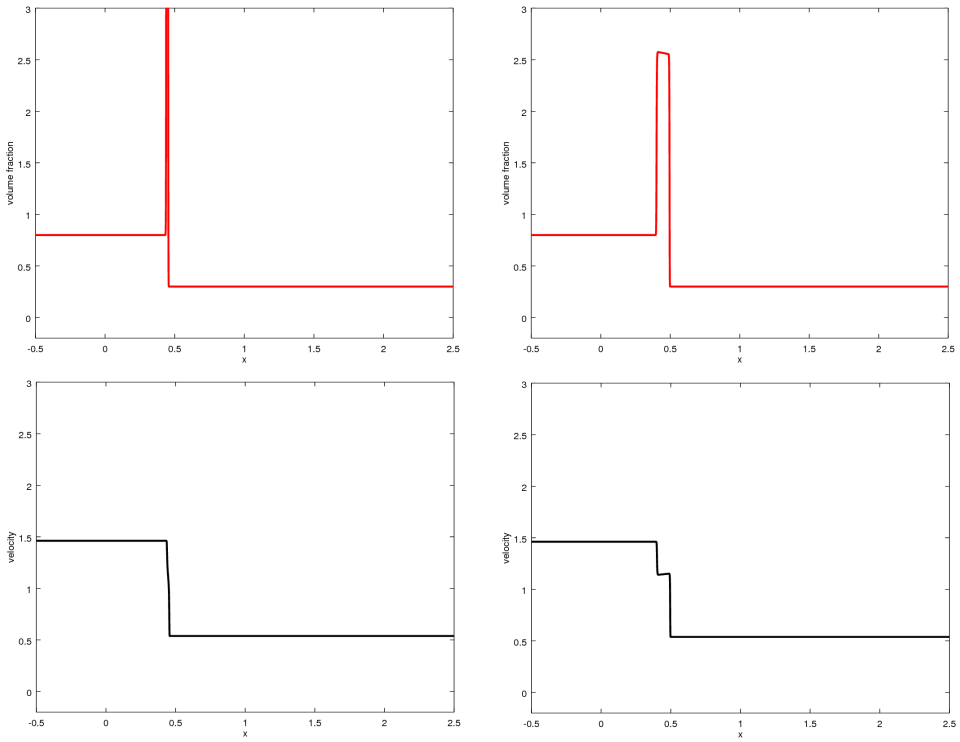

$\kappa_0 = 0$ $\kappa_0 = 0.02$

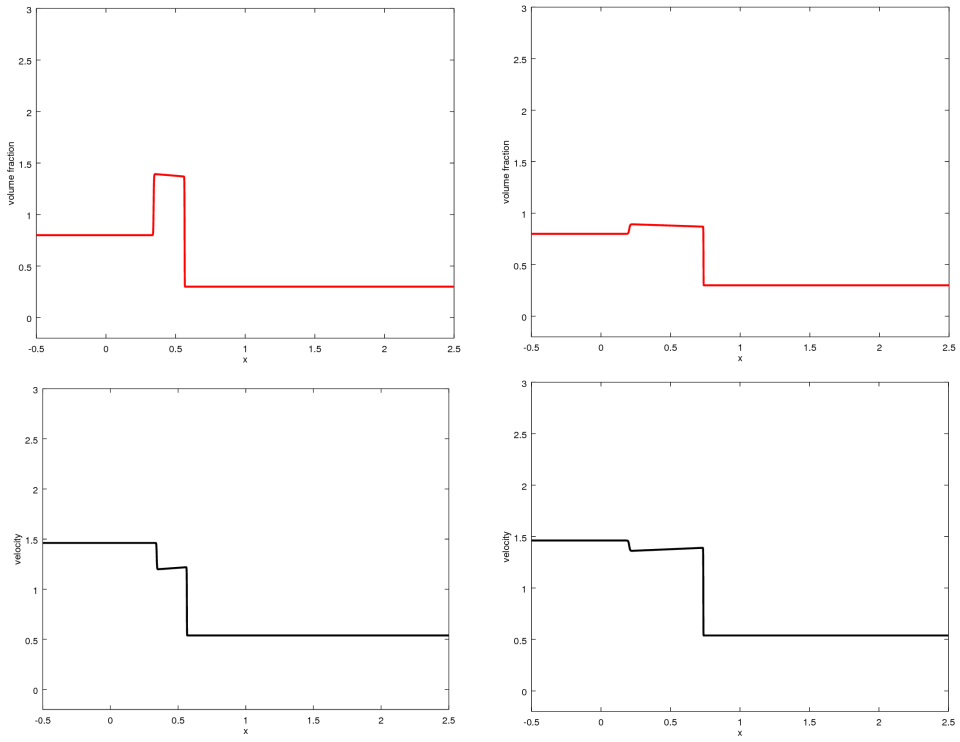

$\kappa_0 = 0.1$ $\kappa_0 = 0.5$

Figure 5.1: Delta shock prevention in Model EP. $t = 0.4$, $u_a = 1.0$, $K_D = 0.2$, $\Delta x = 10^{-3}$ and $\Delta t = 10^{-4}$.

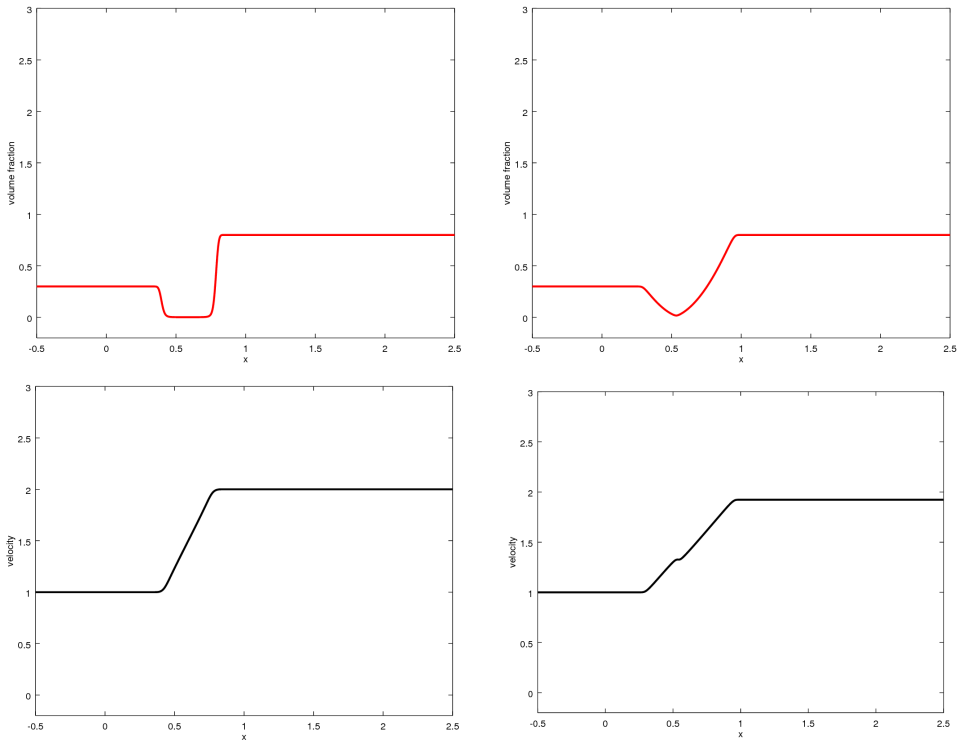

$\kappa_0 = 0$ $\kappa_0 = 0.1$

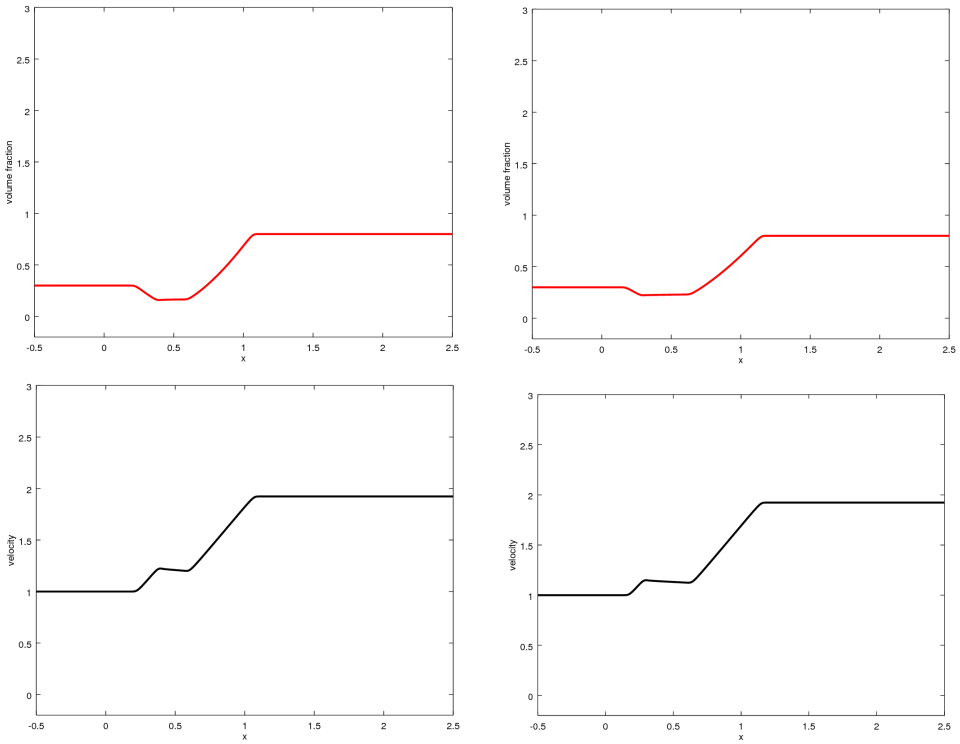

$\kappa_0 = 0.3$ $\kappa_0 = 0.5$

Figure 5.2: Vacuum state prevention in Model EP. $t = 0.4$, $u_a = 1.0$, $K_D = 0.2$, $\Delta x = 10^{-3}$ and $\Delta t = 10^{-4}$.

Chapter 6

A new hierarchy of two-phase flow models

In chapter 3, we analysed an Eulerian droplet model (Model E). It turns out that this model may develop delta shocks and vacuum states. In chapter 5, we proposed an Eulerian droplet model with particle pressure (Model EP) that could be an extension of Model E in order to avoid delta shocks and vacuum states. These two models are one-way coupling, i.e. momentum transfer is assumed from the carrier fluid to the particles but not vice-versa. The carrier fluid is simply considered as a physical body acting on the particles (droplets), and is modeled separately from the particles, for instance by Euler or Navier-Stokes equations. To be more realistic, the effects of the particles on the carrier fluid should also be taken into account. In this chapter, we derive a hierarchy of two-phase flow models including two-way coupling (i.e. the carrier fluid and the particles interact with each other) and two-pressure modelling (i.e. one for the carrier fluid and one for the dispersed phase).

This chapter is divided as follows. The first three sections are devoted to the derivation and brief analysis of the different models. Section 6.4 summarizes the connections between the models. A brief literature review on particle pressure modelling is performed in section 6.5. Numerical comparisons are carried out in section 6.6.

6.1 A two-way coupling Eulerian droplet model

In 2000, Bouchut [10] proposed a hierarchy of Eulerian models (see chapter 2, subsection 2.2.1) for gas-liquid flows. In this section, we derive a two-way coupling Eulerian model from Model I of Bouchut [10]. Then, we discuss its advantages with respect to the Model I and Model E.

The first model in the hierarchy of Bouchut [10], referred to as Model I, reads as

$$\begin{cases} \partial_t((1-\alpha)\rho) + \partial_x((1-\alpha)\rho v) = 0, \\ \partial_t((1-\alpha)\rho v) + \partial_x((1-\alpha)\rho v^2) + (1-\alpha)\partial_x p = -\dfrac{1}{\epsilon}\mu\alpha(1-\alpha)(v-u), \\ \partial_t\alpha + \partial_x(\alpha u) = 0, \\ \partial_t(\alpha u) + \partial_x(\alpha u^2) + \epsilon\alpha\partial_x p + C_p(v-u)^2\partial_x\alpha = \mu\alpha(1-\alpha)(v-u), \end{cases} \tag{I}$$

where $\rho > 0$, $1-\alpha$ and v are the density, volume fraction and velocity of the carrier fluid, respectively; $\alpha > 0$ and u are the volume fraction and velocity of the particles, respectively; p is the common pressure for the two phases and satisfies the state equation for isentropic gas flow (4.0.1); and μ is the drag coefficient. The density ratio $\epsilon = \frac{\rho^{\text{ref}}}{\rho_l^{\text{ref}}}$, where ρ^{ref} and ρ_l^{ref} are the reference densities for the carrier fluid and the particles, respectively. The differential term $C_p\rho_l(v-u)^2\partial_x\alpha$ is called pressure correction term, where C_p is a positive constant. Note that in this model, the density ρ_l of the material constituting the particles is assumed to be constant and equal to ρ_l^{ref}. It is then factorized from the third and fourth equations.

Remark 6.1.1. *The density ratio ϵ comes from the density perturbation method [28] applied to the reduced two-fluid model. This method is a convenient way to describe the behaviour and well-posedness of two-phase flow models. For more details, see [28, 10].*

A necessary condition (at least in the linear case) for the Cauchy problem to be well-posed is that it be stable in the sense of von Neumann. Stability of a system of partial differential equations of first order in the sense of von Neumann is equivalent to the hyperbolicity of the system, i.e. all the eigenvalues of the Jacobian matrix of the system are real [79].

If there is no pressure correction term, i.e. $C_p \equiv 0$, model (I) is known as *the basic equal pressure model* for two-phase flows [85]. This latter is known to possess complex eigenvalues [28]. Several modifications to the equations of the basic equal pressure model have been proposed to remedy this shortcoming. The most common technique is the addition of first-order differential terms called *pressure correction terms* in the momentum equation. These differential terms are mathematically relevant, as they make the system hyperbolic by transforming the complex eigenvalues into real ones. Several variants of pressure correction terms were proposed in the past [28]. The one derived in [61] for bubbly flows, is used in Model I.

We now derive, starting from Model I, a new model which is an intermediate between the models (I) and (E). Assume that $0 < \alpha < 1$. By expanding the first and

second equations of (I), this system can be written as

$$\begin{cases} \partial_t\rho + \partial_x\big(\rho v\big) = \dfrac{\rho}{1-\alpha}\big(\partial_t\alpha + v\partial_x\alpha\big), \\ \partial_t(\rho v) + \partial_x(\rho v^2) + \partial_x p = -\dfrac{1}{\epsilon}\mu\alpha(v-u) + \dfrac{\rho v}{1-\alpha}\big(\partial_t\alpha + v\partial_x\alpha\big), \\ \partial_t\alpha + \partial_x(\alpha u) = 0, \\ \partial_t(\alpha u) + \partial_x(\alpha u^2) + C_p(v-u)^2\partial_x\alpha = \mu\alpha(1-\alpha)(v-u) - \epsilon\alpha\partial_x p. \end{cases} \tag{6.1.1}$$

In many industrial applications on gas-particle flows, the particles are water droplets carried by air. Hence, the reference density for droplets is around $1000kg/m^3$ and the reference density for the carrier fluid is around $1kg/m^3$. This gives a density ratio ϵ of order 10^{-3}. We denote $\frac{D_v\alpha}{dt} = \partial_t\alpha + v\partial_x\alpha$ and make the two following assumptions:

$$\Big|\frac{D_v\alpha}{dt}\Big| \approx 0, \text{ i.e. the variation of the volume fraction } \alpha \text{ along the characteristic curves defined by the gas velocity } v \text{ is negligible;} \tag{6.1.2}$$

$$\epsilon\alpha|\partial_x p| \text{ is negligible with respect to the other terms in the fourth equation of system (6.1.1).} \tag{6.1.3}$$

By neglecting the terms $\frac{D_v\alpha}{dt}$ and $\epsilon\alpha\partial_x p$, system (6.1.1) reduces to

$$\begin{cases} \partial_t\rho + \partial_x\big(\rho v\big) = 0, \\ \partial_t\big(\rho v\big) + \partial_x\big(\rho v^2 + p\big) = -\dfrac{1}{\epsilon}\mu\alpha\big(v-u\big), \\ \partial_t\alpha + \partial_x\big(\alpha u\big) = 0, \\ \partial_t\big(\alpha u\big) + \partial_x\big(\alpha u^2\big) + C_p(v-u)^2\partial_x\alpha = \mu\alpha(1-\alpha)(v-u), \end{cases} \tag{6.1.4}$$

which can be written in quasilinear form with respect to the primitive variables (ρ, v, α, u) as

$$\begin{pmatrix} \rho \\ v \\ \alpha \\ u \end{pmatrix}_t + \begin{pmatrix} v & \rho & 0 & 0 \\ \dfrac{p'(\rho)}{\rho} & v & 0 & 0 \\ 0 & 0 & u & \alpha \\ 0 & 0 & \dfrac{C_p(u-v)^2}{\alpha} & u \end{pmatrix} \begin{pmatrix} \rho \\ v \\ \alpha \\ u \end{pmatrix}_x = \begin{pmatrix} 0 \\ -\dfrac{1}{\epsilon}\dfrac{\mu\alpha}{\rho}(v-u) \\ 0 \\ \mu(1-\alpha)(v-u) \end{pmatrix}. \tag{6.1.5}$$

The Jacobian matrix of this system has four distinct real eigenvalues

$$\lambda_1 = v - c, \quad \lambda_2 = v + c, \quad \lambda_3 = u - \sqrt{C_p}|v-u| \quad \text{and} \quad \lambda_4 = u + \sqrt{C_p}|v-u|, \tag{6.1.6}$$

where $c = c(\rho) = \sqrt{p'(\rho)}$. Hence, system (6.1.4) is stable in the sense of von Neumann. Recall that these pressure correction terms are added in Model I in order to achieve well-posedness. There is some questioning on the physical relevance of the pressure corrections. In fact, some studies argued that pressure correction terms can introduce nonphysical effects [90, 78] and lead to non-conservative system (as with Model I). To avoid these drawbacks, we simply remove the pressure correction term (i.e. we set $C_p \equiv 0$) from system (6.1.4) and the latter reduces to

$$\begin{cases} \partial_t \rho + \partial_x(\rho v) = 0, \\ \partial_t(\rho v) + \partial_x(\rho v^2 + p) = -\dfrac{1}{\epsilon}\mu\alpha(v-u), \\ \partial_t \alpha + \partial_x(\alpha u) = 0, \\ \partial_t(\alpha u) + \partial_x(\alpha u^2) = \mu\alpha(1-\alpha)(v-u). \end{cases} \tag{IA}$$

System (IA) is a new two-way coupling Eulerian droplet model. In the following, this model will also be referred to as Model IA.

6.1.1 Advantages of Model IA versus the models (I) and (E)

Model IA is a two-way coupling model for gas-particle flows. It is a system of conservation laws with zeroth-order linear source terms and can be written in quasilinear form as

$$\begin{pmatrix} \rho \\ v \\ \alpha \\ u \end{pmatrix}_t + \begin{pmatrix} v & \rho & 0 & 0 \\ \dfrac{p'}{\rho} & v & 0 & 0 \\ 0 & 0 & u & \alpha \\ 0 & 0 & 0 & u \end{pmatrix} \begin{pmatrix} \rho \\ v \\ \alpha \\ u \end{pmatrix}_x = \begin{pmatrix} 0 \\ -\dfrac{1}{\epsilon}\dfrac{\mu\alpha}{\rho}(v-u) \\ 0 \\ \mu(1-\alpha)(v-u) \end{pmatrix}. \tag{6.1.7}$$

The Jacobian matrix is composed of two blocks (one for each phase) with zero off-diagonal blocks and has three real eigenvalues given by

$$\lambda_1 = v - c, \quad \lambda_2 = v + c \quad \text{and} \quad \lambda_3 = u. \tag{6.1.8}$$

Model IA has many advantages compared to Model I. In fact, it is written naturally in conservative form as opposed to Model I, which cannot be written in conservative form. Classical theories for conservation laws may be applied to Model IA, while Model I requires less standard theories for non-conservative hyperbolic systems, for instance, see [32]. Model IA is a common-pressure two-phase model which does not require any additional pressure correction term for stability in the sense of von Neumann as opposed to Model I, which does need a pressure correction term.

In many air-particle flow applications, the particle volume fraction α is very small. For instance, during in-flight icing, the volume fraction of water droplets is

of order 10^{-6} [15] and the density ratio ϵ is around 10^{-3}. Therefore, for small drag coefficient μ, the term on the r.h.s of the second equation of Model IA can be neglected with respect to the terms on the l.h.s. The first and the second equation of (IA) can be written as

$$\begin{cases} \partial_t \rho + \partial_x \big(\rho v\big) = 0, \\ \partial_t \big(\rho v\big) + \partial_x \big(\rho v^2 + p\big) = 0, \end{cases} \tag{6.1.9}$$

which are nothing but the isentropic Euler equations (IE) studied in chapter 4. For α small, $1-\alpha$ can be approximated by 1, and thus the term on the r.h.s of the fourth equation of (IA) reduces to $\mu\alpha(v-u)$. The third and fourth equation of (IA) can be written as

$$\begin{cases} \partial_t \alpha + \partial_x \big(\alpha u\big) = 0, \\ \partial_t \big(\alpha u\big) + \partial_x \big(\alpha u^2\big) = \mu\alpha(v-u), \end{cases} \tag{6.1.10}$$

which form the Eulerian droplet model (E) studied in chapter 3. Hence, Model IA leads to Model E while predicting air-droplet flows with low concentration of droplets. A variant of Model E, where the carrier fluid is modeled separately using Navier-Stokes equations, is used in [15, 75, 6, 50, 14]. To our knowledge, Model IA has not yet been proposed in the literature. Whence, the denomination "a new Eulerian droplet model".

6.1.2 Shortcomings of Model IA

Model IA is a system of conservation laws with zeroth-order linear source term. The Jacobian matrix has three distinct real eigenvalues given by (6.1.8) and is not diagonalizable. Therefore, it is a *weakly hyperbolic* system of conservation laws. While this is better than systems with complex eigenvalues, weakly hyperbolic systems still lead to difficulties, particularly the occurrence of delta shocks and vacuum states which are usually nonphysical and very hard to solve numerically. These difficulties restrict their use in some applications. Model IA is no more valid in presence of delta shocks since the primordial saturation constraint $0 \leqslant \alpha \leqslant 1$ for the mixture is violated.

6.2 A two-way coupling two-pressure Eulerian droplet model

In the previous section, we saw that Model IA purports to be more realistic than Model E in the sense that it takes into account two-way momentum transfer between the carrier fluid and the particles, however it is weakly hyperbolic and may develop delta shocks and vacuum states. In chapter 5, we saw that adding a particle pressure

gradient in the momentum equation of the particulate phase prevents the occurrence of delta shocks and vacuum states. Combining these results, we introduce a two-way coupling two-pressure Eulerian model

$$\begin{cases} \partial_t \rho + \partial_x(\rho v) = 0, \\ \partial_t(\rho v) + \partial_x(\rho v^2 + p) = -\dfrac{1}{\epsilon}\mu\alpha(v-u), \\ \partial_t \alpha + \partial_x(\alpha u) = 0, \\ \partial_t(\alpha u) + \partial_x(\alpha(u^2+\pi)) = \mu\alpha(1-\alpha)(v-u), \end{cases} \tag{IAP}$$

where π is the pressure of the carrier fluid and satisfies (5.2.1). The other variables and parameters in (IAP) have the same meaning as in Model IA.

Remark 6.2.1. *Model IAP is obtained by including a particle pressure in the momentum equation for the dispersed phase in Model IA. Therefore, we refer to this model as Model IAP. We use the formulation adopted in Model EP to add the particle pressure. This will be discussed in the next section. Note that in (IAP), the density ρ_l of particles is assumed to be constant and factorized from the third and fourth equations. There is a ratio $\frac{1}{\rho_l}$ (coming from this factorization) that multiplies the pressure π. To simplify the notation, we include this ratio in the particle pressure coefficient. The denomination "two-pressure" comes from the fact that the pressures of the two phases are different.*

Model IAP can be written in the conservative variables (ρ, r, α, q) as

$$\begin{cases} \partial_t \rho + \partial_x r = 0, \\ \partial_t r + \partial_x\left(\dfrac{r^2}{\rho} + p\right) = -\dfrac{1}{\epsilon}\mu\alpha\left(\dfrac{r}{\rho} - \dfrac{q}{\alpha}\right), \\ \partial_t \alpha + \partial_x q = 0, \\ \partial_t q + \partial_x\left(\dfrac{q^2}{\alpha} + \alpha\pi\right) = \mu\alpha(1-\alpha)\left(\dfrac{r}{\rho} - \dfrac{q}{\alpha}\right), \end{cases} \tag{6.2.1}$$

where $r = \rho v$ and $q = \alpha u$. The Jacobian matrix of (6.2.1) rewritten using primitive variables (ρ, v, α, u) gives

$$\begin{pmatrix} 0 & 1 & 0 & 0 \\ p' - v^2 & 2v & 0 & 0 \\ 0 & 0 & 0 & 1 \\ 0 & 0 & \pi + \alpha\pi' - u^2 & 2u \end{pmatrix}. \tag{6.2.2}$$

It is composed of two blocks (one for each phase) with zero off-diagonal blocks, and has four distinct real eigenvalues

$$\lambda_1 = v - c, \quad \lambda_2 = v + c, \quad \lambda_3 = u - c_\pi, \quad \lambda_4 = u + c_\pi, \tag{6.2.3}$$

where $c = \sqrt{p'} > 0$ and $c_\pi = \sqrt{\pi + \alpha\pi'} > 0$ since the pressures p and π satisfy (4.0.1) and (5.2.1), respectively. Hence, Model IAP is a *strictly hyperbolic* system in conservative form.

6.3 A general Eulerian gas-particle model

Model IA and Model IAP are derived under the assumption that the variation of the particle volume fraction is slow. This condition is not always satisfied, for instance when discontinuous solutions occur. This is a weakness in the two models. Recall that the basic equal-pressure model (Model I with $C_p \equiv 0$) is an ill-posed problem since it can have complex eigenvalues [28]. Several modifications have been proposed to remedy this ill-posedness. Some authors proposed to add a pressure correction term in the momentum equation of the particulate phase as it is done in Model I [10]. Gidaspow [43] suggested to modify the common pressure gradient terms $(1-\alpha)\partial_x p$ and $\alpha\partial_x p$ in the momentum equations to read $\partial_x((1-\alpha)p)$ and $\partial_x(\alpha p)$, respectively. This modification has two main advantages. It makes the system hyperbolic without additional pressure correction term. Moreover, it allows to write the system in conservative form. This is the reason behind the formulation that we have adopted to add a particle pressure in the models (IAP) and (EP). Following this idea, but with different pressures for the two phases and without any assumption on the variation of the particle volume fraction, we derive the gas-particle flow model

$$\begin{cases} \partial_t\big((1-\alpha)\rho\big) + \partial_x\big((1-\alpha)\rho v\big) = 0, \\ \partial_t\big((1-\alpha)\rho v\big) + \partial_x\big((1-\alpha)(\rho v^2 + p)\big) = -\mu\rho_l\alpha(1-\alpha)(v-u), \\ \partial_t(\alpha\rho_l) + \partial_x(\alpha\rho_l u) = 0, \\ \partial_t(\alpha\rho_l u) + \partial_x\big(\alpha(\rho_l u^2 + \pi)\big) = \mu\rho_l\alpha(1-\alpha)(v-u), \end{cases} \tag{6.3.1}$$

where the variables and parameters have the same meaning as in Model IAP. Here, the pressures p and π are taken more general, i.e. both may depend on the carrier fluid density and the particle volume fraction. To simplify, we assume that the particle density ρ_l is constant and is equal to the particle reference density ρ_l^{ref}. The pressures are assumed to satisfy

$$p(\rho,\alpha) \geqslant 0, \quad \partial_\rho p > 0, \quad \partial_\alpha p \geq 0, \quad \pi(\rho,\alpha) \geqslant 0, \quad \partial_\rho \pi \geq 0, \quad \partial_\alpha \pi > 0. \tag{6.3.2}$$

These assumptions are physically acceptable and ensure hyperbolicity in most cases as we will see later. With these assumptions, system (6.3.1) reduces to

$$\begin{cases} \partial_t\big((1-\alpha)\rho\big) + \partial_x\big((1-\alpha)\rho v\big) = 0, \\ \partial_t\big((1-\alpha)\rho v\big) + \partial_x\big((1-\alpha)(\rho v^2 + p)\big) = -\dfrac{1}{\epsilon}\mu\alpha(1-\alpha)(v-u), \\ \partial_t\alpha + \partial_x(\alpha u) = 0, \\ \partial_t(\alpha u) + \partial_x\big(\alpha(u^2 + \pi)\big) = \mu\alpha(1-\alpha)(v-u). \end{cases} \tag{G}$$

In the following, system (G) is also referred to as Model G.

Remark 6.3.1. ***(i)*** *As in model (IAP), the factorization of ρ_l from the fourth equation of (6.3.1) gives rise to a ratio $\frac{1}{\rho_l}$ that multiplies the pressure π. This ratio is simply included in the pressure π.*
(ii) *The density ratio ϵ comes from the nondimensionalization of the carrier fluid density as it is done in Model I.*
(iii) *We will see later that the models studied in the previous sections can all be derived from Model G. Hence, the denomination "general Eulerian gas-particle model".*

System (G) can be written in the conservative variables (w, r, α, q) as

$$\begin{cases} \partial_t w + \partial_x r = 0, \\ \partial_t r + \partial_x \left(\dfrac{r^2}{w} + (1-\alpha)p \right) = -\dfrac{1}{\epsilon}\mu\alpha(1-\alpha)\left(\dfrac{r}{w} - \dfrac{q}{\alpha} \right), \\ \partial_t \alpha + \partial_x q = 0, \\ \partial_t q + \partial_x \left(\dfrac{q^2}{\alpha} + \alpha\pi \right) = \mu\alpha(1-\alpha)\left(\dfrac{r}{w} - \dfrac{q}{\alpha} \right), \end{cases} \tag{6.3.3}$$

where $w = (1-\alpha)\rho$, $r = (1-\alpha)\rho v$ and $q = \alpha u$. The Jacobian matrix of this last system, rewritten in the primitive variables (ρ, v, α, u), is given by

$$\begin{pmatrix} 0 & 1 & 0 & 0 \\ \partial_\rho p - v^2 & 2v & \rho\partial_\rho p + (1-\alpha)\partial_\alpha p - p & 0 \\ 0 & 0 & 0 & 1 \\ \frac{1}{1-\alpha}\alpha\partial_\rho \pi & 0 & \pi + \frac{\alpha\rho}{1-\alpha}\partial_\rho \pi + \alpha\partial_\alpha \pi - u^2 & 2u \end{pmatrix}. \tag{6.3.4}$$

The characteristic polynomial Υ of the Jacobian matrix (6.3.4) can be written as

$$\Upsilon(\lambda) = \big(\lambda - V_-\big)\big(\lambda - V_+\big)\big(\lambda - U_-\big)\big(\lambda - U_+\big) - \frac{\alpha\partial_\rho \pi}{1-\alpha}\big(\rho\partial_\rho p + (1-\alpha)\partial_\alpha p - p\big), \tag{6.3.5}$$

where

$$\begin{aligned} V_- &= v - \sqrt{\partial_\rho p}, & V_+ &= v + \sqrt{\partial_\rho p}, \\ U_- &= u - \sqrt{\big(\pi + \frac{\alpha\rho\partial_\rho \pi}{1-\alpha} + \alpha\partial_\alpha \pi\big)}, & U_+ &= u + \sqrt{\big(\pi + \frac{\alpha\rho\partial_\rho \pi}{1-\alpha} + \alpha\partial_\alpha \pi\big)}. \end{aligned} \tag{6.3.6}$$

The terms in (6.3.6) are all well defined in $\mathbb{R}$ since the pressures p and π satisfy (6.3.2). If $|\frac{\alpha\partial_\rho \pi}{1-\alpha}\big(\rho\partial_\rho p + (1-\alpha)\partial_\alpha p - p\big)|$ is small compared to the constant term in the characteristic polynomial, then the last expression in the r.h.s of (6.3.5) can be considered as a small perturbation of the characteristic polynomial Υ. In this case, the latter has real roots, i.e. the Jacobian matrix (6.3.4) has real eigenvalues.

Lemma 6.3.2. *If the particle pressure π only depends on the particle volume fraction α then Model G is hyperbolic.*

Proof: If the particle pressure π only depends on the particle volume fraction α then $\partial_\rho \pi = 0$, which implies that $\frac{\alpha \partial_\rho \pi}{1-\alpha}(\rho \partial_\rho p + (1-\alpha)\partial_\alpha p - p) = 0$. Hence, the characteristic polynomial (6.3.5) has real eigenvalues. ∎

We are not able to find analytic expressions for the eigenvalues of the Jacobian matrix (6.3.4). We generated values randomly and calculated numerically the corresponding eigenvalues with different forms for the pressures, but we never saw a case with a complex eigenvalue. We therefore conjecture that Model G is at least *conditionally hyperbolic*.

6.4 Summary of the new hierarchy

Model G is a two-way coupling two-pressure model for two-phase flows, written in conservative form. We conjecture that it is conditionally hyperbolic but we are not able to show that the eigenvalues are always real. However, it is hyperbolic when the particle pressure π only depends on the volume fraction.

Model I [10] is a two-way coupling common-pressure model for two-phase flows, written in non-conservative form. This model is conditionally hyperbolic since it may have complex eigenvalues [28].

Model IAP is a two-way coupling two-pressure model for two-phase flows. It is a strictly hyperbolic system in conservative form. This model can be derived from Model G under the assumption (6.1.2) and for $\frac{p}{1-\alpha}|\partial_x \alpha| \approx 0$.

Model IA is a two-way coupling one-pressure model written in conservative form. It is a weakly hyperbolic system. This model can be derived from Model I (under the assumptions (6.1.2), (6.1.3), and $C_p \equiv 0$) or from Model IAP (by neglecting the particle pressure π).

Model EP-IE is composed of the Eulerian droplet model with particle pressure (EP) and the isentropic Euler equation (IE) with a zeroth order source term. It is a one-way coupling two-pressure model for two-phase flows and is strictly hyperbolic. This model can be derived from Model IAP for $\frac{\mu\alpha}{\epsilon} \ll 1$.

Model E-IE is composed of the Eulerian droplet model (E) and the isentropic Euler equation (IE) with a zeroth order source term. It is a one-way coupling one-pressure model for two-phase flows and is weakly hyperbolic. This model can be derived from Model IA (for $\frac{\mu\alpha}{\epsilon} \ll 1$) or Model EP-IE (by neglecting the particle pressure π).

Figure 6.1 summarises the connections between the different models, the main properties of the models and the hypothesis for the derivation of some models from others.

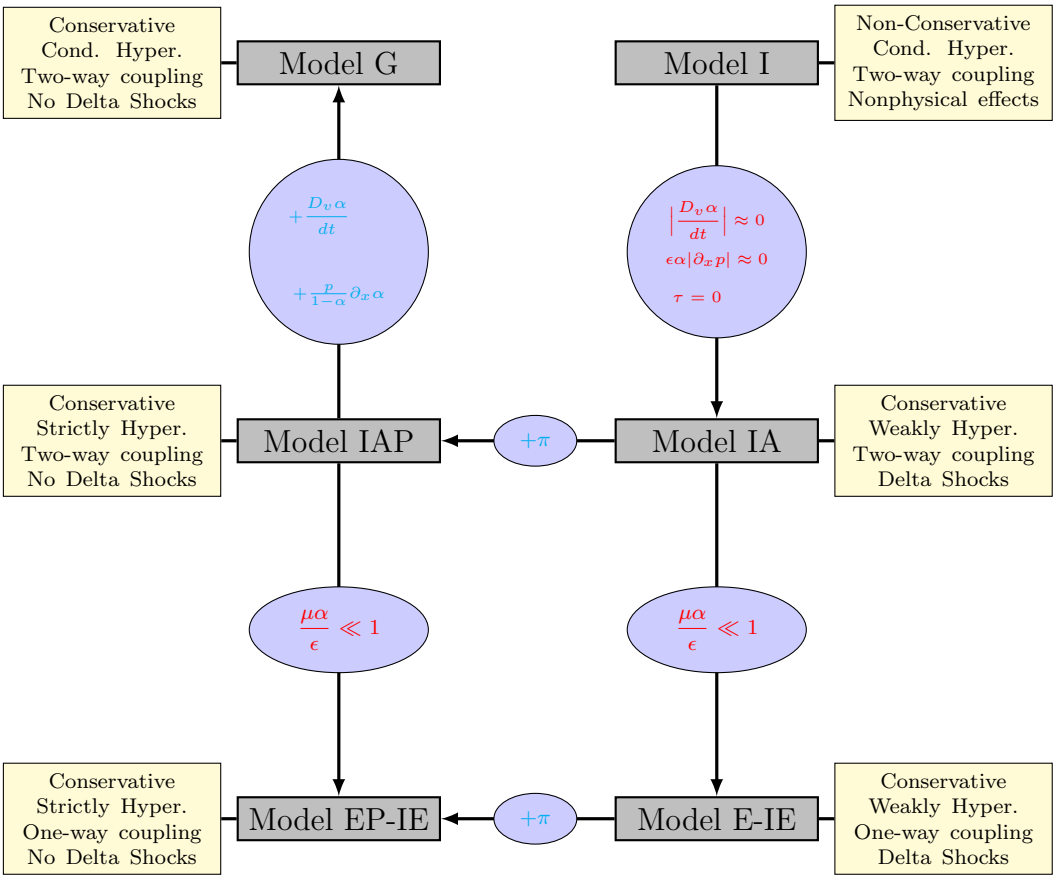

Figure 6.1: Connections between the different models of the new hierarchy.

6.5 Particle pressure modelling

When modelling multiphase flows, a separated set of equations for the conservation of mass, momentum and, if needed, energy, is written for each phase. The individual phase equations are then coupled to each other through interaction terms. Pressures are defined and the pressure gradient of each phase is included in the corresponding momentum conservation equation. When modelling gas-particle flows, the equations that describe the motion of the dispersed phase should contain terms involving a particle pressure gradient. In some mathematical models for gas-particle flows, the particle pressure is ignored. This assumption is made in Model E. In other models, the particle pressure is taken equal to the pressure from the gas phase. This is done in Model I [10]. However, neither of these arguments seems correct. In fact, theoretical and experimental works related to the stability of fluidized beds have shown that a particle pressure gradient has significant effects on the behaviour of multiphase flow models [35, 76, 38, 5]. In chapter 4, we saw that a particle pressure gradient may prevent delta shocks and vacuum states occurring in the solutions of

two-phase flow models. This shows the interest of considering a pressure gradient from the particulate phase .

Particle or granular pressure can be defined as a pressure generated by the action of particles and their interactions in a particulate multiphase flow. This pressure could be generated, for instance, during particle collisions or through interaction by the carrier fluid when particles get close to each other without necessarily colliding. A particle pressure should be positive and increasing as the particle volume volume fraction increases [35]. There are several attempts to measure the pressure generated by particles [35, 76, 38, 5].

In 1983, Needham and Merkin [76] proposed, as a first approximation for a particle pressure, the simple linear function

$$\pi = \kappa_0 \alpha, \tag{6.5.1}$$

where κ_0 is a constant, having dimensions of pressure. This choice is based on the suggestion from Drew and Segel [35], saying that the pressure generated from particle interactions is an increasing function of the volume fraction of the dispersed phase.

Foscolo and Gilibaro [38] introduced a force that is applied to the particles in a control volume and calculated from fluid dynamics considerations. This force represents a fluid dynamics phenomenon that arises from the dispersed phase and corresponds to the particle pressure gradient. Their particle pressure, also used in [97], is expressed as

$$\pi = \rho_l u_e^2 \alpha^2, \tag{6.5.2}$$

where u_e is called the "elastic wave velocity" and is given by

$$u_e = \big(3.2gd\frac{\rho_l - \rho}{\rho_l}\big)^{\frac{1}{2}}, \tag{6.5.3}$$

where g is the gravity acceleration, d is the uniform particle diameter and ρ_l is the density of the particle material.

In the work of Batchelor [5], the particle pressure is assumed to approach zero for two limiting cases: as the volume fraction of the particles approaches zero, and as the volume fraction of the particles approaches the close-packed limit. The first limit is due the absence of velocity fluctuations when the number of particle goes to zero, and the second limit is due to the decrease of fluctuations when particles approach a dense state. Batchelor's [5] expression for the particle pressure in an homogeneous bed is

$$\pi = \alpha \rho_l F(\alpha) u_m^2, \tag{6.5.4}$$

where F is a function satisfying the above two limiting cases and u_m is the superficial fluid velocity (referred to by Batchelor as the local mean velocity according to the frame of reference used in his paper). Batchelor suggested the following representation

$$F(\alpha) \approx \frac{\alpha}{\alpha_{cp}}(1 - \frac{\alpha}{\alpha_{cp}}), \tag{6.5.5}$$

where α_{cp} is the closed-packed solid fraction ($\alpha_{cp} \approx 0.62$ for a randomly packed bed of uniform sized particles).

Besides these theoretical studies, some authors tried to experimentally measure the particle pressure. In [62], Kumar et al. described their experiment to measure the particle pressure in solid-liquid flows in fluidized beds. They noticed that the particle pressure increases to a maximum and then decreases to zero as the volume fraction of the solid phase increases. For dilute flow, the increase of particle pressure with particle volume fraction can be ascribed to an enhanced collision rate and granular temperature, while the decrease of particle pressure at high volume fraction is due the increase of energy dissipation due to particle-particle collisions.

In 1991, Campbell and Wang [21] used an experimental system that measures the sum of the particle and fluid forces in a gas-particle mixture and then cancels the fluid contribution. From this, one measures the average pressure generated by the particles. They found that the particle pressure varies as

$$\frac{\pi}{\rho_l g d_e} \approx 0.08, \tag{6.5.6}$$

where d_e is the equivalent particle diameter, i.e. the diameter of a spherical particle of the same volume as the observed particle, and can be determined through experiments.

Some studies on turbulent dispersed fluid-solid flows also involved particle pressure modeling. In 1995, Abu-Zaid and Ahmadi [1] proposed a particle pressure for a dispersed mixture when particles are not in direct contact except during the relatively short period of collision, and when surface tension and Brownian motion effects are negligible. Their particle pressure is expressed as

$$\pi = \alpha p_f, \tag{6.5.7}$$

where p_f is the mean pressure in the carrier fluid phase.

In [97], Zenit et al. described a new technique for measuring the collisional particle pressure in a solid-liquid system using a fluidized bed. In their experiment, they found that the magnitude of the measured particle pressure increases from low concentrations ($< 10\%$ particle volume fraction), reaches a maximum for intermediate value of the volume fraction (30-40%), and decreases for more concentrated mixtures ($> 40\%$). Kumar et al. observed a similar behaviour in their experiment [62].

Remark 6.5.1. *The particle pressures obtained from experiments in fluidized beds (see [62], [97] and [21]), and Batchelor's pressure* (6.5.4) *do not satisfy our assumption* $\partial_\alpha \pi > 0$. *We will not use them.*

From the above literature review on particle pressure modelling, it clearly appears that particle pressure force can be expressed as a function of the density of the carrier fluid and the volume fraction of the particulate phase.

6.6 Numerical comparisons

This section is devoted to the numerical comparison of the different models in the new hierarchy of two-phase flow models presented in this chapter. We use the modified Lax-Friedrichs scheme (see section 2.3) from [87] to discretize all the models. This scheme is conservative and satisfies the discrete entropy inequality for conservation law equations. While the scheme is diffusive, it is less so than the classical Lax-Friedrichs scheme. In our context, it is not crucial since we only want to see the general behaviour of the solutions. For all the test cases in this section, the pressure of the carrier fluid satisfies the state equation (4.0.1). As we did in the previous chapters, quantities with different units should be represented in different graphs. However, in this section, different variables are represented in a same graph to avoid having a considerable number of figures. This is possible since these variables are non-dimensional. On all graphs, variables are plotted using the same scale shown at the left on the y-axis.

Suppose that we have a pipe of length 1 that initially contains air (the carrier fluid) at rest, i.e. $v_0(x) = 0$, and almost no particle, i.e. $\alpha_0(x) = 10^{-15}$ (we take this positive small value to avoid vacuum states). The air has a constant initial density $\rho_0(x) = 1$. Then, we start injecting particles with initial velocity $u_0(x) = 0.8$ at the inlet ($x = 0$) of the pipe. The boundary conditions on the inlet boundary of the pipe are set as follows:

$$\rho(0,t) = 1, \quad v(0,t) = 0, \quad \alpha(0,t) = \alpha_{\max}(1 - e^{-Rt}), \quad u(0,t) = 0.8, \tag{6.6.1}$$

where $\alpha_{\max}$ is the maximal particle volume fraction allowed at the inlet and R is a positive constant that sets the rate of variation of the particle volume fraction at the inlet. The flow is left free at the outlet ($x = 1$) of the pipe, i.e. no condition is imposed on the outlet boundary of the pipe. We take the reference density $\rho^{\text{ref}} = 1$ for the carrier fluid (air). This test case will be referred to as the *particle jet test case*. With this test case, we want to highlight the general behaviour of the solutions of the different models when solid particles are injected into air at rest, usually resulting in large momentum transfer from the particles to the carrier fluid. The *particle jet test case* will allow us to see how the different models behave for different particle volume fractions, different rates of variation of the particle volume fraction, different particle densities, and important momentum transfer between the two phases.

6.6.1 Comparison of Model I and Model IA

We firstly want to compare the numerical predictions of the models (I) and (IA) when heavy particles are injected at the inlet of the pipe at a low variation rate. For that, we use the *particle jet test case*. We suppose that the particles are droplets of water with reference density $\rho_l^{\text{ref}} = 1000$ (quite heavy) carried by air ($\rho^{\text{ref}} = 1$). The

density ratio calculated from the reference densities is given by $\epsilon = 0.001$. We take a maximal droplet volume fraction $\alpha_{\max} = 0.1$ and a slow rate of variation $R = 0.1$ of the droplet volume fraction at the inlet. We look at the numerical predictions of the two models as time evolves. Numerical solutions for both models at different times are displayed in Figure 6.2. We notice that the two models give almost the same

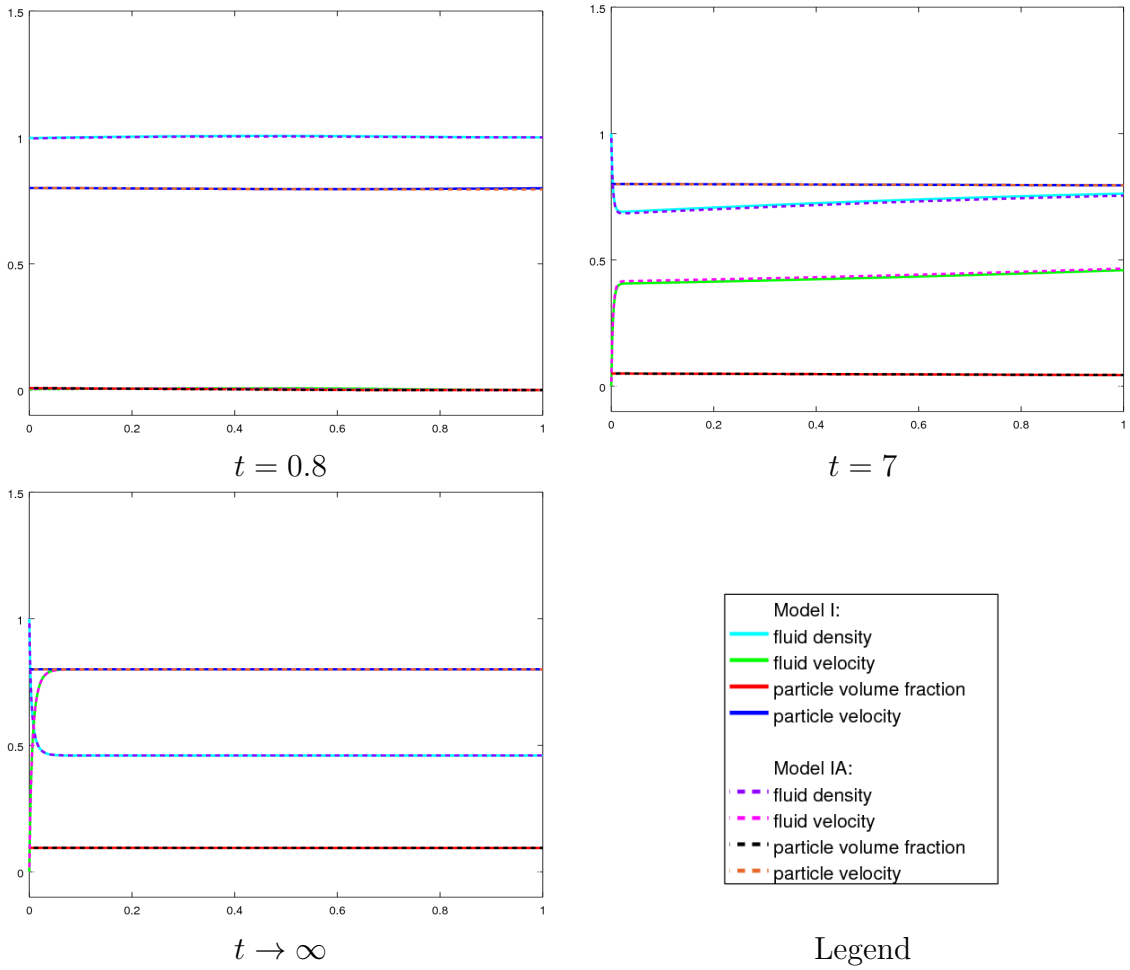

Figure 6.2: Evolution of the solutions of Model I and Model IA for a slow variation of the inlet droplet volume fraction. $\alpha_{\max} = 0.1$, $R = 0.1$, $\epsilon = 10^{-3}$, $\kappa = 1$, $\gamma = 1.4$, $\mu = 0.01$, $C_p = 10^{-4}$, $\Delta x = 10^{-3}$ and $\Delta t = 10^{-4}$.

transition phase solution and stationary solution. This solution is characterized by a momentum transfer from the droplets to the air. In fact, the droplets induce an inertia force that accelerates the air, which was initially at rest. This acceleration stops when the velocity of the air reaches the velocity of the droplets, and thus we reach the stationary state. The boundary layer observed in the solution near the inlet is due to the Dirichlet conditions (6.6.1) imposed on the inlet of the pipe. The flow

quickly settles in this boundary layer with the two models since they both include two-way momentum transfer source terms.

We now want to see the behaviour of the two models for large rates of variation of the droplet volume fraction at the inlet. We repeat the above experiment by increasing the rate of variation R at the inlet. Numerical results are shown in Figure 6.3. The

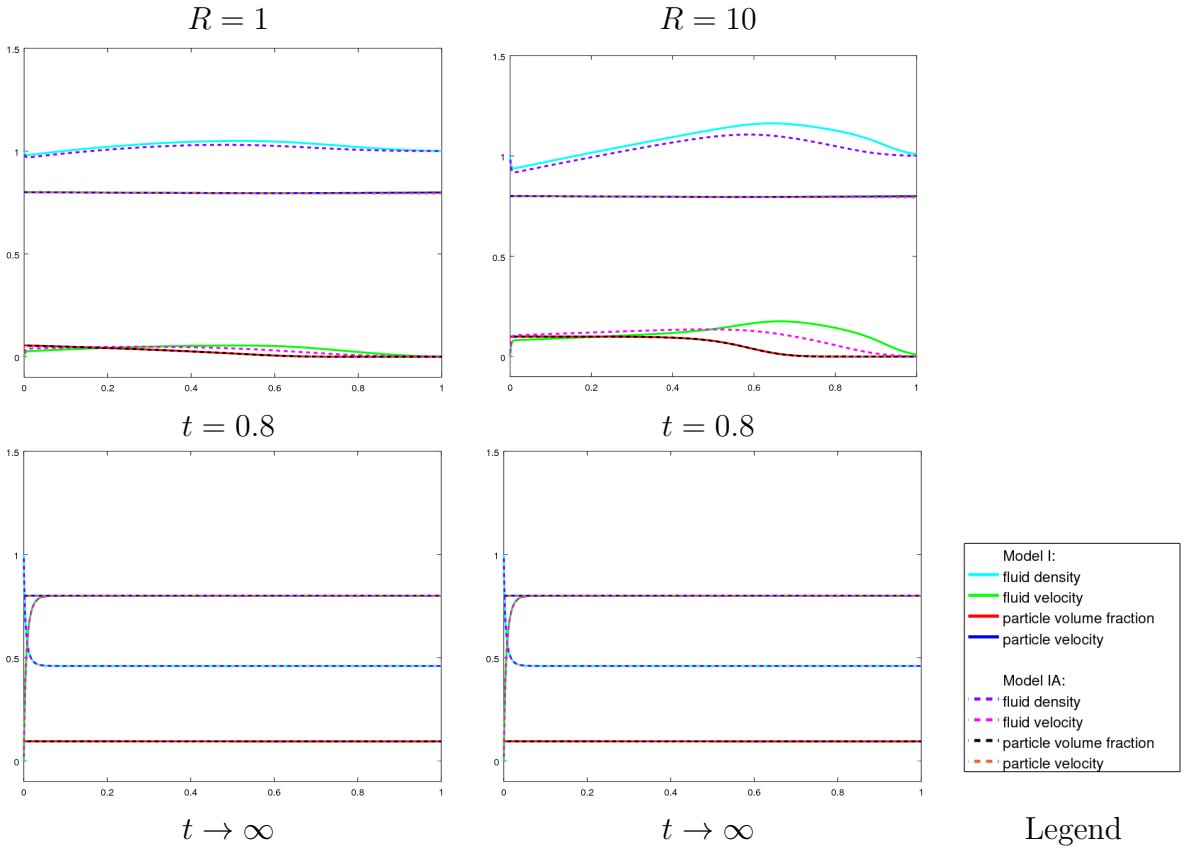

Figure 6.3: Solutions of Model I and Model IA for large rates of variation of the inlet droplet volume fraction. $\alpha_{\max} = 0.1$, $\epsilon = 10^{-3}$, $\kappa = 1$, $\gamma = 1.4$, $\mu = 0.01$, $C_p = 10^{-4}$, $\Delta x = 10^{-3}$ and $\Delta t = 10^{-4}$.

solutions of the two models are no longer similar during the transition phase. The differences lie in the air phase, are more important as the rate of variation R increases, and are due to the fact that condition (6.1.2) ($|\frac{D_v \alpha}{dt}| \approx 0$) of derivation of Model IA fails since the variation of the volume fraction is no longer negligible. However, we get the same stationary solution for both models. This stationary solution is the same as the one obtained with a slow rate of variation of the droplet volume fraction (compare with the stationary solution in Figure 6.2).

We next want to see how the two models behave when light particles are injected at the large rate of variation $R = 10$. For that, we consider two categories of particles:

solid particles that are hundred times lighter than droplets of water, i.e. we take the reference density $\rho_l^{\text{ref}} = 10$ (which implies $\epsilon = 0.1$), and solid particles that are twice heavier than the air, i.e. we take the reference density $\rho_l^{\text{ref}} = 2$ (which implies $\epsilon = 0.5$). Numerical results for both models with both categories of particles are represented in Figure 6.4. Model I predicts an acceleration/deceleration of the

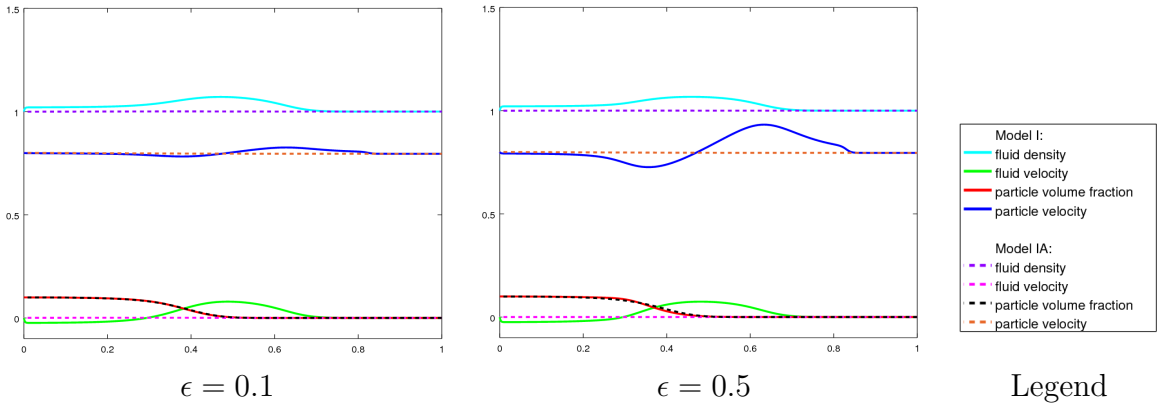

$\epsilon = 0.1$ $\epsilon = 0.5$ Legend

Figure 6.4: Solutions of Model I and Model IA at $t = 0.55$ for two particle densities. $\alpha_{\max} = 0.1$, $R = 10$, $\kappa = 1$, $\gamma = 1.4$, $\mu = 0.01$, $C_p = 10^{-4}$, $\Delta x = 10^{-3}$ and $\Delta t = 10^{-4}$.

particles in the pressure drop/pressure rise area during the transition phase. The particles are light, so that they react to small variations in the fluid pressure. This acceleration/deceleration is not observed with heavier particles (droplets of water, see Figure 6.3). The variation in the particle velocity is also not observed with Model IA because the term $\epsilon\alpha\partial_x p$ that induces this variation is neglected in Model IA. We do not show the stationary solution for these test cases because it is the same as for the above two first experiments.

We saw from these three experiments that Model IA can be used in place of Model I when looking for stationary solutions or dealing with flows that involve slow rates of variation of the particle volume fraction. The two models may differ during transition phases for flows involving light particles (ϵ closer to 1) or large rates of variation of the particle volume fraction.

6.6.2 Comparison of Model IA and Model E-IE

Here, we highlight the limitations of Model E-IE. In fact, we want to show that Model E-IE is not valid when momentum transfer from the dispersed phase to the carrier fluid becomes important. For that, we consider the *particle jet test case* because this test case involves a strong momentum transfer from the particles to the air as we already have seen with Model IA in the previous subsection.

We first suppose that the particles are droplets of water with reference density $\rho_l^{\text{ref}} = 1000$. We compute the solutions of both models with two different inlet volume fractions $\alpha_{\max}$ of droplets. Stationary solutions at the middle of the pipe ($x = 0.5$) are displayed in Table 6.1. Next, we consider two categories of particles: solid particles

	$\alpha_{\max} = 1.000 \times 10^{-4}$				$\alpha_{\max} = 0.01$			
	ρ	v	α	u	ρ	v	α	u
Model IA	0.999	0.001	0.993×10^{-4}	0.795	0.459	0.797	0.010	0.799
Model E-IE	1.000	0.000	0.993×10^{-4}	0.795	1.000	0.000	0.010	0.795

Table 6.1: Stationary solutions of Model IA and Model E-IE at the middle of the pipe ($x = 0.5$) for different droplet volume fractions. $\epsilon = 10^{-3}$, $\kappa = 1$, $\gamma = 1.4$, $\mu = K_D = 0.01$, $\Delta x = 10^{-3}$ and $\Delta t = 10^{-4}$.

with reference density $\rho_l^{\text{ref}} = 500$, and solid particles with reference density $\rho_l^{\text{ref}} = 2$. The solutions for both categories of particles are computed with the same particle inlet volume fraction $\alpha_{\max} = 0.01$. Stationary solutions computed at the middle of the pipe ($x = 0.5$) are displayed in Table 6.2. The rate of variation of the droplet

	$\epsilon = 0.002$ ($\rho_l = 500$)				$\epsilon = 0.5$ ($\rho_l = 2$)			
	ρ	v	u	α	ρ	v	u	α
Model IA	0.465	0.784	0.010	0.799	0.995	0.005	0.010	0.795
Model E-IE	1.000	0.000	0.010	0.795	1.000	0.000	0.010	0.795

Table 6.2: Stationary solutions of Model IA and Model E-IE at the middle of the pipe ($x = 0.5$) for two particle densities. $\alpha_{\max} = 0.01$, $\kappa = 1$, $\gamma = 1.4$, $\mu = K_D = 0.01$, $\Delta x = 10^{-3}$ and $\Delta t = 10^{-4}$.

volume fraction is $R = 1$ for all these experiments. The two models give almost the same solution when the quantity $\frac{\mu\alpha}{\epsilon}$ is small ($\leqslant 10^{-3}$). However, the two solutions are different when $\frac{\mu\alpha}{\epsilon}$ is big enough($> 10^{-3}$). Momentum transfer from particles to air progressively increases when the quantity $\frac{\mu\alpha}{\epsilon}$ gets larger than 10^{-3}.

These experiments show that Model E-IE is not valid when momentum transfer occurs from the dispersed phase to the carrier fluid because it is a one-way coupling model that only takes into account the effects of the carrier fluid on the dispersed phase and not vice versa.

6.6.3 Model IA: Evolution of discontinuous solutions

Here, we are interested in how discontinuous solutions of Model IA evolve in time. For that, we consider three cases corresponding to Riemann problems on the line, and choose initial velocities as follows:

Case 1: the fluid initially moves faster than the particles:

$$v_0(x) = \begin{cases} 1.7, & x \leqslant 0.1, \\ 0.7, & x > 0.1, \end{cases} \qquad u_0(x) = \begin{cases} 1.5, & x \leqslant 0, \\ 0.5, & x > 0. \end{cases}$$

Case 2: the fluid and the particles have the same initial velocity:

$$v_0(x) = u_0(x) = \begin{cases} 1.5, & x \leqslant 0, \\ 0.5, & x > 0. \end{cases}$$

Case 3: the fluid initially moves slower than the particles:

$$v_0(x) = \begin{cases} 1.5, & x \leqslant 0, \\ 0.5, & x > 0, \end{cases} \qquad u_0(x) = \begin{cases} 1.7, & x \leqslant 0.1, \\ 0.7, & x > 0.1. \end{cases}$$

We take an initial fluid density $\rho_0(x) = 0.6$ and an initial particle volume fraction $\alpha_0(x) = 0.001$.

This test case will allow us to see how initial discontinuous (in velocities) solutions of Model IA evolve in time. We look at the solution on the whole real line. However, we solve (IA) in the bounded domain $[-0.5, 3.5]$. We impose a zero slope for each variable on the inlet boundary $x = -0.5$ of the computational domain. Numerical results are displayed in Figure 6.5. The displayed volume fraction α is rescaled ($\times 100$). The solution is composed of a 1-shock and 2-shock waves for the continuous phase, and a delta shock wave for the dispersed phase. It has the same general configuration as if we solve separately the continuous phase using the Euler equation (IE), and the dispersed phase using the Eulerian droplet model (E). However, the intermediate state between the 1-shock and 2-shock waves is no longer constant, as opposed to the model (IE), where this intermediate state is constant. The left and right states of the delta shock depend on both space and time, as opposed to Model E, where these states only depend on time. The difference is due to the two-way coupling. The delta shock wave either catches up with the 1-shock wave (*Case 1*) or is caught up by the 2-shock wave (*Case 3*), depending on its initial position with respect to the two shock waves. In the three cases, the delta shock wave lies between the 1-shock and 2-shock waves for larger times (see right column of Figure 6.5). The Rankine-Hugoniot conditions for the two shocks are determined in the classical way. It is a challenge to derive the generalized Rankine-Hugoniot conditions for the delta shock wave. The difficulty lies in the r.h.s of the momentum equation for the dispersed phase. In fact, this term should be considered as a product of distributions since α evolves as a Dirac delta distribution.

The same experiment with Model I (without pressure correction term) gives qualitatively the same solution as for Model IA. This confirms that Model IA can be used in place of Model I even if the conditions (6.1.2) and (6.1.3) fail for some points in the domain.

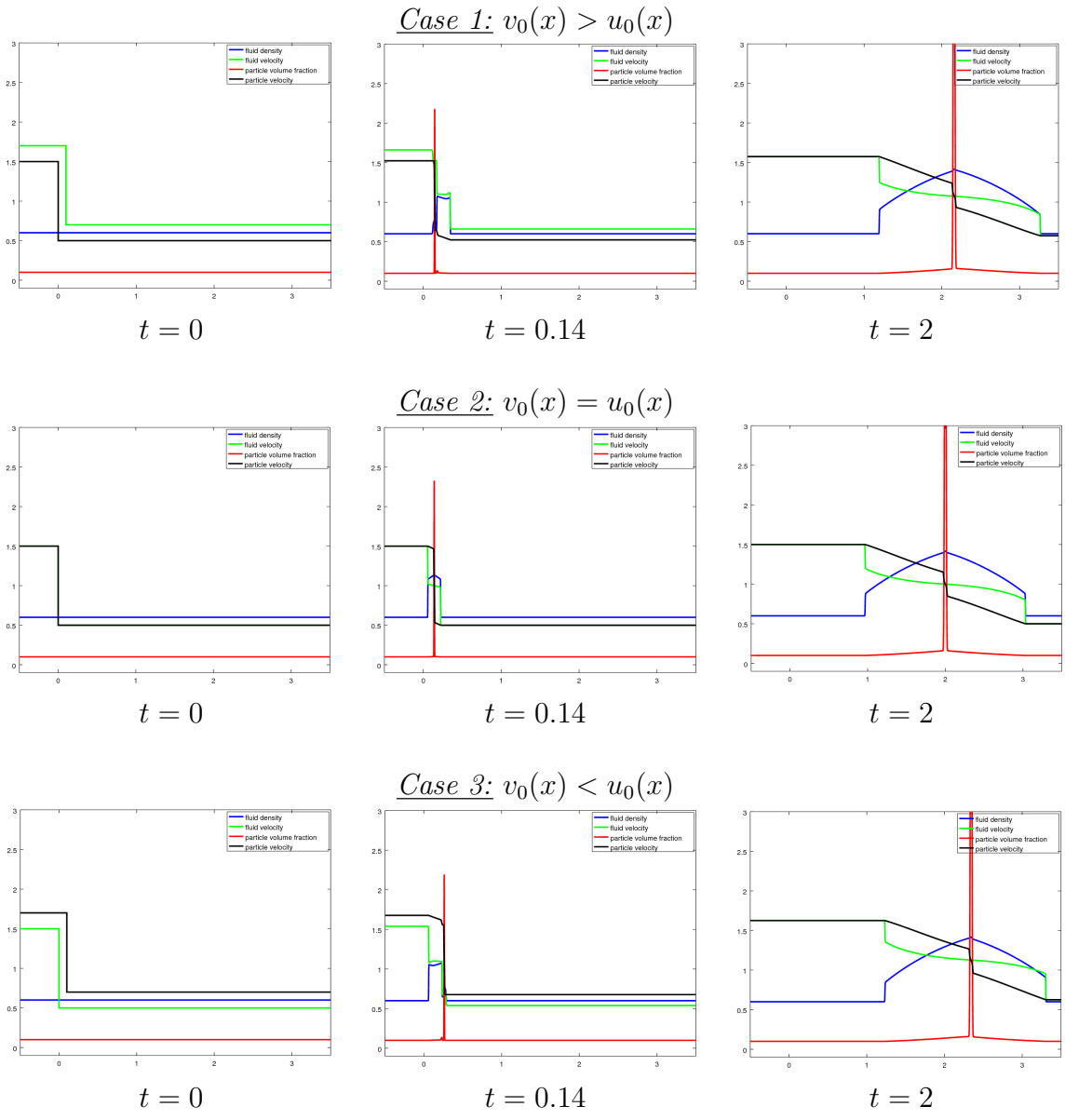

Figure 6.5: Model IA: Evolution in time of a 1-shock and 2-shock waves for the fluid phase, and a delta shock wave for the particulate phase. $\epsilon = 10^{-3}$, $\kappa = 0.5$, $\gamma = 1.4$, $\mu = 1$, $\Delta x = 2 \times 10^{-4}$ and $\Delta t = 4 \times 10^{-5}$.

6.6.4 Model IAP: Comparison of different particle pressures

In section 6.5, we reviewed the most common particle pressure expressions proposed in the literature for gas-particle flows. Here, we are interested in the effects of a particle pressure gradient on particles in movement.

We consider a cloud of droplets of water ($\rho_l^{\text{ref}} = 1000$) represented by an initial volume fraction $\alpha_0(x) = \alpha_{\max} \exp(-50(x-0.5)^2)$, where $\alpha_{\max}$ is the maximal droplet volume fraction allowed. This cloud moves at a uniform initial velocity $u_0(x) = 0.5$ in a fluid (air) with the same initial velocity as the droplets, and initial density $\rho_0(x) = 1$. The computational domain is $[0, 3]$. We impose the following Dirichlet conditions on the inflow boundary ($x = 0$):

$$\rho(0,t) = 1, \quad v(0,t) = u(0,t) = 0.5, \quad \alpha(0,t) = \alpha_{\max} \exp(-50(-0.5)^2). \tag{6.6.2}$$

The flow is left free at the outflow boundary ($x = 3$). This test case will be referred to as *particle cloud test case*. This test case will allow us to see and compare the effects of different particle pressure gradients on droplets in movement.

We take $\alpha_{\max} = 0.005$. Numerical predictions of Model IAP with different particle pressure functions ((6.5.7), (6.5.1) and (6.5.2)) are represented in Figure 6.6. The displayed droplet volume fraction is scaled ($\times 100$). We observe a dispersion of the cloud of droplets as time evolves. This dispersion is more important as the particle pressure gradient is important. We also notice an acceleration (resp. deceleration) of the particles when the particle pressure decreases (resp. increases). The fluid phase remains almost constant with respect to its initial state. With the same experiment, Model IA predicts an uniform translation of the cloud of droplets. There is no dispersion, acceleration or deceleration of the particles. Hence, the particle pressure gradients are responsible of the dispersion, acceleration or deceleration of the particles.

6.6.5 Model IA versus Model IAP: effects of a particle pressure gradient on a delta shock wave

We saw from numerical simulations in the previous subsection that a particle pressure acts on particles by dispersing the latters. Here, we illustrate how a particle pressure prevents the formation of a huge concentration of particles at a specific point (delta shock wave) as it may happen with Model I and Model IA (see Figure 6.5.)

We repeat the test case from Figure 6.5 with Model IAP using Needham's particle pressure given in (6.5.1). Numerical results for *Case 2* at $t = 2$, are displayed in Figure 6.7. In Model IAP, the presence of a particle pressure gradient prevents the accumulation of droplets at the point of discontinuity of the droplet velocity, as opposed to Model IA, where this accumulation is observed. In fact, the particle pressure gradient breaks the initial discontinuity in the particle velocity into two discontinuities (shocks waves). The droplet volume fraction between these two discontinuities then remains bounded.

This shows the importance of taking into account pressure resulting from the dispersed phase when modeling gas-particle flows. Note that a pressure coming only

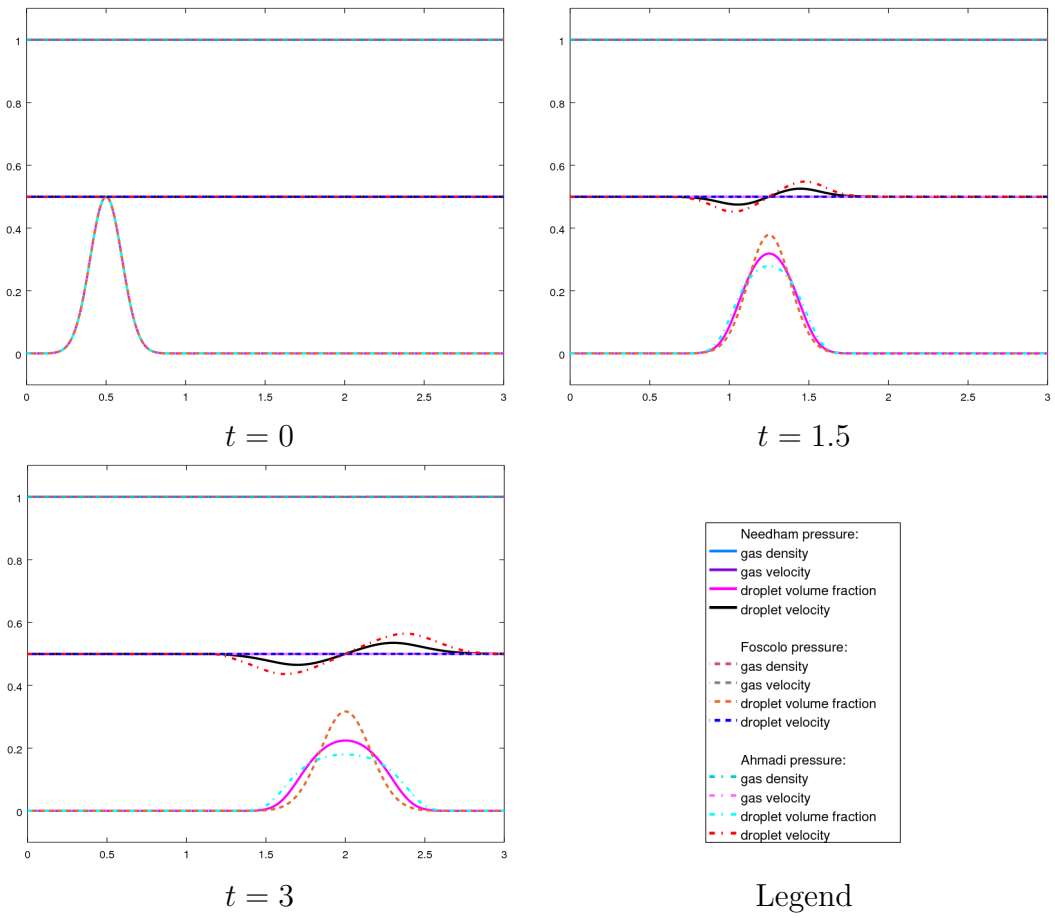

Figure 6.6: Model IAP: Evolution of a cloud of droplets with different particle pressures. $\alpha_{max} = 0.005$, $\epsilon = 10^{-3}$, $\kappa = 1$, $\gamma = 1.4$, $\mu = 0.01$, $\kappa_0 = 0.5$, $d = 1\mu m$, $g = 9.8m/s^2$, $\Delta x = 10^{-3}$ and $\Delta t = 10^{-4}$.

from the continuous phase cannot prevent from the accumulation of particles as we checked with Model I.

6.6.6 Comparison of Model G and the others models

This subsection is devoted to the numerical comparison of the general two-phase flow model (G) with some others models in the new hierarchy of two-phase flow models.

We first consider the *particle cloud test case*. This test case allows a comparison of the models (IAP) and (G) for a flow of droplets of water with a small particle pressure coefficient (we take the particle pressure in (6.5.1), with $\kappa_0 = 0.1$), moving in a fluid with a high fluid pressure coefficient $\kappa = 20$. Numerical results for both models with

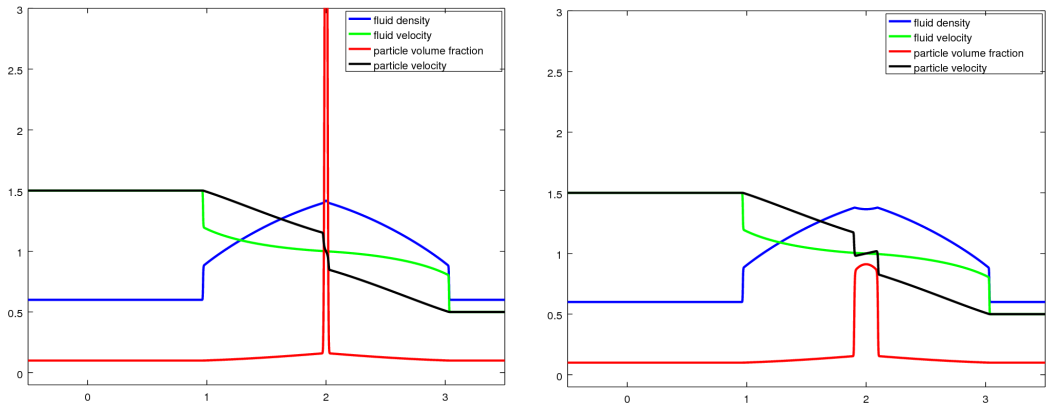

Model IA Model IAP

Figure 6.7: Solutions of Model IA and Model IAP at $t = 2$. $\epsilon = 10^{-3}$, $\kappa = 0.5$, $\gamma = 1.4$, $\mu = 1$, $\kappa_0 = 1$, $\Delta x = 2 \times 10^{-4}$ and $\Delta t = 4 \times 10^{-5}$.

different volume fractions are shown in Figure 6.8. The displayed droplet volume fraction is rescaled ($\times 5$). The two models predict that the droplets are advected with a progressive dispersion of the cloud (due to the particle pressure gradient) as time evolves. The droplets accelerate (resp. decelerate) in particle pressure drop (resp. rise) zones. The fluid phase solutions of the two models are very similar for the low droplet volume fraction $\alpha_{\max} = 0.01$. However, they slightly differ for the larger droplet volume fraction $\alpha_{\max} = 0.1$. The difference is due to the contribution of the terms $\frac{D_v \alpha}{dt}$ and $\frac{p}{1-\alpha}\partial_x \alpha$, which are neglected in the equations for the fluid phase in Model IAP. Hence, Model G should be used for large particle volume fractions.

We finally consider the test case from Figure 6.3, again to compare Model G and Model IAP. We take Needham's particle pressure (6.5.1), with $\kappa_0 = 0.2$. Numerical results for the models (IAP) and (G) are shown in Figure 6.9. Looking at figures 6.3 and 6.9, on can compare the models (I), (IA), (IAP) and (G) for large rates of variation of the particle volume fraction at the inlet of the computational domain. We see that all the models predict the same stationary solution. However, they slightly differ during the transition phase. The difference is more important as the rate R of variation of the particle volume fraction increases. This is due to the fact that the terms $\frac{D_v \alpha}{dt}$ and $\frac{p}{1-\alpha}\partial_x \alpha$ are not negligible when the variation of the particle volume fraction is important. We picked $\alpha_{\max} = 0.1$ to see what happens at very high volume fraction of particles. However, in most applications, the particle volume fraction is small (less than 0.01). In this range of particle volume fractions, all the models give very similar solutions.

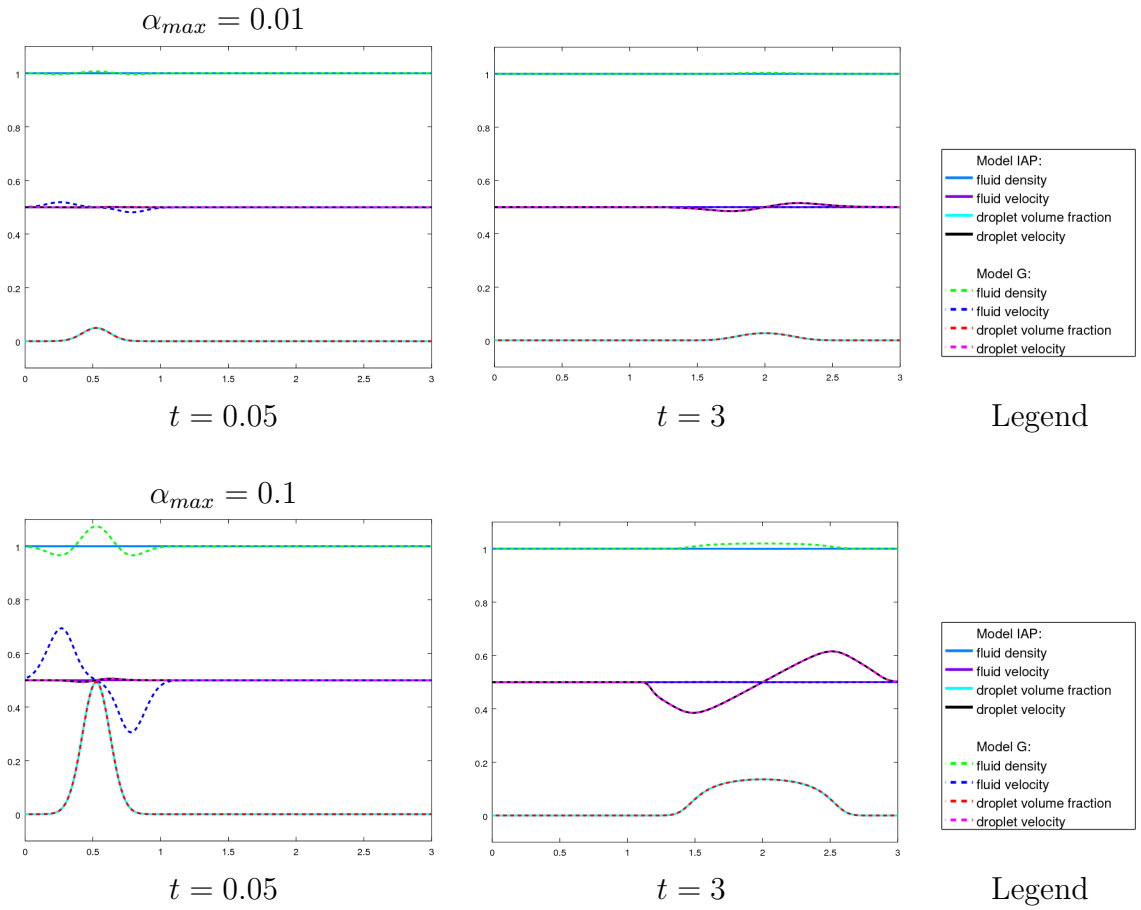

Figure 6.8: Model IAP vs Model G: Evolution of a cloud of droplets for different droplet volume fraction. $\epsilon = 10^{-3}$, $\kappa = 20$, $\gamma = 1.4$, $\mu = 0.01$, $\kappa_0 = 0.1$, $\Delta x = 10^{-3}$ and $\Delta t = 10^{-4}$.

6.7 Conclusion

In this chapter, we derived a new hierarchy of Eulerian models for two-phase flows starting from two relatively general models. The first general model (the first model in the hierarchy of Bouchut [10]) is stated as a two-way common pressure, conditionally hyperbolic non-conservative model with a pressure correction term. For small variations of the volume fraction, no pressure correction term, and if the quantity $\epsilon\alpha\partial_x p$ is small, we could reduce this model to a two-way one-pressure, conservative and weakly hyperbolic model (Model IA). If the quantity $\frac{\mu\alpha}{\epsilon}$ is small then Model IA could be reduced to a one-way one-pressure, conservative and weakly hyperbolic model (Model E-IE). The second general model (Model G) is stated as a two-way coupling two-pressure, conditionally hyperbolic conservative model. For small varia-

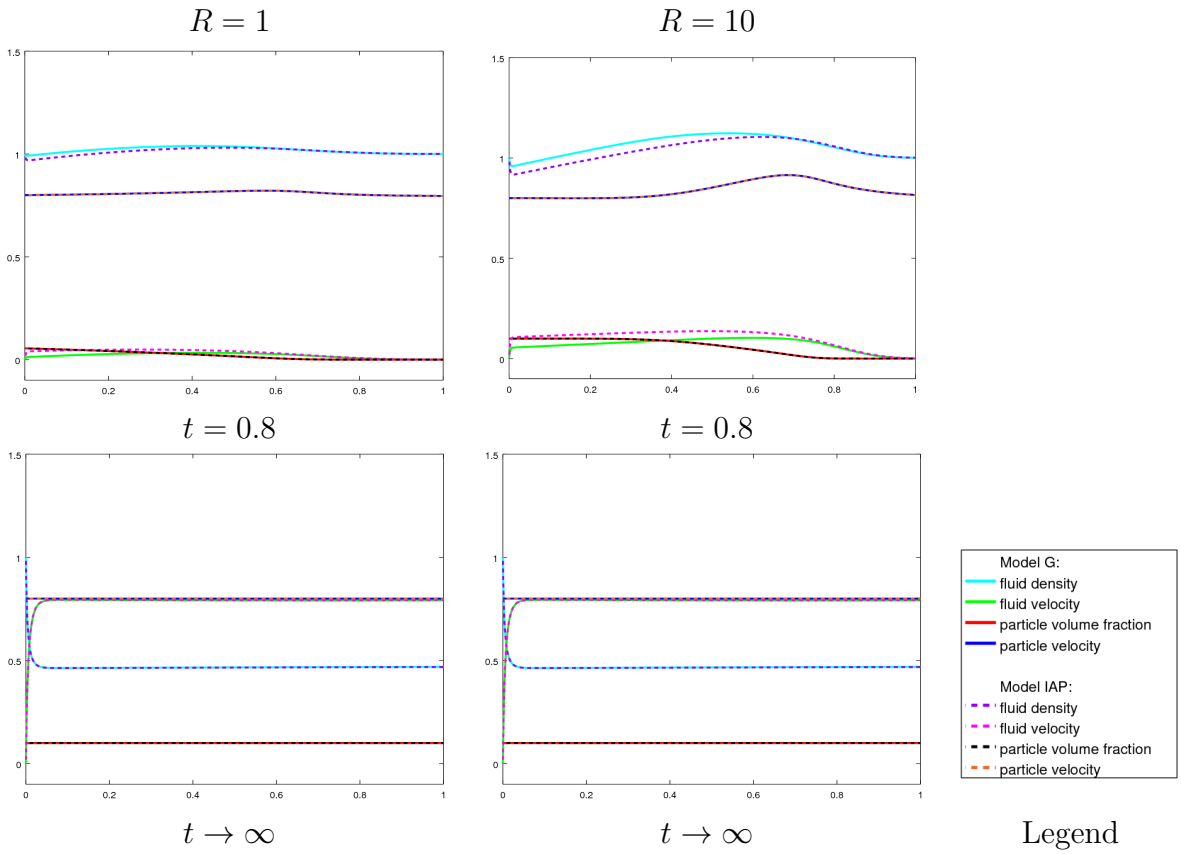

Figure 6.9: Solutions of Model G and Model IAP for large rates of variation of the inlet droplet volume fraction. $\alpha_{\max} = 0.1$, $\epsilon = 10^{-3}$, $\kappa = 1$, $\gamma = 1.4$, $\mu = 0.01$, $\kappa_0 = 0.2$, $\Delta x = 10^{-3}$ and $\Delta t = 10^{-4}$.

tions of the volume fraction, we could reduce this model to a two-way two-pressure, conservative and strictly hyperbolic model (Model IAP). The latter reduces to Model IA when the pressure from the dispersed phase is neglected. If the quantity $\frac{\mu\alpha}{\epsilon}$ is small then Model IAP could be reduced to a one-way two-pressure, conservative and strictly hyperbolic model (Model EP-IE).

We also reviewed particle pressure modelling in gas-particle flows and examined the eigenstructures of two-pressure models for two-phase flows. This study provides a better understanding of the impact of particle pressure gradients in the momentum equation of models for two-phase flows, and allows to identify a physical mechanism to avoid delta shocks from occurring in Eulerian two-phase flow models.

The main conclusion of this chapter is that two-way coupling two-pressure models should be used in general, for instance Model IAP or, even better, Model G.

Chapter 7

Applications to two-dimensional air-particle flows

The non-conservative form of the Eulerian droplet model (E) was used for in-flight icing simulations [15, 75, 6, 50, 17] and recently for air-particle flows in airways [14, 16]. However, we showed in chapter 3 that this model may develop delta shock waves that are not physical since the volume fraction should remain bounded. Moreover, the conservative form should be used when discontinuous travelling waves are present in the solutions. In chapters 5 and 6, we saw that a particle pressure prevents the formation of delta shocks. In this chapter, we use an Eulerian droplet model with a particle pressure (EP) for the prediction of air-particle flows. This model is written in conservative form and does not develop the non desirable delta shocks.

The chapter is organized as follows. In section 7.1, we present theoretical arguments leading to the use of Model EP for the proposed applications. In section 7.2, we discuss a finite element method for the numerical solution of Model EP for two-dimensional applications. Numerical results are carried out in section 7.3.

7.1 Mathematical model

Eulerian models for air-particle flows are based on a set of partial differential equations that express the conservation of mass, momentum and, if needed, of energy for the continuous air phase and the dispersed particulate phase. We make the following assumptions regarding the behaviour of the particles and the air flow:

1) The air phase flow is incompressible;

2) Particle mass loading is small, i.e. the bulk density (mass of the phase in the mixture per unit volume of mixture) of the particle over the bulk density of the gas is small enough so that two-way coupling is not needed;

3) The particles are spherical with same diameter and without any deformation;

4) No heat and mass exchange between the particles and the carrier fluid;

5) The only forces acting on the particles are due to air drag and particle pressure.

As we already have seen in chapter 6, no modifications of the carrier fluid equations is needed for small particle mass loading (see also [30]). Therefore, the air phase is kept independent from the particulate phase. The classical incompressible Navier-Stokes equations are the basis of incompressible flow computations. These equations are expressed as

$$\begin{aligned} \partial_t \mathbf{v} + \mathbf{v} \cdot \nabla \mathbf{v} - \nu \Delta \mathbf{v} + \nabla p = 0, \\ \nabla \cdot \mathbf{v} = 0, \end{aligned} \tag{7.1.1}$$

where $\mathbf{v}$ is the fluid velocity field; p is the pressure; and ν is the kinematic viscosity. The Navier-Stokes equations (7.1.1) are used to model the air phase.

Remark 7.1.1. *The Euler equations can also be used to model the air phase. Here, we use Navier-Stokes equations since the air flow is assumed to be incompressible and we will consider internal flows where viscous effects are important. This was also done in [15, 17, 75, 6, 50, 14, 16].*

The equations for the particulate phase are derived using an averaging procedure as in [34]. They can be written as

$$\begin{cases} \partial_t(\alpha\rho_l) + \nabla \cdot (\alpha\rho_l \mathbf{u}) = 0, \\ \partial_t(\alpha\rho_l \mathbf{u}) + \nabla \cdot (\alpha(\rho_l \mathbf{u} \otimes \mathbf{u} + \pi \mathcal{I})) = K C_D Re_d \alpha \big(\mathbf{v} - \mathbf{u}\big), \end{cases} \tag{7.1.2}$$

where $0 < \alpha < 1$, ρ_l, $\mathbf{u}$ and π are the volume fraction, density, velocity field and pressure of the particles, respectively, and $\mathcal{I}$ is the identity matrix. The momentum transfer between the two phases is due to the drag force given by the term on the r.h.s of the second equation, where

$$Re_d = \frac{\rho d |\mathbf{v} - \mathbf{u}|}{\mu} \tag{7.1.3}$$

is the particle Reynolds number; ρ is the air density; d is the diameter of the particles; μ is the dynamic viscosity of the air; and C_D is a dimensionless drag coefficient which depends on the particle Reynolds number. We will use the widely accepted correlation for spherical particles [49]:

$$C_D = \begin{cases} \dfrac{24}{Re_d}\big(1 + 0.15 {Re_d}^{0.687}\big), & \text{if} \quad Re_d < 1000, \\ 0.44, & \text{if} \quad Re_d \geqslant 1000. \end{cases} \tag{7.1.4}$$

The inertia parameter K comes from the averaging procedure and is given by (see [49])

$$K = \frac{3\mu}{4d^2}. \tag{7.1.5}$$

Remark 7.1.2. *The air density ρ is constant since the air flow is assumed to be incompressible.*

In the following, we also assume that the particle mass density ρ_l is constant. With this simplification, model (7.1.2) can be written as

$$\begin{cases} \partial_t \alpha + \nabla \cdot (\alpha \mathbf{u}) = 0, \\ \partial_t (\alpha \mathbf{u}) + \nabla \cdot (\alpha(\mathbf{u} \otimes \mathbf{u} + \pi \mathcal{I})) = K_D \alpha \big(\mathbf{v} - \mathbf{u}\big), \end{cases} \tag{7.1.6}$$

where $K_D = \frac{KC_D Re_d}{\rho_l}$. For smooth solutions with no vacuum state ($\alpha > 0$), system (7.1.6) can be written in the non-conservative form

$$\begin{cases} \partial_t \alpha + \nabla \cdot (\alpha \mathbf{u}) = 0, \\ \partial_t \mathbf{u} + (\mathbf{u} \cdot \nabla)\mathbf{u} + \dfrac{1}{\alpha} \nabla \cdot (\alpha \pi \mathcal{I}) = K_D(\mathbf{v} - \mathbf{u}). \end{cases} \tag{7.1.7}$$

Remark 7.1.3. ***i)*** *There is a ratio $\frac{1}{\rho_l}$ (coming from the simplification of ρ_l) that multiplies the particle pressure π. To simplify the notation, this ratio is included in the particle pressure as a coefficient.*
ii) *System* (7.1.6) *is nothing else but Model EP (with a non constant drag coefficient) in the multi-dimensional case.*
iii) *If the particle pressure $\pi = 0$, systems* (7.1.6) *and* (7.1.7) *reduce to Model E in the multi-dimensional case, written in conservative and non-conservative form, respectively.*

7.2 Finite element methods

Finite element methods have been introduced in the early 1950s and are known to be useful for solving many problems arising in engineering, physics and mathematics. Finite element methods are capable of solving complex PDEs and handling physical problems with complex geometries. Finite element methods are based on a weak formulation of the PDE. This section is devoted to finite element methods for air phase equations (7.1.1) and particulate phase equations (7.1.6).

Let $\Omega \subset \mathbb{R}^2$ be an open and bounded domain. The boundary $\partial\Omega$ of the domain Ω is split in three parts:

$$\Gamma_- = \Big\{(x, y) \in \partial\Omega : \mathbf{u} \cdot \mathbf{n} < 0\Big\}, \tag{7.2.1}$$

$$\Gamma_0 = \Big\{(x,y) \in \partial\Omega : \mathbf{u}\cdot\mathbf{n} = 0\Big\}, \tag{7.2.2}$$

$$\Gamma_+ = \Big\{(x,y) \in \partial\Omega : \mathbf{u}\cdot\mathbf{n} > 0\Big\}, \tag{7.2.3}$$

where $\mathbf{n}$ is outward unit normal of the domain. We consider a regular triangulation $\mathcal{T}_h$ (see [37]) of this domain, consisting of a finite number of triangles $\mathcal{K}$,

$$\Omega = \bigcup_{\mathcal{K}\in\mathcal{T}_h} \mathcal{K}. \tag{7.2.4}$$

The discretization parameter h is the maximal element length (generally h is taken as the maximum of the diameters of the triangles $\mathcal{K}$). The time interval $[0,T]$ is discretized as

$$\Delta t = \frac{T}{N}, \quad t_n = n\Delta t, \quad n = 0,1,2,...,N, \tag{7.2.5}$$

where Δt is the time step used.

7.2.1 Finite element methods for the air phase equations

To solve the Navier-Stokes equations (7.1.1), we use the Taylor-Hood finite element discretization in space (continuous piecewise quadratic polynomial for velocity and linear polynomial for pressure). The Taylor-Hood element satisfies the well-known inf-sup condition required for stability [8]. Let $\mathcal{V}_{\Phi_i h}$ and $\mathcal{M}_h$ be the following spaces of piecewise continuous finite element functions satisfying

$$\begin{aligned}
\mathcal{V}_{\Phi_i h} &= \Big\{v_h \in \mathcal{C}^0(\Omega,\mathbb{R}) : v_{h|_\mathcal{K}} \in \mathbb{P}_2,\ \forall \mathcal{K} \in \mathcal{T}_h,\ v_{h|_{\partial\Omega}} = \Phi_i\Big\},\\
\mathcal{M}_h &= \Big\{v_h \in \mathcal{C}^0(\Omega,\mathbb{R}) : v_{h|_\mathcal{K}} \in \mathbb{P}_1,\ \forall \mathcal{K} \in \mathcal{T}_h\Big\},
\end{aligned} \tag{7.2.6}$$

where $\mathbb{P}_k$ denotes the vector space of polynomials in two variables of degree less thant or equal to k on any element $\mathcal{K}$, and Φ_i is a given function that belongs to the trace space of the finite element functions on the boundary $\partial\Omega$. We approximate the unknowns $\mathbf{v} = (v_1, v_2)$ and p by the finite element functions $\mathbf{v}_h = (v_{1h}, v_{2h})$ and p_h from $\mathcal{V}_{\Phi_1 h} \times \mathcal{V}_{\Phi_2 h}$ and $\mathcal{M}_h$, respectively. For the time derivative discretization, we use the characteristic method [45], which is already implemented in FreeFem++ [51] and gives good numerical results for the incompressible Navier-Stokes equations. The Taylor-Hood finite element formulation for the incompressible Navier-Stokes (7.1.1) with the characteristic method reads:

Find $\mathbf{v}_h^n \in \mathcal{V}_{\Phi_1 h} \times \mathcal{V}_{\Phi_2 h}$ and $p_h^n \in \mathcal{M}_h$ such that

$$\begin{aligned}
\int_\Omega \mathbf{v}_h^n \cdot \boldsymbol{\psi}_h\, dx + \nu\Delta t \int_\Omega \nabla\mathbf{v}_h^n \cdot \nabla\boldsymbol{\psi}_h\, dx - \Delta t \int_\Omega p_h^n \nabla\cdot\boldsymbol{\psi}_h\, dx &= \int_\Omega \mathbf{v}_h^{n-1}\circ\chi^{n-1}\cdot\boldsymbol{\psi}_h\, dx,\\
\int_\Omega \beta p_h^n \varphi_h\, dx - \int_\Omega \nabla\cdot v_h^n \varphi_h\, dx &= 0,
\end{aligned} \tag{7.2.7}$$

for all $\boldsymbol{\psi}_h \in \mathcal{V}_{0h} \times \mathcal{V}_{0h}$ and $\varphi_h \in \mathcal{M}_h$, where χ^{n-1} is an approximation of the characteristic $\chi(x, t_n; t_{n-1})$ solution of

$$\begin{cases} \dfrac{d\chi}{ds}(x, t_n; s) = \mathbf{v}_h^n(\chi(x, t_n; s), s), \quad s \in [t_n, t_{n-1}], \\ \chi(x, t_n; t_n) = x, \end{cases} \tag{7.2.8}$$

on the time interval $[t_{n-1}, t_n]$. For more details on the characteristic method and its use to solve Navier-Stokes equations, see [45, 39].

Remark 7.2.1. *The matrix from the discretization* (7.2.7) *may be singular from the unspecified average pressure in Navier-Stokes equations with boundary conditions on the velocity* $\mathbf{v}$ *only. To avoid this drawback, one can force the average pressure or add a small term* $\int_\Omega \beta p_h^n \varphi_h \, dx$*, with* $0 < \beta \ll 1$*, in the variational formulation. This explains the presence of this term in the variational formulation.*

7.2.2 Finite element methods for the particle equations

The particulate phase equations (7.1.6) form a pure convection problem with a zeroth-order linear source term. It is known that the classical Galerkin discretization of convective terms generally produces spurious oscillations, also known as wiggles. Moreover, explicit time-stepping schemes applied to classical Galerkin methods are usually unstable. Various stabilization techniques mimicking "upwinding" methods, have been developed [52, 53, 86]. These stabilized finite element methods help to remove the unwanted oscillations but very often introduce too much numerical diffusion, leading to poor accuracy. Another drawback with these methods is the loss of consistency, reducing the order of accuracy and convergence rate. An important improvement came with the streamline upwind/Petrov-Galerkin (SUPG) method developed by Brooks and Hughes [55, 20], which substantially eliminates almost all the difficulties mentioned above. The SUPG method only introduces numerical diffusion along streamlines in a consistent manner. Consequently, stability is obtained without compromising the order of accuracy. The SUPG method is one of the most widely used stabilized methods in finite element computations of compressible flows, however, it still struggles to remove unwanted oscillations (known as undershoots and overshoots) in the neighbourhood of sharp layers and shock waves. This deficiency of the SUPG method comes from the lack of monotonicity of the resulting scheme. As a remedy, researchers proposed to add an isotropic artificial diffusion term in the SUPG formulation in a proper way so that the resulting scheme satisfies the discrete maximum principle, at least in some problems. The maximum principle is very important since it ensures monotonicity of the solution near shocks and sharp layers, and thus no oscillation is observed. To ensure high accuracy, this artificial diffusion should depend on the discrete solution in a nonlinear way since linear monotone schemes can

be at most first order accurate. This additional term is known as *discontinuity shock-capturing term* [56]. The idea behind the shock capturing stabilization technique is to add artificial diffusion only in the direction in which oscillations are observed in the solution from the SUPG method.

Stabilized finite element methods

Let $\mathcal{W}_{\Psi_i h}$ be the space of continuous piecewise linear finite element functions satisfying

$$\mathcal{W}_{\Psi_i h} = \Big\{ u_h \in \mathcal{C}^0(\Omega, \mathbb{R}) : u_{h|_\mathcal{K}} \in \mathbb{P}_1, \ \forall \mathcal{K} \in \mathcal{T}_h, \text{ and } u_{h|_{\Gamma_-}} = \Psi_i \Big\}, \tag{7.2.9}$$

where Ψ_i is a given function that belongs to the trace space of the finite element functions on the boundary $\partial\Omega$. Set $\mathbf{q} = \alpha\mathbf{u} = (\alpha u_1, \alpha u_2)$. We approximate the solutions α and $\mathbf{q}$ by the finite element functions α_h from $\mathcal{W}_{\omega h}$ and $\mathbf{q}_h = (q_{1h}, q_{2h})$ from $\mathcal{W}_{\Psi_1 h} \times \mathcal{W}_{\Psi_2 h}$, respectively. We use the backward Euler formulation for the discretization of the time derivative. We define the residual of the differential equations (7.1.6) at time t_n as

$$\begin{aligned} \mathcal{R}^n_{\alpha_h} &= \frac{\alpha_h^n - \alpha_h^{n-1}}{\Delta t} + \nabla \cdot \mathbf{q}_h^n, \\ \mathcal{R}^n_{q_{ih}} &= \frac{q_{ih}^n - q_{ih}^{n-1}}{\Delta t} + \nabla \cdot \Big(\frac{q_{ih}^n}{\alpha_h^n}\mathbf{q}_h^n\Big) + \partial_{x_i}(\alpha_h^n \pi_h^n) + K_D(q_{ih}^n - \alpha_h^n v_{ih}^n), \quad i = 1, 2. \end{aligned} \tag{7.2.10}$$

We set $\mathcal{R}^n_{\mathbf{q}_h} = (\mathcal{R}^n_{q_{1h}}, \mathcal{R}^n_{q_{2h}})$. The variational formulation of (7.1.6) with the SUPG method [20] combined with a shock-capturing term is given as follows:

Find $\alpha_h^n \in \mathcal{W}_{\omega h}$ and $\mathbf{q}_h^n \in \mathcal{W}_{\omega\Phi_1 h} \times \mathcal{W}_{\omega\Phi_2 h}$ such that

$$\begin{aligned} &\underbrace{\int_\Omega \mathcal{R}^n_{\alpha_h}\varphi_h\,dx + \int_\Omega \mathcal{R}^n_{\alpha_h}\tau(\mathbf{u}_h^n\cdot\nabla)\varphi_h\,dx}_{\text{SUPG formulation for the continuity equation}} + \underbrace{\int_\Omega \mathcal{R}^n_{\alpha_h}\sigma_{\alpha_h}(\widehat{\mathbf{u}}^n_{\alpha_h}\cdot\nabla)\varphi_h\,dx}_{\text{Shock-capturing term}} = 0, \\ &\underbrace{\int_\Omega \mathcal{R}^n_{\mathbf{q}_h}\cdot\boldsymbol{\psi}_h\,dx + \int_\Omega \mathcal{R}^n_{\mathbf{q}_h}\cdot\tau(\mathbf{u}_h^n\cdot\nabla)\boldsymbol{\psi}_h\,dx}_{\text{SUPG formulation for the momentum equation}} + \underbrace{\int_\Omega \mathcal{R}^n_{\mathbf{q}_h}\cdot(\boldsymbol{\sigma}_{\mathbf{q}_h}\widehat{\mathbf{u}}^n_{\mathbf{q}_h}\cdot\nabla)\boldsymbol{\psi}_h\,dx}_{\text{Shock-capturing term}} = 0, \end{aligned} \tag{7.2.11}$$

for all $\varphi_h \in \mathcal{W}_{0h}$ and $\boldsymbol{\psi}_h \in \mathcal{W}_{0h} \times \mathcal{W}_{0h}$, where the scalars τ and σ_{α_h}, and the matrix $\boldsymbol{\sigma}_{\mathbf{q}_h}$ are stabilization parameters. The vector $\widehat{\mathbf{u}}^n_{\alpha_h}$ and the matrix $\widehat{\mathbf{u}}^n_{\mathbf{q}_h}$ will be defined in the next subsection. The advection velocity $\mathbf{u}_h^n = \dfrac{\mathbf{q}_h^n}{\alpha_h^n}$. It is well defined since we assume there is no vacuum state.

Brief review of Petrov-Galerkin finite element methods

Consider the scalar convection-diffusion problem

$$\partial_t u + \mathbf{b} \cdot \nabla u - \eta \Delta u = f, \quad \text{in } \Omega, \qquad u = u_b \text{ on } \partial\Omega, \tag{7.2.12}$$

where $\mathbf{b}$, u_b and f are given functions and η is a positive constant. The SUPG formulation combined with a shock-capturing term for (7.2.12) is as follows:

Find $u_h \in \mathcal{V}_{u_b h}$ such that

$$\int_\Omega \mathcal{R}_{u_h} \varphi \, dx + \int_\Omega \mathcal{R}_{u_h} \tau (\mathbf{b}_h \cdot \nabla)\varphi \, dx + \int_\Omega \mathcal{R}_{u_h} \sigma (\widehat{\mathbf{b}}_{u_h} \cdot \nabla)\varphi \, dx = 0, \tag{7.2.13}$$

for all $\varphi \in \mathcal{V}_{u_b h}$. Here, $\mathcal{R}_{u_h} = \partial_t u_h + \mathbf{b}_h \cdot \nabla u_h - \eta \Delta u_h - f$ is the residual of (7.2.12) computed on each element, τ is the SUPG stabilization parameter, σ is the shock-capturing stabilization parameter. The vector $\widehat{\mathbf{b}}_{u_h}$ will be defined later.

A big challenge with the SUPG method is the choice of the stabilization parameter τ. An "optimal" value is not yet known in the case of a general advection-diffusion system. The judicious selection of the stabilization parameter τ plays an important role in determining the accuracy of the SUPG formulation. Christie et al. [27] showed for the one-dimensional stationary problem associated to (7.2.12) that the SUPG method with piecewise linear finite elements on a uniform mesh (equally spaced nodes) gives exact values at the nodes of the mesh if

$$\tau = \frac{h}{2|b|} \zeta(Pe), \tag{7.2.14}$$

where $\zeta(Pe) = \coth(Pe) - \frac{1}{Pe}$ and $Pe = \frac{|b|h}{2\eta}$ is the numerical *Péclet number* for element size h. The generalization in the multidimensional case takes the form

$$\tau = \frac{h}{2|\mathbf{b}|} \zeta(Pe). \tag{7.2.15}$$

In practice, the stabilization parameter τ is locally computed as

$$\tau_{\mathcal{K}} = \frac{h_{\mathcal{K}}}{2|\mathbf{b}_h|} \zeta(Pe_{\mathcal{K}}), \tag{7.2.16}$$

where $\mathcal{K}$ is any element of the triangulation $\mathcal{T}_h$, $h_{\mathcal{K}}$ is the local element size of $\mathcal{K}$ and $Pe_{\mathcal{K}} = \frac{|\mathbf{b}_h| h_{\mathcal{K}}}{2\eta}$ is the local Péclet number. Note that for the pure advection problem, i.e. $\eta = 0$, the Péclet number goes to infinity, and thus $\zeta(Pe_{\mathcal{K}})$ goes to one.

For the shock-capturing term, the key point is also the judicious selection of the stabilization parameter σ and the vector $\widehat{\mathbf{b}}_{u_h}$. Various expressions for σ and $\widehat{\mathbf{b}}_{u_h}$ have

been proposed in the literature [56, 60, 59, 40]. In case of a scalar advection-diffusion equation as in (7.2.12), Hughes et al. [56] first proposed to take

$$\sigma = \max\left\{0, \widehat{\tau}(\widehat{\mathbf{b}}_h) - \tau\right\}, \tag{7.2.17}$$

where

$$\widehat{\tau}(\widehat{\mathbf{b}}_h) = \frac{h}{2\|\widehat{\mathbf{b}}_h\|} \quad \text{and} \quad \widehat{\mathbf{b}}_h = \left(\frac{\mathbf{b}_h \cdot \nabla u_h}{\|\nabla u_h\|^2}\right) \nabla u_h. \tag{7.2.18}$$

The vector $\widehat{\mathbf{b}}_h$ is the projection of the advection velocity $\mathbf{b}_h$ into the direction ∇u_h. It corresponds to the direction in which oscillations in SUPG solutions are often observed. With this choice, the shock-capturing term in (7.2.13) can be written as

$$\int_\Omega \sigma \frac{(\mathbf{b}_h \cdot \nabla u_h)\mathcal{R}_{u_h}}{\|\nabla u_h\|^2} \nabla u_h \cdot \nabla \varphi \, dx. \tag{7.2.19}$$

We immediately see that this last term becomes negative and may destabilize the finite element discretization (7.2.13) if $(\mathbf{b}_h \cdot \nabla u_h)\mathcal{R}_{u_h} < 0$. Galẽao and do Carmo [40] redefine the corresponding vector $\widehat{\mathbf{b}}_h$ using the residual of the governing equation instead of the convective derivative

$$\widehat{\mathbf{b}}_h = \left(\frac{\mathcal{R}_{u_h}}{\|\nabla u_h\|^2}\right) \nabla u_h. \tag{7.2.20}$$

This was also suggested in [60, 59] and turns out to be the best choice currently available for $\widehat{\mathbf{b}}_h$. For vector equations, the shock-capturing parameters σ and $\widehat{\mathbf{b}}_{u_h}$ are matrices. The theoretical results to guide their selection are less obvious.

We now return to the formulation (7.2.11). The advection velocity is given by $\mathbf{u}_h$. According to the above discussion, we choose the SUPG stabilization parameter

$$\tau = \frac{h}{2\|\mathbf{u}_h^n\|} \tag{7.2.21}$$

and the shock-capturing stabilization parameter

$$\sigma_{\alpha_h} = \max\left\{0, \widehat{\tau}(\widehat{\mathbf{u}}_{\alpha_h}^n) - \tau\right\}, \tag{7.2.22}$$

where $\widehat{\tau}$ is defined as in (7.2.18) and $\widehat{\mathbf{u}}_{\alpha_h}^n = \left(\frac{\mathcal{R}_{\alpha_h}^n}{\|\nabla \alpha_h^n\|^2}\right)\nabla \alpha_h^n$. For the momentum equation, we calculate the shock-capturing parameter $\sigma_{q_{i_h}}$ and the vector $\widehat{\mathbf{u}}_{q_{i_h}}^n$ for each component of the vector equation as above. We obtain

$$\sigma_{q_{i_h}} = \max\left\{0, \widehat{\tau}(\widehat{\mathbf{u}}_{q_{i_h}}^n) - \tau\right\}, \quad i = 1, 2, \tag{7.2.23}$$

where $\widehat{\mathbf{u}}^n_{q_{ih}} = \left(\frac{\mathcal{R}^n_{q_{ih}}}{\|\nabla q_{ih}^n\|^2}\right)\nabla q_{ih}^n$. Then we construct the shock-capturing parameter $\boldsymbol{\sigma}_{\mathbf{q}_h}$ and the matrix $\widehat{\mathbf{u}}^n_{\mathbf{q}_h}$ by setting

$$\boldsymbol{\sigma}_{\mathbf{q}_h} = \mathrm{diag}(\sigma_{\mathrm{q_{1h}}}, \sigma_{\mathrm{q_{2h}}}) \quad \text{and} \quad \widehat{\mathbf{u}}^{\mathrm{n}}_{\mathbf{q}_{\mathrm{h}}} = \begin{pmatrix} \widehat{\mathbf{u}}^{n^T}_{q_{1h}} \\ \widehat{\mathbf{u}}^{n^T}_{q_{2h}} \end{pmatrix}. \tag{7.2.24}$$

In a similar fashion, we obtain the SUPG formulation with a shock capturing term for the non-conservative form (7.1.7):

Find $\alpha_h^n \in \mathcal{W}_{\omega h}$ and $\mathbf{u}_h^n \in \mathcal{W}_{\Phi_1 h} \times \mathcal{W}_{\Phi_2 h}$ such that

$$\begin{aligned} &\int_\Omega \mathcal{R}^n_{\alpha_h}\varphi\,dx + \int_\Omega \mathcal{R}^n_{\alpha_h}\tau(\mathbf{u}_h^n\cdot\nabla)\varphi\,dx + \int_\Omega \mathcal{R}^n_{\alpha_h}\sigma_{\alpha_h}(\widehat{\mathbf{u}}^n_{\alpha_h}\cdot\nabla)\varphi\,dx, \\ &\int_\Omega \mathcal{R}^n_{\mathbf{u}_h}\cdot\boldsymbol{\psi}\,dx + \int_\Omega \mathcal{R}^n_{\mathbf{u}_h}\cdot\tau(\mathbf{u}_h^n\cdot\nabla)\boldsymbol{\psi}\,dx + \int_\Omega \mathcal{R}^n_{\mathbf{u}_h}\cdot(\boldsymbol{\sigma}_{\mathbf{u}_h}\widehat{\mathbf{u}}^n_{\mathbf{u}_h}\cdot\nabla)\boldsymbol{\psi}\,dx = 0, \end{aligned} \tag{7.2.25}$$

for all $\varphi \in \mathcal{V}_0^h$ and $\boldsymbol{\psi} \in \mathcal{V}_0^h \times \mathcal{V}_0^h$, where $\boldsymbol{\sigma}_{\mathbf{u}_h}$ is a stabilization matrix for the shock-capturing term and $\mathcal{R}^n_{\mathbf{u}_h} = (\mathcal{R}^n_{u_{1h}}, \mathcal{R}^n_{u_{2h}})$ with

$$\begin{aligned} \mathcal{R}^n_{\alpha_h} &= \frac{\alpha_h^n - \alpha_h^{n-1}}{\Delta t} + \nabla\cdot(\alpha_h^n\mathbf{u}_h^n), \\ \mathcal{R}^n_{u_{ih}} &= \frac{u_{ih}^n - u_{ih}^{n-1}}{\Delta t} + (\mathbf{u}_h^n\cdot\nabla)u_{ih}^n + \frac{1}{\alpha_h^n}\partial_{x_i}(\alpha_h^n\pi_h^n) + K_D(u_{ih}^n - v_{ih}^n). \end{aligned} \tag{7.2.26}$$

Again here, the stabilization matrix is constructed as $\boldsymbol{\sigma}_{\mathbf{u}_h} = \mathrm{diag}(\sigma_{\mathrm{u_{1h}}}, \sigma_{\mathrm{u_{2h}}})$, where

$$\sigma_{u_{ih}} = \max\left\{0, \widehat{\tau}(\widehat{\mathbf{u}}^n_{u_{ih}}) - \tau\right\}, \quad \widehat{\mathbf{u}}^n_{u_{ih}} = \left(\frac{\mathcal{R}^n_{u_{ih}}}{\|\nabla u_{ih}^n\|^2}\right)\nabla u_{ih}^n, \quad i = 1, 2, \tag{7.2.27}$$

and the matrix $\widehat{\mathbf{u}}^n_{\mathbf{q}_h}$ as

$$\widehat{\mathbf{u}}^n_{\mathbf{q}_h} = \begin{pmatrix} \widehat{\mathbf{u}}^{n^T}_{u_{1h}} \\ \widehat{\mathbf{u}}^{n^T}_{u_{2h}} \end{pmatrix}. \tag{7.2.28}$$

Note that here each component of the advection velocity $\mathbf{u}_h^n$ is discretized with $\mathbb{P}_1$ finite elements, as opposed to the conservative form weak formulation (7.2.11), where each component of the advection velocity is a quotient of two $\mathbb{P}_1$ functions on each element.

7.3 Numerical results

This section is devoted to two-dimensional test cases. All the finite element formulations are solved using the FreeFem++ software [51]. The numerical results are displayed and analyzed with the Paraview software [91].

7.3.1 2D plug flow in a channel

We start with a simple computational domain $\Omega_1 = [0,5] \times [0,1]$ represented in Figure 7.1. This domain is a rectangular channel composed of inflow Γ_- and outflow Γ_+ boundaries, and two walls $\Gamma_{0,1}$ and $\Gamma_{0,2}$.

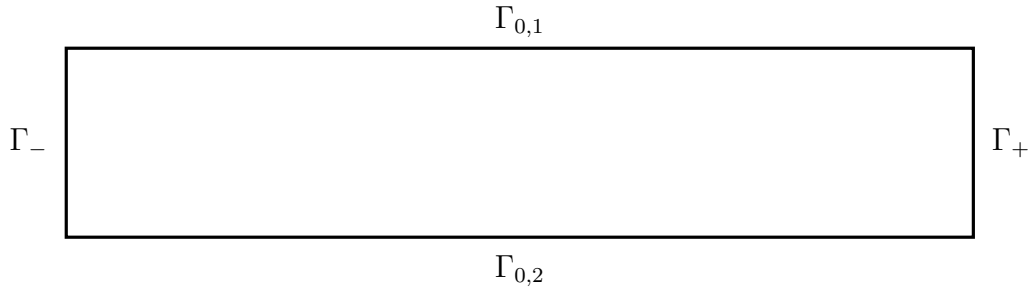

Figure 7.1: Rectangular channel (domain Ω_1).

The air flow in this domain is computed with the formulation (7.2.7) of the Navier-Stokes equations using a kinematic viscosity $\nu = 0.01$. We take an initial air velocity $\mathbf{v}_0(x,y) = (1,0)$ and set the boundary conditions $\mathbf{v} = (1,0)$ on the inflow boundary Γ_-, $\mathbf{v} = (0,0)$ on the walls $\Gamma_{0,1}$ and $\Gamma_{0,2}$. The outflow boundary Γ_+ is left free, i.e. $(-p\mathcal{I} + \mu\nabla\mathbf{v}) \cdot \mathbf{n} = 0$ on Γ_+. We consider a triangular mesh of the domain Ω_1, composed of 50 elements along the inflow and outflow boundaries, and 250 elements along each of the walls $\Gamma_{0,1}$ and $\Gamma_{0,2}$. This gives a mesh with 27794 triangles and 14198 nodes. The solution is computed with a time step $\Delta t = 0.02$ till a steady solution is reached. Figure 7.2 shows the steady air flow in the channel. The air flow

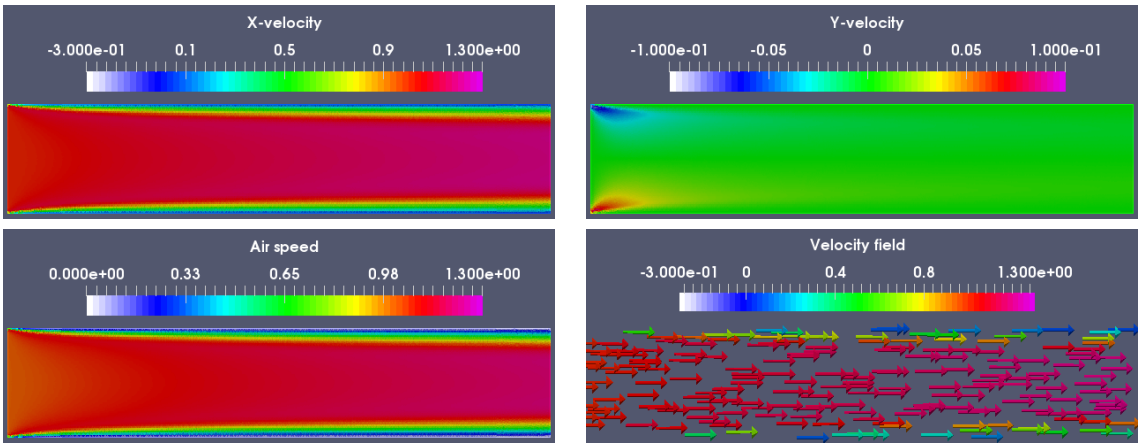

Figure 7.2: Plug flow in the channel.

streamlines are represented in Figure 7.3. Starting from a uniform velocity field at

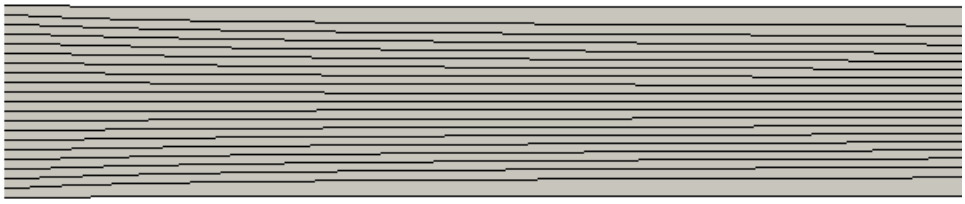

Figure 7.3: Air flow streamlines in the channel.

the inlet, the velocity field progressively settles to a parabolic profile, characteristic of Poiseuille flows.

We are interested in the time-evolution of a jet of droplets (spherical particles with density $\rho_l = 1000kg/m^3$) injected at the inflow boundary Γ_- and advected by the air flow that is assumed to be in its steady state by the time the particles enter the channel. A particle volume fraction $\alpha = 0.5 \times \exp(-50(y-0.5)^2)$ and a particle velocity equal to the air velocity ($\mathbf{u} = \mathbf{v} = (1,0)$) are imposed on the inflow boundary Γ_-. The rest of the domain initially contains a volume fraction $\alpha_0 = 10^{-10}$ of droplets at rest, i.e. $\mathbf{u}_0 = (0,0)$. We choose Needham's particle pressure given in (6.5.1), with a particle pressure coefficient $\kappa_0 = 0.2$. To compute the solution of the Eulerian droplet model, we use a finer mesh. We consider a triangular mesh composed of 100 elements on the inflow and outflow boundaries, and 500 elements on each of the walls $\Gamma_{0,1}$ and $\Gamma_{0,2}$. This gives a mesh with 106578 triangles and 53890 nodes.

Remark 7.3.1. ***i)*** *We have chosen a very small initial volume fraction $\alpha_0 = 10^{-10}$ to avoid vacuum state ($\alpha = 0$) since the particle velocity $\mathbf{u} = \frac{\mathfrak{q}}{\alpha}$ is not defined in a vacuum state.*
ii) *The particle volume fraction $\alpha = 0.5 \times \exp(-50(y-0.5)^2)$ imposed on the inflow boundary is sufficiently large that it may not satisfy the assumption on small particle loading made for one-way coupling (see assumption 2 at the beginning of section 7.1). However, it is not crucial for this test case since we only want to test the numerical method and highlight the effect of a particle pressure on droplets in 2D computations.*

Figure 7.4 shows the time-evolution of the volume fraction with/without particle pressure for droplets with diameter $d = 1\mu m$. The small droplets injected at the inflow boundary are simply transported by the air towards the outflow boundary. The droplet velocity field adjusts rapidly to the air velocity field as one can see by comparing the Figures 7.2 and 7.5. The inertia parameter K which determines the

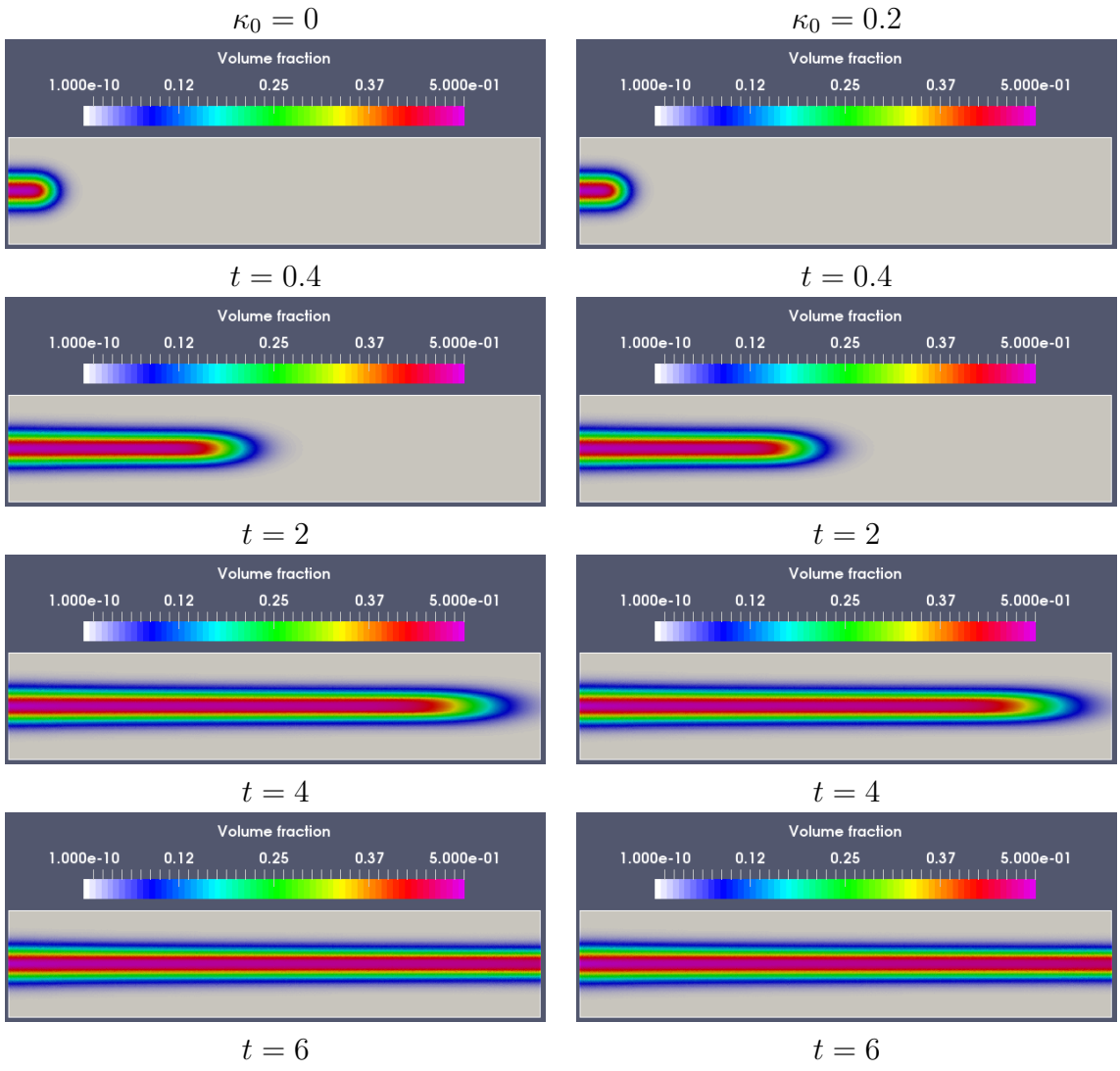

Figure 7.4: Particle volume fraction as a function of time for droplets with diameter $d = 1\mu m$. At left: solution without particle pressure ($\kappa_0 = 0$). At right: solution with particle pressure ($\kappa_0 = 0.2$). $\Delta t = 0.02$.

amplitude of the drag force between the air and the droplets, is inversely proportional to the square of the particle diameter. For small particles ($d \leqslant 1\mu m$), the drag force is so important that the contribution of the particle pressure force ($\kappa_0 \leqslant 0.2$) in the resulting force acting on the droplets is negligible. The drag force and the inertia are the leading forces acting on the droplets.

Figure 7.6 shows the time-evolution of the volume fraction with/without particle pressure for droplets with diameter $d = 100\mu m$. On can see a progressive dispersion

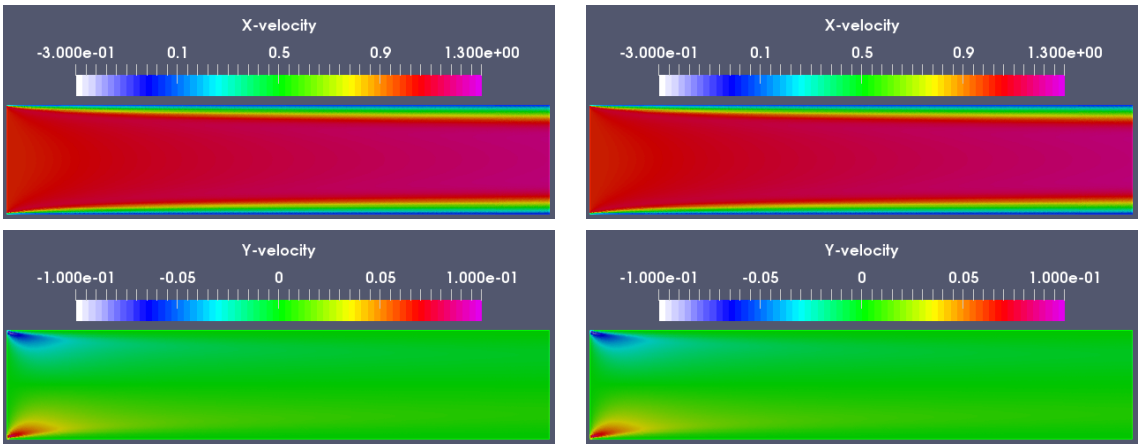

Figure 7.5: Velocity of droplets with diameter $d = 1\mu m$ after $t = 0.4$. At left: solution without particle pressure ($\kappa_0 = 0$). At right: solution with particle pressure ($\kappa_0 = 0.2$). $\Delta t = 0.02$.

of the droplets in the presence of a particle pressure (see solution on the right column of Figure 7.6). Figure 7.7 shows the velocity field for droplets with diameter $d = 100\mu m$. Comparing the Figures 7.2 and 7.7 (for velocities) and Figure 7.8 (for streamlines), on can see small differences in the droplet velocity field with respect to the air velocity field in the solution with a particle pressure. These small differences are due to the particle pressure, which affects the droplet velocity field. As the droplet diameter reaches $100\mu m$, inertial forces are in equilibrium with both the drag force and particle pressure gradient as opposed to only the dominant drag force for small droplets. The effects of the particle pressure on the droplets cause the progressive dispersion of the droplets away from the centerline of the jet.

Comparing the left columns of the Figures 7.4 and 7.6 (for volume fractions) and the left columns of the Figures 7.5 and 7.7 (for velocities), it can be seen that small ($d = 1\mu m$) and large ($d = 100\mu m$) droplets behave in the same way when there is no particle pressure force. In this case, the drag force between the air and the droplets and the inertia are the leading forces acting on the droplets and the latter are simply advected by the air flow. In presence of a pressure particle force, larger droplets progressively disperse as time evolves. This was also observed in the 1D computations performed in the previous chapters.

We repeated all the above test cases using the non-conservative formulation (7.2.25). We get exactly the same solutions as with the conservative formulation (7.2.11) since these solutions are smooth. For instance, some plots of the solutions for both forms for droplets with diameter $d = 100\mu m$ and a particle pressure coeffi-

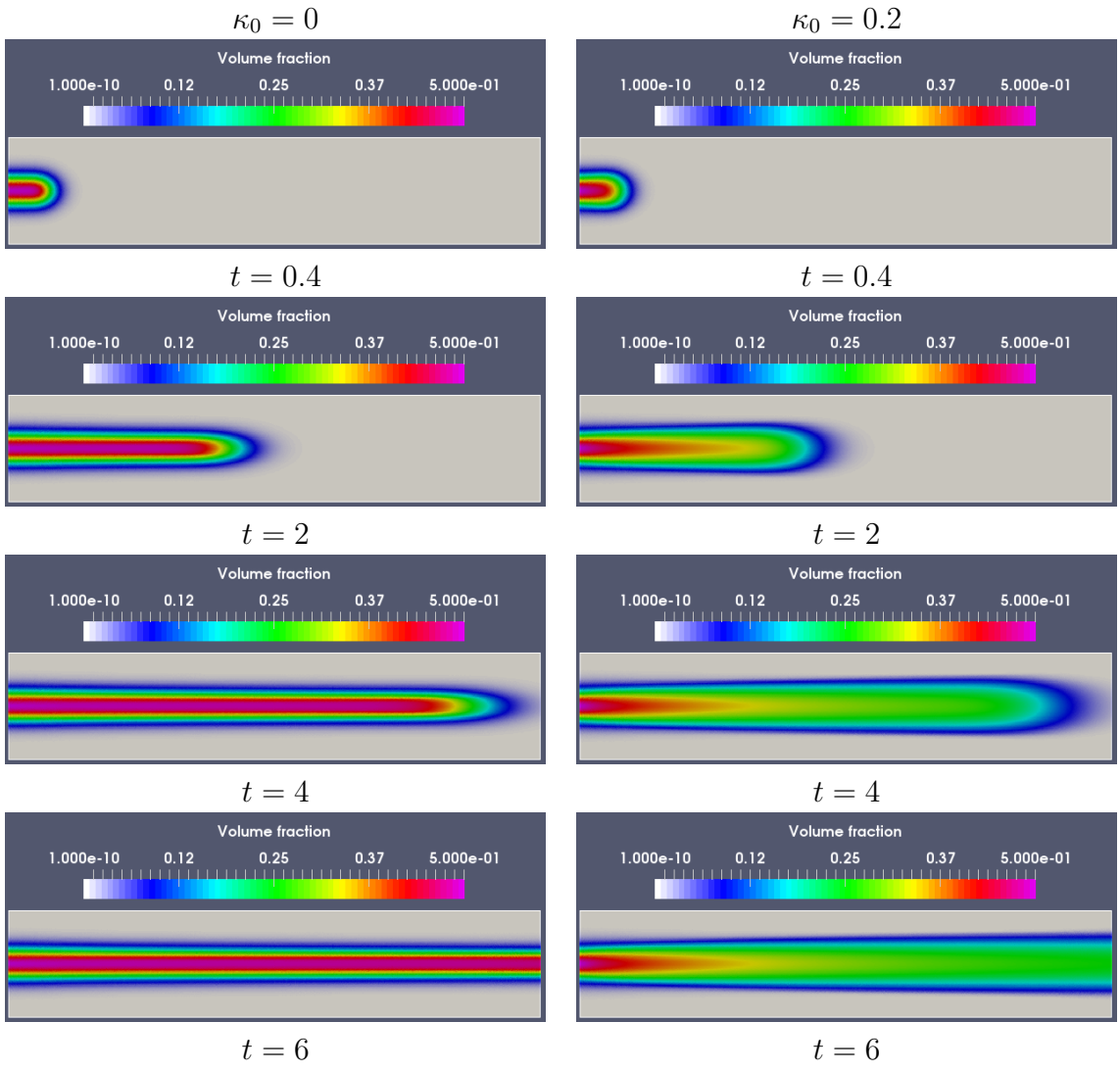

Figure 7.6: Particle volume fraction as a function of time for droplets with diameter $d = 100\mu m$. At left: solution without particle pressure ($\kappa_0 = 0$). At right: solution with particle pressure ($\kappa_0 = 0.2$). $\Delta t = 0.02$.

cient $\kappa_0 = 0.2$ are represented in Figure 7.9.

The test cases performed in this subsection show that the SUPG method combined with a shock-capturing term can be used to discretize the droplet equations (7.1.6) for 2D computations. However, as is true for many stabilized finite element methods, this method is diffusive, which calls for finer grid resolution.

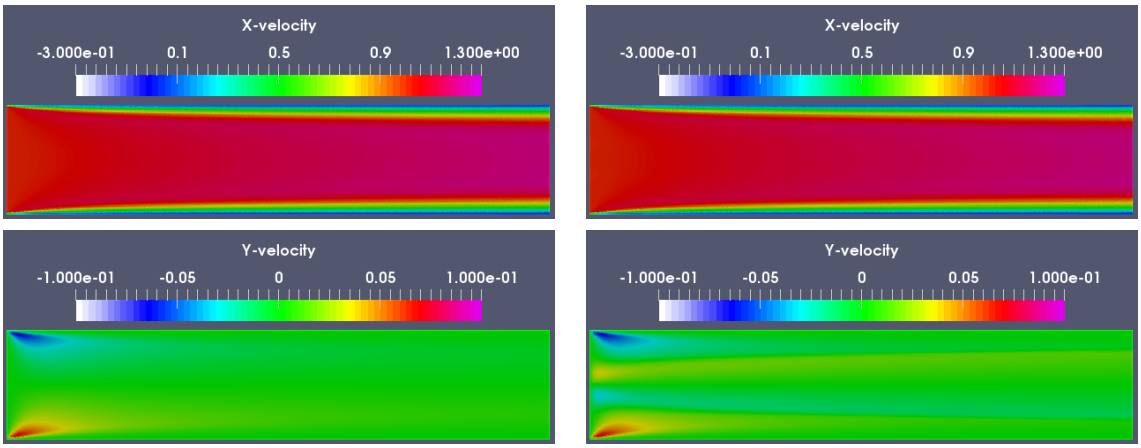

Figure 7.7: Velocity of droplets with diameter $d = 100\mu m$ at $t = 6$. At left: solution without particle pressure ($\kappa_0 = 0$). At right: solution with particle pressure ($\kappa_0 = 0.2$). $\Delta t = 0.02$.

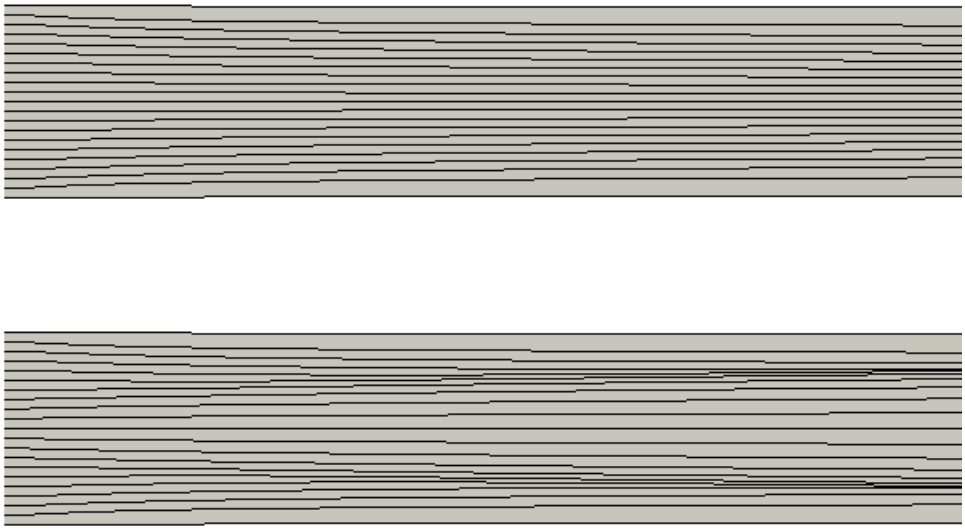

Figure 7.8: Streamlines of the particle velocity field for droplets with diameter $d = 100\mu m$. Top: solution without particle pressure. Bottom: solution with particle pressure.

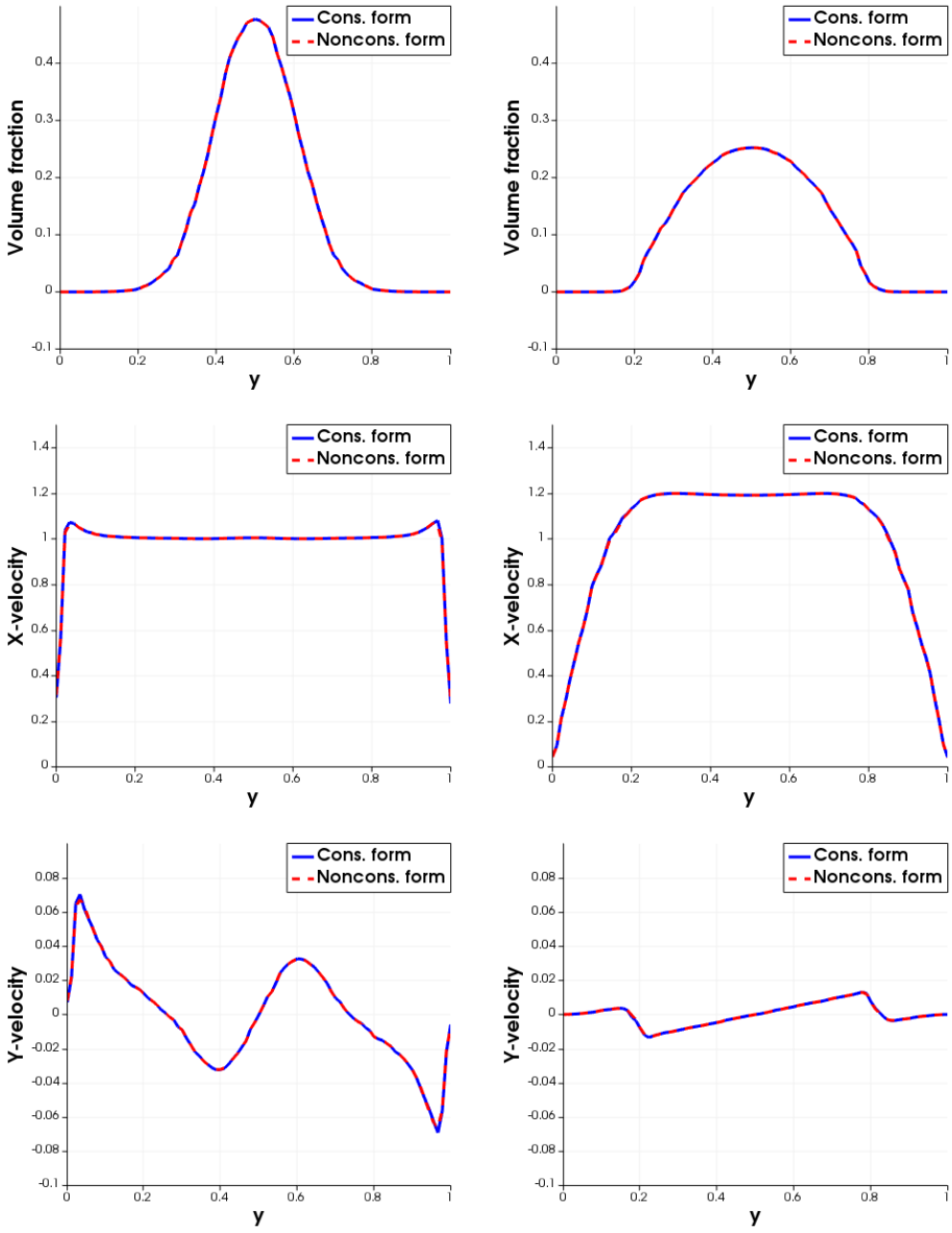

Figure 7.9: Conservative vs non-conservative form: Plot of the solution along vertical cuts for different values of x. At left: solution near the inflow boundary Γ_- ($x = 0.1$). At right: solution near the outflow boundary Γ_+ ($x = 4.9$). $t = 6$, $d = 100\mu m$, $\kappa_0 = 0.2$, $\Delta t = 0.02$.

7.3.2 2D flow in the upper airways

Here, we use another domain, noted Ω_2, represented in Figure 7.10. This 2D

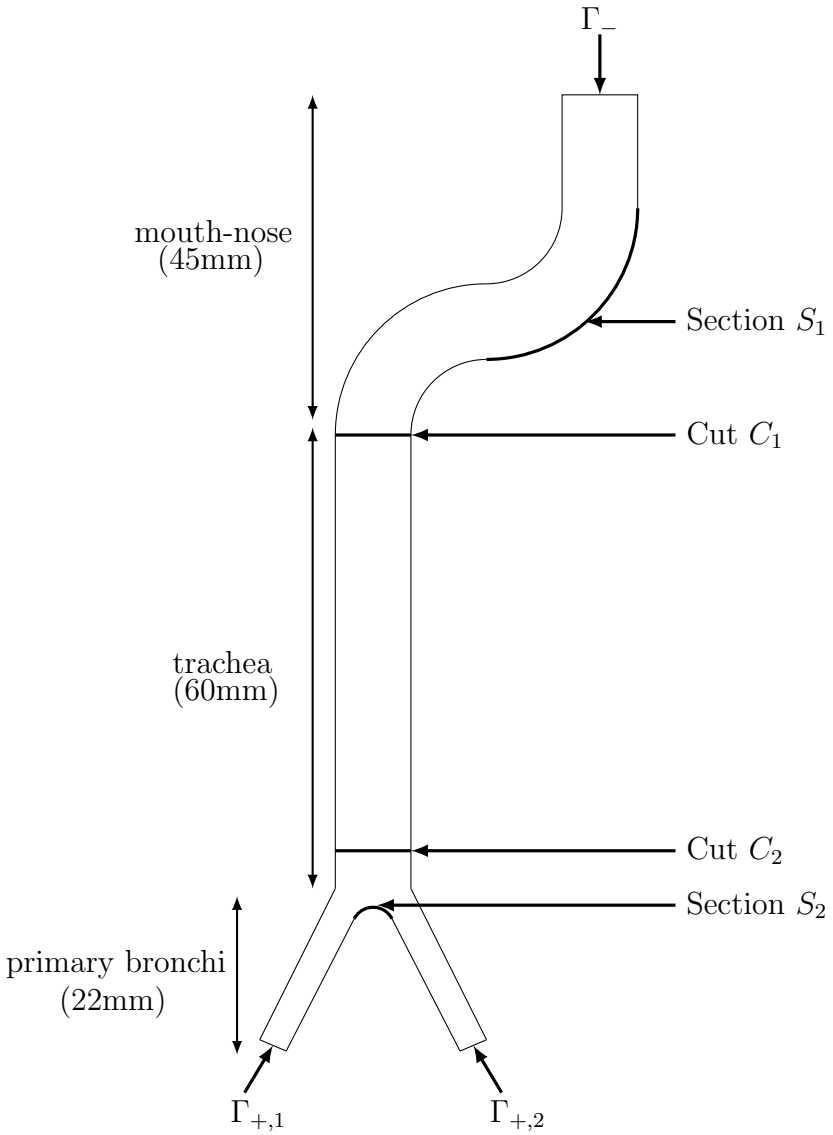

Figure 7.10: Upper airways geometry (domain Ω_2).

domain mimicks the geometry of the upper airways including a nose-mouth region and the trachea down to the first generation bronchi. The trachea has a length of $60mm$ and a diameter of $10mm$. The primary bronchi have a length of $23mm$ and a diameter of $4mm$. This geometry includes an inflow boundary Γ_- and two outflow boundaries $\Gamma_{+,1}$ and $\Gamma_{+,2}$.

The air flow in this domain is computed using the finite element formulation (7.2.7) of the Navier-Stokes (7.1.1) with a kinematic viscosity $\nu = \frac{1}{Re}$. The Reynolds number defined by $Re = \rho UD/\mu$ is calculated using a typical velocity during inhalation of $U = 1m/s$, a characteristic length of $D = 0.01m$ (diameter of the upper airways), an air density $\rho = 1.3kg/m^3$, and a dynamic viscosity of air at ambient temperature $\mu = 1.65 \times 10^{-5} Pa \cdot s$. With these parameters, the Reynolds number is about 788. We set the boundary condition $\mathbf{v} = (0, -1)m/s$ on the inflow boundary Γ_-, the outflow boundaries $\Gamma_{+,1}$ and $\Gamma_{+,2}$ are left free, and we assume no-slip velocity $\mathbf{v} = (0, 0)m/s$ on the rest of the boundary of the domain. We take an initial air velocity $\mathbf{v}_0 = (0, -1)m/s$. We consider a triangular mesh of the domain, composed of 60 elements on the inflow boundary Γ_-, 180 elements on the boundary of the nose-mouth region, 240 elements along the trachea, 80 elements along each primary bronchi, 30 elements on each outflow boundary $\Gamma_{+,1}$ and $\Gamma_{+,2}$, and 30 elements on the curve connecting the two primary bronchi. This gives a mesh with 51227 elements and 26362 nodes. The solution is computed with a time step $\Delta t = 0.018$ till a steady solution is reached. Figure 7.11 shows the stationary solution for the air flow field. With a Reynolds number $Re = 788$, the air flow presents several recirculations near

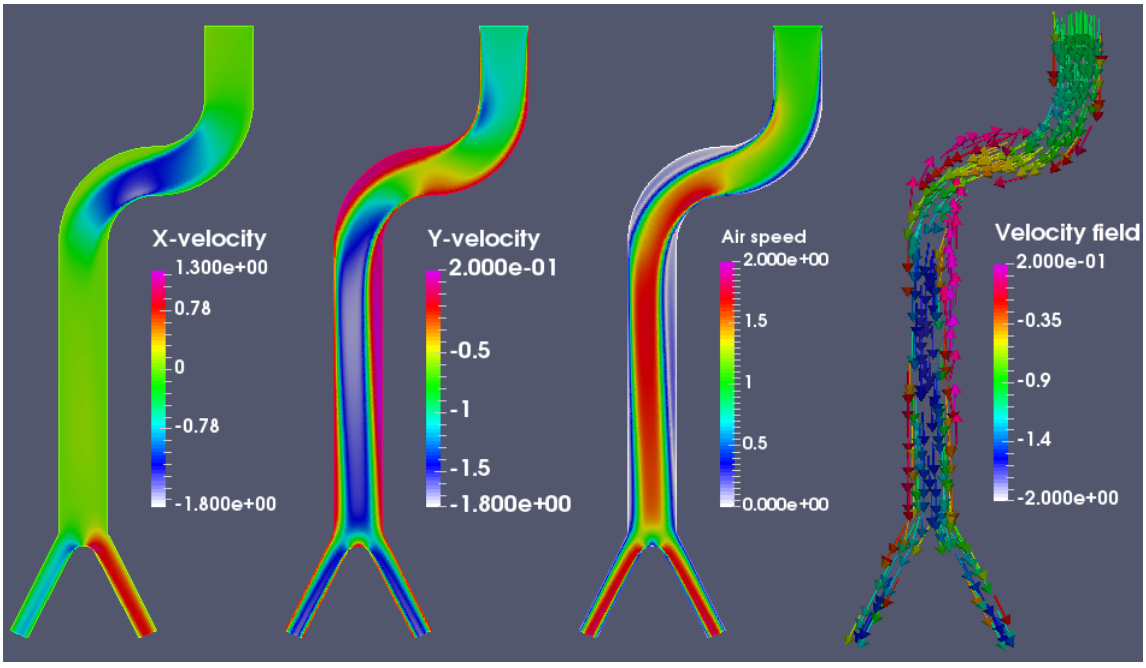

Figure 7.11: Steady air flow field in the upper airways.

the left down boundary of the nose-mouth and the right boundary of the trachea as one can see from the streamlines shown in Figure 7.12.

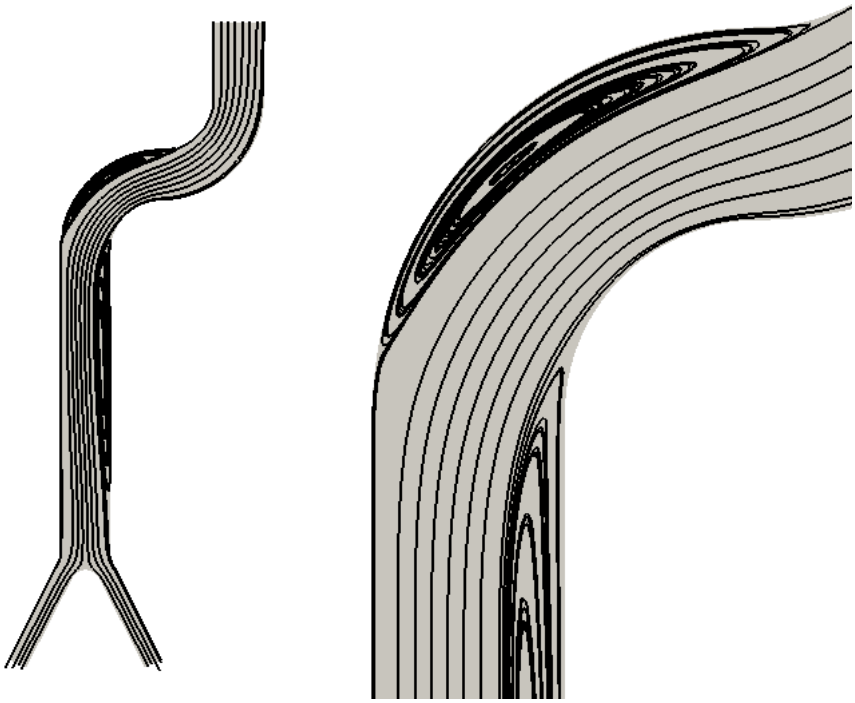

Figure 7.12: Air flow streamlines in the upper airways (left). Zoom near the junction of the nose-mouth and the trachea (right).

We are interested in the time-evolution of particles injected at the inflow boundary Γ_- and advected by the air flow. Here also, to solve the Eulerian droplet model, we have to use a finer mesh. We consider a triangular mesh of the domain, composed of 100 elements on the inflow boundary Γ_-, 300 elements on the boundary of the nose-mouth region, 400 elements along the trachea, 150 element each primary bronchi, 40 elements on each outflow boundary $\Gamma_{+,i}$, 50 elements on the corner connecting the two primary bronchi. This gives a mesh with 155064 triangles and 78838 nodes. We take an initial particle volume fraction $\alpha_0 = 10^{-10}$ and particle velocity $\mathbf{u}_0 = (0, 0)m/s$. We choose Needham's particle pressure given in (6.5.1).

We first suppose that the particles are droplets of water with density $\rho_l = 1000kg/m^3$. A particle volume fraction $\alpha = 10^{-5} \times \exp(-2(x - 1.5)^2)$ and a particle velocity $\mathbf{u} = \mathbf{v} = (0, -1)m/s$ are imposed on the inflow boundary Γ_-. The rest of the boundary of the domain is left free. The numerical solutions are computed with the finite element formulation (7.2.11). Figure 7.13 shows the time-evolution of the volume fraction computed with a particle pressure coefficient $\kappa_0 = 10$ for droplets with diameter $d = 1\mu m$. As time evolves, the droplets advected by the air progressively fill the domain. It takes about $t = 8.4$ for the jet of particles to first reach the primary bronchi and $t = 10$ to exit from these primary bronchi. Some particles progressively

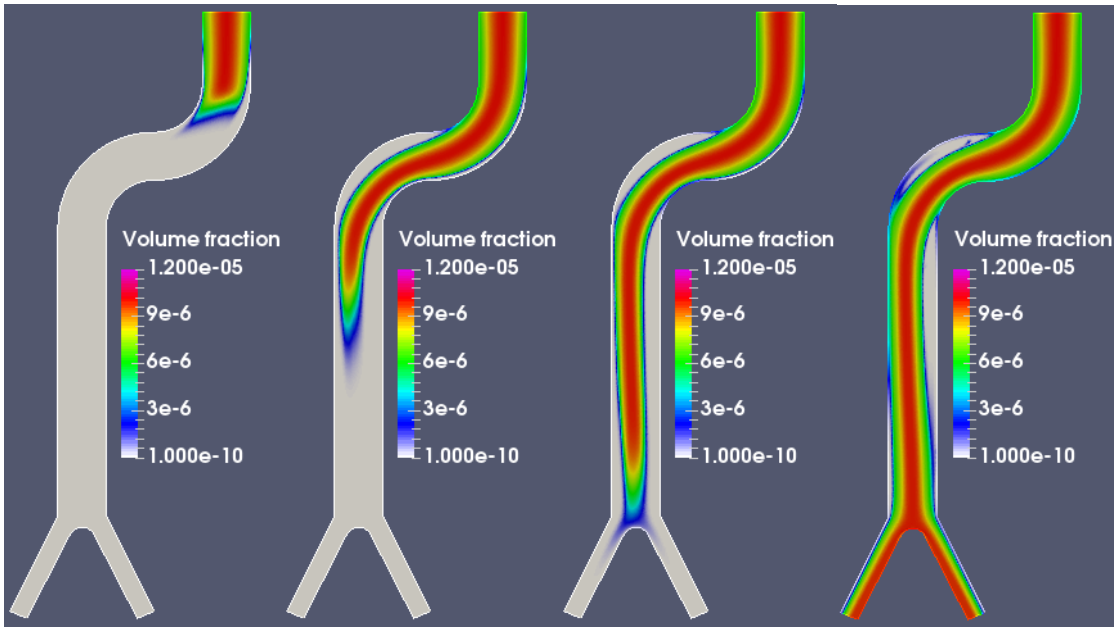

$t = 2$ $t = 6$ $t = 8.4$ $t = 20$

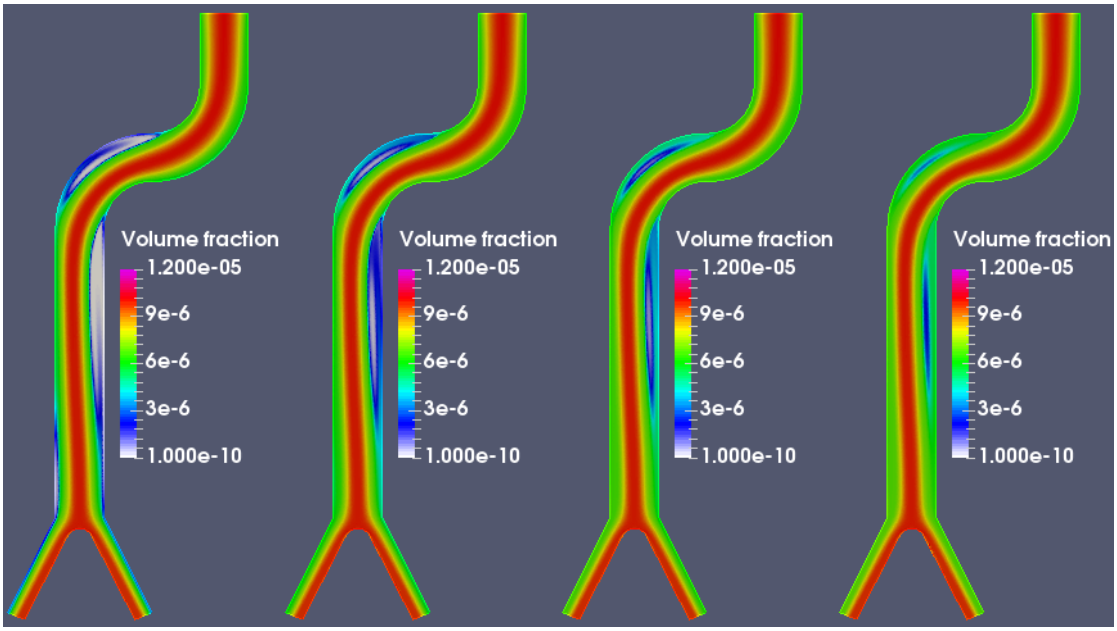

$t = 30$ $t = 60$ $t = 100$ $t = 180$

Figure 7.13: Model EP: Particle volume fraction as a function of time. $\rho_l = 1000kg/m^3$, $\kappa_0 = 10$, $d = 1\mu m$, $\Delta t = 0.02$.

enter in the air flow recirculations (near the left down boundary of the nose-mouth region and the right boundary of the trachea). After $t = 140$, the whole domain is filled assuming a steady inflow of particles. The droplet velocity field is shown in Figure 7.14. Comparing the Figures 7.11 and 7.14, one can see that the droplet velocity

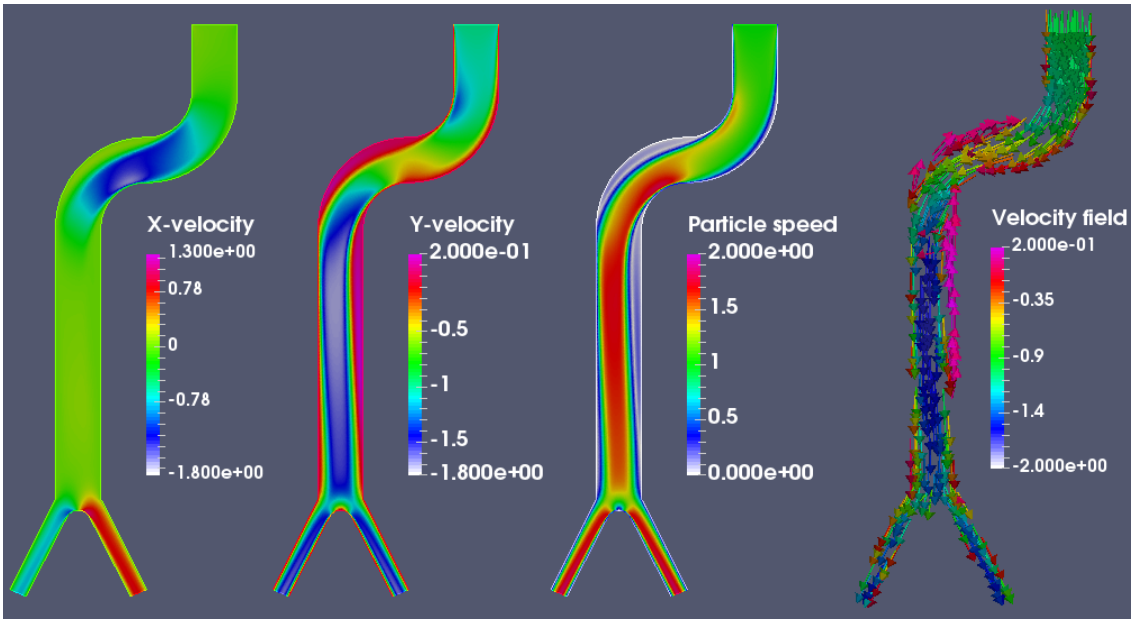

Figure 7.14: Model EP: Particle velocity field after $t = 0.1$. $\rho_l = 1000kg/m^3$, $d = 1\mu m$, $\kappa_0 = 10$, $\Delta t = 0.02$.

field is very close to the air velocity field. The velocity of the droplets, that was initially null, adjusts rapidly to the air velocity. Small droplets ($d = 1\mu m$) with density $\rho_l = 1000kg/m^3$ do not have enough inertia to cross boundary layers and impinge on walls. They are simply advected by the air flow from the nose to the primary bronchi.

We repeat this test case but without a particle pressure, i.e. we set the particle pressure coefficient $\kappa_0 = 0$. Note that this corresponds to solving Model E with a non constant drag coefficient. The time-evolution (not shown here) of the droplet volume fraction computed with Model E is similar to the one computed with Model EP with a particle pressure coefficient $\kappa_0 = 10$. Figure 7.15 shows a plot of the solutions for both models, along the horizontal cut C_1 (see Figure 7.10), at $t = 100$. The effects of the particle pressure on the droplets are not seen because for small particles ($d = 1\mu m$), the drag force between the droplets and the air is much more important than the particle pressure force for small mass loading. The drag force and the inertia are the leading forces acting on the droplets.

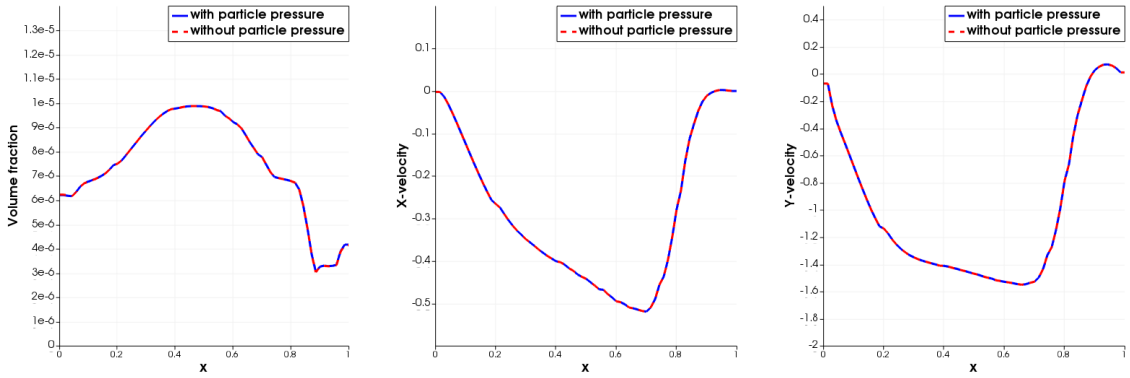

Figure 7.15: Plot of the solutions with/without particle pressure along the horizontal cut C_1. $t = 100$, $d = 1\mu m$, $\rho_l = 1000kg/m^3$, $\Delta t = 0.02$.

We repeat again the first test case but for droplets with diameter $d = 100\mu m$. The time-evolution of the droplet volume fraction computed with a particle pressure coefficient $\kappa_0 = 10$ is shown in Figure 7.16. It can be seen by comparing the solutions in Figures 7.13 and 7.16 that large droplets ($d = 100\mu m$) are less deviated by the air flow than small droplets ($d = 1\mu m$). Most of the large droplets are advected towards the left side of the trachea and exit by the left primary bronchi, as opposed to small droplets for which the repartition of particles between the left and right primary bronchi is more even. Large particles also take more time to entirely fill the recirculation zones since their larger inertia to some extent prevents them from being trapped by the recirculations.

The previous test case is repeated but without a particle pressure, i.e. with $\kappa_0 = 0$. Here also, the solution computed without particle pressure is the same as the one obtained with a particle pressure coefficient $\kappa_0 = 10$. Figure 7.17 shows a plot of the solutions with/without particle pressure over along the horizontal cut C_1. Comparing figures 7.15 and 7.17, differences are seen on the volume fraction while varying the diameter of the particles. Differences are minor on the particle velocity which remains almost the same and is identical to the air velocity.

These test cases show that the models (E) and (EP) give similar results for particles with diameter in the range $1 - 100\mu m$ and density $\rho_l = 1000kg/m^3$ advected by air in movement inside the domain Ω_2. There is no a significant effect of the particle pressure force on the droplets because the particle mass loading is small. The drag force between the air and the droplets and the inertia are the leading forces acting on the droplets.

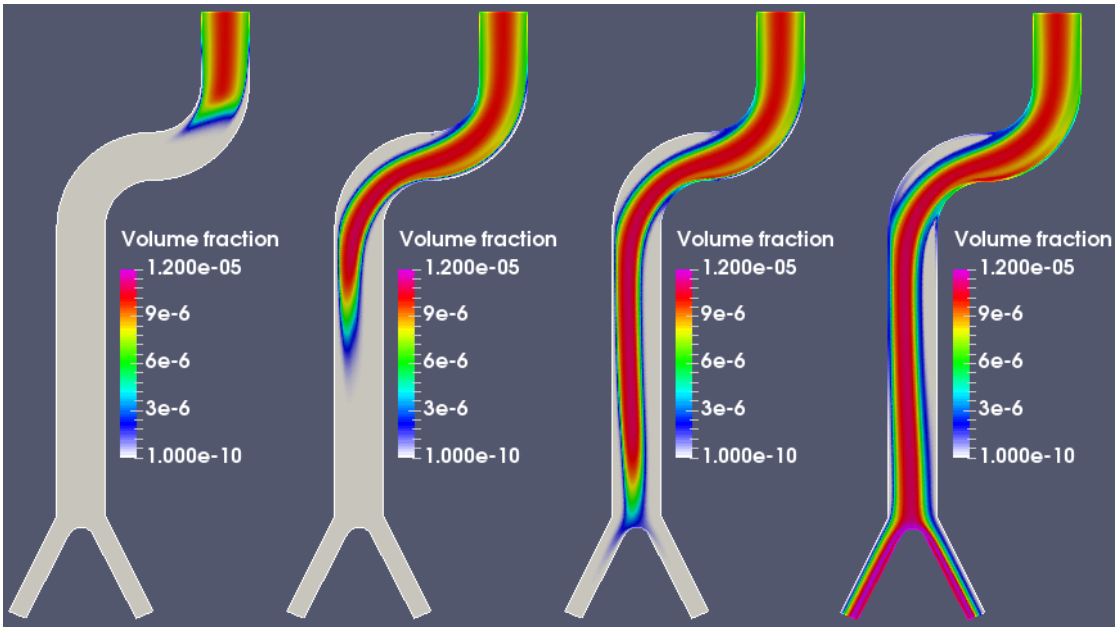

$t = 2$ $t = 6$ $t = 8.4$ $t = 20$

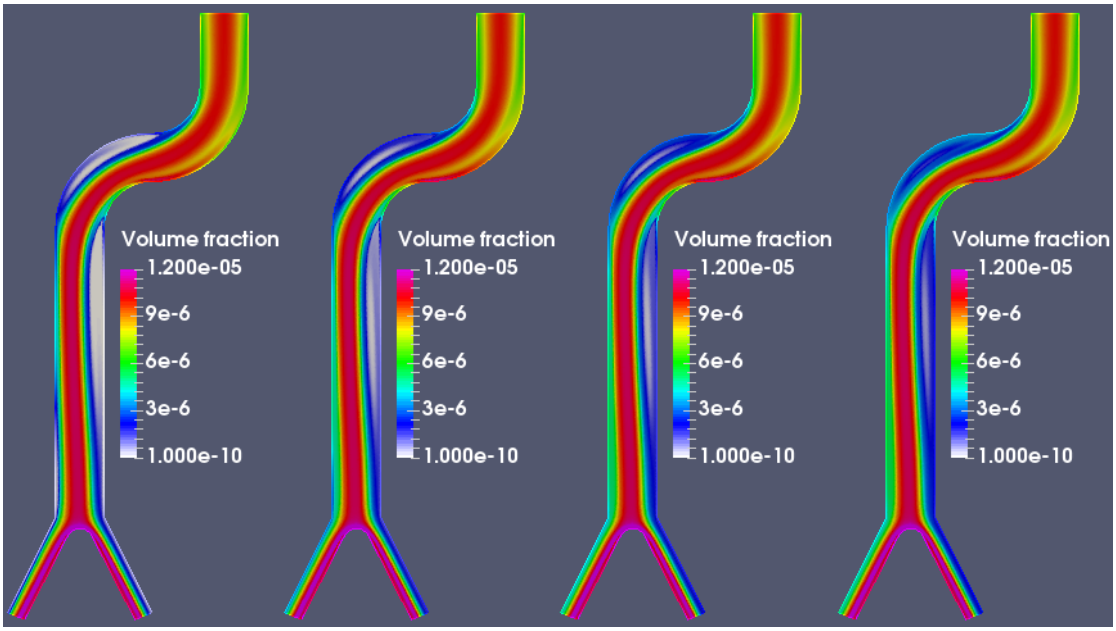

$t = 30$ $t = 60$ $t = 100$ $t = 180$

Figure 7.16: Model EP: Particle volume fraction as a function of time. $\rho_l = 1000kg/m^3$, $\kappa_0 = 10$, $d = 100\mu m$, $\Delta t = 0.02$.

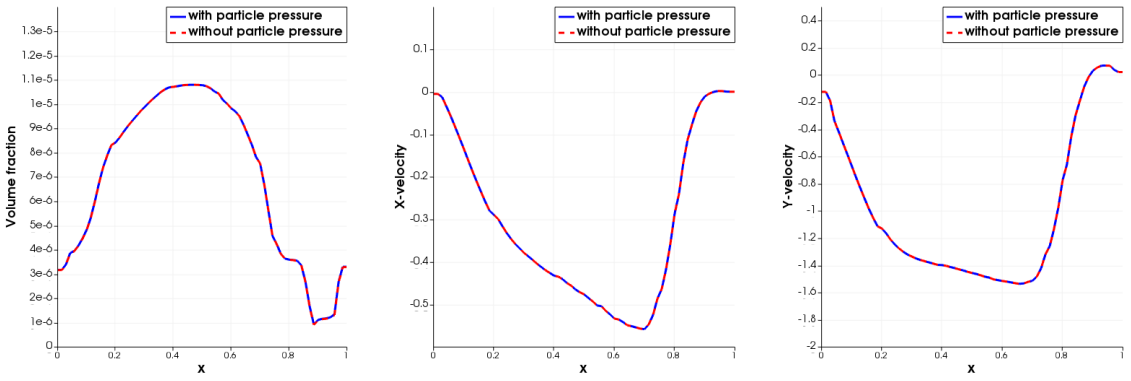

Figure 7.17: Plot of the solutions with/without particle pressure along the horizontal cut C_1. $t = 100$, $d = 100\mu m$, $\rho_l = 1000kg/m^3$, $\Delta t = 0.02$.

Next, we consider heavier particles with density $\rho_l = 4000kg/m^3$. A particle volume fraction $\alpha = 10^{-4} \times \exp(-2(x - 1.5)^2)$ and a particle velocity $\mathbf{u} = \mathbf{v}$ are imposed on the inflow boundary Γ_-. The rest of the boundary of the domain is left free. The numerical solutions are computed with the finite element formulation (7.2.25). Figure 7.18 shows the time-evolution of the particle volume fraction computed with a particle pressure coefficient $\kappa_0 = 10$ for particles with diameter $d = 100\mu m$. One can see that heavier particles are less deviated by the air flow. Most of the particles are advected along the left wall of the trachea and exit through the left primary bronchi.

This test case is repeated but without a particle pressure, i.e. by setting $\kappa_0 = 0$. Figure 7.19 shows the time-evolution of the particle volume fraction without particle pressure. Comparing Figures 7.18 and 7.19, one can see a slow dispersion of the particles in the solution with particle pressure. This dispersion is more important in the recirculation zones, namely near the lower left boundary of the nose-mouth region and the right boundary of the trachea. A plot of the solutions with/without particle pressure along the horizontal cut C_2 (see Figure 7.10) is represented in Figure 7.20. One can see that the particle volume fraction is larger near the left and right boundaries of the trachea and slightly smaller in between for the solution with particle pressure. There is a smaller difference on the velocity field between the solutions with/without particle pressure. Nevertheless, the difference on velocities is consistent with the difference between the volume fractions, given the smaller magnitude of this latter variable. These results show that for heavier ($\rho_l = 4000kg/m^3$) and larger ($d = 100\mu$) particles, the drag force and the particle pressure gradient become equally important for inducing variations of the particle inertia.

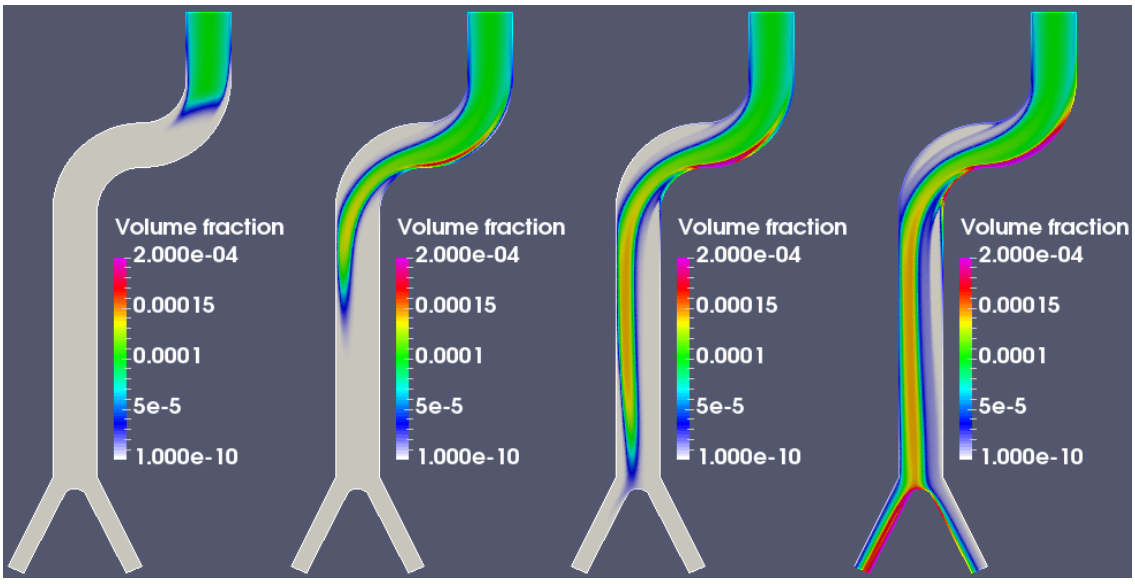

$t = 2$ $t = 6$ $t = 8.4$ $t = 20$

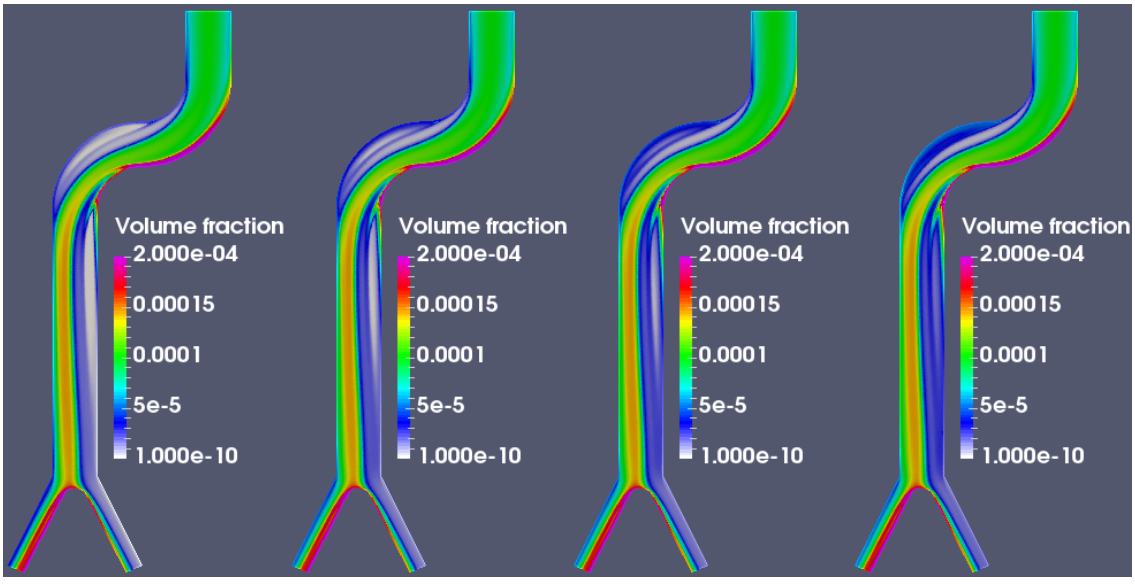

$t = 30$ $t = 60$ $t = 100$ $t = 180$

Figure 7.18: Model EP: Particle volume fraction as a function of time. $\rho_l = 4000kg/m^3$, $d = 100\mu m$, $\kappa_0 = 10$, $\Delta t = 0.02$.

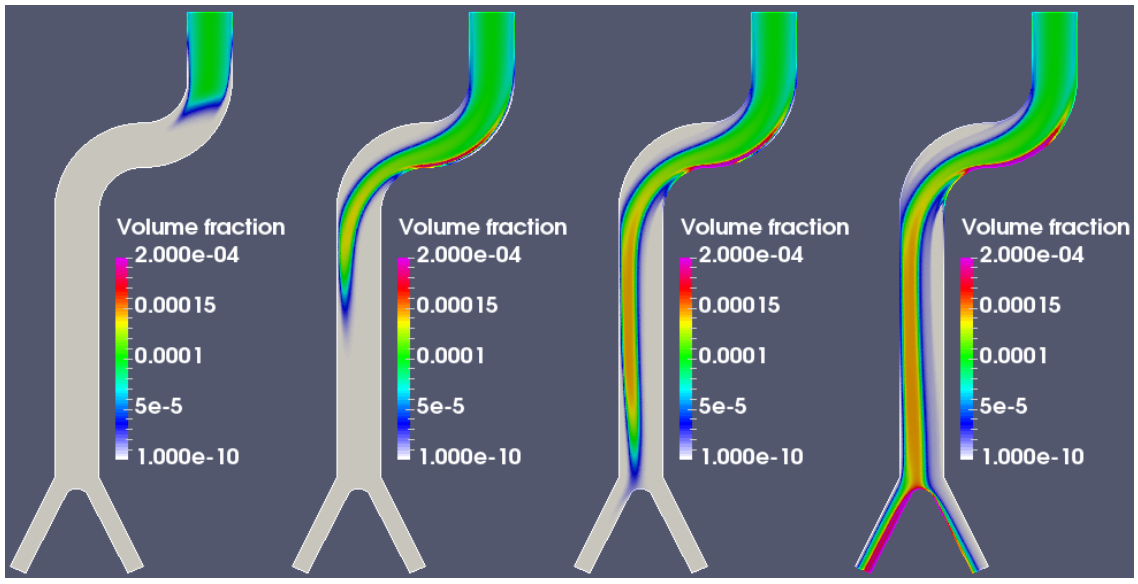

$t = 2$ $t = 6$ $t = 8.4$ $t = 20$

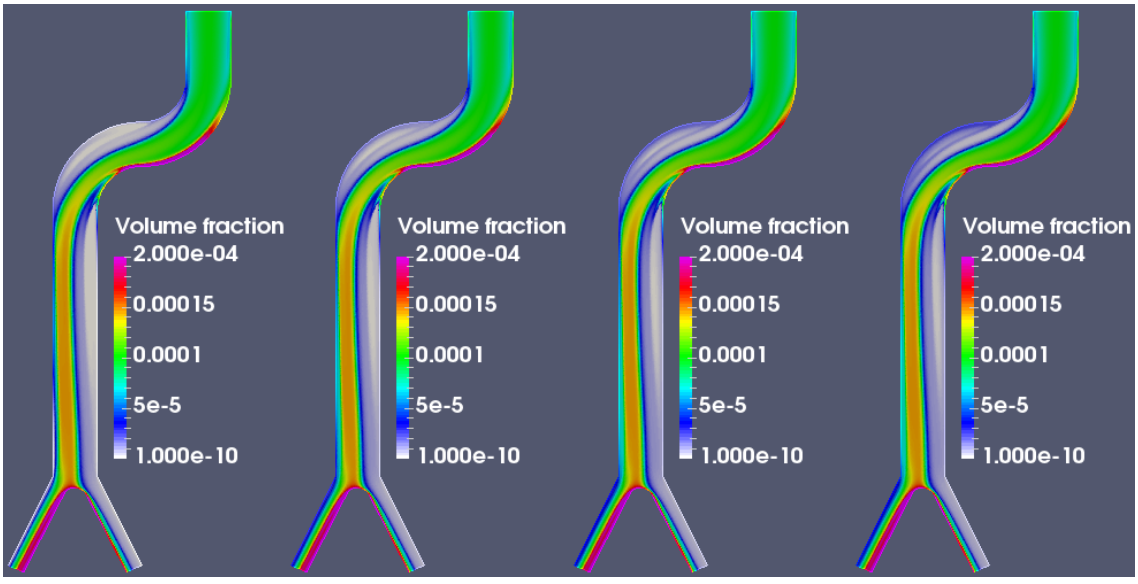

$t = 30$ $t = 60$ $t = 100$ $t = 180$

Figure 7.19: Model E: Particle volume fraction as a function of time. $\rho_l = 4000kg/m^3$, $d = 100\mu m$, $\Delta t = 0.02$.

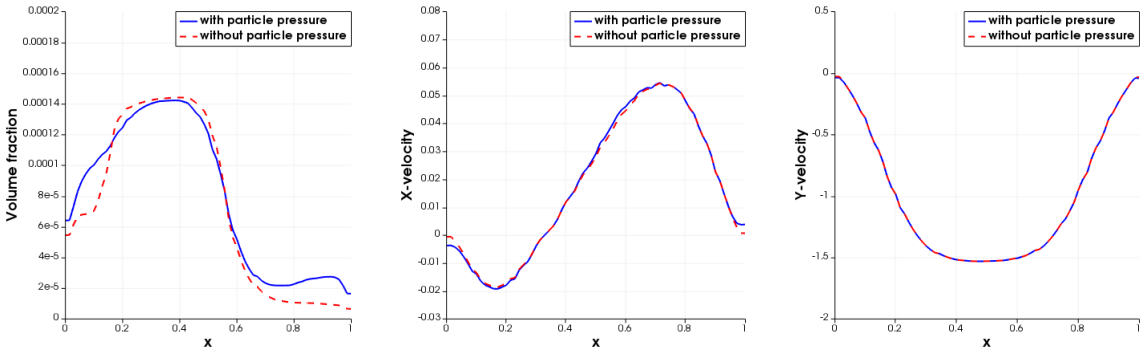

Figure 7.20: Plot of the solutions with/without particle pressure along the horizontal cut C_2 at $t = 180$. $\rho_l = 4000kg/m^3$, $d = 100\mu m$, $\Delta t = 0.02$.

Finally, we are interested in the collection efficiency. The Eulerian droplet model yields volume fraction α and velocity field $\mathbf{u}$ of the particles at any specific location in space over time. The collection efficiency on walls can then be calculated as $\beta = \alpha \mathbf{u} \cdot \mathbf{n}$, where $\mathbf{n}$ is the outward normal of the domain. This expression measures the quantity of particles that deposit on the walls. The present approach eliminates the well-known limitations of the Lagrangian tracking method which requires elaborate algorithms and large computational resources for computing the collection efficiency on complex geometries. The Eulerian droplet model (E) can provide accurate droplet impingement predictions when an adequate droplet size distribution is provided [17, 16]. Here, we compare the collection efficiency profiles computed with the models (E) and (EP). Considering the second test case, we compute the collection efficiency on the right boundary of the nose-mouth region (section S_1 in Figure 7.10) and on the circular arc connecting the primary bronchi (section S_2 in Figure 7.10). Figure 7.21 shows the collection efficiency with/without particle pressure. The abscissa x is the horizontal distance along the considered sections. The two models give similar collection efficiency profiles. Minor differences are noticed due to the effects of the particle pressure. In fact, the latter disperses the particles, and thus affects the particle volume fraction, particularly in regions where particles accumulate or recirculations occur. Overall, the differences are small. This shows the potential of Model EP since it can recover predictions from Model E that is already validated for smooth solutions against experimental data in aerodynamics [17], but also extends the validity range of Model E to those situations where particle pressure matters.

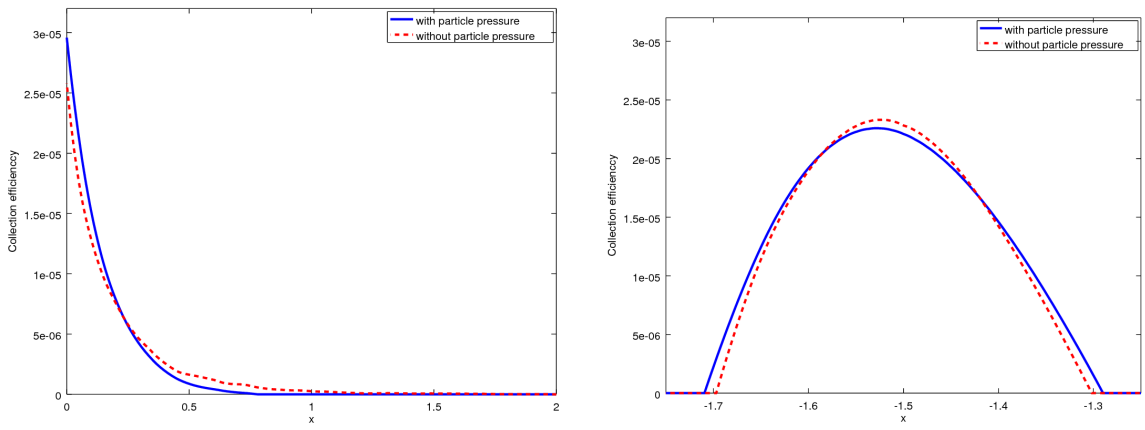

Figure 7.21: Collection efficiency $\beta = \alpha \mathbf{u} \cdot \mathbf{n}$ computed for the solutions with/without particle pressure at $t = 180$. At left: collection efficiency along the section S_1. At right: collection efficiency along the section S_2 . $\rho_l = 4000 kg/m^3$, $d = 100 \mu m$, $\Delta t = 0.02$.

7.4 Conclusion

The standard non-conservative form of the Eulerian droplet model (E) has been used in the past for the prediction of droplets impingement on airfoils and ice accretion on airplane wings during in-flight icing events [15, 17, 75, 6, 50] and more recently for the prediction of air-particle flows in airways [14, 16]. As far as we know, the conservative Eulerian droplet model with particle pressure (EP) was never used. Some theoretical justifications for the use of this new model have been given here and in the previous chapters. The 2D computations performed here show that the SUPG method combined with a shock capturing term can be used to solve the conservative form of the particle equations with/without particle pressure. However, it is diffusive. The models (E) and (EP) give almost identical solutions for the test cases presented in this chapter. Small differences between the two models can be noticed in the recirculation regions for heavier and larger particles. These differences are due to the particle pressure. The results in this chapter show that Model EP can recover predictions from Model E. Model EP could also be used as an extension of Model E in situations where particle pressure has larger impact (e.g. discontinuous travelling waves, large particle loading, high-speed flows, etc). Of course, a extensive validation of Model EP is needed in such cases. Moreover, the limitation on the smallness of the particle mass loading for the one-way coupling to be valid could be removed by adding momentum transfer terms in the Navier-Stokes equations.

Chapter 8

Conclusion and perspectives

In this thesis, we considered Eulerian models for dispersed two-phase flows. We focused on the mathematical analysis of a one-way coupling Eulerian model for air-particle flows, which can be seen as the pressureless gas system with a zeroth-order source term. We also worked on the improvement of Eulerian models for dispersed two-phase flows, as well as the use of such models for numerical predictions of air-particle flows in airways.

8.1 Contributions

The condition for the loss of regularity of smooth solutions of the inviscid Burgers equation with a zeroth-order source term is established. The same condition applies to the Eulerian droplet model. The Riemann problems associated, respectively, to the Burgers equation with a source term and the Eulerian droplet model are solved. As far as we know, this had not been done before for the inviscid Burgers equation and the pressureless gas system, both including a zeroth-order source term as the one in Model E. As for the pressureless gas system, the solution of the Riemann problem for the Eulerian droplet model is either a contact discontinuity, or a delta shock, or a two-contact discontinuity with a vacuum state, but the left and right states are no longer constant. The zeroth-order source term acts as a relaxation term by weakening the delta shocks as time evolves. The generalized Rankine-Hugoniot conditions are given by a nonlinear system of ODEs of first order that is hard or impossible to solve analytically. The difficulty in the solution comes from the contribution of the source term, which also leads to characteristic curves that are no longer straight lines, but curves that tend asymptotically to straight lines. The existence of an entropic solution to the generalized Rankine-Hugoniot conditions is proven. However, all this analysis is carried out in one-dimensional space and for a drag coefficient and air velocity that are both constant.

Chen and Liu [23] analyzed the behaviour of the solutions of the Riemann problem for the isentropic Euler equations when the pressure vanishes. They showed that the formation of delta shocks and vacuum states in the pressureless gas system results from an asymptotically vanishing pressure in the isentropic Euler equations. Two cases were only partially covered by their analysis, namely the 1-shock combined with the 2-rarefaction and the 1-rarefaction combined with the 2-shock wave. We performed a complete analysis of these two cases and showed that any Riemann solution composed of a 1-shock wave combined with a 2-rarefaction wave converts to a two-shock waves when the pressure coefficient gets smaller than a fixed value determined by the Riemann data. In contrast, any Riemann solution composed of a 1-rarefaction wave combined with a 2-shock wave converts to a two-rarefaction waves when the pressure coefficient gets smaller than a fixed value determined by the Riemann data. These results were mentioned by Chen and Liu [23] without proof. Our analysis completes the picture on the degeneracy of the isentropic Euler equations to the pressureless gas system.

Based on the results from chapters 3 and 4, we proposed an Eulerian droplet model with a particle pressure. This new model is written in conservative form and is strictly hyperbolic. The conservative form should be used when traveling waves with discontinuities appear in the solution and propagate as time evolves. We illustrated numerically that this new Eulerian model does not develop the undesirable delta shocks and vacuum states. Nevertheless, we are not able to solve the Riemann problem associated to this model and analyze the behaviour of the solutions in the vanishing pressure limit. The difficulty lies in the presence of the source term which makes the standard theory for strictly hyperbolic conservation laws not applicable.

We discussed the mathematical and physical relevance of particle pressures in Eulerian models for dispersed two-phase flows. The usual approach in the literature is to consider the pressure coming from the carrier phase as a common pressure for the two phases. The gradient of this pressure times the volume fraction is included in the momentum equation of the corresponding phase. Neither of these two modeling assumptions seems correct. In fact, this requires additional pressure correction terms for well-posedness and leads to non-conservative systems as the general common-pressure two-fluid model (the starting model in the hierarchy of Bouchut [10]). Different pressures (one for each phase) should be considered and the gradient of the product of the pressure and the volume fraction is to be included in the momentum equation of the corresponding phase. This has two main advantages. It makes the system hyperbolic without additional pressure correction term. Moreover, it allows us to write the system in conservative form. The idea of including the pressure gradients in such way was proposed in the 70s [43], but not considered further in the literature. Following these ideas, we derived a new hierarchy of two-way coupling two-pressure models for dispersed two-phase flows and discussed the validity of each model. However, mathematical analysis and numerical validations are still needed for

some models.

Much of the literature on the propagation and deposition of aerosols in airways relies on the Lagrangian tracking approach. A common justification for the use of the Lagrangian approach is that air flows in airways are internal and pulsatile, and present recirculation regions which potentially lead to crossing particle trajectories. One major concern of the Lagrangian approach is the large computational expense that may be experienced because of the requirement to track a substantial number of particles to attain good statistical information of the dispersed phase. The computations conducted in this thesis show that the Eulerian formulation could provide a viable approach to compute internal dilute gas-particle flows, even in the presence of reverse flow regions. Our test cases for internal flows representative of airways showed that crossing trajectories are unlikely to happen since the particle velocity remains close to the air velocity, even for very large and heavy particles. On the one hand, these results confirm that Model E could be used for smooth solutions of dilute gas-particle flows. On the other hand, they show the potential of Model EP, which should be used in situations where particle pressure matters (large particle loading, discontinuous traveling waves, etc). The implementation of the Eulerian approach is simple and results in relatively small computational time to get the volume fraction, velocity and collection efficiency for aerosol flows. No particle tracking has to be done. These advantages make the Eulerian model very attractive. Nevertheless, there are some difficulties in the use of Eulerian models for air-particle flows. A major concern is the modeling of the boundary conditions for the dispersed phase, as the current approach assumes that the particles hitting the walls just vanish (basically stick to the walls). A proper treatment of the particle-wall impaction at wall boundaries is still far from adequate for more complex physical situations, e.g. splash-back of particles, particle breakup, etc.

8.2 Future work

In the future, it would be desirable to provide a rigorous mathematical proof of the non-occurrence of delta shocks and vacuum states Model EP. A good deal of work needs to go into solving the Riemann problem for the isentropic Euler equations with a zeroth-order source term as the one in Model E. The primary difficulty stems from the presence of this zeroth order source term which renders the characteristic variables non constant along the characteristic curves that are no longer straight lines. Additionally, in this thesis we only performed the analysis in the one-dimensional case. A challenging problem would be to extend this analysis to multi-dimensional cases to see how travelling waves evolve in multi-dimensional space.

The comparison of the models in chapter 6 shows that the one-way coupling assumption is only valid for dilute gas-particle flows. Two-way momentum transfer should be considered for large particle loading. This can be achieved by adding

a momentum transfer term in the carrier fluid equations (Euler or Navier-Stokes equations). A way of adding such term in the Euler equations is known. Navier-Stokes equations are commonly used for internal flows where viscous effects are important. In the future, it would be interesting to investigate how momentum transfer terms can be added in the Navier-Stokes equations. Another direction of improvement would be the use of a more sophisticated droplet model that could account for the size of the droplets, droplet splashing and droplet-wall impaction at boundary surfaces.

The numerical methods used in chapter 7 are clearly not the "optimal" ones to solve the Navier-Stokes and particle equations, respectively. More accurate and efficient methods should be considered for the Navier-Stokes equations, as well as for the droplet equations. The numerical solution of these equations requires accurate methods that are efficient to handle advective terms and singular problems since the computation of the particle velocity vector field using the conservative form of the particle equations leads to singular equations in regions where the particle volume fraction tends to zero.

Appendix A

List of the models

Model I from Bouchut [10] (introduced on page 17):

$$\begin{cases} \partial_t((1-\alpha)\rho_g) + \partial_x((1-\alpha)\rho_g v) = 0, \\ \partial_t((1-\alpha)\rho_g v) + \partial_x((1-\alpha)\rho_g v^2) + (1-\alpha)\partial_x p = \dfrac{\mu}{\epsilon}\alpha(1-\alpha)(u-v), \\ \partial_t \alpha + \partial_x(\alpha u) = 0, \\ \partial_t(\alpha u) + \partial_x(\alpha u^2) + \epsilon\alpha\partial_x p + C_p(v-u)^2\partial_x\alpha = \mu\alpha(1-\alpha)(v-u), \end{cases} \tag{I}$$

Model II from Bouchut [10] (introduced on page 17):

$$\begin{cases} \partial_t((1-\alpha)\rho_g) + \partial_x((1-\alpha)\rho_g u) = \epsilon\partial_x(\dfrac{\rho_g}{\mu\alpha}(1-\alpha)\partial_x p), \\ \partial_t \alpha + \partial_x(\alpha u) = 0, \\ \partial_t(\alpha u) + \partial_x(\alpha u^2 + \epsilon p) = 0. \end{cases} \tag{II}$$

Model III from Bouchut [10] (introduced on page 17):

$$\begin{cases} \partial_t \alpha + \partial_x(\alpha u) = 0, \\ \partial_t(\alpha u) + \partial_x(\alpha u^2) = 0. \end{cases} \tag{III}$$

Model IV from Bouchut [10] (introduced on page 18):

$$\begin{cases} \partial_t \alpha + \partial_x(\alpha u) = 0, \\ \partial_t(\alpha u) + \partial_x(\alpha u^2 + \Pi) = 0, \\ \lim\limits_{\epsilon\to 0} \epsilon p = \Pi, \text{ with } (1-\alpha)\Pi = 0. \end{cases} \tag{IV}$$

Model E (introduced on page 22):

$$\begin{cases} \partial_t \alpha + \partial_x(\alpha u) = 0, \\ \partial_t(\alpha u) + \partial_x(\alpha u^2) = K_D\alpha(u_a - u), \end{cases} \tag{E}$$

Equation (B) (introduced on page 22):

$$\partial_t u + \partial_x(\frac{u^2}{2}) = K_D(u_a - u). \tag{B}$$

System E' (introduced on page 23):

$$\begin{cases} \partial_t \alpha + \partial_x(\alpha u) = 0, \\ \partial_t u + \partial_x(\frac{u^2}{2}) = K_D(u_a - u). \end{cases} \tag{E'}$$

Model IE (introduced on page 67):

$$\begin{cases} \partial_t \rho + \partial_x(\rho v) = 0, \\ \partial_t(\rho v) + \partial_x(\rho v^2 + p) = 0, \end{cases} \tag{IE}$$

Model EP (introduced on page 86):

$$\begin{cases} \partial_t \alpha + \partial_x(\alpha u) = 0, \\ \partial_t(\alpha u) + \partial_x(\alpha(u^2 + \pi)) = K_D \alpha(u_a - u), \end{cases} \tag{EP}$$

Model IA (introduced on page 100):

$$\begin{cases} \partial_t \rho + \partial_x(\rho v) = 0, \\ \partial_t(\rho v) + \partial_x(\rho v^2 + p) = -\dfrac{1}{\epsilon}\mu\alpha(v - u), \\ \partial_t \alpha + \partial_x(\alpha u) = 0, \\ \partial_t(\alpha u) + \partial_x(\alpha u^2) = \mu\alpha(1 - \alpha)(v - u). \end{cases} \tag{IA}$$

Model IAP (introduced on page 102):

$$\begin{cases} \partial_t \rho + \partial_x(\rho v) = 0, \\ \partial_t(\rho v) + \partial_x(\rho v^2 + p) = -\dfrac{1}{\epsilon}\mu\alpha(v - u), \\ \partial_t \alpha + \partial_x(\alpha u) = 0, \\ \partial_t(\alpha u) + \partial_x(\alpha(u^2 + \pi)) = \mu\alpha(1 - \alpha)(v - u), \end{cases} \tag{IAP}$$

Model G (introduced on page 103):

$$\begin{cases} \partial_t\big((1 - \alpha)\rho\big) + \partial_x\big((1 - \alpha)\rho v\big) = 0, \\ \partial_t\big((1 - \alpha)\rho v\big) + \partial_x\big((1 - \alpha)(\rho v^2 + p)\big) = -\dfrac{1}{\epsilon}\mu\alpha(1 - \alpha)(v - u), \\ \partial_t \alpha + \partial_x(\alpha u) = 0, \\ \partial_t(\alpha u) + \partial_x\big(\alpha(u^2 + \pi)\big) = \mu\alpha(1 - \alpha)(v - u). \end{cases} \tag{G}$$

Appendix B

Derivation of Model II

Consider Model I

$$\begin{cases} \partial_t((1-\alpha)\rho_g) + \partial_x((1-\alpha)\rho_g v) = 0, \\ \partial_t((1-\alpha)\rho_g v) + \partial_x((1-\alpha)\rho_g v^2) + (1-\alpha)\partial_x p = \dfrac{\mu}{\epsilon}\alpha(1-\alpha)(u-v), \\ \partial_t\alpha + \partial_x(\alpha u) = 0, \\ \partial_t(\alpha u) + \partial_x(\alpha u^2) + \epsilon\alpha\partial_x p + C_p(v-u)^2\partial_x\alpha = \mu\alpha(1-\alpha)(v-u). \end{cases} \tag{I}$$

We carry out the Chapman-Enskog expansion for Model I, i.e. we seek solution v of Model I in the form

$$v = u + \epsilon w. \tag{B.0.1}$$

Substituting v by $u + \epsilon w$ in (I) leads to

$$\begin{cases} \partial_t((1-\alpha)\rho_g) + \partial_x((1-\alpha)\rho_g u) = -\epsilon\partial_x((1-\alpha)\rho_g w), \\ \partial_t((1-\alpha)\rho_g u) + \partial_x((1-\alpha)\rho_g(u+\epsilon w)^2) + (1-\alpha)\partial_x p = -\mu\alpha(1-\alpha)w, \\ \partial_t\alpha + \partial_x(\alpha u) = 0, \\ \partial_t(\alpha u) + \partial_x(\alpha u^2) + \epsilon\alpha\partial_x p + C_p(\epsilon w)^2\partial_x\alpha = \epsilon\mu\alpha(1-\alpha)w. \end{cases} \tag{B.0.2}$$

which can be written in term of $O(\epsilon)$ as

$$\begin{cases} \partial_t((1-\alpha)\rho_g) + \partial_x((1-\alpha)\rho_g u) = O(\epsilon), \\ \partial_t((1-\alpha)\rho_g u) + \partial_x((1-\alpha)\rho_g u^2) + (1-\alpha)\partial_x p + O(\epsilon) = -\mu\alpha(1-\alpha)w, \\ \partial_t\alpha + \partial_x(\alpha u) = 0, \\ \partial_t(\alpha u) + \partial_x(\alpha u^2) = O(\epsilon). \end{cases} \tag{B.0.3}$$

Developing the fourth equation of (B.0.3) and using the third equation of the latter lead to

$$\partial_t u + u\partial_x u = O(\epsilon). \tag{B.0.4}$$

Developing the second equation in (B.0.3) leads to

$$u\big(\partial_t((1-\alpha)\rho_g)+\partial_x((1-\alpha)\rho_g u)\big)+(1-\alpha)\rho_g\big(\partial_t u+u\partial_x u\big)+(1-\alpha)\partial_x p+O(\epsilon)=-\mu\alpha(1-\alpha)w. \tag{B.0.5}$$

Substituting the first equation of (B.0.3) and (B.0.4) in (B.0.5), one gets

$$-\mu\alpha(1-\alpha)w=(1-\alpha)\partial_x p+O(\epsilon). \tag{B.0.6}$$

In one hand, assuming $\mu\alpha>0$, on can divide (B.0.6) by $\alpha\mu$ to obtain

$$-(1-\alpha)w=\frac{1}{\mu\alpha}(1-\alpha)\partial_x p+O(\epsilon). \tag{B.0.7}$$

Multiplying (B.0.7) by ρ_g, taking the x-derivative and multiplying again by ϵ, one obtains

$$-\epsilon\partial_x((1-\alpha)\rho_g w)=\epsilon\partial_x(\frac{\rho_g}{\mu\alpha}(1-\alpha)\partial_x p)+O(\epsilon^2). \tag{B.0.8}$$

Substituting (B.0.8) in the first equation of (B.0.2), the latter equation reduces to

$$\partial_t((1-\alpha)\rho_g)+\partial_x((1-\alpha)\rho_g u)=\epsilon\partial_x(\frac{\rho_g}{\mu\alpha}(1-\alpha)\partial_x p)+O(\epsilon^2). \tag{B.0.9}$$

In the other hand, multiplying (B.0.6) by ϵ leads to

$$-\epsilon\mu\alpha(1-\alpha)w-\epsilon(1-\alpha)\partial_x p=O(\epsilon^2). \tag{B.0.10}$$

Rewritting α in the third term on the l.h.s of the fourth equation of (B.0.2) as $1-(1-\alpha)$, the latter equation gives rise to

$$\partial_t(\alpha u)+\partial_x(\alpha u^2)+\epsilon\partial_x p-\epsilon(1-\alpha)\partial_x p-\epsilon\mu\alpha(1-\alpha)w+C_p(\epsilon w)^2\partial_x\alpha=0. \tag{B.0.11}$$

Using (B.0.10) in (B.0.12), the latter reduces to

$$\partial_t(\alpha u)+\partial_x(\alpha u^2)+\epsilon\partial_x p=O(\epsilon^2). \tag{B.0.12}$$

Using (B.0.9) and (B.0.12), system (B.0.2) gives rise to

$$\begin{cases}\partial_t((1-\alpha)\rho_g)+\partial_x((1-\alpha)\rho_g u)=\epsilon\partial_x(\frac{\rho_g}{\mu\alpha}(1-\alpha)\partial_x p)+O(\epsilon^2),\\ \partial_t((1-\alpha)\rho_g u)+\partial_x((1-\alpha)\rho_g(u+\epsilon w)^2)+(1-\alpha)\partial_x p=-\mu\alpha(1-\alpha)w,\\ \partial_t\alpha+\partial_x(\alpha u)=0,\\ \partial_t(\alpha u)+\partial_x(\alpha u^2+\epsilon p)=O(\epsilon^2).\end{cases} \tag{B.0.13}$$

Note that the second equation of (B.0.2) gives rises to (B.0.8) which is used in the others equations of (B.0.2) to get the system (B.0.13). By ignoring this second equation in (B.0.13) and the terms in $O(\epsilon^2)$, one obtains

$$\begin{cases}\partial_t((1-\alpha)\rho_g)+\partial_x((1-\alpha)\rho_g u)=\epsilon\partial_x(\frac{\rho_g}{\mu\alpha}(1-\alpha)\partial_x p),\\ \partial_t\alpha+\partial_x(\alpha u)=0,\\ \partial_t(\alpha u)+\partial_x(\alpha u^2+\epsilon p)=0.\end{cases} \tag{II}$$

Bibliography

[1] S. Abu-Zaid and G. Ahmadi. A thermodynamically consistent rate-dependent model for turbulent two-phase flows. *Int. J. Non-Linear Mechanics*, 30(4):509 – 529, 1995.

[2] Federal Aviation Administration. *Airplane and Engine Certification Requirements in Supercooled Large Drop, Mixed Phase, and Ice Crystal Icing Condition*. FAA–2010–0636, 2010.

[3] K. L. Aplin and R. G. Harrison. The interaction between air ions and aerosol particles in the atmosphere. *Inst. Phys. Conf. Ser.*, 163:411–414, 1999.

[4] B. Arcen and A. Tanière. Simulation of a particle-laden turbulent channel flow using an improved stochastic Lagrangian model. *Physics of Fluids*, 21(4), 2009.

[5] G. K. Batchelor. A new theory of the instability of a uniform fluidized bed. *J. Fluid Mech.*, 193:75–110, 1988.

[6] H. Beaugendre, F. Morency, and W. G. Habashi. Developpement of a second generation in-flight icing simulation code. *J. Fluids Eng.*, 128(2):378–387, 2006.

[7] United States. National Transportation Safety Board. *In-flight Icing Encounter and Loss of Control, Simmons Airlines, D.b.a. American Eagle Flight 4184, Avions de Transport Regional (ATR) Model 72-212, N401AM, Roselawn, Indiana, October 31, 1994*. Aircraft accident report. National Transportation Safety Board, 1996.

[8] D. Boffi, F. Brezzi, and M. Fortin. *Mixed Finite Element Methods and Applications*, volume 44 of *Springer Series in Computational Mathematics*. Springer, Heidelberg, 2013.

[9] F. Bouchut. On zero pressure gas dynamics. In *Advances in kinetic theory and computing*, volume 22 of *Ser. Adv. Math. Appl. Sci.*, pages 171–190. World Sci. Publ., River Edge, NJ, 1994.

[10] F. Bouchut, Y. Brenier, J. Cortes, and J.-F. Ripoll. A hierarchy of models for two-phase flows. *J. Nonlinear Sci.*, 10:639–660, 2000.

[11] F. Bouchut and F. James. Duality solutions for pressureless gases, monotone scalar conservation laws, and uniqueness. *Comm. Partial Differential Equations*, 24(11–12):2173–2189, 1999.

[12] F. Bouchut, S. Jin, and X. Li. Numerical approximations of pressureless and isothermal gas dynamics. *SIAM J. Numer. Anal*, 41(1):135–158, 2001.

[13] L. Boudin and J. Mathiaud. A numerical scheme for the one-dimensional pressureless gases system. *Numer. Methods Partial Differential Equations*, 28(6):1729–1746, 2012.

[14] Y. Bourgault. Computing gas-particle flows in airways with an Eulerian model. In *European Conference on Computational Fluid Dynamics-ECCOMAS CFD*, 2006.

[15] Y. Bourgault, W. G. Habashi, J. Dompierre, and G. S. Baruzzi. A finite element method study of Eulerian droplets impingement models. *Int. J. Numer. Methods Fluids*, 29(4):429–449, 1999.

[16] Y. Bourgault and M. Thiriet. Critical aspects of flow and aerosol simulations in the airway tract. In *European Conference on Computational Fluid Dynamics–ECCOMAS CFD 2008*, Venice, Italy, 2008.

[17] Z. Boutanios, Y. Bourgault, S. Cober, G. A. Isaac, and W. G. Habashi. 3D Droplets impingement analysis around an aircraft's nose and cockpit using FENSAP-ICE. In *36th AIAA Aerospace Science Meeting and Exhibit*, Egmond ann Zee, The Netherlands, 1997.

[18] Y. Brenier and E. Grenier. Sticky particles and scalar conservation laws. *SIAM J. Numer. Anal.*, 35(6):2317–2328, 1998.

[19] M. Breuer, H. T. Baytekin, and E. A. Matida. Prediction of aerosol deposition in 90° bends using LES and an efficient Lagrangian tracking method. *J. of Aerosol Sc.*, 37(11):1407–1428, 2006.

[20] A. N. Brooks and T. J. R. Hughes. Streamline upwind/Petrov-Galerkin formulations for convection dominated flows with particular emphasis on the incompressible Navier-Stokes equations. *Comput. Methods in Appl. Mech. Eng.*, 32(1):199–259, 1982.

[21] C. S. Campbell and D. G. Wang. Particle pressures in gas-fluidized beds. *J. Fluid Mech.*, 227:495–508, 1991.

[22] G.-Q. Chen, C. D. Levermore, and T.-P. Liu. Hyperbolic conservation laws with stiff relaxation terms and entropy. *Comm. Pure Appl. Math.*, 47(6):787–830.

[23] G.-Q. Chen and H. Liu. Formation of delta-shocks and vacuum states in the vanishing pressure limit of solutions to the isentropic Euler equations. *SIAM J. Math. Anal.*, 34(4):925–938, 2003.

[24] G.-Q. Chen and H. Liu. Concentration and cavitation in the vanishing pressure limit of solutions to the Euler equations for nonisentropic fluids. *Physica D. Nonlinear Phenomena*, 189(1–2):141–165, 2004.

[25] G.-Q. Chen and D. Wang. The Cauchy problem for the Euler equations for compressible fluids. In *Handbook of Mathematical Fluid Dynamics, Vol. I*, pages 421–543. North-Holland, Amsterdam, 2002.

[26] S. Cheng, J. Li, and T. Zhang. Explicit construction of measure solutions of Cauchy problem for transportation equations. *Science in China Series A: Mathematics*, 40(12):1287–1299, 1997.

[27] I. Christie, D. F. Griffiths, A. R. Mitchell, and O. C. Zienkiewicz. Finite element methods for second order differential equations with significant first derivatives. *Int. J. Numer. Meth. Eng.*, 10(6):1389–1396, 1976.

[28] J. Cortes, A. Debussche, and I. Toumi. A density perturbation method to study the eigenstructure of two-phase flow equation systems. *J. Comput. Phys.*, 147:463–484, 1998.

[29] M. Crouzeix and A. L. Mignot. *Analyse Numérique des Equations Différentielles*. Collection Mathématiques Appliquées pour la Maîtrise. Masson, 1984.

[30] C. T. Crowe. Review - Numerical models for dilute gas-particle flows. *ASME Transactions J. Fluids Eng.*, 104:297–303, 1982.

[31] C. M. Dafermos. *Hyperbolic Conservation Laws in Continuum Physics*. Grundlehren der mathematischen Wissenschaften [Fundamental Principles of Mathematical Sciences]. Springer-Verlag, Berlin, 2016.

[32] G. Dal Maso, P. G. LeFloch, and F. Murat. Definition and weak stability of nonconservative products. *J. Math. Pures Appl.*, 74(6):483–548, 1995.

[33] D. A. Drew. Mathematical modeling of two-phase flow. *Annual Review of Fluid Mechanics*, 15(1):261–291, 1983.

[34] D. A. Drew and S. L. Passman. *Theory of Multicomponent Fluids*, volume 135 of *Applied Mathematical Sciences*. Springer-Verlag, New York, 1999.

[35] D. A. Drew and L. A. Segel. Averaged equations for two-phase flow. *Stud. Appl. Math.*, 50(3):205–231, 1971.

[36] Weinan E, Yu. G. Rykov, and Ya. G. Sinai. Generalized variational principles, global weak solutions and behavior with random initial data for systems of conservation laws arising in adhesion particle dynamics. *Comm. Math. Phys.*, 177(2):349–380, 1996.

[37] A. Ern and J.-L. Guermond. *Theory and Practice of Finite Elements*, volume 159 of *Applied Mathematical Sciences*. Springer-Verlag, New York, 2004.

[38] P. U. Foscolo and L. G. Gibilaro. Fluid dynamic stability of fluidised suspensions: the particle bed model. *Chem. Eng. Sci.*, 42(6):1489–1500, 1987.

[39] G. Fourestey. Une méthode des caractéristiques d'ordre deux sur maillages mobiles pour la résolution des équations de Navier-Stokes incompressible par éléments finis. Technical Report RR-4448, INRIA, 2002.

[40] A. C. Galeão and E. G. D. do Carmo. A consistent approximate upwind Petrov-Galerkin method for convection-dominated problems. *Comput. Methods in Appl. Mech. Eng.*, 68(1):83–95, 1988.

[41] T. Gallouët, P. Helluy, J.-M. Hérard, and J. Nussbaum. Hyperbolic relaxation models for granular flows. *ESAIM: M2AN*, 44(2):371–400, 2010.

[42] T. Gemci, B. Shortall, G. M. Allen, T. E. Corcoran, and N. Chigier. A CFD study of the throat during aerosol drug delivery using heliox and air. *J. of Aerosol Sc.*, 34(9):1175–1192, 2003.

[43] D. Gidaspow. Modelling of two-phase flow. In *Round Table Discussion, Proceedings of the 5th International Heat Transfer Conference*, volume VII, pages 163–168, 1974.

[44] D. Gidaspow. *Multiphase Flow and Fluidization*. Academic Press, Inc., Boston, MA, 1994. Continuum and kinetic theory descriptions.

[45] R. Glowinski and O. Pironneau. Finite element methods for Navier-Stokes equations. In *Annual review of fluid mechanics, Vol. 24*, pages 167–204. Annual Reviews, Palo Alto, CA, 1992.

[46] E. Godlewski and P.-A. Raviart. *Numerical Approximation of Hyperbolic Systems of Conservation Laws*, volume 118 of *Applied Mathematical Sciences*. Springer-Verlag, New York, 1996.

[47] Abhijit Guha. A unified Eulerian theory of turbulent deposition to smooth and rough surfaces. *J. of Aerosol Sc.*, 28(8):1517–1537, 1997.

[48] F. Guichard and F. Couvreux. A short review of numerical cloud-resolving models. *Tellus A: Dynamic Meteorology and Oceanography*, 69(1), 2017.

[49] M. Gurris, D. Kuzmin, and S. Turek. Finite element simulation of compressible particle-laden gas flows. *J. Comput. Appl. Math.*, 233(12):3121–3129, 2010.

[50] W. G. Habashi. Recent advances in CFD for in-flight icing simulation. *Journal of Japan Society of Fluid Mechanics*, 28:99–118, 2009.

[51] F. Hecht. New development in freefem++. *J. Numer. Math.*, 20(3–4):251–265, 2012.

[52] J. C. Heinrich, P. S. Huyakorn, O. C. Zienkiewicz, and A. R. Mitchell. An upwind finite element scheme for two-dimensional convective transport equation. *Int. J. Numer. Meth. Eng.*, 11(1):131–143, 1977.

[53] J. C. Heinrich and O. C. Zienkiewicz. Quadratic finite element schemes for two-dimensional convective-transport problems. *Int. J. Numer. Meth. Eng.*, 11(12):1831–1844, 1977.

[54] R. Honsek. Development of a three-dimensional Eulerian model of droplet-wall inter-action mechanisms. Master's thesis, McGill University, Montréal, Québec, June 2005.

[55] T. J. R. Hughes and A. N. Brooks. A multi-dimensional upwind scheme with no crosswind diffusion. *In: Hughes, T.J.R, Ed., Finite Element Methods for Convection Dominated Flows*, 34:19–35, 1979.

[56] T. J. R. Hughes, M. Mallet, and M. Akira. A new finite element formulation for computational fluid dynamics: II. beyond SUPG. *Comput. Methods in Appl. Mech. Eng.*, 54(3):341–355, 1986.

[57] M. Ishii. *Thermo-Fluid Dynamic Theory of Two-Phase Flow.* Eyrolles, Paris, 1975.

[58] M. Z. Jacobson and Y. J. Kaufman. Wind reduction by aerosol particles. *Geophysical Research Letters*, 33(24), 2006.

[59] V. John and P. Knobloch. On discontinuity—capturing methods for convection—diffusion equations. In *Numerical Mathematics and Advanced Applications: Proceedings of ENUMATH 2005, the 6th European Conference on Numerical Mathematics and Advanced Applications Santiago de Compostela, Spain, July 2005*, pages 336–344. Springer Berlin Heidelberg, 2006.

[60] V. John and P. Knobloch. On spurious oscillations at layers diminishing (SOLD) methods for convectiondiffusion equations: Part II - analysis for P1 and Q1 finite elements. *Comput. Methods in Appl. Mech. Eng.*, 197(21–24):1997–2014, 2008.

[61] R. T. Lahey Jr. The prediction of phase distribution and separation phenomena using two-fluid models. In *Boiling Heat Transfer*, pages 85–122. Elsevier, 1992.

[62] S. Kumar, D. P. Hart, and C. E. Brennen. Granular pressure measurement in fluidized bed. In *ASME Cavitation and Multiphase Flow Forum*, Toronto, Canada, 1900.

[63] P. Lax and B. Wendroff. Systems of conservation laws. *Communications on Pure and Applied Mathematics*, 13(2):217–237, 1960.

[64] P. D. Lax. *Hyperbolic Systems of Conservation Laws and the Mathematical Theory of Shock Waves*. Society for Industrial and Applied Mathematics, 1973.

[65] P. G. LeFloch and M. Westdickenberg. Finite energy solutions to the isentropic Euler equations with geometric effects. *Math. Pures Appl.*, 88(5):389–429, 2007.

[66] R. J. LeVeque. *Numerical Methods for Conservation Laws*. Lectures in Mathematics ETH Zürich. Birkhäuser Verlag, Basel, second edition, 1992.

[67] R. J. LeVeque. *Finite Volume Methods for Hyperbolic Problems*. Cambridge Texts in Applied Mathematics. Cambridge University Press, Cambridge, 2002.

[68] J. Li and G. Warnecke. Generalized characteristics and the uniqueness of entropy solutions to zero-pressure gas dynamics. *Adv. Differential Equations*, 8(8):961–1004, 2003.

[69] J. Li and H. Yang. Delta-shocks as limits of vanishing viscosity for multidimensional zero-pressure gas dynamics. *Quart. Appl. Math.*, 59(2):315–342, 2001.

[70] J. Li, T. Zhang, and S. Yang. *The Two-Dimensional Riemann Problem in Gas Dynamics*, volume 98 of *Pitman Monographs and Surveys in Pure and Applied Mathematics*. Longman, Harlow, 1998.

[71] T.-P. Liu. Hyperbolic conservation laws with relaxation. *Comm. Math. Phys.*, 108(1):153–175, 1987.

[72] S. Marčič, M. Marčič, and Z. Praunseis. Mathematical model for the injector of a common rail fuel-injection system. *Engineering*, 7(6):307–321, 2015.

[73] E. A. Matida, W. H. Finlay, C. F. Lange, and B. Grgic. Improved numerical simulation of aerosol deposition in an idealized mouththroat. *J. of Aerosol Sc.*, 35(1):1–19, 2004.

[74] MATLAB. *version 8.0.1.604 (R2013a)*. The MathWorks Inc., Natick, Massachusetts, 2013.

[75] F. Morency, H. Beaugendre, and W. G. Habashi. FENSAP-ICE: A comprehensive 3D simulation tool for in-flight icing. In *15th AIAA Computational Fluid Dynamics Conference*, 2001.

[76] D. J. Needham and J. H. Merkin. The propagation of a voidage disturbance in a uniformly fluidized bed. *J. Fluid Mech.*, 131:427–454, 1983.

[77] O. Oleinik. Discontinuous solutions of nonlinear differential equations. *Amer. Math. Soc. Transl. (2)*, 26:95–172, 1957.

[78] H. Pokharna, M. Mori, and V. H. Ransom. Regularization of two-phase flow models: A comparison of numerical and differential approaches. *J. Comput. Phys.*, 134(2):282–295, 1997.

[79] V. H. Ransom and D. L. Hicks. Hyperbolic two-pressure models for two-phase flow. *J. Comput. Phys.*, 53(1):124–151, 1984.

[80] W. Rudin. *Principles of Mathematical Analysis*. International series in pure and applied mathematics. McGraw-Hill, 1976.

[81] D. Serre. *Systems of Conservation Laws: Hyperbolicity, Entropies, Shock Waves*. Cambridge University Press, Cambridge, 1999.

[82] W. Sheng and T. Zhang. *The Riemann Problem for the Transportation Equations in Gas Dynamics*. American Mathematical Society: Memoirs of the American Mathematical Society. American Mathematical Society, 1999.

[83] W. A. Sirignano. *Fluid Dynamics and Transport of Droplets and Sprays*. Cambridge University Press, 1999.

[84] J. Smoller. *Shock Waves and Reaction-Diffusion Equations*. Grundlehren der mathematischen Wissenschaften. Springer-Verlag New York, 1994.

[85] H. B. Stewart and B. Wendroff. Two-phase flow: models and methods. *J. Comput. Phys.*, 56(3):363–409, 1984.

[86] M. Tabata. A finite element approximation corresponding to the upwind finite differencing. *Mem. Numer. Math.*, 4:47–63, 1977.

[87] E. Tadmor. Numerical viscosity and the entropy condition for conservative difference schemes. *Math. Comp.*, 43(168):369–381, 1984.

[88] A. F. Tena and P. C. Clarà. Deposition of inhaled particles in the lungs. *Archivos de Bronconeumologa (English Edition)*, 48(7):240–246, 2012.

[89] Z. F. Tian, J. Y. Tu, and G. H. Yeoh. Numerical simulation and validation of dilute gas-particle flow over a backward-facing step. *Aerosol Science and Technology*, 39(4):319–332, 2005.

[90] I. Toumi. An upwind numerical method for two-fluid two-phase flow models. *Nucl. Sci. Eng.*, 123(2):147–168, 1996.

[91] A. Utkarsh. The Paraview Guide: A Parallel Visualization Application, Kitware, 2015, ISBN 978-1930934306.

[92] N. E. Veremei, Yu. A. Dovgalyuk, and E. N. Stankova. Numerical simulation of convective clouds developing in the atmosphere in emergency situations (explosions, fires). *Izvestiya, Atmospheric and Oceanic Physics*, 43(6):731–744, 2007.

[93] Z. Wang and X. Ding. Uniqueness of generalized solution for the Cauchy problem of transportation equations. *Acta Math. Scientia*, 17(3):341–352, 1997.

[94] M. J. Woodhouse, A. J. Hogg, J. C. Phillips, and R. S. J. Sparks. Interaction between volcanic plumes and wind during the 2010 Eyjafjallajökull eruption, Iceland. *J. of Geophysical Research: Solid Earth*, 118(1):92–109, 2013.

[95] H. Yang and J. Wang. Delta-shocks and vacuum states in the vanishing pressure limit of solutions to the isentropic Euler equations for modified Chaplygin gas. *J. Math. Anal. Appl.*, 413(2):800–820, 2014.

[96] G. Yin and W. Sheng. Delta shocks and vacuum states in vanishing pressure limits of solutions to the relativistic Euler equations for polytropic gases. *J. Math. Anal. Appl.*, 355(2):594 – 605, 2009.

[97] R. Zenit, M. L. Hunt, and C. E. Brennen. Collisional particle pressures measurement in solid-liquid flows. *J. Fluid Mech.*, 353:216–283, 1997.

[98] Z. Zhang, C. Kleinstreuer, and C. S. Kim. Cyclic micron-size particle inhalation and deposition in a triple bifurcation lung airway model. *J. of Aerosol Sc.*, 33(2):257–281, 2002.

[99] L. Zhou. Two-phase turbulence models in Eulerian-Eulerian simulation of gas-particle flows and coal combustion. *Procedia Engineering*, 102:1677–1696, 2015.